# DEVELOPMENT AND APPLICATION OF PROTEOMIC TOOLS TO QUANTIFY THE REDOX STATUS CHANGE IN BLOOD CELLS

by

Ru Li

B.Sc., Nanjing University, 2010

A THESIS SUBMITTED IN PARTIAL FULFILLMENT OF

THE REQUIREMENTS FOR THE DEGREE OF

DOCTOR OF PHILOSOPHY

in

THE FACULTY OF GRADUATE AND POSTDOCTORAL STUDIES

(Chemistry)

THE UNIVERSITY OF BRITISH COLUMBIA

(Vancouver)

August 2016

## Abstract

Cardiovascular diseases (CVDs) remain the number one killer around the world, representing a huge unmet need in innovative therapies. Platelet activation and their interaction with monocytes are critical in the development of CVDs, particularly atherosclerosis. Activated platelets release the contents of their granules, commonly called "platelet releasate", and recruit monocytes to damaged endothelium. However, the molecular mechanisms of the redox regulation in monocytes in response to platelet releasate are not fully understood. To extend our knowledge in this area, the modified biotin switch assays were developed and applied to an atherosclerotic model in sequential experiments, *i.e.* the quantification of reversible cysteine oxidations and sulfenic acid modification. We found that monocytes treated with platelet releasate activated NADPH oxidase (NOX) to produce reactive oxygen species (ROS) and resulted in cysteine oxidations. The proteome of reversible cysteine oxidations was analyzed in the atherosclerotic model using the modified biotin switch assay, and several biological processes were identified including glycolysis, cytoskeleton arrangement, and redox regulation. To better understand redox regulation in monocytes, the proteome of the sulfenic acid modification, a subtype of reversible cysteine oxidations, was obtained in the same model. Bioinformatics analysis of the proteome of sulfenic acid modification highlighted the biological process of monocyte transendothelial migration, which included integrin $\beta_2$. Flow cytometry confirmed the activation of LFA-1 ($\alpha_L\beta_2$), a subfamily of integrin $\beta_2$ complex, on human primary monocytes following platelet releasate treatment, which was mediated by the NOX-derived ROS. Furthermore, dyslipidemia is closely associated with hyperactivity of platelets in atherosclerosis and the generation of biologically active oxidized phospholipids including oxidized phosphatidylcholine (oxPC). Through our studies, we found a previous unknown inhibitory effect of oxPC species on platelet activation via

soluble guanylyl cyclase (sGC)– cyclic guanosine monophosphate (cGMP) pathway. In summary, the versatile modified biotin switch assay provides an approach for the quantification of reversible cysteine oxidation in biological systems. The application of this assay has extended our understanding of redox regulation in platelet-monocyte interaction and platelet function in atherosclerosis. The better understanding of redox regulation in atherosclerosis has the potential to advance the design of more targeted antioxidant therapies for CVDs.

## Preface

A version of chapter 2 has been published. Ru Li, Jiqing Huang, Juergen Kast, Identification of Total Reversible Cysteine Oxidation in an Atherosclerosis Model Using a Modified Biotin Switch Assay, J. Proteome Res., 2015, 14 (5), 2026–2035. I was the primary researcher involved in this project. I developed the modified biotin switch assay for the enrichment of reversible cysteine oxidation, and applied the method on an atherosclerotic model. Jiqing Huang helped me with the isolation of primary monocyte. Primarily I, with editing help from Dr. Juergen Kast, wrote the manuscript.

A version of chapter 3 has been submitted for publication. Ru Li, Cordula Klockenbusch, Liwen Lin, Shujun Lin, Juergen Kast, Quantitative Protein Sulfenic Acid Analysis Identifies Platelet Releasate-induced Activation of Integrin $\beta_2$ on Monocytes via NADPH Oxidase. I was the primary researcher involved in this project. I adapted the method of the biotin switch assay for the enrichment of protein sulfenic acid, and tested the method on an atherosclerotic model. Liwen Lin and Cordula Klockenbusch provided intellectual input on optimization of the method, Shujun Lin helped to run samples on mass spectrometers. The manuscript was written primarily by me, with editing help and writing contribution from Cordula Klockenbusch and Juergen Kast.

Ethical approval for platelet and monocyte isolation from whole blood from healthy blood donors was obtained from the Clinical Research Ethics Board at University of British Columbia (H12-00757) and written consent was granted by the blood donors.

## Table of Contents

## List of Tables

## List of Figures

## List of Abbreviations

| | |
|---|---|
| AA | Arachidonic acid |
| AC | Adenylyl cyclase |
| ADP | Adenosin 5'-diphosphate |
| Akt | Protein kinase B |
| AP-1 | Activator protein-1 |
| ApoE | Apolipoprotein E |
| Biotin-HPDP | N-[6-(Biotinamido)hexyl]3'-(2'-pyridyldithio)propion-amid |
| cAMP | Cyclic adenosine monophosphate |
| cGMP | Cyclic guanosine monophosphate |
| CID | Collision-induced dissociation |
| $cPLA_2$ | Cytosolic phospholipase $A_2$ |
| CVD | Cardiovascular disease |
| $Cys_{OX}$ | cysteine oxidation |
| cysTMT | Cysteine-reactive tandem mass tag |
| DAG | Diacylglycerol |
| DC | Dendritic cell |
| DPI | Diphenyleneiodonium |
| DTT | DL-dithiothreitol |
| ECD | Electron capture dissociation |
| eNOS | Endothelial nitric oxide synthase |
| ESI | Electrospray ionization |
| ETD | Electron transfer dissociation |
| FACS | Fluorescence-activated cell sorting |
| FcRγ | Fc-receptor γ-chain |
| FT-ICR | Fourier transform ion cyclotron resonance |
| GAPDH | Glyceraldehyde 3-phosphate dehydrogenase |
| GO | Gene ontology |
| GP | Glycoprotein |
| GPCR | G protein-coupled receptors |
| GSH | Glutathione |
| IAA | Iodoacetamide |
| ICAM-1 | Intrecellular adhesion molecule-1 |
| ICAT | Isotope-coded affinity tags |
| IMS | Imaging mass spectrometry |
| $IP_3$ | Inositol trisphosphate |
| IPA | Ingenuity Pathway Analysis |
| ITAM | Immunoreceptor tyrosine-based activation motif (ITAM) |
| iTRAQ | Isobaric tag for relative and absolute quantitation |

| | |
|---|---|
| JNK | c-Jun N-terminal kinase |
| KO | Knockout |
| LC | Liquid chromatography |
| LC-MS/MS | Liquid chromatography tandem mass spectrometry |
| LDL | Low density lipoprotein |
| LFA-1 | Integrin $\alpha_L\beta_2$ |
| LPA | Lysophosphatidic acid |
| LPAPR | LPA-induced platelet releasate |
| LPS | lipopolysaccharide |
| m/z | Mass-to-charge ratio |
| Mac-1 | Integrin $\alpha_M\beta_2$ |
| MALDI | Matrix-assisted laser desorption/ionisation |
| MALDI-TOF | Matrix-assisted laser desorption/ionisation-time of flight |
| ML 171 | 2-acetylphenothiazine |
| MS | Mass spectrometry |
| MS/MS | Tandem mass spectrometry |
| NADH | Nicotinamide adenine dinucleotide |
| NADPH | Nicotinamide adenine dinucleotide phosphate |
| NEM | N-Ethylmaleimide |
| NF-κB | Nuclear factor-κB |
| NO | Nitric oxide |
| NOX | NADPH oxidase |
| Nrf2 | Nuclear factor (erythroid-derived 2)-like 2 |
| oxLDL | Oxidized low density lipoprotein |
| oxPC | Oxidized phosphatidylcholine |
| p38MAPK | p38 mitogen-activated protein kinase |
| p53 | Tumor protein p53 |
| PAPC | 1-palmitoyl-2-arachidonoyl-*sn*-phosphatidylcholine |
| PAR | protease activated receptor |
| PBMC | Peripheral blood mononuclear cell |
| PC | Phosphatidylcholine |
| PDE | Phosphodiesterase |
| PF4 | Platelet factor 4 |
| $PGI_2$ | Prostacylin |
| PKA | Protein kinase A |
| PKC | Protein kinase C |
| PKG | Protein kinase G |
| $PLC_\beta$ | Phospholipase $C_\beta$ |
| PMA | Platelet-monocyte aggregate |
| PPP | Platelet poor plasma |

| | |
|---|---|
| PR | Platelet releasate |
| PR | Platelet releasate |
| PRP | Platelet rich plasma |
| PSGL-1 | P-selectin glycoprotein ligand-1 |
| PTM | Post-translational modification |
| QQQ | Triple quadrupole |
| RANTES | Chemokine(C-C motif) ligand 5 |
| rcf | Relative centrifugal force |
| RNS | Reactive nitrogen species |
| ROS | Reactive oxygen species |
| SDS-PAGE | Sodium dodecyl sulfate polyacrylamide gel electrophoresis |
| sGC | soluble guanylate cyclase |
| SILAC | Stable isotope labeling by amino acids in cell culture |
| SOD | Superoxide dismutase |
| TCEP | Tris(2-carboxyethyl) phosphine |
| THP-1 | The human acute monocytic leukemia cell line |
| Thr | Thrombin |
| ThrPR | Thrombin-induced platelet releasate |
| TPI | Triose phophate isomerase |
| $TXA_2$ | Thromboxane $A_2$ |
| VASP | Vasodilator-stimulated phosphoprotein |
| VCAM-1 | Vascular adhesion molecule-1 |
| VSMC | Vascular smooth muscle cell |
| vWF | von Willebrand factor |

## Acknowledgements

I would like to start off by giving enormous thanks to my supervisor Dr. Juergen Kast for his guidance and encouragement when I knew very little about scientific research. Dr. Kast taught me a lot of things from critical thinking, experimental design to scientific writing, and helped me see the big picture when I was overwhelmed by small details. I appreciate his trust in me to pursue my research interest, his endless support for my research projects, and giving me the opportunity to attending international and national conferences. Over the years, Dr. Kast helped me become an independent scientist.

I would like to thank Dr. David Chen, Dr. Michael Blades, and Dr. Roman Krems, for being members of my supervisory committee, and giving me valuable insight and discussion regarding my research and thesis.

I am extremely lucky to be surrounded by many brilliant scientists during my PhD studies. I would not be able to complete the research in this thesis without their help. Herein, thank you to our former master student, Liwen Lin, who taught me all the fundamentals about wet-lab work; Dr. Cordula Klockenbusch, who gave me valuable advices on designing many of my experiments; Dr. Jane O'Hara and Dr. Geraldine Walsh for helping me improve my writing and constantly encouraging me during these six years; Dr. Iris Egner, one of the most cheerful people I have ever met, who made my research incredibly smoothly through recruiting blood donors; Dr. Chengcheng Zhang, who taught me how to give presentations, prepare papers, and proofread my papers; Shujun Lin for assistance with mass spectrometer and insight advice about life; our amazing platelet team Jiqing Huang and Honghui Jiang for their teamwork. To all the other

members of Kast Lab, both past and present, I would like to thank you all for all your help and suggestions over the years.

I'd next like to thank Dr. Nikolay Stoynov from Foster Lab and Jason Rogalski for helping me running samples on mass spectrometers. I would like to thank UBCFlow, especially Andy Johnson, who trained me with flow cytometry. I would also like to thank everyone in the Biomedical Research Centre (BRC), particularly Dr. Hermann Ziltener, Dr. Yanni Wang and Dr. Doug Carlow for proofreading my paper and my thesis, attending my BRC talks, and giving me input on my research.

In addition, I offer my enduring gratitude to all the blood donors who made the research possible. Thank you to Iren Constantinescu, Brana Culibrk in Centre of Blood Research, and UBC hospital for the phlebotomy services. I'd also like to extend my appreciation to Natural Sciences and Engineering Research Council of Canada (NSERC) and Canadian Institute of Health Research (CIHR) for our operating funding.

At last but not least, special thanks to my parents for being there with me for all the up and down, and encouraging me through all the difficulties.

**Dedication**

*To my parents and my family*

# Chapter 1: Introduction

## 1.1 Atherosclerosis

Cardiovascular diseases (CVDs) are the major cause of mortality worldwide, accounting for 17.5 million deaths or 31% of all deaths in 2012 (1). One repetitive cause of CVDs is atherosclerosis, which is developed through the formation of atherosclerotic plaques. The build-up of plaques over time causes hardening and narrowing of elastic arteries, which limits oxygen and nutrients in downstream tissue (2). The sudden rupture of atherosclerotic plaque activates platelets to form thrombus. The formation of thrombus and subsequent arterial occlusion in the heart (heart attack) or brain (stroke) are particularly devastating, as they lead to permanent tissue damage in vital organs (3). The plaque of atherosclerosis may be present throughout a person's lifetime, with the earliest type of lesion known as fatty streak. A fatty streak is a purely inflammatory lesion only with monocyte-derived macrophages and T lymphocytes, and has been found in infants and young children (4). It is still unclear how a plaque begins to form and its molecular mechanism driving disease progression. Thus, a better understanding of the basic pathophysiologic mechanism of atherosclerosis is crucial to provide the early prognosis and better therapies for preventing and curing CVDs.

### 1.1.1 The development of the atherosclerotic plaque

Healthy endothelium is critical to maintain the vascular tone in blood vessels (5). However, a wide variety of risk factors such as physical or chemical forces and infection can damage endothelial cells (endothelial dysfunction). Of the identified risk factors, oxidized low-density lipoprotein (oxLDL) from cholesterol in plasma is regarded as a principal cause (6). Endothelial dysfunction in turn leads to the increase of endothelial permeability to oxLDL and other plasma

constituents, up-regulation of adhesion molecules, and the release of chemotactic factors (7). The expression of adhesion molecules and the secretion of chemotactic factors facilitate tethering, adhesion, and transendothelial migration of leukocytes, particularly monocytes (a leukocyte subset), into the underlying tunica intima (8). Subsequently, monocytes differentiate into macrophages, which become foam cells upon ingestion of accumulated oxLDL. The accumulation of foam cells and T lymphocytes initiates the formation of the fatty streak. The fatty streaks progress to intermediate and advanced plaques through the continuing influx of monocytes, vascular smooth muscle cells (VSMC), and lipids (Figure 1-1) (9, 10).

### 1.1.2 Platelet-monocyte interaction in atherosclerosis

The rupture of vulnerable large plaque exposes coagulation factors, extracellular matrix, and its lipid content, which trigger platelet activation (3). Activated platelets can interact with monocytes to form platelet-monocyte aggregate (PMA). Circulating PMAs in blood have been found to be an early marker for acute cardiovascular events, i.e. acute myocardial infarction (11), stroke (12), and acute coronary syndromes (13). The PMAs are mainly mediated through the interaction between P-selectin on the surface of activated platelets and P-selectin glycoprotein ligand (PSGL-1) on monocytes (14). The formation of PMA triggers the production of reactive oxygen species (ROS), activation of the GTPase Ras, and phosphorylation of various cytoplasmic proteins in monocytes (15). This series of events lead to the up-regulation and activation of integrin $\beta_1$ and $\beta_2$, and the secretion of various bioactive molecules from monocytes (16). The PMA formation also increases the adhesion of monocytes to endothelial cells, and subsequent transmigration of monocytes across the endothelial layer (Figure 1-1) (17, 18). In addition to direct binding to monocytes, platelets release soluble factors, proteins, i.e. RANTES

and platelet factor (PF4), and microparticles that increase adhesion of monocytes to endothelial cells (19).

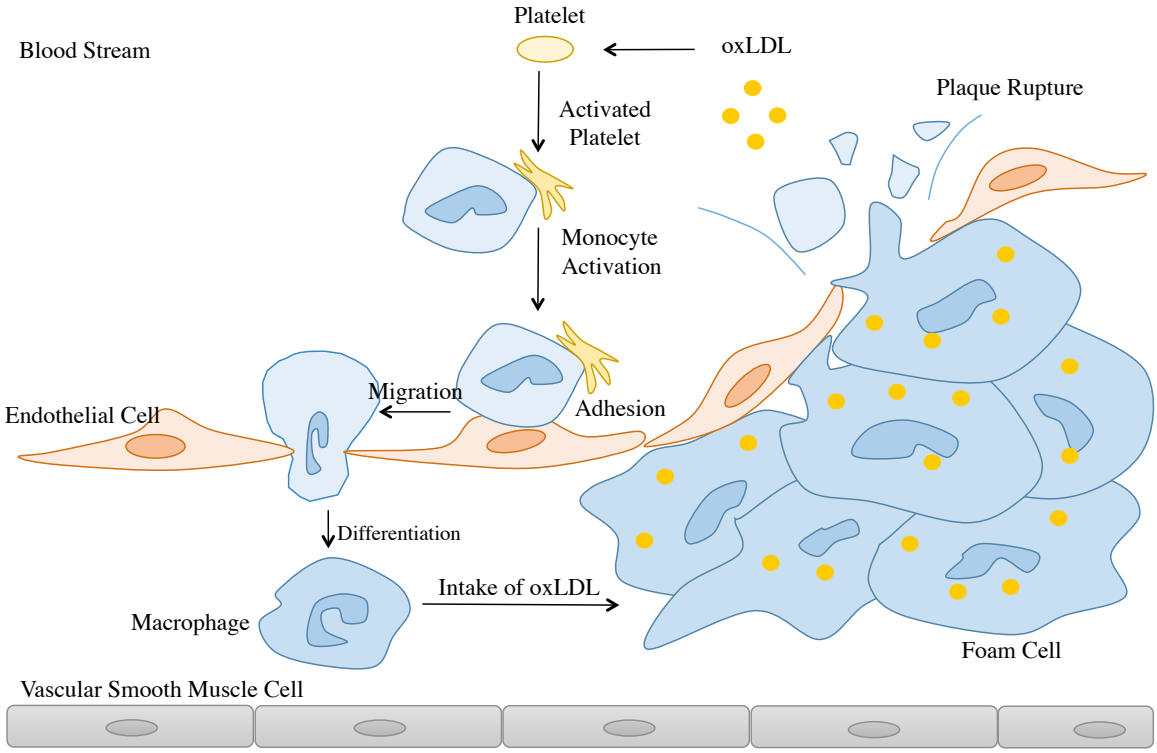


**Figure 1-1. The development of an atherosclerotic plaque in vascular system.** Endothelial dysfunction leads to the increase of endothelial permeability to oxidized low-density lipoprotein (oxLDL), and recruits monocytes into the adjacent tissue. The infiltrated monocytes then differentiate into macrophages. Macrophages as well as vascular smooth muscle cells take in oxLDL and become foam cells. The accumulation of foam cells results in the formation of fatty streak, and then the development of a plaque. The rupture of vulnerable plaque triggers platelet activation and aggregation by exposing coagulation factors, extracellular matrix, and its lipid content. Activated platelets interact with monocytes to promote the adhesion of monocytes on endothelial cells. Adapted from a grant figure made by Jiqing Huang with permission.

### 1.1.3 Platelets

Platelets are key components in the hemostatic system, which is crucial to maintain blood flow under physiological conditions, and react to vascular injury in a rapid manner. Platelets are fragments of megakaryocytes, which contain cytoplasm, membranes, and mitochondria. They are the smallest corpuscular components of human blood (2 to 5 μm in diameter), have no nucleus, and their physiological concentration varies from $200 \times 10^9$/L to $400 \times 10^9$/L. Resting platelets have a smooth discoid shape, and circulate passively in the blood for 10 days before being removed by spleen macrophages (20). The major secretory organelles within platelets are α-granules, dense granules, and lysosomes. The numerous α-granules contain many proteins, including fibrinogen, vWF, PF4, and albumin (21). Dense granules, which are easily recognized by their dense core surrounded by a clear halo, store and secrete small molecules, including serotonin, ADP, adenosine triphosphate (ATP), and divalent cations such as $Mg^{2+}$ and $Ca^{2+}$ (22). Lysosomes contain acid hydrolases (23).

At the site of endothelial injury, platelets adhere to the exposed sub-endothelial matrix. The initial adhesion of platelets is mainly mediated by interactions of glycoprotein (GP) complex Ib-IX-V on platelets with vWF on endothelium (24), and GPVI on platelets with collagen in the extracellular matrix (25). Once adhered, platelets undergo a shape change to a spherical form and become activated. In activated platelets, granules migrate to and fuse with the platelet membrane to release their contents, e.g. ADP and ATP, or molecules synthesized by activated platelets like thromboxane $A_2$ ($TxA_2$) (26). These secondary agonists recruit circulating platelets and further activate them to form aggregates. The platelet aggregation is formed by the activation of the platelet specific integrin $\alpha_{IIb}\beta_3$ from a low affinity state to a high affinity state (27), which then

binds to its primary ligand fibrinogen to form bridges between adjacent platelets. Once a primary layer of adhesive platelets has covered the exposed endothelial injury, subsequent adhesion will continue in the form of platelet aggregation.

#### 1.1.3.1 Platelet agonists in hemostasis

A number of agonists can be locally available at the site of endothelial injury, including thrombin, collagen, $TxA_2$, ADP, and epinephrine. Thrombin, collagen, and $TxA_2$ are considered strong platelet agonists, as they can cause platelet aggregation, $TxA_2$ synthesis, and granule secretion. ADP and epinephrine are weak platelet agonists that trigger platelet aggregation without inducing granule release.

***Thrombin*** is the main serine protease in the coagulation cascade, generated from prothrombin by coagulation factor Xa and factor Va. As the most potent physiological agonist of platelets, thrombin causes all the hallmarks of platelet activation, and is able to activate platelets at concentrations as low as 0.1 nM (28). Thrombin mediates its action through binding to cell-surface G-protein coupled protease-activated receptors (PARs). Four PARs have been identified so far, and PAR1 and PAR4 are expressed on human platelets, both of which are activated by cleavage of its extended N-terminus by thrombin (29). The newly formed N-terminus then serves as a tethered ligand for PAR1 or PAR4 to initiate transmembrane signaling (Figure 1-2) (30). PAR1 and PAR4 trigger downstream $G_{12/13}$ and $G_q$ signaling. $G_{12/13}$ regulates actin cytoskeletal rearrangement via the activation of small GTPase Rho and Rac, which leads to platelet shape change and degranulation (31). Activation of $G_q$ leads to strong activation of phospholipase Cβ (PLCβ), which mediate cleavage of phosphatidylinositol 4,5-bisphosphate ($PIP_2$) to 1,4,5-inositol

triphosphate ($IP_3$) and diacylglycerol (DAG) (32). These in turn increase concentration of cytosolic $Ca^{2+}$, activate protein kinase C (PKC) and integrin $\alpha_{IIb}\beta_3$, and stimulate the synthesis of $TxA_2$. PAR1 is also coupled to $G_i$, which inhibits adenylyl cyclase (AC) and leads to decreased level of cyclic adenosine monophosphate (cAMP) (33). The AC-cAMP pathway is one of the two dominant physiological inhibition pathways in platelets, through which the endothelial derived platelet antagonist $PGI_2$ signal to inhibit platelet activation.

***Collagen*** is an extracellular matrix protein that is exposed at sites of endothelial damage or ruptured plaques, and a key initiator of increased platelet adhesion and subsequent activation. There are two types of receptors on platelet that bind directly to collagen: GPVI, a receptor of the immunoglobulin superfamily, and integrin $\alpha_2\beta_1$ (34). GPVI is considered to be the main platelet collagen receptor (35). Firm adhesion of platelets on collagen under high shear pressure requires prior activation of integrins through "inside-out" signaling generated by GPVI (36). GPVI is associated with Fc-receptor γ-chain (FcRγ). Activation of GPVI leads to phosphorylation of immunoreceptor tyrosine-based activation motif (ITAM) in FcRγ by Src kinase. This causes the activation of Syk kinase, initiates downstream activation of PLCγ, and results in full platelet activation (Figure 1-2) (37). The activation signal from collagen binding to GPVI is reinforced by the release of ADP and the generation of $TxA_2$ (25). Integrin $\alpha_2\beta_1$ is an $Mg^{2+}$-dependent collagen receptor and involved in the initial rolling of platelets on collagen (38).

***ADP*** is secreted from the dense granules in activated platelets and damaged cells at the injured vessel wall, and acts as a potentiator of platelet responses to other agonists (39). Adenosine nucleotides interact with the P2 receptor family, which consists of two distinct classes: P2Y G

protein-coupled receptors (GPCRs), and P2X ligand-gated ion channels. ADP activates $P2Y_1$ and $P2Y_{12}$ (Figure 1-2), while ATP activates $P2X_1$ on human platelets. $P2Y_1$ signals through $G_q$ to trigger $Ca^{2+}$ mobilization from internal stores, activates PKC, and leads to platelet shape change through small GTPase Rac. The $P2Y_{12}$ receptor is coupled to $G_{i2}$, which is responsible for the activation of phosphoinositide-3 kinase (PI3K), the small GTPase Rap1b, and integrin $\alpha_{IIb}\beta_3$ (40, 41). Due to the important contribution of ADP to platelet function through $P2Y_1$ and $P2Y_{12}$, a number of pharmacological agents have been developed against ADP receptors and provided effective antithrombotic therapy (42). Given the ubiquitous expression of $P2Y_1$ receptor on other cells, most clinical agents are designed to inhibit $P2Y_{12}$, such as clopidogrel, prasugrel, ticagrelor, cangrelor, and elinogrel (43).

#### 1.1.3.2 Platelet agonists in atherosclerosis

The sudden rupture of vulnerable atherosclerotic plaque exposes the subendothelium, which contains collagen, vWF, and tissue factor-derived thrombin. Besides these platelet agonists relevant to hemostasis, ruptured plaques also release the content in their large necrotic lipid core, which contains multiple thrombogenic species, including oxidized low-density lipoprotein (oxLDL), lysophosphatidic acid (LPA), and oxidized phosphatidylcholine (oxPC).

***Oxidized low-density lipoprotein (oxLDL)*** is generated from low-density lipoprotein (LDL) that is trapped in the tunica intima, and plays an important role in CVDs through their pro-thrombotic and pro-inflammatory properties. Oxidized LDL behaves as a mild platelet activator, and the response of platelet to oxLDL seems to be dependent on the degree of LDL oxidation. Below 30% of oxidation, oxLDL primarily sensitizes platelets through p38 mitogen-activated protein

kinase ($p38^{MAPK}$) signaling pathway (44). Increased oxidation of LDL is associated with $Ca^{2+}$ mobilization and leads to platelet activation. However, part of this effect may be attributed to the production of LPA, a platelet agonist, during LDL oxidation (45). Moreover, oxLDL binds to the macrophage scavenger receptor CD36 to activate the c-Jun N-terminal kinase 2 (JNK2) and its upstream kinase MKK4. The activation of JNK2 leads to assemble of a signaling complex, which consists of Fyn, Lyn, and Src kinases (46). Highly oxidized LDL was suggested to be an inhibitor of platelet activation, as it was observed to inhibit thrombin receptor-activating peptide (TRAP)-induced platelet aggregation (45). Oxidized LDL also plays a role in activating NADPH oxidase 2 (NOX2) for ROS generation, which rapidly reacts with endothelial-derived nitric oxide (NO) and desensitizes the inhibitory cGMP signaling pathway (47). The soluble guanylyl cyclase (sGC) –cyclic guanosine monophosphate (cGMP) pathway is an important inhibitory pathway in platelets that is initiated by NO.

***Lysophosphatidic acid (LPA)*** is a bioactive lipid accumulating in human atherosclerotic plaque, and acyl- and alkyl-LPA was identified as the oxLDL component most strongly activating platelets (48). LPA is enzymatically produced by autotaxin using lysophosphatidylcholine (lysoPC) as a substrate (49), which is derived from the oxidation of LDL (50). Different forms of LPA are present in plaques with variance in the types of fatty acid and the linkage to the glycerol backbone (Scheme 1-1). LPA molecules also differ greatly in their potency for platelet activation (48), e.g. alkyl-LPA is 20 times stronger compared to acyl-LPA in activating human platelets (51). However, the signaling mechanisms by which LPA activates platelets and the receptors that LPA binds to are still under investigation. To date, six LPA receptors are confirmed, $LPA_1$ - $LPA_6$ (52-54), and a few others, i.e. GPR87 (55), $P2Y_{10}$ (56), GPR35 (57), and PPARγ (58),

require more validation. According to their structures, $LPA_1$, $LPA_2$, and $LPA_3$ are classified into the endothelial differentiation gene (EDG) subfamily of GPCRs (52); $LPA_4$, $LPA_5$, and $LPA_6$ are P2Y GPCRs (54). The mRNA of all six LPA receptors has been found in human platelets, with $LPA_4$ and $LPA_5$ being the most abundant (59) (Figure 1-2). The downstream signaling pathways mediated by LPA are not very well characterized. It has been suggested that LPA receptors couple to $G_{12/13}$ to activate the small GTPase Rho and induce platelet shape change (60). LPA also act on platelets by activating ADP receptors (48). Moreover, the activation effect of LPA on human platelets is donor dependent, such that platelets of 20% of healthy donors do not response to LPA (61). Inhibition of cAMP production partially restores platelet aggregation induced by LPA, and LPA4 is proposed to regulate inhibitory pathways in human platelets (61). What exactly causes these differences is currently unknown.

***Phosphatidylcholine (PC)*** is the main phospholipid within low-density lipoprotein (LDL) in all mammalian cells (40~50%) (62). The oxidations of LDL by multiple pathways give rise to a family of bioactive oxidized phosphatidylcholine (oxPC), which has been structurally characterized by mass spectrometry (63). This study identified a class of oxPC comsisting of two subgroups, four species derived from oxidized 1-palmitoyl-2-arachidonyl-PC (PAPC) and four species from oxidized 1-palmitoyl-2-linoleoyl-PC (PLPC) (64). These eight oxPC species are markedly increased in the plasma of patients with low high-density lipoprotein (HDL) (62, 65). OxPC species have been demonstrated to serve as high-affinity ligands for the CD36 receptor. The scavenger receptor CD36 on macrophage recognizes oxLDL, and assists foam cell formation from macrophage through the uptake of oxLDL. For human platelets, some oxPC species are observed to activate integrin $\alpha_{IIb}\beta_3$, increase p-selectin expression, and induce ROS

production through activation of NOX2 in a CD36-dependent manner (47, 65). However, the exact mechanism of oxPC on platelet activation and its relevance to CD36 are still not clear, which requires more systematic analysis.

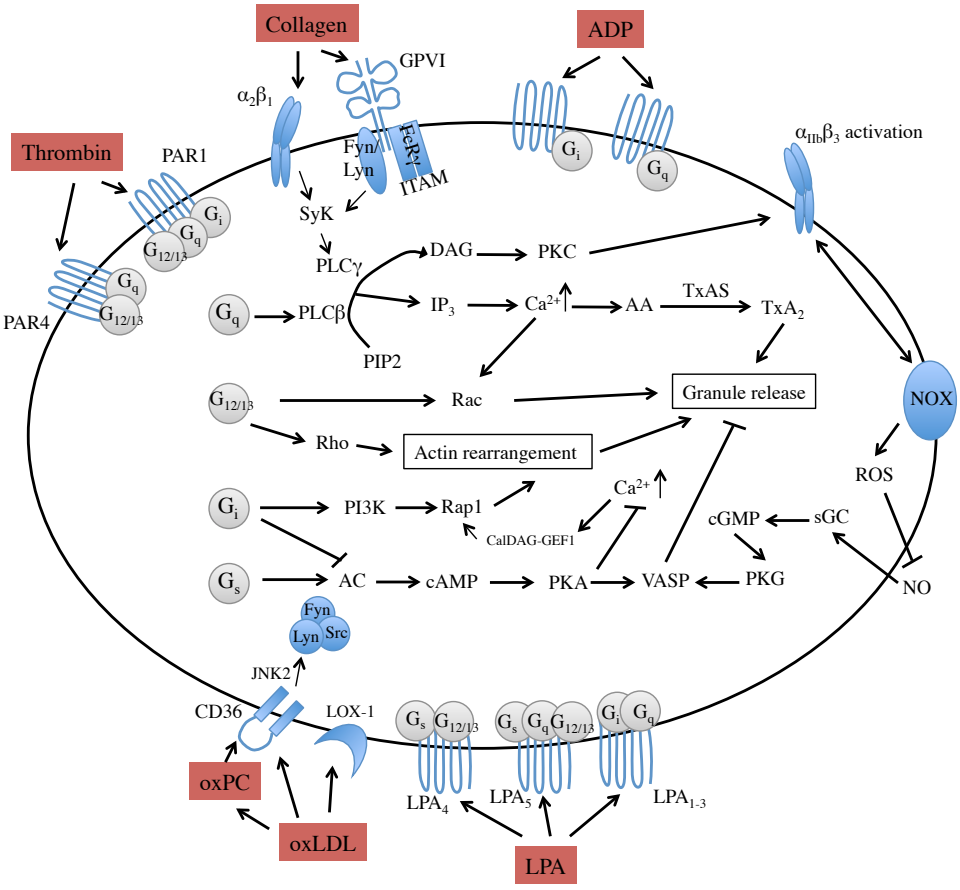


**Figure 1-2. Schematic view of signaling transductions in platelet activation.** Platelet activation is achieved through different receptors by thrombin (PAR1 and PAR4), collagen (GPVI and $\alpha_2\beta_1$), and ADP ($P2Y_1$ and $P2Y_{12}$), and coordinated with components from atherosclerotic plaque, e.g. LPA ($LPA_{1\text{-}5}$), oxLDL, and oxPC (CD36 and LOX-1). Some of these receptors couple to different G-proteins, whose signaling events downstream in platelets lead to granule release and platelet aggregation. PLCβ, phospholipase C β; PLCγ, phospholipase γ; PIP2, phosphatidylinositol 4,5-bisphosphate; DAG, diacylglycerol; $IP_3$, inositol triphosphate; AA, arachidonic acid; $TxA_2$, thromboxane A2; TxAS, thromboxane synthase; SyK, spleen tyrosine kinase; PKA, protein kinase A; PKC protein kinase C; PKG protein kinase G; PI3K, phosphoinositide 3-kinase; CalDAG-GEF1, calcium and DAG-regulated

guanine exchange factor 1; AC, adenylate cyclase; sGC, soluble guanylate cyclase; VASP, vasodilator-stimulated phosphoprotein; NO nitric oxide; ROS reactive oxygen species; NOX, NADPH oxidase. Adapted from a grant figure made by Jiqing Huang with permission.

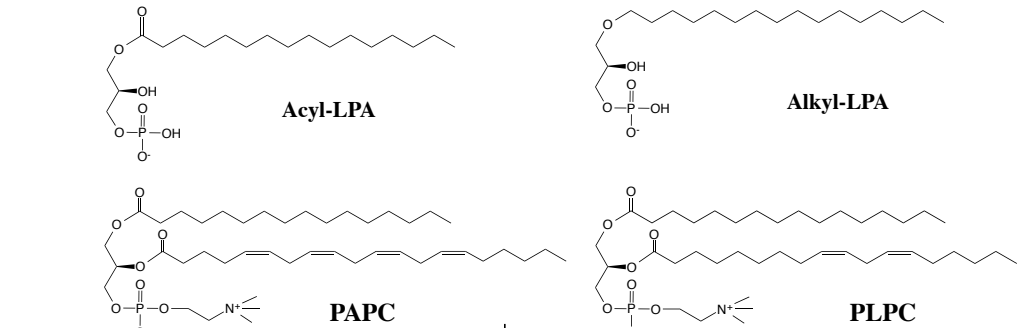


| PAPC series n=1 | X | Y |
|---|---|---|
| **HOdiA-PC** | OH | OH |
| **KOdiA-PC** | =O | OH |
| **HOOA-PC** | OH | H |
| **KOOA-PC** | =O | H |

| PLPC series n=5 | X | Y |
|---|---|---|
| **HDdiA-PC** | OH | OH |
| **KDdiA-PC** | =O | OH |
| **HODA-PC** | OH | H |
| **KODA-PC** | =O | H |

**Scheme 1-1. Chemical structures of bioactive phospholipids formed during the oxidation of LDL.** LPA, Lysophosphatidic acid; PAPC, 1-palmitoyl-2-arachidonyl-phosphatidylcholine; PLPC, 1-palmitoyl-2-linoleoyl-phosphatidylcholine.

### 1.1.4 Monocytes

Monocytes originate from myeloid progenitors in the bone marrow, and circulate in the peripheral blood for several days without proliferation. Mature monocytes constitute ~5-10% of peripheral blood leukocytes in humans. During their trip throughout the body, monocytes scavenge dead cells and toxic molecules, and give rise to a variety of tissue-resident

macrophages and dendritic cells (DCs). The morphology of mature monocytes is heterogeneous in size, degrees of granularity, and the shape of nucleus. Differential expression of CD14, a receptor for lipopolysaccharide, and CD16, also known as FcγRII, divides monocytes into three subsets: the classical $CD14^{hi}CD16^{-}$ monocytes, which express high level of CD14 and no CD16, and represent 85% ~95% of the monocytes in healthy individuals; the non-classical $CD14^{+}CD16^{hi}$ monocytes, which express low level of CD14 and high level of CD16, and have been suggested to resemble mature tissue macrophages; and the intermediate $CD14^{hi}CD16^{+}$ monocytes, which express high level of CD14 and low level of CD16 (66, 67). Phenotypic differences, for example distinct chemokine-receptor expression profiles, are also recognized between these subsets (68).

Monocytes mediate host antimicrobial defense (69) and play a central role in several pathophysiological diseases, particularly when the diseases arise from underlying inflammatory reactions, e.g. atherosclerosis (70). In the processes of hemostasis, infection, or inflammation, monocytes leave the blood stream and migrate to lymphoid and nonlymphoid tissues (71). Subsequently, monocytes get activated and differentiate into macrophages or DCs to ingest apoptotic cells, microbes, and toxic molecules such as oxLDL (72, 73). Meanwhile, activated monocytes release more than 100 different biological active molecules, such as coagulation factors, growth factors, cytokines, chemokines, and reactive oxygen species (66, 74).

In the context of atherosclerosis, blood monocytes accumulate at sites of inflammation and enter atherosclerotic plaque (75). When they encounter fatty deposits in intima and subintima, monocytes differentiate into macrophages, and take up oxLDL and other lipids through their

scavenger receptors (76). These monocyte-derived macrophages subsequently become foam cells in the subintima and develop into fatty streaks. The accumulation and continued infiltration of monocytes are key to the development of advanced plaque (77).

As a direct relationship among platelet activation, oxLDL accumulation, and CVDs has been established, current therapies target primarily platelet and oxLDL as treatment options. For patients at increased risk of acute atherothrombotic events, low-dose aspirin is one of the main therapeutic interventions as an antiplatelet treatment. Aspirin therapy inhibits $TxA_2$ synthesis via the enzyme cyclooxygenase-1 (COX-1) in activated platelets to reduce overall platelet aggregation (78). However, aspirin therapy targets signals shared by atherothrombotic and hemostatic pathways, and increases the risk of bleeding (79). Statin therapy, which lowers the oxLDL level, provides an alternative, but the use of statins may be limited by hepatotoxicity, muscle damage (80), acute renal failure (81), and increased diabetes risk (82). Moreover, the side effects associated with high doses of statin and their interactions with other drugs may be more severe in older patients (8.3% of adverse events in adults $\geq$ 65 years) than middle-aged patients (7.9% adverse events in adults < 65 years) (83).

Neither aspirin therapy nor statin therapy affects monocyte function, the key contributor to the development of atherosclerosis. The signaling events induced by platelet-monocyte interactions open a novel approach for therapeutic treatments of atherosclerosis. In order to fully exploit such an approach, a thorough understanding of the mechanism of platelet-monocyte interactions and platelet activation that lead to atherosclerosis is required.

## 1.2 Redox modulation in atherosclerosis

### 1.2.1 Reactive oxygen species (ROS) - a double-edged sword in cells

The processes of cell respiration are accompanied by the production of free radicals as byproducts named reactive oxygen/nitrogen species (ROS/RNS). ROS is a collective term, including hydrogen peroxide ($H_2O_2$), superoxide ($O_2^-$), and hydroxyl radical (OH•); RNS includes nitric oxide (NO), nitroxyl (HNO), and peroxynitrite ($ONOO^-$). Since the first published article on ROS in 1954, thousands of studies have been conducted in this area (84).

It is universally acknowledged that oxidative stress, the accumulation of ROS/RNS, is a major contributor to human aging and diseases such as cancer, diabetes, cardiovascular disease, and Alzheimer's disease (85). However, numerous studies also suggest that ROS/RNS at relatively low concentrations can also promote cell proliferation, act as a protective mechanism and secondary messengers in physiological processes. For instance, ROS is essential for both innate and acquired immune defense. Activated monocytes/macrophages present in the local inflammatory milieu exaggerate ROS production to generate an oxidative burst against the invading pathogens. Excess ROS continue to be locally produced by the activated monocytes/macrophages to decrease the activation threshold within the T lymphocytes to initiate the acquired immune response (86). Besides their involvement in the immune system, ROS/RNS also participate extensively in regulating vascular tone. Endothelium-derived relaxing factor nitric oxide (NO) inhibits platelet activation, and induces relaxation of vascular smooth muscle (87).

ROS/RNS are also proposed as second messengers (88). For example, ROS/RNS regulate signaling pathways by affecting transcription factors, e.g. nuclear factor-κB (NF- κB) (89), activator protein-1 (AP-1) (90), and nuclear factor (erythroid-derived 2)-like 2 (Nrf2) (91). In the meantime, ROS/RNS can oxidatively modify redox-sensitive signaling proteins, such as tumor protein p53 (p53), protein kinase B (Akt), c-Jun N-terminal kinase (JNK), and p38 mitogen-activated protein kinase ($p38^{MAPK}$) (92). In ROS/RNS mediated signaling pathways and oxidative stress, cysteine thiols play a central part, as the thiol groups are well suited as targets of diverse oxidative modifications. The reversible cysteine oxidations can function as redox switches and are able to integrate the intracellular changes in redox state to biochemical processes. Therefore, my emphasis in this thesis is mainly on redox regulations in platelet-monocyte interaction through reversible cysteine oxidation.

### 1.2.2 Association of atherosclerosis with increased production of ROS

A substantial body of evidence from both research and clinical studies now implicate ROS in various aspects of atherosclerosis development (Figure 1-3). It has been demonstrated that ROS is able to inactivate endothelial nitric oxide synthase (eNOS) to decrease the NO level in endothelium dysfunction. $O_2^-$ reacts with NO three times faster than with $Cu^{2+}/Zn^{2+}$-superoxide dismutase (SOD) (93). The lower level of NO and the consumption of NO by $O_2^-$ lead to the increased risk of platelet activation, PMA formation, and a pro-inflammatory state in the vascular system. Moreover, oxidation of NO by $O_2^-$ also results in the formation of peroxynitrite, which in combination with other ROS enhance oxidative stress, and augment the oxidation of LDL (94). OxLDL contributes to the atherosclerotic plaque formation and progression (95), produces LPA, oxPC, and other bioactive lipid mediators found in the lipid–rich core of the

atherosclerotic plaques (96). In addition, ROS also induces the expression of adhesion molecules such as intercellular adhesion molecule-1 (ICAM-1) and vascular adhesion molecule-1 (VCAM-1) on endothelial cells, which assist in the recruitment of monocytes and oxLDL deposition in the intimal layer (97).

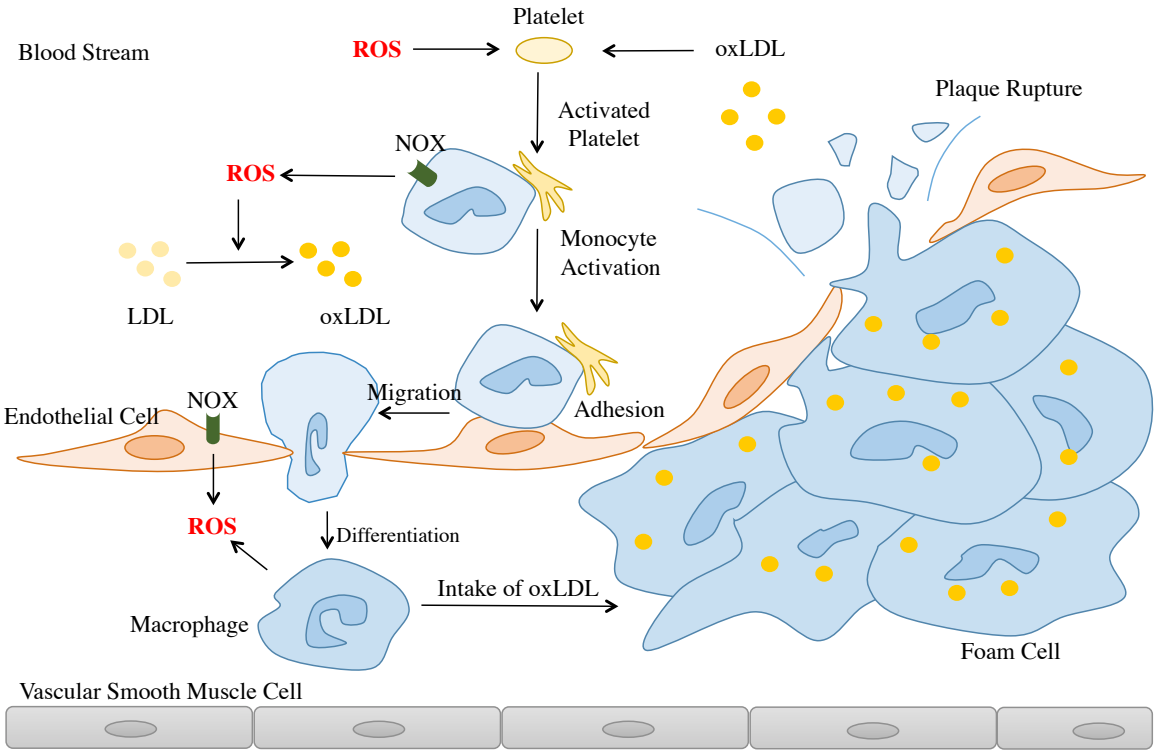


**Figure 1-3. Interactions between reactive oxygen species (ROS), platelets, monocytes, and endothelial cells in the presence of platelet agonists are crucial for atherosclerosis.** NADPH oxidase (NOX)-derived ROS are actively involved in various aspects of plaque development, including activation of platelets and monocytes, and oxidation of LDL. The role of ROS in platelet activation and monocyte recruitment is the focus of our study. Adapted from grant application by Jiqing Huang. Adapted with permission.

### 1.2.3 NADPH oxidase and atherosclerosis

NADPH oxidase (NOX) is a family of membrane associated multicomponent enzymes that primarily catalyze the generation of superoxide and/or hydrogen peroxide. This property is

distinct from other oxidoreductases that produce ROS as by-products of their catalytic pathways. In addition to the originally discovered phagocytic NOX2, six isoforms of NOX2 (NOX1, -3, -4, -5, and DUOX1, -2) have been described in nonphagocytic cells (98, 99).

Under physiological conditions, the expression levels of NOX1 and NOX2 are low in the vasculature, but are up-regulated in atherosclerosis (100). The NOX1/4-targeting inhibitor, streptozotocin (STZ), resulted in an anti-atherosclerotic effect in Apolipoprotein E (ApoE) knockout (KO) mice (101). Three studies have further supported the role of NOX1 in atherosclerosis. In the first study, laboratory mice received an atherogenic diet for 18 weeks to induce lesion formation. NOX1/ApoE double KO mice exhibited decreased lesion area and macrophage infiltration in comparison with ApoE KO mice (102), while the depletion of NOX4 did not decrease lesion area (103). The second study showed decreased atherosclerotic lesion formation and cellular surface adhesion factor CD44 expression on vascular smooth muscle cells (VSMCs) in ApoE KO mice treated with GKTB6901, a NOX specific inhibitor (104). The third study revealed reduced proliferation and migration response from NOX1-deficient VSMCs, whereas NOX1 overexpression had the opposite effect (105).

Monocytes are the prototype of a NOX2-expressing phagocyte, which utilizes the NOX2-derived ROS in antimicrobial defense. The activation of monocytes leads to the activation of NOX2, and the mechanism of NOX2 activation is summarized in Figure 1-4. In brief, the activation of monocyte leads to the influx of calcium through receptor-regulated channels and the mobilization of intracellular calcium (106), which then activate protein kinase C (PKC) (107) and cytosolic phospholipase $A_2$ ($cPLA_2$) (108). PKCδ phosphorylates p47phox and p67phox

(117), the two regulatory subunits of NOX2, resulting in their activation and translocation to cell membrane for the assembly and activation of NOX2. The activation of $cPLA_2$ leads to its translocation from the cytosol to the membrane, and the production of arachidonic acid (AA), which is also an essential regulator of NOX2 in monocytes (109). Monocytes/macrophages are most likely a significant source of NOX2-derived superoxide in atherosclerotic lesions, and NOX2-derived ROS has been shown to promote atherogenesis through provoking LDL oxidation (110), monocyte adhesion and proliferation (111-113). Thus, the regulatory pathways of NOX2 in monocytes are potential therapeutic targets for controlling atherosclerosis.

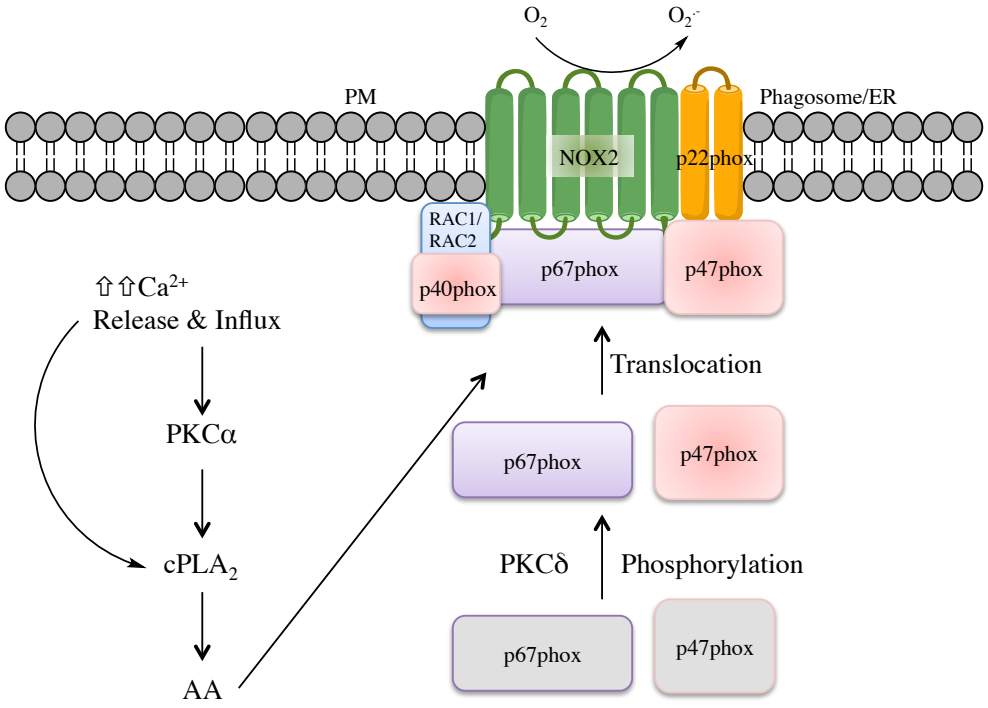


**Figure 1-4. The activation mechanism and regulation pathways of NOX2 in monocytes.** Activation of NOX2 depends on the binding of its organizer protein (p47phox and Rac), the activator protein (p67phox), and p40phox. The translocation of p47phox and p67phox from cytosol to membrane for NOX2 activation requires their phosphorylation by protein kinase Cδ (PKCδ). The increase of intracellular Ca2+ level also induces the activation of

PKCα and cytosolic phospholipase $A_2$ ($cPLA_2$), which produce arachidonic acid (AA) for NOX2 activation in monocytes.

Another important contributor to the development of atherosclerosis and atherothrombosis are platelets. A variety of stimuli activate NOX in platelets, and the NOX-derived ROS in turn promote platelet activation (47, 114-116). Platelets appear to only express NOX2, based on Western blots of p47phox, p67phox, p22phox and gp91phox (117-119). However, these findings do not exclude the presence of other NOX isoforms, since only incomplete suppression of platelet $O_2^-$ production was observed with a specific NOX2 inhibitor (120). NOX2-derived $O_2^-$ affects platelet activation by interfering with NO activity (121), $cPLA_2$-dependent arachidonic acid (AA) release from the membrane (122), and the downstream formation of F2-isoprostane (123, 124). NOX2-derived $O_2^-$ also acts as a secondary messenger to elicit the formation of $H_2O_2$, which induces calcium mobilization, AA and $TxA_2$ production, and phospholipase C (PLC) up-regulation (125). Inhibition of platelet aggregation by NOX2 inhibitors is associated with down-regulation of integrin $\alpha_{IIb}\beta_3$ activation, a central response in platelet aggregation, indicating that integrin $\alpha_{IIb}\beta_3$ may be the receptor through which $H_2O_2$ and $O_2^-$ affect platelets (126).

The beneficial effects of statin therapy, a common intervention strategy for lowering cholesterol, have been partially attributed to the indirect inhibition of NOX by statin through Rac isoprenylation (127). The NOX-derived ROS are, therefore, compelling targets for the prevention and treatment of atherosclerosis. However, our understanding is limited in the redox regulation of platelet-monocyte interaction and platelet activation in contact with atherosclerosis.

Clearly, a systems-level functional analysis involving redox regulation, platelets, and monocytes would help identify possible pathways to potentially facilitate drug development.

## 1.3 System biology and the "omics" era

With the first draft of the sequenced human genome introduced in 2000, systems biology, a new way of exploring human health, became available (128, 129). Systems biology consists of "omics" techniques and bioinformatics to provide information on the global state of biological systems (130). "Omics" approaches make it possible to comprehensively analyze DNA (genomics), mRNA (transcriptomics), proteins (proteomics), and metabolites (metabolomics) using large-scale, high throughput techniques (131). Bioinformatics focuses on integrating, interpreting, and translating the information collected through omics approaches into an understandable format (132).

### 1.3.1 Mass spectrometry and proteomics

The sequenced human genome reveals which protein sequences are coded. However, the protein environment is much more complicated than simple sequence information, e.g. post-translational modifications (PTMs), splicing variants, tertiary structure, formation of complexes and ligand interactions. These intricate networks determine how biological functions occur, and understanding of them requires information beyond genome, which forms the basis of proteomics (133). Proteomics is the study of protein in cells or tissues under certain conditions, and aims to understand the biological activities that are happening in the complex environment on the protein level (134). For different fields of "omics" techniques, proteomics has experienced

novel technical advances in the past decade due to the rapid development of mass spectrometry (MS).

MS is an analytical technology that characterizes individual molecules by converting them into gas-phase ions and manipulating them in electric and magnetic fields. Samples are converted to gas-phase ions by adding or removing charged particles in an ion source. The gas-phase ions are then separated in a mass analyzer on the basis of their mass-to-charge ratio (m/z). A detector records the mass spectrum that delineates a statistical representation of the type and abundance of each ion in a complex mixture.

The two major ionization techniques utilized in mass spectrometry-based proteomics, which enable MS analysis of intact biological macromolecules, are electrospray ionization (ESI) (135) and matrix-assisted laser desorption/ionization (MALDI) (136, 137). ESI liberates ions out of a solution, and is readily coupled online with liquid chromatography for separation before MS analysis. Hence, ESI is commonly applied to complex peptide/protein samples (138). Distinct from ESI, MALDI volatizes ions out of a crystalline matrix via a focused laser beam. MALDI-MS is, therefore, preferred for the analysis of relatively simple peptide mixtures, and has higher tolerance of the presence of salts and detergents (139).

Four basic types of mass analyzers are currently used in proteomics research: ion trap, time-of-flight (TOF), quadrupole, and Fourier Transform ion cyclotron resonance (FT-ICR). These mass analyzers are very different in their strengths and weaknesses, and can be used alone, or put together in sequence as a tandem mass spectrometer (hybrid instrument) to take advantage of the

beneficial effects of each mass analyzer (140). For instance, LTQ-FTICR consists of a linear ion trap (LTQ) and a FTICR. A linear ion trap captures ions in a two-dimensional radio frequency (RF) field. With high sensitivity and fast in peptide sequencing, LTQ is able to study post-translational modifications (PTMs) but has lower mass accuracy (141). FT-ICR traps ions under vacuum in a high magnetic field, and acquire mass spectra based on Fourier Transformation of image current of trapped ions. FT-ICR is able to provide high sensitivity, mass accuracy, resolution, and dynamic range (142). The combination of LTQ with FTICR allows analysis of PTMs with ultra-high resolution and sensitivity with sub ppm mass accuracy (143). The principle of fourier transformation is also applied in Orbitrap MS, but without the use of a static magnetic field. The recently introduced Orbitrap instrument provides similar accuracy and resolution to FT-ICR at relatively high speed, and in most cases is coupled with other MS analyzers, such as LTQ (144). Another example is quadrupole/time-of-flight (QqTOF), where Q refers to a mass-resolving quadrupole, and q refers to an RF-only quadrupole collision cell. TOF has the advantages of simplicity, excellent mass accuracy, and comparability with different ion sources (145).The QqTOF enable high mass accuracy and sensitivity with ESI for high-throughput proteomic analysis (146).

### 1.3.2 Peptide sequencing by MS/MS: bottom up proteomics

MS-based proteomics can be categorized into two broad approaches, top-down and bottom-up, based on the size of the analyte that enter the mass spectrometer. The “top-down” proteomic analysis provides an effective methodology for analyzing modifications on large peptides and intact proteins (147). Under rapid development, the mass range of intact proteins analyzed in top-down proteomics has been extended to more than 200 kDa, with more and more intact proteins

being detected in a single analysis (148). The more widely used "bottom-up" proteomics analyzes proteolytically digested samples with peptides of 25 amino acids or less (149), and is the main method utilized in this thesis. The advantages of bottom-up proteomics is the determination of the peptide amino acid sequence, and the types and sites of post-translational modification (PTM) via tandem mass spectrometry (MS/MS) (150). Tandem mass spectrometry is comprised of two mass analyzers connected by a fragmentation cell. The first mass analyzer, MS1, selects an ion from an ion source. The selected precursor ion then undergoes fragmentation in the collision cell through several different methods: collision-induced dissociation (CID), electron capture dissociation (ECD), and electron transfer dissociation (ETD). The resulting daughter ions are separated in the second mass analyzer, MS2, and the mass spectra are recorded by a detector. Under CID conditions, the charged peptide precursor ions collide with a target neutral gas (He, $N_2$, or Ar), and the ion translational energy can partially transfers to the ion internal energy. The collision results in ion dissociation occurring primarily at the amide bounds to generate a-, b-, and y- type fragment ions, or losses of small neutral molecules, e.g. water, ammonia, or other fragments derived from side chains of amino acids. CID can be performed in two different energy regimes. Low-energy CID is conduced in most instruments, in which the selected precursor ions undergo multiple collisions with a target gas molecule. In a TOF-TOF instrument, high-energy CID can be performed using single kilo electron-volts collisions with He to provide more informative and thus complex tandem mass spectra. CID is currently the most prevalently applied fragmentation method for proteomic analysis. However, CID is more effective for small, low-charged peptides and stable modifications, but not for the intact proteins and peptides with labile PTMs, like phosphorylation (151).

Complementary to CID, ECD and ETD allow the direct introduction of low energy electrons to or the transfer of electrons between the gas-phase peptide/protein ions. They primarily lead to the cleavage of N-C α-bonds to give rise to c- and z-type fragment ions (152). The advantages of these approaches are the potential application in intact protein ions and PTM characterization. ECD is preferred when dealing with phosphorylation, N- and O-glycosylation, and sulfation, as it is able to efficiently break down the peptide backbone while leaving the modification intact (153). ETD can fragment intact proteins in the top-down strategy, and perform better than CID on highly-charged peptides (154).

Computational approaches are essential to fully decipher the enormous amount of data generated by mass spectrometers. To identify a peptide/protein, the theoretical MS data of a peptide/protein predicted from genomic database *in silico* is compared with experimental data using search algorithms. The most widely used databases are Entrez Protein, Reference Sequence (RefSeq), Swiss-Prot, GPMDB, and International Protein Index (IPI). A number of database search algorithms have been described in the literature, including SEQUEST (155), MASCOT (156), ProteinProspector (157), TANDEM (158), and OMSSA (159). These search engines have scoring functions that measure the degree of similarity between experimental spectra and the theoretical spectra. The matching score is used to establish false discovery rate (FDR) to statistically validate the identification result and reduce false positives.

### 1.3.3 Quantitative proteomics

In a mass spectrometer, the signal intensity of a particular molecule is only a relative measurement to its quantitation due to the variance in ionization, transmission and detection

efficiency of different molecules. In order to quantitatively measure a protein/peptide in a mixture, a lot of effort has been put into the field, and the state-of-the-art methods are reviewed thoroughly and engagingly elsewhere (160, 161). Despite methods for label-free quantitative proteomics still being an active area of research, metabolic- and chemical-labeling based quantitative proteomics are widely applied in human health research to study drug effects, biomarkers of disease, and pathways involved in disease processes. The core of the majority of the quantitative proteomic techniques is the differential stable isotope labeling, which generate chemically identical peptides/proteins but with mass difference to quantify small differences between two or more states of a biological system.

#### 1.3.3.1 Metabolic incorporation of stable isotopes

Stable isotope labeling by amino acids in cell culture (SILAC) was first introduced in 2002 (162), and by far is the most accurate proteomic quantitation method. In general, cells are grown in media containing $^{13}C/^{15}N$-labeled arginine or lysine, treated with agents, and then mixed with those untreated cells grown in normal media. Proteins and peptides are extracted from the cell lysate, and subjected to MS analysis. (163). In MS analysis, the peptides will be separated from a column, and ionized with identical efficiency. To ensure every digested peptide has at least one heavy-labeled arginine or lysine, trypsin is the most commonly used protease to digest proteins, as it specifically cleaves the amine bonds next to the carbonyl group of either an arginine or a lysine residue. The peak area of the two chemically identical co-eluting peptides can then be directly compared to obtain their relative abundance (164).

The accuracy of SILAC is mostly due to the ability to introduce the mass differences of the same protein at the intact cell level, thus minimizing errors involved in sample preparation (162). Different forms of isotopically-labeled arginine and/or lysine give rise to as many as eight conditions to be performed in a single experiment (165). In spite of these strengths, SILAC is limited to cultured cells, but not comparable to analyze human primary cells that cannot be cultured *in vitro*. Although SILAC labeled mice have been successfully developed (166), it is very expensive and time consuming for most research projects, and still not applicable to human samples. An alternative method, named super-SILAC, has been explored recently (167). It uses a mix of multiple SILAC-labeled cells to provide a physical proteome database as an internal standard to compare with light isotope-labeled human tissue for quantitation.

#### 1.3.3.2 Chemical tagging approaches

Chemical labeling methods quantitate the relative concentration of peptides or proteins through an isotope-coded mass tags attaching to cysteines, amine groups or carboxylic groups. The first chemical labeling method isotope-coded affinity tag (ICAT) was introduced in 1999, using a mass tag containing eight hydrogen or deuterium to label cysteine residue (168). The labeled peptides were then enriched using avidin chromatography against the biotin moiety in the tag, and subsequently analyzed by MS. One limitation with ICAT is that it depends on the modification of cysteine residues, which is a less common amino acid accounting for only 1.42% of all amino acids in a sample (169). A large number of peptides and even some proteins, which do not carry cysteine residues, can therefore not be quantitated by ICAT.

An alternative to ICAT was the isobaric tags for relative and absolute quantitation (iTRAQ) label developed in 2004 (Applied Biosystems; http://www.appliedbiosystems.com) (170). An iTRAQ reagent consists of an isotope-coded reporter group, a peptide-reactive group, and an isotope-labeled balancing group to give the same total mass when all three groups are combined. The isobaric tags are attached to a peptide through the reaction between the peptide-reactive group and primary amines on lysine side chains or the N-terminal of peptides. Peptides from samples under different conditions are labeled with different isobaric tags, and mixed together for MS/MS analysis. During the fragmentation of the labeled peptides in MS/MS analysis, the tags form a marker ion from the reporter group, each of which will be specific and highly sensitive for each condition to be compared (171). With eight tags commercially available, iTRAQ is suitable to analyze the proteome of human cells or tissues that cannot not be cultured.

Another recently introduced chemical labeling technique is the tandem mass tag (TMT) strategy by Thermo Scientific (172). TMT utilize similar principle of iTRAQ, with up to 10 different tandem mass tags. A set of six iodoTMT reagents was also developed to label cysteine residues (173).

The disadvantage associated with chemical tagging approaches is the risk of introducing systematic errors during sample preparation, as quantitative labeling and the combination of differential labeled samples occurs late in the workflow.

### 1.3.4 Post-translational modifications

#### 1.3.4.1 Post-translational modification - functional modifications on proteins

Post-translational modifications (PTMs), the modifications on proteins after their translation, profoundly affect various aspects of a protein, including protein structure, solubility, activity, location in the cells, and binding to interaction partners. Of the twenty amino acids, cysteine is one of the most susceptible residues for PTMs, such as oxidation and disulfide formation in protein folding. All the PTMs on cysteine are due to the change of the oxidation state of the thiol group on the side chain, and reflect the redox state of a cell. The analysis of PTMs on cysteine therefore allows the understanding of the cellular oxidation state as well as redox regulations.

#### 1.3.4.2 Cysteine oxidation modifications: a major modulator of cell signaling by ROS

Cysteine residues in proteins can be divided in four categories: 1) permanent structural disulfide bonds which are typically observed in oxidizing environments; 2) thiols that coordinate with metals, typically Fe, Zn or Cu; 3) those that are maintained in the reduced state; and 4) those that are susceptible to reversible and irreversible oxidation (174).

The reactivity of cysteine thiol group is determined by protein microenvironments that enable thiolate formation at neutral pH through reducing its pKa (Figure 1-5). Oxidation of cysteine thiol group by hydrogen peroxide yields sulfenic acid modification (R-SOH), also known as sulfenylation, as a reversible, labile moiety with a mass shift of + 16 Da. As the first PTM generated by oxidation of a thiolate, sulfenic acid can be stabilized within certain protein microenvironment (175), but is also vulnerable to be further irreversibly oxidized to sulfinic acid ($R\text{-}SO_2H$) and sulfonic acid ($R\text{-}SO_3H$) with mass shifts of + 32 and + 48 Da, respectively.

Sulfenic acid can also react with a neighboring amide nitrogen to form the stabilized cyclic 5-membrane ring structure sulfenamide, characterized by a mass shift of 31 Da (176). Besides ROS, RNS react with cysteine to form *S*-nitrosylation (R-SNO), which is a chemical intermediate. Although found in low abundance, *S*-nitrosylation has been shown to be involved in a variety of dynamic redox-signaling/regulation events, and implicated in cardioprotection by several studies (177-179). A leading hypothesis for its protective effect is that reversible *S*-nitrosylation modification protects critical cysteines from subsequent irreversible oxidation (178, 179). Another type of PTM on cysteines is the disulfide derivatives formed with another protein cysteine (R-S-S-R', as an intramolecular or intermolecular interaction), or with a small molecular thiol like glutathione (R-SS-G) or cysteine. The disulfide bond has been initially regarded as a static structural feature that occurs during protein folding in the oxidizing environment of the endoplasmic reticulum, and is preserved throughout the lifetime of the protein. Nowadays, more and more disulfides have been found to be dynamically interchangeable in the cellular redox environment to alter protein conformation, association, and function (180). The mixed disulfide bond formed between protein thiol and GSH, termed as *S*-glutathionylation, has now been recognized as another potential modulator of redox-sensitive proteins in signal transduction. Similar to *S*-nitrosylation, *S*-glutathionylation has also been proposed to function as a temporary thiol cap to protect critical cysteines from potentially irreversible oxidative modifications (181). The branch of proteomics that analyze oxidatively modified proteins, particularly oxidative modifications of cysteine, is named redox proteomics.

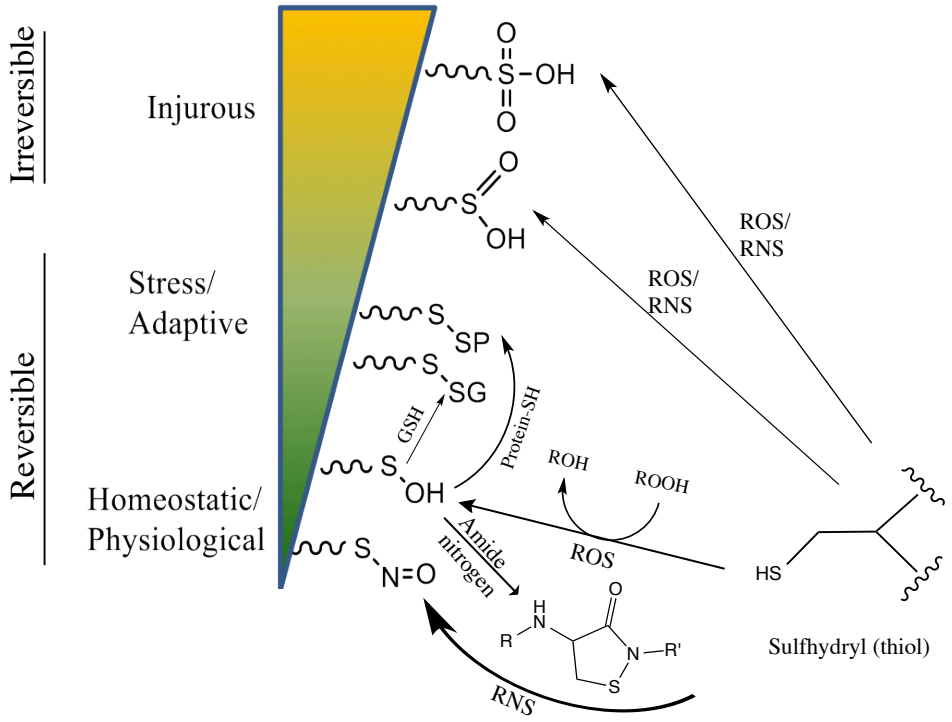


**Figure 1-5. Schematic overview of various oxidative modifications on cysteines.** The thiol group on cysteine can be oxidized into different modifications, which range from protective, reversible modifications: S-nitrosylation (-S-NO), sulfenic acid (-S-OH), S-glutathionylation (-S-SG), sulfenamide, disulfide (-S-SP), to detrimental, irreversible modifications: sulfinic acid (-S-$O_2$H), sulfonic acid (-S-$O_3$H).

### 1.3.5 Mass spectrometry-based redox proteomics analysis of cysteine oxidation

In order to study the *S*-nitrosylation, Jaffrey *et al* introduced the biotin switch method in 2001, which enabled the enrichment and detection of *S*-nitrosylation in complex biological samples (182). Since then, several variations of the biotin switch assay have been developed and expanded it to other reversible cysteine modifications. By switching the modification of interest to a biotin moiety, these assays leverage the high affinity between biotin and avidin ($K_d = 10^{-15}$ M) to enrich the modification (Figure 1-6). For all modified biotin switch assays, the logic of the

strategy is the same. Briefly, free thiols are blocked with different cysteine alkylation reagents. Cysteine modifications of interest are then reduced with selected reducing reagents, and labeled with a thiol-reactive biotin. Once the modified sites are labeled with the stable biotin group, they can easily be enriched by avidin beads and analyzed by MS to determine their positions in corresponding proteins (Figure 1-7).

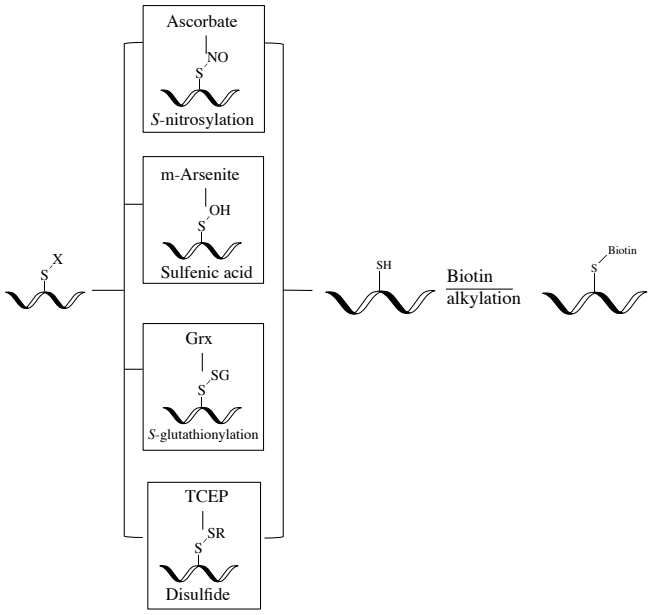


**Figure 1-6. Schematic diagram of the biotin switch method.** Different reversible cysteine oxidative modifications (-S-X) are selectively reduced by their corresponding reducing agents to free thiols (-SH). The newly released free thiols are then alkylated with biotin agent (-S-Biotin).

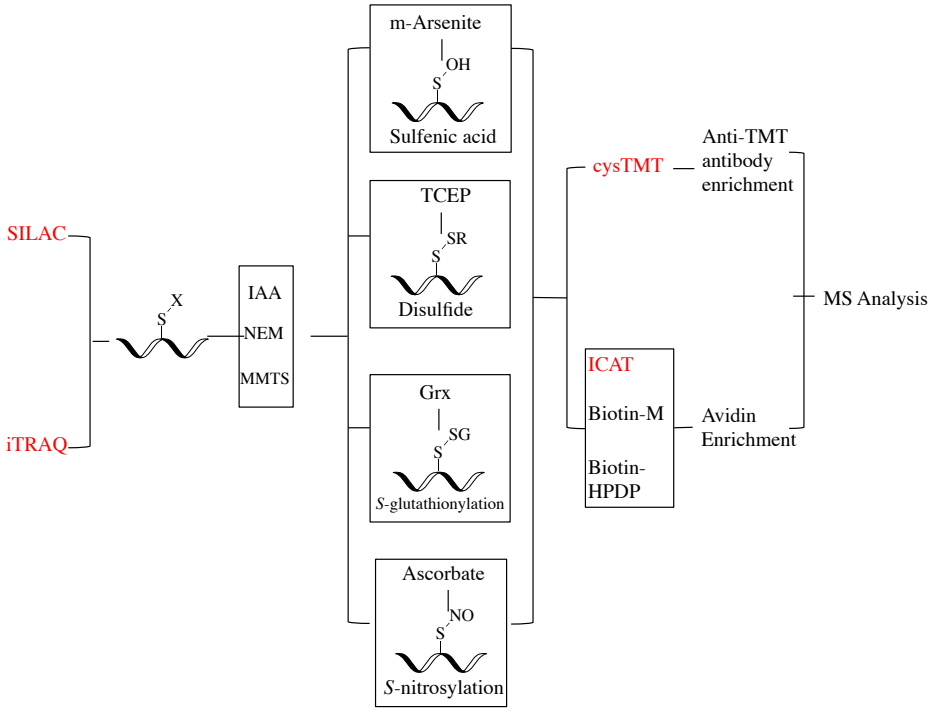


**Figure 1-7. General workflow for mass spectrometry-based quantification of reversible cysteine oxidative modifications.** The various options and developments are available for detection, identification, and site mapping of proteins with reversible cysteine oxidative modifications. Steps in the protocol can be customized depending on the target modification and goals of the investigation. iTRAQ, isobaric tags for relative and absolute quantitation; SILAC, stable labeling by amino acids in cell culture; MMTS, S-methyl methanethiosulfonate; NEM, N-ethylmaleimide; IAA, iodoacetamide; TCEP, tris(2-carboxyethyl)phosphine;Grx, glutaredoxin; Biotin-HPDP, N-[6-(Biotinamido)hexyl]3'-(2'pyridyldithio) propionamide: Biotin-M, N-Biotinoyl-N′-(6-maleimidohexanoyl)hydrazide; ICAT, isotope coded affinity tag; and cysTMT, cysteine-reactive tandem mass tag.

In order to target sulfenic acid modification, the Eaton group has developed a biotin switch assay utilizing m-arsenite to selectively reduce the sulfenic acid modification (183). However, this approach has not been widely adopted due to the uncertainty of arsenite selectivity. Besides arsenite, a widely applied strategy for identification of sulfenic acid modification uses dimedone

as a specific targeting reagent (184). Dimedone-based probes take advantage of the highly selective condensation reaction between sulfenic acid and dimedone (1,3-diketone), therefore, eliminating blocking and reducing steps (185). Once labeled, the biotin group conjugated with dimedone, or the azide group with a click reaction to add a biotin group, can be used for enrichment and detection.

Different from the previous two labile modifications, *S*-glutathionylation is a relative stable modification with a unique mass shift of 305 Da, making direct MS analysis possible. However, even though it is relatively stable, enrichment procedures are still necessary for *S*-glutathionylation due to its low abundance. Until now, three different enrichment strategies have been developed. The modified biotin switch assay employs glutaredoxin (Grx) to enzymatically reduce *S*-glutathionylation, and make it available for biotin labeling and avidin enrichment and detection (186). The second way is still based on the biotin-avidin interaction, but applies a biotin-labeled GSH ester, a cell-permeable ester, to capture *S*-glutathionylation directly (187). The third potential option is an antibody-based immuno-assay for *S*-glutathionylation detection and enrichment (188). As developed against a GSH epitope, the antibody has only been tested on an individual protein (189).

Regulatory disulfide identification currently favors site-directed determination of particular Cys residues. To achieve an unbiased assessment of the disulfide proteome, enrichment techniques have been widely used. For example, the biotin switch assay can be adapted for disulfide identification through the reduction of disulfide with tris(2-carboxyethyl)phosphine or dithiothreitol to release the disulfide-bonded Cys. After reduction, the uncovered cysteine

residues can be either labeled with biotin and captured by avidin, or directly captured by activated thiol sepharose (190). Another commercially available approach is to use the ICAT reagent to quantitatively analyze disulfide formation in response to oxidative stress (191).

In addition to detection and mapping of the sites of different modifications on cysteine residues, another important aspect of redox proteomics is to measure the extent of a given cysteine modification, which can be achieved through quantitative proteomic methods such as ICAT, iTRAQ, and SILAC. All these quantitative proteomic methods can be coupled with various biotin switch assays. The newly developed cysteine-reactive TMT (iodoTMT) is an alternative option for quantitation. The iodoTMT has six isotopic versions that release different reporter ions (126~131 Da) during fragmentation, allowing comparing the extent of modification of each cysteine across samples (173). The iodoTMT-labeled peptides can be reversibly captured by an immunoaffinity resin, or combined with biotin switch assay for the enrichment.

ROS is actively involved in the progress of atherosclerosis on many aspects, particularly in platelet activation and platelet-monocyte interaction through cysteine oxidation. However, the reversible cysteine oxidation modifications and their effect on cell behaviors are not well established in platelet-monocyte interaction and platelet activation. A variety of technologies are now available in redox proteomics, which allow us to develop a versatile proteomic method to study the redox regulation in these processes.

## 1.4 Aims

Based on the current evidence and knowledge, we hypothesize that platelet releasate can induce the production of ROS and cysteine oxidation in monocytes, and redox regulation is actively involved in platelet-monocyte interaction and platelet activation. Consequently, there is an urgent need to develop quantitative redox proteomic tools to analyze redox regulation in monocytes and platelets in the context of atherosclerosis.

The first aim of this thesis was to establish redox states in monocytes treated with platelet releasate. To achieve this, we decided to employ flow cytometry to investigate the intracellular ROS level. To quantify the total reversible cysteine oxidations in monocytes, we chose to develop a modified biotin switch assay and apply it to an atherosclerotic model (chapter 2).

As our second aim, we wanted to extend our understanding of redox regulation in platelet-monocyte interaction by focusing on an individual cysteine oxiation. To this purpose, we decided to further modify the biotin switch assay to selectively quantify sulfenic acid modification in monocytes treated with platelet releasate (chapter 3).

In the third and final aim, we sought to establish the involvement of ROS in platelet function, and identify the differences of platelet behavior in hemostasis and atherothrombosis. We opted for the analysis of the effects of different stimuli on platelet activation via ROS production using platelet functional assays as a prerequisite of future redox proteomics studies (chapter 4).

# Chapter 2: Identification of Total Reversible Cysteine Oxidation in an Atherosclerosis Model Using a Modified Biotin Switch Assay

## 2.1 Introduction

According to the World Health Organization, cardiovascular diseases (CVDs) are the leading cause of death worldwide, accounting for 17.5 million deaths in 2012 and representing 31% of all global deaths (1). The complication of atherosclerosis, a chronic inflammatory disease, results in the majority of CVDs (2). Clinical studies have shown that direct binding between activated platelets and monocytes promotes recruitment of the latter to the inflamed vascular endothelium, which is critical to the development of atherosclerosis (192, 193). In addition, the degranulation of activated platelets releases soluble molecules and microparticles, which are termed platelet releasate (194). Chemokines and cytokines that are present in platelet releasates, e.g., RANTES or platelet factor 4, have been shown to promote monocyte survival and LDL uptake and induce monocyte differentiation (195, 196). In contrast to direct binding, which results in the formation of platelet-monocyte aggregates, the concerted impact of platelet releasates on monocytes (particularly those induced by platelet agonists in the atherosclerotic environment such as lysophosphatidic acid (LPA), a bioactive phospholipid) is largely unknown.

Studies have correlated oxidative stress and the consequent oxidative modification of lipids and proteins in vascular walls with atherosclerosis (197-199). For example, the oxidation of low density lipoproteins (LDL) by reactive oxygen species (ROS) can generate LPA, which accumulates at a high concentration in atherosclerotic plaques (200). In redox signaling pathways, the oxidative modification of proteins is linked to ROS via the sequential reversible or

irreversible oxidation of cysteine (Cys) (201-203). Upon reaction with ROS, cysteine residues can be reversibly modified into undergoing *S*-nitrosylation, *S*-glutathionylation, and sulfenic acid or disulfide bond formation (204). These protein modifications have been identified in human atherosclerotic plaques and implicated in promoting LDL oxidation and lesion formation *in vivo* (205, 206). However, the mechanism of the oxidative signaling from activated platelets to monocytes, especially through platelet releasate, has not yet been well characterized. Thus the establishment of an assay to monitor the cysteine oxidation within this process becomes paramount.

For the study of reversible cysteine oxidation ($Cys_{OX}$), several methods have been developed (204, 207). Among them is the biotin switch method described by Jaffrey and Snyder in 2001, which has been widely used in mass spectrometry analysis (182). Numerous studies have employed selective reducing reagents, such as ascorbic acid and arsenite, to identify specific forms of reversible $Cys_{OX}$, *e.g., S*-nitrosylation or sulfenic acid (182, 183, 208). However, most of these studies did not quantify the extent of the cysteine modification. Assessing the reversible redox states of specific $Cys_{OX}$ modifications may not reflect the global cellular redox status of protein thiols. To address these issues, we modified the biotin switch assay by utilizing tris(2-carboxyethyl) phosphine (TCEP) to analyze all reversible forms of $Cys_{OX}$ by combining it with the stable isotope labeling by amino acids in cell culture (SILAC) technique for quantitation (209).

In this study, the modified biotin switch assay was applied to THP-1 monocytic cells, a model system used to quantify $Cys_{OX}$ change in monocytes that are in contact with platelet releasate.

THP-1, a human monocytic leukemia cell line, has been successfully used to study monocyte function and is amenable to SILAC labeling (210). We stimulated platelets from healthy donors with different stimuli (LPA and thrombin) and collected platelet releasate to use for incubating THP-1 cells. Through applying the modified biotin switch assay, we were able to quantify the reversible $Cys_{OX}$ in THP-1 cells upon platelet releasate stimulation. In addition, the intercellular ROS level was also monitored in THP-1 cells and human primary monocytes in response to platelet releasate.

## 2.2 Methods

### 2.2.1 Chemicals and reagents

N-Ethylmaleimide (NEM), DL-dithiothreitol (DTT), iodoacetamide (IAA), 2', 7'-dichlorodihydrofluorescein diacetate ($H_2$DCFDA), thrombin and 4-(2-aminoethyl)-benzenesulfonyl fluoride hydrochloride (AEBSF) from human plasma, α-glycerophosphate dehydrogenase, DL-glyceraldehyde 3-phosphate, β-NAD, and NADH were obtained from Sigma (ON, Canada); EZ-Link Biotin-HPDP, NeutrAvidin agarose resins, and TCEP·HCl from Pierce, diphenyleneiodonium chloride (DPI) from Cayman Chemical, 2-acetylphenothiazine (ML171) from Tocris bioscience (ON, Canada), alkyl-LPA (16:0) from Avanti Polar Lipids (AL, USA), and sequencing grade modified trypsin from Promega (WI, USA).

### 2.2.2 Cell culture

Human THP-1 monocytic cells (American Type Culture Collection, MD, USA) were cultured in RPMI-1640 medium (Gibco, Life Technologies, Canada) supplemented with 10% FBS and 1% penicillin/streptomycin. Cells were maintained at 37°C in 5% $CO_2$ and 95% humidity. For all

experiments, only cells less than two months old were used. The SILAC labeling was performed as described previously (209). Briefly, lysine- and arginine-free RPMI medium (Caisson Labs, UT, USA) was supplemented with 2 mM L-glutamine, 10% dialyzed FBS (Invitrogen Corporation, CA, USA), 1% penicillin/streptomycin, heavy isotope Lys4 (L-[$^{2}H_{4}$]lysine), Arg6 (L-[$^{13}C_{6}$]arginine), or light isotope (the normal lysine and arginine) (Cambridge Isotope Labs, MA, USA). Heavy isotopes were incorporated into THP-1 cells for two weeks before use. During incorporation, the THP-1 cells were maintained at $0.5 \times 10^{6}$ /mL of medium, which was changed every two to three days.

### 2.2.3 Ethics statement of blood donation and platelet releasate preparation

Ethical approval for the platelet and primary monocyte isolation from healthy volunteers was granted by the University of British Columbia Research Ethics Board (certificate number H12-00757). Platelets were isolated as described previously (211). Briefly, platelet-rich plasma (PRP) was isolated from whole blood that was anticoagulated with 15% acid citrate dextrose (ACD) following centrifugation at 150 relative centrifugal force (rcf) for 15 minutes at room temperature. The PRP was then centrifuged at 720 rcf for 10 minutes with half volume ACD buffer supplemented. Finally, pelleted platelets were washed twice in CGSA buffer (10 mM trisodium citrate, 30 mM dextrose, 1 U/mL apyrase) by centrifugation at 720 rcf for 10 minutes and suspended at physiological concentration ($200 – 350 \times 10^{9}$ /L) in RPMI medium. Platelet numbers were determined by counting with a hemocytometer.

After isolation, platelets were allowed to rest for 30 minutes then activated with either LPA (20 μM) or thrombin (1 U/mL) for 10 minutes at 37 °C(48). The platelets were then separated from

releasate by centrifugation (750 rcf at 4 °C). The supernatant was subjected to centrifugation again and the resulting supernatant was collected as platelet releasates.

### 2.2.4 Primary monocyte isolation and labeling

Peripheral blood mononuclear cells (PBMCs) were isolated from whole blood by density gradient centrifugation over Ficoll-Paque (GE Healthcare, Canada) according to the manufacturer's protocol. Cells were then washed in HBSS (Gibco, Life Technologies, Canada) and resuspended in RoboSep® buffer (StemCell Technologies, Canada) at a density of $1 \times 10^7$/mL. Human primary monocytes were isolated from PBMCs by negative selection using the EasySep™ Human Monocyte Enrichment Kit without CD16 depletion (StemCell Technologies, Canada) according to the manufacturer's instructions. After being washed with RoboSep® buffer, the monocytes were resuspended in RPMI1640 at a density of $5 \times 10^5$/mL, labeled with Pacific blue antihuman CD14 and APC antihuman CD16 antibodies, and subjected to platelet releasate treatments.

### 2.2.5 Fluorescence-activated cell sorting (FACS) analysis

For the FACS method development, THP-1 cells were incubated with 100 μM / 1 mM $H_2O_2$ for one or six hours. For the FACS method application, THP-1 cells or primary monocytes ($CD14^+/CD16^+$) were treated with 10 μM alkyl-LPA (LPA), 0.5 U/mL thrombin or releasate from LPA (LPA-PR) / thrombin (Thr-PR) for 1, 6 or 24 h. After incubation, THP-1 cells were washed twice with cold PBS and then treated with 1 μM 2', 7'-dichlorodihydrofluorescein diacetate for 20 minutes (212). The mean fluorescence intensity of the intracellular ROS level was quantified on a BD LSR II flow cytometer (BD™ Bioscience, Canada).

For NOX inhibitor experiments, the THP-1 cells or primary monocytes ($CD14^+/CD16^+$) were treated with 10 μM DPI, 10 μM ML171 or 10 μM AEBSF for one hour to block NOX; DMSO was used as vehicle control. After incubation, the cells were washed with PBS to remove inhibitors or DMSO and then treated with platelet releasate for six hours. Finally, the intracellular ROS level in the THP-1 cells or monocytes were measured by FACS as described above.

### 2.2.6 Modified biotin switch assay

We developed a method to quantify $Cys_{OX}$ by combining SILAC with a modified biotin switch assay. After two weeks of incorporation in cell culture with SILAC medium, heavy-isotope-labeled THP-1 cells were treated with either 100 μM $H_2O_2$ or platelet releasate from LPA or thrombin for six hours and light-isotope-labeled THP-1 cells were used as control. The heavy- and light-SILAC-labeled THP-1 cells were then mixed in a 1:1 ratio and lysed with RIPA buffer (25 mM Tris•HCl pH 7.6, 150 mM NaCl, 1% NP-40, 1% sodium deoxycholate, and 0.1% SDS) in the presence of protease inhibitors.

On the basis of the original protocols (182), we modified the biotin switch assay as follows. In a first step starting with 2 mg protein, free thiols were blocked with NEM (12 mM) for one hour, and the extra NEM was reacted with excess L-cysteine (48 mM) for one hour. Following that all the reversible cysteine oxidations (including disulfide, S-nitrosothiols, and sulfenic acid) were reduced with TCEP (3 mM), and the extra reducing reagent was removed by methanol-chloroform precipitation. The precipitated protein pellet was then dissolved in 8 M urea and the

newly released free thiols were labeled with biotin-HPDP (1.2 mM), followed by another methanol chloroform precipitation to remove excess biotin-HPDP. Urea (8 M) was used to dissolve the protein pellet and diluted to less than 1 M before undergoing trypsin digestion overnight at 37 °C. After digestion, the peptide mixture was first incubated with sepharose 6B beads for one hour and then NeutrAvidin agarose resins (1 mL) for 1.5 h. The NeutrAvidin-bound peptides were then eluted with DTT (10 mM) and alkylated with IAA (31 mM). The purified Cys-containing peptides were fractionated by anion exchange tip (213) into six fractions and then desalted with a solid phase extraction on C18 stage tips (214). Purified peptides were analyzed using a linear ion trap – FT-ICR cell (LTQ-FT, Thermo Fisher Scientific, USA) mass spectrometer, online coupled to an Agilent 1100 Series nanoflow HPLC using a nanospray ionization source (Proxeon Biosystems) and holding columns packed into 15 cm long, 75 μm ID fused silica emitters (8 μm diameter opening, pulled on a P-2000 laser puller from Sutter Instruments) using 3 μm diameter Reprosil-Pur C-18-AQ beads (Dr. Maisch, Germany, www.Dr-Maisch.com). Buffer A consisted of 0.5% aqueous acetic acid, and buffer B consisted of 0.5% acetic acid and 80% acetonitrile in water. Gradients were run from 6 to 30% B over 75 minutes (with a flow rate of 0.2 μL/minute), then from 30 to 80% B in the next 20 minutes, held at 80% B for 8 minutes (while increasing the flow rate from 0.2 to 0.6 μL/minute), and then dropped to 6% B to recondition the column. The LTQ-FT was set to acquire a full-range scan at 25000 resolution from 350 to 1500 Th in the FTICR cell, and the scan was followed by the MS/MS of the top 5 ions in the LTQ (minimum intensity: 500 counts). The mass window for the precursor ion selection was 1.0, and the normalized collision energy was 35. The selected ions were then excluded from MS/MS for the next 180 sec. Singly charged ions were excluded.

For inhibitor experiments, heavy-isotope-labeled THP-1 cells were incubated with DPI, and light-isotope-labeled THP-1 cells were treated with DMSO as the vehicle control for one hour. After that, 6-hour incubation with LPA-induced platelet releasate was performed, and the $Cys_{OX}$ containing peptides were enriched by the modified biotin switch assay as described above.

### 2.2.7 Database Search, quantification and bioinformatics analysis

The identification of peptides from THP-1 cell lysates was performed by searching each MS raw file against the human Swiss-Prot database (version: May 30th, 2013; 540261 sequences; 191876607 residues) using Mascot Distiller (version 2.4.3.3). The following search criteria were used: Lys + 4, Arg + 6 in quantitation; *homo sapiens* (20258 sequences) in taxonomy; trypsin/P for digestion and cleavage specificity with up to two missed cleavage sites; no fixed modifications; variable modifications of carbamidomethyl, NEM-modified cysteines, and oxidized methionines; ± 20 ppm peptide tolerance; ± 0.6 Da MS/MS tolerance; ESI-TRAP as instrument type. For peptide scoring, the significance threshold was 0.01. The cutoff score that we used for peptide identification was > 23 ($p < 0.05$). The quantification of peptides in Mascot Distiller was performed with the following parameters: the extracted ion chromatogram (XIC) threshold was set to 0.1, XIC smooth to 3, and maximum XIC width to 250. The correlation score, a quantification quality parameter, was set to 0.7. The median of the heavy/light isotope ratio (H/L) of the peptide in the data set was used as the normalization factor. The percentage of $Cys_{OX}$ was calculated using H/L in an equation: percent of $Cys_{OX} = 1 - [1/ (H/L)]*100\%$. The quantified proteins were clustered by cellular component and biological function on the basis of DAVID Functional Annotation, version 6.7 (215, 216). The mass spectrometry proteomics data

have been deposited to the ProteomeXchange Consortium (217) via the PRIDE partner repository using the data set identifier PXD001802 and 10.6019/PXD001802.

### 2.2.8 Enzyme activity assay of glyceraldehyde 3-phosphate dehydrogenase (GAPDH), triose phosphate isomerase (TPI) and α-Enolase

GAPDH activity was measured as described previously (218). After incubation with or without NOX inhibitors followed by a 6-hour platelet releasate treatment, the THP-1 cell pellet was lysed in RIPA buffer in the presence of a protease inhibitor. The protein concentrations of cell lysates were determined by BCA assay. For the GAPDH enzyme activity assay, the cell lysate containing 30 μg cellular protein was mixed with a reaction buffer containing 13 mM sodium pyrophosphate, 26 mM sodium arsenate, 10 mM DTT, 750 μM β-NAD and 2.5 mM D, L-glyceraldehyde-3-phosphate (pH 7.0). Absorbance at 340 nm was recorded at 10 sec intervals for 5 minutes. Enzyme activity was determined by the molar absorption coefficient of NADH and then normalized to vehicle control.

TPI activity was measured for the same batch of samples used in the GAPDH activity assay using a protocol that described in a previous study (219). Briefly, assays were carried out in 100 μL of 0.1 M triethanolamine buffer, pH 7.4, containing 10 mM EDTA, 0.05% BSA, 0.2 mM NADH, 50 U/mL α-glycerophosphate dehydrogenase, and 1 mM D, L-glyceraldehyde 3-phosphate**.** The reaction was started by the addition of 30 μg of cellular protein. The TPI activity was determined on the basis of the reduction in absorbance at 340 nm due to the NADH consumption.

The α-enolase activity was determined by measuring the conversion of NADH to NAD as described elsewhere (220) with some modification. The enzymatic reaction was performed at 37 °C in 100 mM HEPES buffer (pH 7.0) containing 5.0 mM $MgSO_4$, 0.2 mM NADH, 0.25 mM 2-phosphoglycerate (2-PGE), 1.2 mM ADP, 15 U/mL lactate dehydrogenase and 5 U/mL pyruvate kinase in a final volume of 100 µL. The reaction was started by adding 30 µg cellular protein. The α-enolase activity was again determined on the basis of the conversion of NADH to NAD and the resulting drop in absorbance at 340 nm.

## 2.3 Results

### 2.3.1 Adaptation of the biotin switch assay to quantify $Cys_{OX}$

Among different reactive oxygen species (ROS), $H_2O_2$ is one of the most important signaling molecules. For method validation, we used $H_2O_2$ to treat THP-1 cells to mimic oxidative stress. Before applying the proteomic assay, we used FACS-based experiments to screen $H_2O_2$ treatment conditions. The FACS results showed that the intracellular ROS levels significantly increased after $H_2O_2$ treatment for both one hour ($p<0.1$) and six hours ($p<0.01$) and six-hour incubation induced more ROS production than an incubation of one hour. With six-hour incubation, 100 µM and 1 mM $H_2O_2$ had similar effects on ROS production (Appendix A.1). Taking into account the FACS results and the toxicity of $H_2O_2$ (221), a 6-hour incubation with 100 µM $H_2O_2$ was chosen for the subsequent proteomics study.

The modified biotin switch assay was then applied to THP-1 cells treated with 100 µM H2O2 for six hours. We were able to quantify 1506 peptides on average in three biological replicates. The average percentage of Cys-containing peptides out of all enriched peptides was 40% (Table 2-1).

There were 599 enriched peptides shared among the three biological replicates, which contained 245 Cys-containing peptides (Figure 2-1).

**Table 2-1. Enrichment efficiency of the modified biotin switch assay.** THP-1 Cells were first treated with 100 µM $H_2O_2$ for six hours, and then enriched with the modified biotin switch assay. After in-solution digestion, mass spectrometric analysis of three replicates, the corresponding number of peptides, Cys-containing peptides were extracted from the MaxQuant result file.

| Replicate | Total number of peptide | Number of Cys-containing Peptide |
|---|---|---|
| 1 | 1423 | 613 |
| 2 | 1734 | 639 |
| 3 | 1360 | 532 |
| Average | 1506 | 595 |

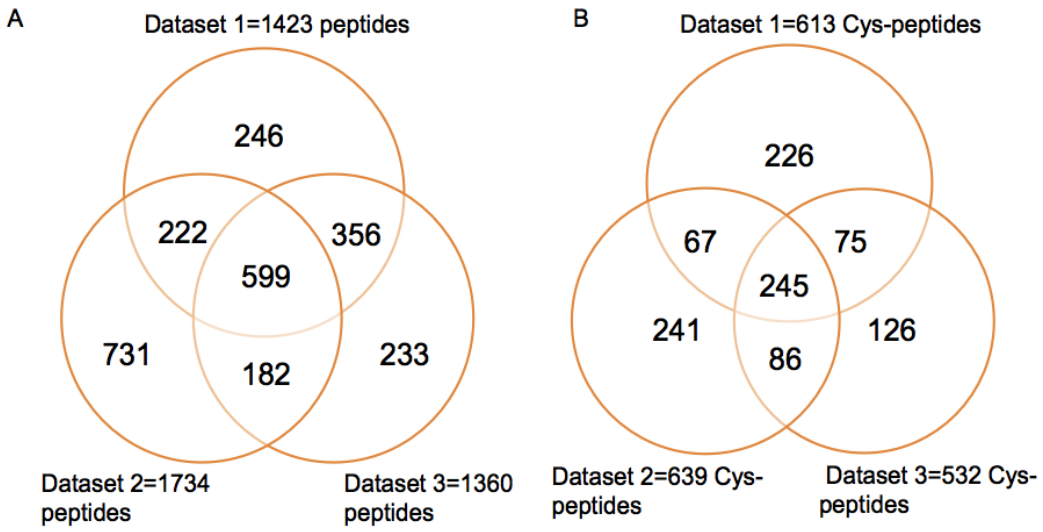


**Figure 2-1. Overlap of three replicates in THP-1 cells.** THP-1 Cells were first treated with 100 µM $H_2O_2$ for six hours, and then enriched with the modified biotin switch assay. After in-solution digestion, peptides were identified using mass spectrometric analysis. The Venn diagrams represent the common (A) peptides, and (B) Cys-containing peptides among three repeats.

### 2.3.2 ROS level in THP-1 monocytic cells in response to 6-hour platelet releasate incubation

To determine whether platelet releasate induces ROS production, we incubated THP-1 cells with platelet releasates collected from platelets stimulated with LPA (20 μM) (LPA-PR) or thrombin (1 U/mL) (Thr-PR). The ROS levels remarkably increased ($p<0.01$) in THP-1 cells in response to both LPA-PR and Thr-PR for one hour. LPA alone (10 μM) doubled the intracellular ROS levels ($p<0.01$) compared to those of control, whereas thrombin alone had no effect on ROS production. For 6-hour incubation, intracellular ROS levels in LPA-PR or Thr-PR-treated THP-1 cells were three times higher than those of control ($p<0.001$) and were also significantly higher than those of LPA alone ($p<0.01$) or thrombin alone ($p<0.01$). After 24 h incubation, only the platelet releasates notably increased in intracellular ROS levels in the THP-1 cells ($p<0.01$) (Figure 2-2). LPA had previously been shown to significantly increase intracellular ROS production and DNA synthesis in THP-1 cells (200). Our results indicated that LPA-PR induced more intracellular ROS generation than LPA alone. In summary, incubation with platelet releasate for six hours resulted in a large amount of ROS production, and this method was chosen to study reversible cysteine oxidation change in THP-1 cells in more detail.

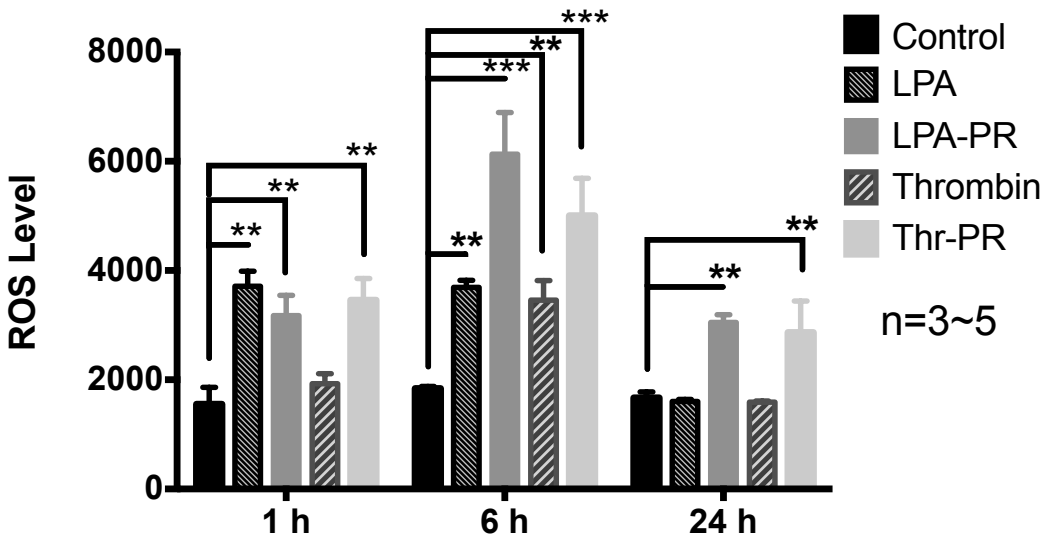


**Figure 2-2. The accumulation of ROS in THP-1 cells with different treatments.** THP-1 cells were treated with LPA (10 μM), thrombin (0.5 U/mL), alkyl-LPA-induced platelet releasate (LPA-PR) and thrombin-induced platelet releasate (Thr-PR) for one, six and 24 hours. Results are expressed as the mean ± SD, and asterisks indicate significance (**, $p<0.01$; ***, $p<0.001$;two-way ANOVA plus Tukey's post hoc test, n= 3-5).

### 2.3.3 Application of the modified biotin switch assay to platelet-releasate-treated THP-1 monocytic cells

The modified biotin switch assay was applied to THP-1 cells treated with LPA-PR for six hours. On average, 1859 peptides were identified and 550 were shared among three biological replicates (Appendix A.2, A.5). Out of a total of 550 peptides, 224 Cys-containing peptides could be quantified on the basis of their H/L ratios. According to a standard power calculation (n = 3, 10% RSD, 95% confidence interval), H/L=1.3, or more than a 20% increase of cysteine oxidation, was set as the cutoff criteria for the determination of reversible $Cys_{OX}$. Of the 224 Cys-containing peptides, 120 peptides (corresponding to 86 proteins) were identified with reversible

$Cys_{OX}$ (H/L >1.3) (Appendix A.6). For Thr-PR, an average of 1692 peptides were identified in three biological replicates. Of the 584 peptides shared among the three replicates, 239 were Cys-containing peptides (Appendix A.3, A.7). Out of 239 Cys-containing peptides, 104 peptides (corresponding to 73 proteins) were quantified with reversible $Cys_{OX}$ (Appendix A.8). There were 75 reversible $Cys_{OX}$-containing peptides shared between LPA-PR and Thr-PR, corresponding to 53 proteins (Figure 2-3 and Appendix A.9). This accounted for 63% or 71% of $Cys_{OX}$-containing peptides quantified in LPA-PR or Thr-PR, respectively. For 23 out of the 75 peptides), the oxidized Cys residues had been reported in previous studies (Table 2-2).

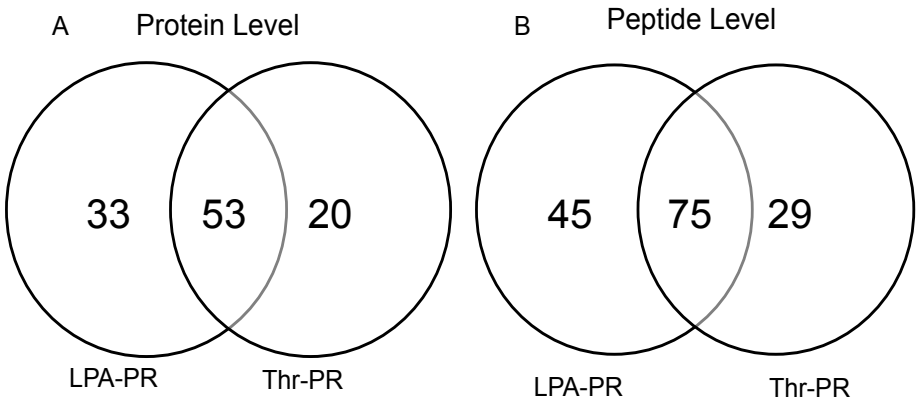


**Figure 2-3. Overlap of proteomics result from LPA-PR and Thr-PR. Heavy SILAC-labeled THP-1 cells were first treated with** LPA-PR or Thr-PR for six hours, and then mixed 1:1 with untreated light SILAC-labeled THP-1 cells. After enrichment, in-solution digestion, and mass spectrometric analysis of three replicates for each treatment condition, the Venn diagrams show the 75 peptides (B) with $Cys_{OX}$, corresponding to 53 proteins (A) shared between LPA-PR and Thr-PR.

**Table 2-2. List of selected $Cys_{OX}$ peptides that were quantified across two conditions with literature Reference.** Proteins quantified across all conditions (LPA-PR, Thr-PR treatment) were extracted from the corresponding results files, and listed with their name, the peptide sequence carrying the $Cys_{OX}$ modifications, and the heavy/light (H/L) ratio obtained using three replicates each.

| Protein name | Sequence | H/L ± SD | | Ref |
|---|---|---|---|---|
| | | LPA-PR | Thr-PR | |
| ***Glycolysis, Total 6*** | | | | |
| Alpha-enolase | SCNCLLLK | 9.03±2.97 | 1.95±0.23 | (222-225) |
| | VNQIGSVTESLQACK | 4.18±2.25 | 2.22±0.91 | (222-225) |
| L-lactate dehydrogenase A chain | VIGSGCNLDSAR | 2.54±1.17 | 16.67±0.78 | (225) |
| Phosphoglycerate kinase 1 | GCITIIGGGDTATCCAK | 1.71±0.13 | 1.7±0.41 | (225) |
| Triosephosphate isomerase | IAVAAQNCYK | 2.00±0.82 | 1.95±0.58 | (222) |
| ***Cytoskeleton organization, Total 11*** | | | | |
| Actin, cytoplasmic 1 | CDVDIR | 2.67±1.1 | 2.7±0.82 | (226, 227) |
| | LCYVALDFEQEMATAASSSSL | 2.02±0.47 | 2±0.31 | (226, 227) |
| Cofilin-1 | AVLFCLSEDK | 6.6±1.06 | 2.77±0.88 | (228) |
| | HELQANCYEEVK | 3.25±0.63 | 1.37±0.07 | (228) |
| Ras-related C3 botulinum toxin substrate | YLECSALTQR | 3.27±0.82 | 1.35±0.05 | (229) |
| Tubulin alpha-1B chain | SIQFVDWCPTGFK | 1.63±0.3 | 1.49±0.13 | (222-225, 230) |
| Tubulin beta-3 chain | NMMAACDPR | 6.82±4.48 | 1.49±0.14 | (223-225, 230) |
| ***Translation, Total 7*** | | | | |
| Elongation factor 2 | STLTDSLVCK | 4.15±2.17 | 1.48±0.19 | (231) |
| | TFCQLILDPIFK | 2.31±0.97 | 1.64±0.48 | (231) |
| 60S ribosomal protein L23 | ISLGLPVGAVINCADNTGAK | 1.96±0.68 | 1.85±0.17 | (225) |
| ***Protein folding, Total 6*** | | | | |
| Heat shock 70 kDa protein 4 | GCALQCAILSPAFK | 2.93±1.33 | 2.58±0.79 | (231) |
| Heat shock cognate 71 kDa protein | VCNPIITK | 2.25±0.26 | 1.54±0.33 | (225) |
| Peptidyl-prolyl cis-trans isomerase A | KITIADCGQLE | 1.93±0.7 | 1.89±0.95 | (225) |
| ***Oxidation reduction, Total 6*** | | | | |
| Glutathione S-transferase P | ASCLYGQLPK | 2.44±0.72 | 1.78±0.13 | (232, 233) |
| Peroxiredoxin-6 | DINAYNCEEPTEK | 1.41±0.06 | 1.33±0.13 | (234) |
| Thioredoxin | CMPTFQFFK | 2.62±0.94 | 2.42±0.4 | (225) |
| ***Other*** | | | | |
| Macrophage migration inhibitory factor | LLCGLLAER | 1.48±0.15 | 1.49±0.08 | (225) |
| 14-3-3 protein zeta/delta | YDDMAACMK | 2.62±1.51 | 2.54±0.81 | (235) |

### 2.3.4 Bioinformatics analysis of proteins with $Cys_{OX}$

The protein lists of reversible $Cys_{OX}$ for LPA-PR and Thr-PR were submitted for Gene Ontology (GO) enrichment by the DAVID Functional Annotation Analysis, and the resulting top 10 biological functions were extracted (Figure 2-4 A, B). GO enrichment revealed several biological functions that were shared between LPA-PR and Thr-PR, including glycolysis, translation, and actin cytoskeleton organization. Cellular component distribution was also performed (Figure 2-4 C, D). For LPA-PR, 30% of the proteins were associated with the cytoplasm, 30% with the ribosome, 16% with the cytoskeleton, 11% with the nucleus, and 6% with the plasma membrane. For Thr-PR, cytoplasmic proteins made up 40% of the total proteins, with another 22% of proteins originating from the cytoskeleton, 15% from the nucleolus, 8% from the plasma membrane, and 11% from the ribosome.

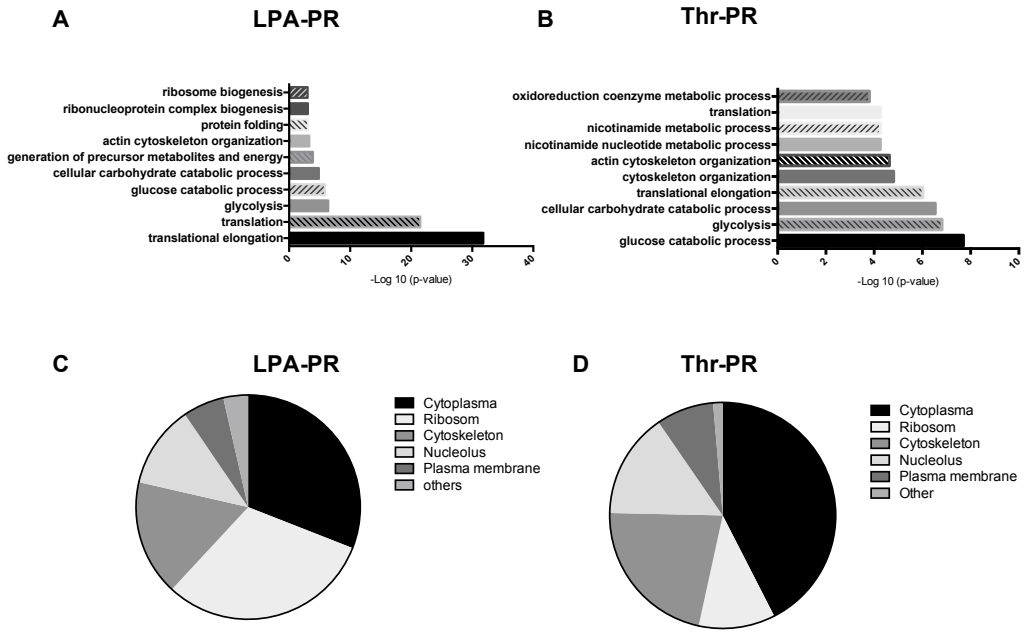


**Figure 2-4. Bioinformatics analysis of proteins quantified with $Cys_{OX}$ in THP-1 cells during platelet releasate treatments.** The proteins detected with $Cys_{OX}$ were subjected to David Functional Annotation Analysis. Shown are

the calculated p-value for the top 10 biological functions (A, B) and cellular component (C, D) distribution of (A, C) LPA-PR and (B, D) Thr-PR.

### 2.3.5 Inhibition of NADPH oxidase in THP-1 monocytic cells

NADPH oxidase (NOX) is known as the major contributor of intracellular ROS in the vascular system (236, 237). Thus, we introduced three different NOX inhibitors, DPI, AEBSF and ML171 to evaluate the role NOX played in our model. Both DPI and AEBSF are nonspecific NOX inhibitors, and incubation with the inhibitors alone did not affect intracellular ROS production. Preincubation with DPI or AEBSF significantly reduced intracellular ROS production following LPA-PR/Thr-PR treatments for six hours ($p<0.01$). Exposure to ML171, which specifically targets the NOX1 isoform, inhibited the ROS production in THP-1 cells induced by platelet releasate treatment ($p<0.01$) to a similar extent as the nonspecific NOX inhibitors (Figure 2-5).

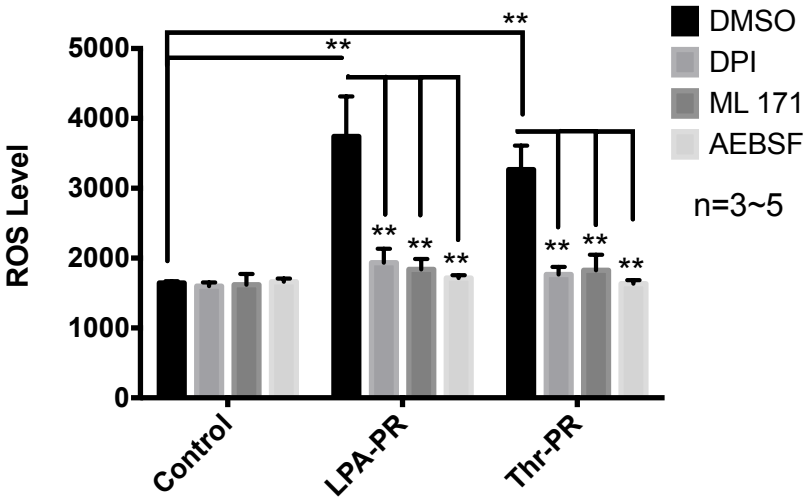


**Figure 2-5. Quantification of ROS accumulation in THP-1 cells upon platelet releasate treatment and DPI, ML171, and AEBSF inhibition of NOX.** THP-1 cells were first treated with DPI, ML171, AEBSF or DMSO as a control for one hour. After that, THP-1 cells were incubated with different platelet releasate (LPA-PR and Thr-PR)

or RPMI medium as a control for six hours. Results are expressed as the mean ± SD; asterisks indicate significance. (*, $p<0.05$, **, $p<0.01$; two-way ANOVA plus Tukey's post hoc test, n= 3).

We then applied the modified biotin switch assay to quantify reversible Cys oxidation upon DPI preincubation. There were 1654 peptides being identified on average, and 584 were found to be in common across three biological repeats (Appendix A.10). Among the 584 peptides, 215 were Cys-containing peptides and 43 had reversible $Cys_{OX}$ (Appendix A.4, A.11). A total of 131 Cys-containing peptides were shared between the result of the 6-hour LPA-PR treatment and the DPI pretreatment (Figure 2-6 A). DPI pretreatment reduced the contribution of the $Cys_{OX}$-containing peptides to the total Cys-containing peptides from 40% in LPA-PR to 20% (Figure 2-6 B). We further classified the 42 reversible $Cys_{OX}$-containing peptides following the LPA-PR treatment on the basis of the change of their H/L ratios upon DPI pretreatment (Table 2-3). There were 32 peptides in which $Cys_{OX}$ was blocked upon DPI pretreatment. This group included Cys152 in glyceraldehyde 3-phosphate dehydrogenase (GAPDH) and Cys39 and Cys139 in cofilin. In another nine peptides, $Cys_{OX}$ was partially prevented by DPI-pretreatment. This subset involved additional glucose metabolic enzymes such as triose phosphate isomerase (TPI) and α-enolase, as well as cytoskeleton proteins like actin and tubulin. In only one peptide, $Cys_{OX}$ was not inhibited upon DPI pretreatment.

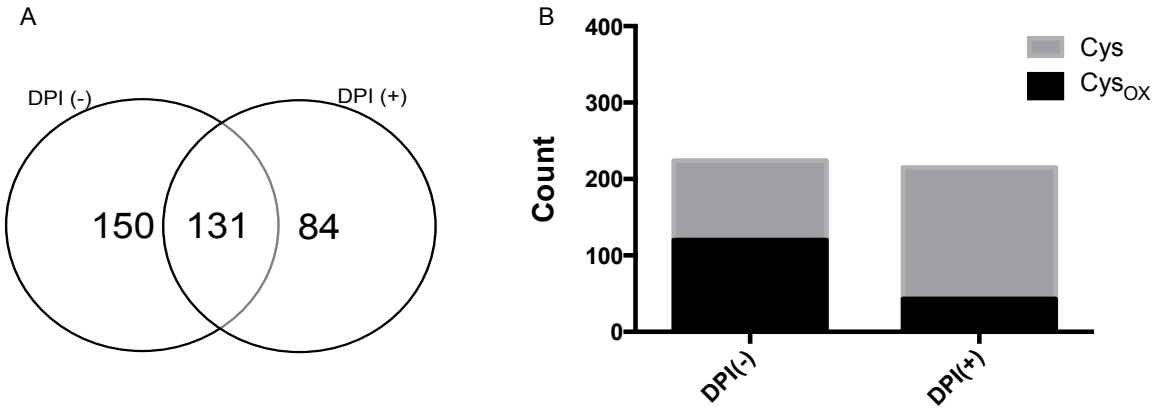


**Figure 2-6. Comparison of the proteomics results of DPI treated THP-1 cells versus normal THP-1 cells upon LPA-PR treatment.** Heavy SILAC-labeled THP-1 cell were first treated with DPI for one hour followed by the treatment with LPA-PR for six hours, and then combined with an equal amount of untreated light SILAC-labeled THP-1 cells. Samples were then subjected to the modified biotin switch assay followed by mass spectrometric analysis. The peptides quantified in samples treated with DPI-LPA-PR were compared with samples treated with LPA-PR. (A) The Venn diagram represents the overlap of Cys-containing peptides across two conditions (DPI-LPA-PR and LPA-PR treatment). (B) Percentage of $Cys_{OX}$ in total Cys-peptides varies different treatments (DPI-LPA-PR and LPA-PR treatment).

**Table 2-3. Classification of 42 Cys-containing peptides that overlapped between DPI-LPA-PR and LPA-PR treated THP-1 cells. Proteins quantified across all conditions** (DPI-LPA-PR, LPA-PR treatment) were grouped based on the H/L ratio, and listed with their name, the peptide sequence carrying the $Cys_{OX}$ modification.

| Protein Name | Peptide Sequence | H/L±SD | |
|---|---|---|---|
| | | DPI(-) | DPI(+) |
| **Inhibition of $Cys_{OX}$ upon DPI treatment** | | | |
| Actin, cytoplasmic 1 | CDVDIR | 2.67±1.1 | 1.25±0.49 |
| Annexin A6 | CLIEILASR | 3.52±3.45 | 0.84±0.59 |
| Calreticulin | HEQNIDCGGGYVK | 1.57±0.23 | 1±0.33 |
| Adenylyl cyclase-associated protein 1 | TDGCHAYLSK | 1.53±0.16 | 1.18±0.41 |
| | NSLDCEIVSAK | 1.69±0.42 | 1.07±0.45 |
| | INSITVDNCK | 1.57±0.19 | 1.05±0.26 |
| | CVNTTLQIK | 2.46±0.97 | 0.99±0.38 |
| | ALLVTASQCQQPAENK | 2.36±1.06 | 0.94±0.17 |
| Chloride intracellular channel protein 1 | LHIVQVVCK | 3.07±0.66 | 0.73±0.42 |
| Elongation factor 2 | TFCQLILDPIFK | 2.31±0.97 | 1.24±0.27 |
| Glyceraldehyde-3-phosphate dehydrogenase | IISNASCTTNCLAPLAK | 1.41±0.03 | 0.99±0.2 |

| Protein Name | Peptide Sequence | H/L±SD | |
|---|---|---|---|
| | | DPI(-) | DPI(+) |
| Guanine nucleotide-binding protein G(i) subunit | IIHEDGYSEEECR | 1.39±0.09 | 0.93±0.19 |
| Heterogeneous nuclear ribonucleoprotein D0 | GFCFLEYEDHK | 1.44±0.09 | 0.97±0.24 |
| Galectin-1 | FNAHGDANTIVCNSK | 1.43±0.12 | 1.08±0.28 |
| Macrophage migration inhibitory factor | LLCGLLAER | 1.48±0.15 | 1.12±0.06 |
| Putative nucleoside diphosphate kinase | GDFCIQVGR | 5.21±0.72 | 1.19±0.19 |
| Poly(rC)-binding protein 2 | LVVPATQCGSLIGK | 2.21±1.03 | 1.18±0.08 |
| | AITIAGIPQSIIECVK | 1.51±0.04 | 1.11±0.17 |
| Peptidyl-prolyl cis-trans isomerase A | KITIADCGQLE | 1.93±0.7 | 1.15±0.19 |
| | IIPGFMCQGGDFTR | 1.97±0.59 | 0.96±0.57 |
| 60S ribosomal protein L23 | ISLGLPVGAVINCADNTGAK | 1.96±0.68 | 1.29±0.3 |
| D-3-phosphoglycerate dehydrogenase | NAGNCLSPAVIVGLLK | 1.56±0.13 | 0.92±0.11 |
| Tubulin alpha-1B chain | SIQFVDWCPTGFK | 1.63±0.3 | 0.91±0.18 |
| Heat shock cognate 71 kDa protein | CNEIINWLDK | 2.47±0.65 | 1.13±0.08 |
| 40S ribosomal protein S5 | TIAECLADELINAAK | 1.9±0.36 | 1.24±0.18 |
| Cofilin-1 | HELQANCYEEVKDR | 3.25±0.63 | 0.81±0.2 |
| Alpha-enolase | VNQIGSVTESLQACK | 4.18±2.25 | 1.03±0.21 |
| Integrin beta-2 | TTEGCLNPR | 2±0.26 | 1.03±0.28 |
| L-lactate dehydrogenase A chain | VIGSGCNLDSAR | 2.54±1.17 | 1.05±0.22 |
| Phosphoglycerate kinase 1 | GCITIIGGGDTATCCAK | 1.71±0.13 | 1.11±0.19 |
| Ubiquitin-like modifier-activating enzyme 1 | YFLVGAGAIGCELLK | 1.46±0.29 | 1.22±0.45 |
| Ras-related C3 botulinum toxin substrate 2 | YLECSALTQR | 3.27±0.82 | 0.8±0.45 |
| **Partially inhibition of $Cys_{OX}$ upon DPI treatment** | | | |
| Chloride intracellular channel protein 1 | FLDGNELTLADCNLLPK | 2.5±1.23 | 1.31±0.38 |
| Alpha-enolase | SCNCLLLK | 9.03±2.97 | 1.56±0.45 |
| Tubulin beta chain | EIVHIQAGQCGNQIGAK | 1.91±0.82 | 1.42±0.05 |
| Triosephosphate isomerase | IAVAAQNCYK | 2±0.82 | 1.8±0.43 |
| Heat shock cognate 71 kDa protein | VCNPIITK | 2.25±0.26 | 1.63±0.06 |
| Phosphoglycerate kinase 1 | DCVGPEVEK | 1.64±0.35 | 1.88±0.81 |
| Ubiquitin-conjugating enzyme E2 N | ICLDILK | 1.6±0.17 | 1.36±0.44 |
| Ras-related C3 botulinum toxin substrate 2 | AVLCPQPTR | 2.18±1 | 1.37±0.5 |
| Actin, cytoplasmic 1 | LCYVALDFEQEMATAASSSSL | 2.02±0.47 | 1.64±0.11 |
| **No inhibition of $Cys_{OX}$ upon DPI treatment** | | | |
| Malate dehydrogenase | TIIPLISQCTPK | 1.7±0.62 | 2.94±0.15 |

### 2.3.6 Analysis of enzymatic activity in THP-1 cells following platelet releasate treatment

The proteomics data indicated that Cys152 in the active site of GAPDH was oxidized in response to LPA-PR treatment (H/L= 1.41, 29%) and restored by DPI treatment (H/L=0.99). However, Thr-PR treatment did not lead to a significantly increased H/L ratio of Cys152 (H/L=1.04) (Table 2-4). To validate the inhibition effect of Cys152 oxidation on GAPDH activity, we measured the GAPDH enzyme activity via the increase of UV absorbance of NADH that is produced when

GAPDH converts DL-glyceraldehyde 3-phosphate to D-glycerate 1,3-biophosphate (Figure 2-7 A). Platelet releasate produced by both thrombin and LPA significantly impaired the GAPDH activity in THP-1 cells by more than 20% ($p<0.01$). The reduced enzyme activity was consistent with the proteomic result for LPA-PR but not with that for Thr-PR. Pretreatment with DPI or ML171 partially restored the enzyme activity to more than 90%, which is in agreement with the proteomic result of DPI treatment.

Another enzyme involved in glycolysis, triose phosphate isomerase (TPI), was also oxidized in THP-1 cells upon both types of platelet releasate treatment. In contrast to the effect on GAPDH, NOX inhibitor treatment did not fully restore the oxidation state of the TPI cysteine we had detected and quantified (Table 2-4). Likewise, platelet releasate treatment reduced TPI activity in THP-1 cells to 50% in the enzyme activity assay, but pretreatment with either DPI or ML171 did not recover TPI activity (Figure 2-7 B), confirming the proteomic results of oxidative inhibition of TPI in our model system.

Finally, we also evaluated α-enolase, a third enzyme involved in glycolysis. Proteomic data indicated that LPA-PR and Thr-PR treatments resulted in a more than 80% and 40% increase in oxidation of the observed cysteine in α-enolase, respectively. DPI pretreatment reduced the extent of the oxidative Cys modification to 35% (Table 2-4). Similarly, the enzyme activity assay revealed more than 70% inhibition upon exposure to either of the two platelet releasates and the NOX inhibitor pretreatment did not recover α-enolase activity (Figure 2-7 C).

**Table 2-4. Proteomic results of three important enzymes in glycolysis with $Cys_{OX}$ modification.** The three enzymes in glycolysis were quantified across all conditions (LPA-PR, Thr-PR, DPI-LPA-PR) with $Cys_{OX}$ and listed with the peptide sequence carrying the $Cys_{OX}$ modification and the H/L raio obtained using three replicates each.

| Protein Name | Sequence | Sample Name | Peptide H/L ratio | Protein H/L ratio |
|---|---|---|---|---|
| GAPDH | IISNASCTTNCLAPLAK | LPA-PR 6 h | 1.41±0.03 | 1.24±0.05 |
| | | Thr-PR 6 h | 1.04±0.08 | 0.99±0.06 |
| | | DPI-LPA-PR 6 h | 0.99±0.2 | 0.93±0.06 |
| TPI | IAVAAQNCYK | LPA-PR 6 h | 2.00±0.82 | 1.08±0.07 |
| | | Thr-PR 6 h | 1.95±0.58 | 0.99±0.28 |
| | | DPI-LPA-PR 6 h | 1.80±0.43 | 1.02±0.09 |
| Alpha-enolase | SCNCLLLK | LPA-PR 6 h | 9.03±2.97 | 0.96±0.13 |
| | | Thr-PR 6 h | 1.95±0.23 | 0.94±0.11 |
| | | DPI-LPA-PR 6 h | 1.56±0.45 | 0.97±0.13 |

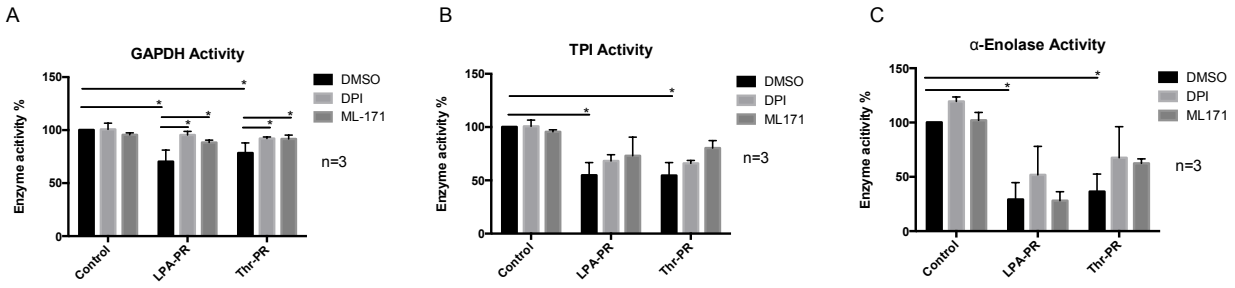


**Figure 2-7. Enzyme activity assays of glyceraldehyde-3-phosphate dehydrogenase (GAPDH), triose phosphate isomerase (TPI), and α-enolase activity in THP-1 cells upon platelet releasate and NOX inhibitor treatments.** (A) GAPDH lost 20% of its activity upon platelet releasate treatment for six hours and recovered it by NOX inhibitor treatment. (B) TPI enzyme activity assay showing the loss of more than 50% of its activity upon platelet releasate treatment after 6 h. The activity did not recover upon NOX inhibitor pretreatments. (C) Results similar to those of TPI seen as in α-Enolase (*, $p<0.05$; two-way ANOVA plus Tukey's *post hoc* test, n = 3 - 5)

### 2.3.7 ROS production induced by platelet releasate in human primary monocytes via NADPH oxidase

To validate the results obtained for THP-1 cells in our model, we isolated human primary monocytes ($CD14^+/CD16^+$) from healthy donors and incubated them with LPA (20 μM)-induced releasate or thrombin (1 U/mL)-induced releasates from platelets of the same donor, or with stimuli alone. The increase in ROS levels observed in THP-1 cells upon treatment was also seen in monocytes. The fold change of intracellular ROS in human primary monocyte treated with platelet releasates was lower than in THP-1 cells, but still reached statistical significance at six hour ($p<0.01$). The incubation of one hour with LPA-PR also significantly increased ROS production in monocytes ($p<0.05$). In contrast to THP-1 cells, the overnight incubation of primary monocytes with Thr-PR also induced ROS production ($p<0.01$). Treatment with LPA or thrombin alone slightly increased ROS production in monocytes at the different time points, but none reached statistical significance (Figure 2-8). In addition, we also exposed primary monocytes to the different NOX inhibitors, followed by 6-hour platelet releasate treatments. Both DPI and ML171 reduced ROS production in primary monocytes, but AEBSF did not block ROS production in monocytes (Figure 2-9).

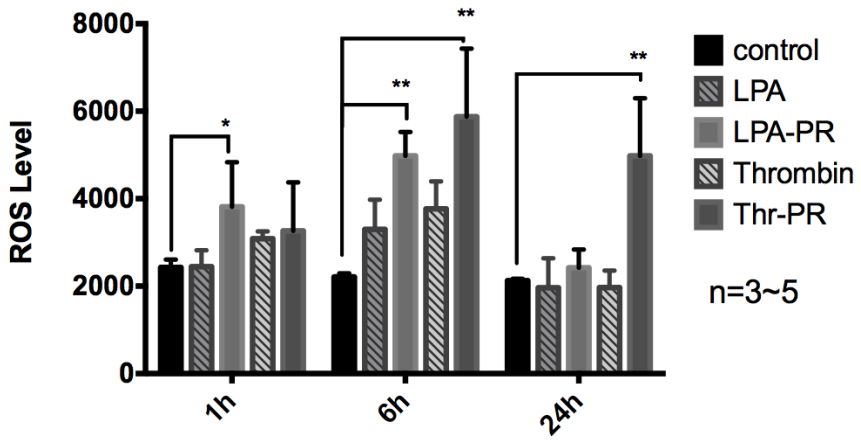


**Figure 2-8. The accumulation of ROS in human primary monocyte with different treatments.** Monocytes were treated with LPA (10 μM), thrombin (0.5 U/mL), alkyl-LPA-induced platelet releasate (LPA-PR) and thrombin-induced platelet releasate (Thr-PR) for 1, 6 and 24 h. Results are expressed as the mean ± SD, and asterisks indicate significance (*, $p<0.05$; **, $p<0.01$; two-way ANOVA plus Tukey's post hoc test, n= 3-5).

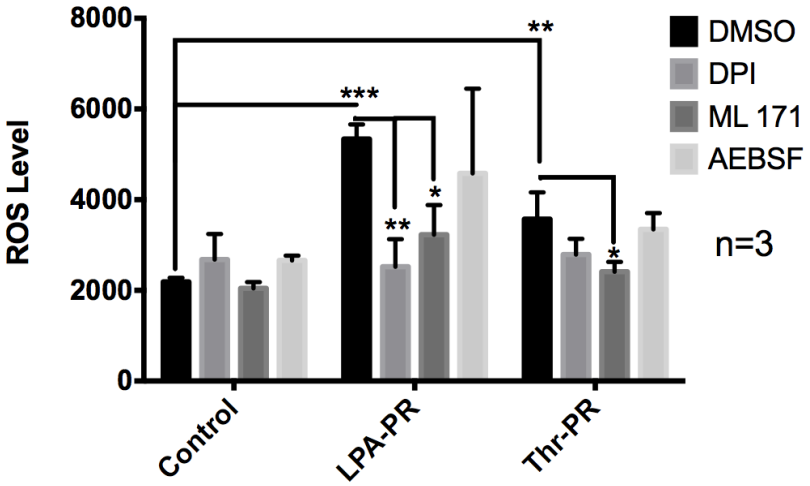


**Figure 2-9. The quantification of ROS accumulation in the primary monocyte upon platelet releasate treamtnes and DPI and ML171 inhibition of NOX.** Monocytes were first treated with DPI, ML171, AEBSF, or DMSO as a control for one hour. After that, monocytes were incubated with different platelet releasate (LPA-PR and Thr-PR) or RPMI medium as a control for six hours. Results are expressed as the mean ± SD, and asterisks indicate significance. (*, $p<0.05$; **, $p<0.01$; ***, $p<0.001$; two-way ANOVA plus Tukey's post hoc test, n= 3)

## 2.4 Discussion

It had already been demonstrated that the direct binding of activated platelets to monocytes induces integrin activation, chemotaxis and intracellular ROS production in monocytes (192). However, a recent study revealed that direct platelet-monocyte interaction is not necessarily required, as proinflammatory signaling events in monocytes could be uncoupled from platelet-monocyte direct binding (238). Interestingly, our results now demonstrate that platelet releasate could also trigger ROS production in both THP-1 cells and primary human monocytes without platelet binding. Furthermore, we identified NADPH oxidase (NOX) as the key enzyme for ROS production in this physiologically relevant process, as preincubation with NOX inhibitors prevented intracellular ROS level increase in both THP-1 cells and primary monocytes as well as oxidative modifications on almost all of the responsive cysteines. This novel mechanistic insight was obtained by combining an established FACS assay with a modified biotin switch assay to monitor the platelet-releasate-induced intracellular ROS level increase and the cysteine oxidation in THP-1 monocytic cells, respectively.

We decided to develop such a modified assay because the existing biotin switch assays that utilize selective reducing reagents have several disadvantages. First, the coverage of modification sites is usually limited due to the instability of the *S*-nitrosylation and sulfenic acid. On average, only 40 modification sites were identified by mass spectrometry in these studies (183, 208, 225, 231). Second, most of these studies did not incorporate quantification methods into the biotin switch assays. Indeed, there is only one report that combines SILAC with the biotin switch assay to quantify endogenous *S*-nitrosylation (231). However, in this study the elution of biotinylated peptides from streptavidin using DTT reduced not only the S-nitrosylation

sites but also the disulfide bonds, which may lead to erroneous assignment. Third, both *S*-nitrosylation and sulfenic acid formations are mostly involved in cell signaling under physiological conditions, and *S*-nitrosyl and sulfenic acid preferentially react with other free cysteines to form disulfide bonds (183, 204). Consequently, their identification provides little information on the global redox state of a system under pathological conditions.

To address these issues, we modified the biotin switch assay in the following aspects. First, instead of detecting specific forms of oxidized cysteines ($Cys_{OX}$), we used TCEP to recover all reversible $Cys_{OX}$ for enrichment. Moreover, we employed avidin enrichment on the peptide level to reduce the amount of non-Cys-containing peptides. We also fractionated the peptide mixture into six fractions by anion exchange to increase coverage. All of these steps help improve the coverage of $Cys_{OX}$ sites. As a result, we significantly increased coverage to more than 200 Cys-containing peptides per experiment. Second, SILAC labeling was introduced into the biotin switch assay to quantify the extent of cysteine oxidation. SILAC is a metabolic labeling strategy that incorporates stable isotopes during cell culture (209). Consequently, our method provides an alternative to iodoTMT (239) and ICAT (240) for quantifying the reversible cysteine oxidation modification that, unlike these chemical labeling strategies, does not depend on the reduction step that would otherwise affect the accuracy of the quantification. Indeed, the modified biotin switch assay also showed improved quantification coverage of $Cys_{OX}$ sites. For a 6-hour 100 μM $H_2O_2$ treatment, over 100 reversible $Cys_{OX}$ out of the more than 200 Cys-containing peptides could be quantified. For the platelet releasate-treated THP-1 cells, similar performance was achieved by enriching approximately 100 reversible $Cys_{OX}$ sites.

The advantages discussed above are partially offset by several shortcomings of our assay. First, due to the multiple labeling steps and the biotin avidin enrichment, milligram amounts of proteins are required. For the analysis of rare samples providing limited material, further optimization may be required to render the assay practical. Second, SILAC as a quantitative metabolic labeling method is generally restricted to cultured cells. Therefore, for primary cells that cannot be cultured, such as primary monocytes or platelets, the biotin switch method will have to rely on other quantitative labeling approaches or use label-free strategies. Alternatively, if a surrogate cell line that adequately mimics the primary cells can be found, e.g., THP-1 cells substituting for human primary monocytes in our case, subsequent validation of the proteomic results on primary cells would also be possible. Third, contamination with non-Cys-containing peptides (which are mostly due to the nonspecific binding of abundant proteins to avidin) currently increases the complexity of the sample. This could result in the missed identification of low abundance proteins as well as reduced reproducibility and coverage, as evident in our study (40% overlap between three biological replicates, 1500 peptides observed). Further optimization of the protocol and the use of state-of-the-art instrumentation to increase throughput and sensitivity may help address this issue.

Despite these limitations, the biotin switch assay presented here has already provided a robust workflow, and it has also produced reliable results. The identified $Cys_{OX}$ sites listed in Table 2 were consistent with literature, including those in key enzymes for glycolysis and cytoskeleton proteins (227, 241). Moreover, oxidation of Cys152 in the active site is known to inactivate the GAPDH (241), and the enzyme assay revealed inhibition of GADPH activity after platelet releasate treatment and restored activity through the inhibition of NOX. In addition to GADPH,

several other enzymes involved in glycolysis also showed increased cysteine oxidation upon platelet releasate treatment. The enzyme activity assay we performed for the other two enzymes that are upstream of GADPH in the glycolytic pathway, TPI and α-enolase, also confirmed their inhibition via cysteine oxidation. The inhibition of TPI and GAPDH by oxidative stress had previously been proposed to reroute the glucose-6-phosphate into the pentose phosphate pathway (PPP), the key pathway of NADPH production, to protect cells from oxidative stress (242). Consequently, the enzyme activity assays not only supported the proteomics results but also were consistent with the literature. The improved coverage of $Cys_{ox}$ sites also enabled us to perform Gene Ontology (GO) enrichment analysis. Both releasates affected proteins in multiple cellular functions that overlapped between the two releasates, which notably included glycolysis. The relative contributions of the various categories appeared to differ, but more detailed biological experimentation will be needed to define whether this has any biological relevance.

In summary, owing to the identification of all reversible $Cys_{OX}$ and the independent high throughput quantification, the modified biotin switch assay has demonstrated its ability to reveal the redox processes in our atherosclerosis model. This new, versatile assay enables the study of the redox state by mapping the oxidative modifications of cysteine involved in redox signaling in biological systems.

# Chapter 3: Quantitative Protein Sulfenic Acid Analysis Identifies Platelet Releasate-induced Activation of Integrin $\beta_2$ on Monocytes via NADPH Oxidase

## 3.1 Introduction

Redox imbalance in cells, due to the accumulation of reactive oxygen species (ROS), has been implicated in the pathogenesis of several diseases, including atherosclerosis. However, the molecular details of redox regulation in atherosclerosis remain to be established (198). During the progression of atherosclerotic plaque formation, ROS are mainly produced by NADPH oxidase (NOX) complexes that are present in vascular cells, particularly in phagocytic cells including monocytes (110). ROS from exogenous or endogenous sources are capable of modifying DNA, lipids, and proteins. Cysteine residue in proteins, despite being one of the least abundant amino acid residues, are a major target of ROS-mediated cell-signaling modulation (201). The ROS-mediated regulation is accomplished through a variety of reversible and irreversible oxidative modifications on cysteines such as sulfenic acid, S-nitrosylation, S-glutathionylation, or sulfonic acid.

Among the reversible cysteine oxidative modifications, sulfenic acid has emerged as an important post-translational modification of proteins (243). Sulfenic acid, as the principle product of the reaction between a thiol and hydrogen peroxide, is a pivotal reactive intermediate under physiological and oxidative stress conditions. Several studies have identified the catalytic or regulatory sulfenic acid formation in proteins such as NADH peroxidase, peroxiredoxins, and protein tyrosine phosphatase (243). Pinpointing the precise location of sulfenic acid modification

in proteins enables the localization of the reactive site where oxidation is initiated. However, the detection of sulfenic acid modification is challenging, as the sulfenic acid moiety is highly reactive and in most situations rapidly converted back to the reduced or further oxidized to a more stable form. Certain protein microenvironments, such as the presence of polar uncharged residues, particularly threonine, and the absence of the charged residues close to the sulfenic acid sites, promote sulfenic acid formation and stabilization (244). In order to be able to conduct proteomic studies of this oxidative modification, various analytical methods have been developed to enrich proteins or peptides bearing sulfenic acid modifications (185).

Introduced first by Jaffrey in 2001, the biotin switch assay has been extensively adapted to identify various cysteine modifications in complex biological samples (182). We had previously combined the biotin switch assay with stable isotope labeling by amino acid in cell culture (SILAC) to quantify total reversible cysteine oxidation, and had applied it to an atherosclerotic model consisting of human platelets and monocytic THP-1 cells. In the development of atherosclerosis, platelet activation facilitates the recruitment of monocytes to sites of inflamed vascular endothelium not only via P-selectin-PSGL-1-mediated direct binding, but also via the released contents of their granules, which are referred to as platelet releasate (PR). Our previous work had demonstrated that thrombin- or LPA- induced PR led to ROS production in THP-1 cells, which in turn altered fundamental biological processes such as glycolysis (245). To further characterize the redox regulation mechanism in this atherosclerotic model, we decided to alter the modified biotin switch assay to selectively quantify sulfenic acid. The Eaton group had modified the biotin switch assay using m-arsenite to selectively reduce sulfenic acid (183). Consequently, we combined SILAC and m-arsenite in the biotin switch assay, and used it to

quantify more than 100 sulfenic acid sites in our model system. Bioinformatics analysis of the proteins showing quantitative changes in sulfenic acid modification highlighted integrin $\beta_2$, which was contained in the leukocyte transendothelium migration category. LFA-1 ($\alpha_L\beta_2$) and Mac-1 ($\alpha_M\beta_2$) are the two integrin $\beta_2$ complexes that are most relevant for the migration of monocytes on endothelial cells (246). Using primary monocytes, we validated the activation of LFA-1 and Mac-1 upon platelet releasate treatment and showed this to be independent of P-selectin-PSGL1 interaction on monocytes. Consequently, the selective quantitative analysis of sulfenic acid modification reveals a new aspect of the crosstalk between platelet releasate and monocytes in the early stage of atherosclerosis.

## 3.2 Method

### 3.2.1 Chemicals and antibodies

N-ethylmaleimide (NEM), DL-dithiothreitol (DTT), iodoacetamide (IAA), arsenite, biotin-maleimide, propidium iodide, aldolase (rabbit), lysozyme (chicken) and thrombin from human plasma were obtained from Sigma; EZ-Link Biotin-HPDP, NeutrAvidin Agarose resins from Pierce (IL, USA); dimedone, diphenyleneiodonium chloride from Cayman Chemical (ON, Canada); 2-acetylphenothiazine (ML171) from Tocris bioscence (ON, Canada); 1-O-hexadecyl-2-hydroxy-*sn*-glycero-3-phosphatidic acid (16:0) from Avanti Polar Lipids (AL, USA); sequencing grade modified trypsin from Promega (WI, USA). All antibodies i.e. anti-human CD14-Pacific blue (Clone: HCD14), anti-human CD16-APC (Clone 3G8), anti-human CD11a/CD18- Alexa Fluor® 488 (LFA-1; Clone m24), and anti-human CD11b- Alexa Fluor® 488 (Mac-1; Clone m44) were purchased from BioLegend (CA, USA).

### 3.2.2 Platelet preparation and releasate collection

Ethics approval for platelet and monocyte isolation from whole blood was obtained from the Clinical Research Ethics Board at the University of British Columbia (H12-00757) and written consent was granted by the blood donors. After discarding the first 2 mL, whole blood from healthy donors was collected in vacutainer blood collection tubes containing acid citrate-dextrose (ACD) (Cat: 364606, BD Biosciences, Canada). Platelet rich plasma (PRP) was separated from whole blood following initial centrifugation at 150 g at room temperature for 15 minutes. Platelets were pelleted from PRP supplemented with half-volume of ACD by centrifugation at 720 g for 10 minutes, washed twice with citrate glucose saline buffer (10 mM tri-sodium citrate, 30 mM glucose, 120 mM sodium chloride and 1 U / mL apyrase, pH=6.5) and resuspended in lysine and arginine free Roswell Park Memorial Institute (RPMI) 1640 medium (Gibco, Life Technologies, Canada) supplemented with 1.8 mM $CaCl_2$. Platelet counts were determined on a hemocytometer, and adjusted to physiological concentration ($300 \times 10^9$/L). Platelets were rested at room temperature for 30 minutes and then activated with 1 U / mL thrombin from human plasma or 20 μM 1-O-hexadecyl-2-hydroxy-*sn*-glycero-3-phosphatidic acid (LPA) at 37°C. Ten minutes after activation, platelet releasate was collected as supernatant after two-time centrifugation at 750 g at 4°C for 10 minutes, and the releasate was stored at -80°C.

### 3.2.3 Cell culture and incubation with platelet releasate

The human monocytic cell line THP-1 (American Type Culture Collection, Rockville, MD) was maintained in RPMI 1640 medium supplemented with 10% fetal bovine serum (FBS; Invitrogen Coporation, Carlsbad, CA) and 100 units / ml of penicillin/streptomycin. For SILAC labeling, THP-1 cells were maintained in lysine and arginine-free RPMI 1640 medium (Caisson Labs, UT,

USA) with 2 mM L-glutamine, 10% heat-inactivated dialyzed FBS, 100 units / ml penicillin/streptomycin, supplemented with either normal, 0.075 mg / mL $^{1}H_{1}$-L-lysine and 0.044 mg / ml $^{12}C_{6}$-L-arginine (light) or $^{2}D_{4}$-L-lysine and $^{13}C_{6}$-L-arginine (heavy) (Cambridge Isotope Labs, Andover, MA, USA). THP-1 cells were cultured in SILAC media for at least two weeks to allow full incorporation of labeled amino acids. The cell density was maintained at 1 - 5 × $10^{5}$ cells / mL. Heavy SILAC-labeled cells were washed, resuspended in heavy SILAC media to 1 × $10^{6}$ cells / mL, and mixed 1:1 (v/v) with platelet releasate or treated with 100 μM $H_2O_2$ for six hours, while light SILAC cells was used as control.

### 3.2.4 Differential alkylation method applied on model protein

Aldolase (1.6 μL from a stock of 25 μg/ μL in $H_2O$) in Tris buffer (50 mM Tris, 0.05 M Guanidine•HCl, pH 6.5) was treated with 10 μM or 20 μM $H_2O_2$ for one hour at 37°C to convert free thiols into sulfenic acid or subsequently disulfides. The mixture was quenched by adding a 100-fold molar ratio of NEM for one hour at 37°C (reagent excess here refers to molar excess over the number of cysteines per protein) to block the free thiols. Excess NEM was removed using Amicon Centrifugal Filter Units with 30 kDa cutoff (Millipore, Canada) and three times buffer exchange with 200 μL Tris buffer. After that, sulfenic acids were reduced by adding a 1000-fold molar ratio of arsenite and alkylated with 3100-fold molar ratio of iodoacetamide (IAA). The pKa of cysteine typically falls into the range of 8.3~8.5 and the conjugate base derived from cysteine, the thiolate, exhibits a high reactivity with sulfenic acid. To avoid thiolate formation and its subsequent reaction with nascent sulfenic acid, the pH of the whole buffer system in this study was set to 6.5. In parallel, this protocol was repeated with arsenite being replaced by DTT. Samples were then labeled with IAA and digested with trypsin (30:1 (w/w)

protein: trypsin) overnight at 37°C and analyzed by mass spectrometry. In the meantime, $H_2O_2$ treated aldolase was also reacted with a 1000-fold molar ratio of dimedone to label sulfenic acid directly for one hour at 37°C.

Similarly, lysozyme (1.8 µl from a stock of 20 µg/µL) in Tris buffer (50 mM Tris, 0.05 M Guanidine•HCl, pH 6.5) was also subjected to this differential alkylation method. Three conditions were applied on lysozyme: no, arsenite, and DTT reduction. Digested peptides were analyzed by mass spectrometry using a Thermo LTQ-FT (CA, USA).

Based on the LC-MS/MS results, the peak area of a thiol group with a modification (i.e. IAA modification or NEM modification) was determined as follows: the ion chromatograms of the Cys-containing peptide with different charge states in the full MS scan were extracted and their peak areas were summed up as the total peak area of this specific cysteine. To quantitatively assess the extent of sulfenic acid modification, the IAA-modification percentage was calculated based on the equation: IAA-modification percentage = peak area of IAA-modification/(peak area of IAA-modification + peak area of NEM-modification). The mass spectrometry proteomics data have been deposited to the ProteomeXchange Consortium (217) via the PRIDE partner repository using the dataset identifier PXD003348 and 10.6019/PXD003348.

### 3.2.5 Modified biotin switch assay development

To determine the optimal arsenite concentration and reaction time for sulfenic acid reduction in whole cell lysates, a pyridine-2-thione assay was performed by utilizing biotin-HPDP. THP-1 cells treated with 100 µM $H_2O_2$ for six hours were lysed in lysis buffer (1% NP-40, 0.1% sodium

deoxycholate, 50 mM Tris, 1 mM EDTA, 150 mM NaCl, pH 6.5) in the presence of protease inhibitors (Roche) to yield a protein concentration of 1 mg/ml, determined by BCA assay. A 200 μL aliquot of the whole cell lysate was treated with an equal amount of NEM (1:1, w/w) for one hour at 37°C, and excess NEM was removed by buffer exchange using Amicon Centrifugal Filter Units with 10 kDa cutoff (Millipore, Canada). The eluted mixture was then incubated with various concentrations of arsenite and 1.2 mM biotin-HPDP. The reaction product of free thiols with biotin-HPDP, pyridine-2-thione, has a molar extinction coefficient of $8.08 \times 10^3$ $M^{-1}cm^{-1}$ at 343 nm. Therefore, the protein mixture was monitored at 343 nm immediately before adding biotin-HPDP to determine background absorbance, and at 15 minutes intervals for two hours during the labeling reaction.

For all subsequent experiments, SILAC labeled THP-1 cells were incubated with 100 μM $H_2O_2$ or platelet releasate at 37°C for six hours. After treatment, light- and heavy-labeled THP-1 cells were washed twice with PBS, and harvested in lysis buffer in the presence of an equal amount of NEM (1:1, w/w) to block free thiols, and excess NEM was removed by buffer exchange using Amicon Centrifugal Filter Units with 10 kDa cutoff. Sulfenic acids were then reduced by adding 200 mM arsenite, the reduced free thiols labeled with 1 mM biotin-maleimide for two hours at 37°C, and the labeled proteins enriched with NeutroAvidin. The proteins enriched by NeutroAvidin were eluted by boiling in 4 × SDS buffer (composition) and 1mM biotin for five minutes and loaded onto 10% SDS gel. Following electrophoretic separation, gels were stained with Coomassie Brilliant Blue, and each lane was cut into five bands. In-gel digestion was performed essentially as described previously (247). The gel pieces were reduced in 10 mM dithiothreitol at 56°C for 30 minutes, followed by alkylation with 55 mM iodoacetamide at room

temperature for 45 minutes. Trypsin digestion was performed in 50 mM $NH_4HCO_3$ at 37°C for at least 16 hours. Then, peptides were extracted from the gel pieces by adding extraction buffer (1:2 (v/v) 5% formic acid / acetonitrile). Samples were analyzed by mass spectrometry using a Bruker Impact Q-TOF.

### 3.2.6 LC-MS/MS analysis

All peptide mixtures were purified by solid phase extraction on C-18 stage tips prior to MS analysis (214). For the model protein experiments, purified peptide mixtures were analyzed using a linear ion trap - FT-ICR cell (LTQ-FT; Thermo Fisher Scientific) mass spectrometer on-line coupled to an Agilent 1100 Series nanoflow HPLC using a nanospray ionization source (Proxeon Biosystems) holding columns packed into a 15 cm long, 75 μm I.D. fused silica emitters (8 μm diameter opening, pulled on a P-2000 laser puller from Sutter Instruments) using 3 μm diameter Reprosil-Pur C-18-AQ beads (Dr. Maisch, Germany, www.Dr-Maisch.com). Buffer A consisted of 0.5% aqueous acetic acid, and buffer B consisted of 0.5% acetic acid and 80% acetonitrile in water. Gradients were run from 6% B to 30% B over 75 minutes (flow 0.2 μL/minute), then from 30% B to 80% B in the next 20 minutes, held at 80% B for 8 minutes (while increasing the flow rate from 0.2 μL/minute to 0.6 μL/minute), before returning to 6% B to recondition the column. The LTQ-FT was set to acquire a full-range scan at 25,000 resolution from 350 to 1500 Th in the FT-ICR cell, followed by MS/MS of the top 5 ions in the LTQ (minimum intensity 500 counts). The mass window for precursor ion selection was 1.0, and the normalized collision energy was 35. The selected ions were then excluded from MS/MS for the next 180 seconds. Singly charged ions were excluded.

For experiments involving THP-1 cell lysates, the purified peptide mixtures were analyzed using an orthogonal quadrupole – time of flight mass spectrometer (Q-TOF) Impact II (Bruker Daltonics) on-line coupled to an Easy nano LC 1000 nanoflow HPLC (Thermo Scientific) using a Captive Spray nanospray ionization source (Bruker Daltonics) including a 2-cm-long, 100-µm-inner diameter fused silica trap column, 75-µm-inner diameter fused silica analytical column with an integrated 10 µm opening spray tip (pulled on a P-2000 laser puller from Sutter Instruments). The trap column was packed with 5 µm-diameter Aqua C-18 beads (Phenomenex, www.phenomenex.com), while the analytical column was packed with 3 µm-diameter Reprosil-Pur C-18-AQ beads (Dr. Maisch, www.Dr-Maisch.com). Buffer A consisted of 0.1% formic acid in water, and buffer B consisted of 0.1% formic acid in acetonitrile. Gradients were run at 250 nL/minute from 10% B to 35% B over 74 minutes, then the column was washed with 100% B for 15 minutes. The HPLC autosampler was maintained at 7°C. The Captive Spray Tip holder was modified similarly to an already described procedure (248) – the fused silica spray capillary was removed (together with the tubing which holds it) to reduce the dead volume, and the analytical column tip was fitted in the Bruker spray tip holder using a piece of 1/16" x 0.015 PEEK tubing (IDEX), an 1/16" metal two way connector, and a 16-004 Vespel ferrule. This instrument was operated under OTOF Control 1.8 (version 4.0.17.1840), HiStar 3.2 and Compass 4.2 (Bruker Daltonics) software. The Impact II was set to acquire an MS scan for 0.2 seconds followed by MS/MS scans for the remainder of a three second period using 0.06 seconds per MS/MS scan. The mass range for the MS scan was 300 to 2200 Th and for the MS/MS scans 200 to 2200 Th. The minimum precursor ion intensity for triggering MS/MS was 500 counts. Precursor ions were then excluded from MS/MS for the next 0.3 minutes. Singly charged ions

and ions with unknown charge state were excluded and Strict Active Exclusion was used. The error of mass measurement was usually within 5 ppm and was not allowed to exceed 10 ppm.

### 3.2.7 Protein identification and quantification

LTQ-FT raw files were analyzed using Mascot software. Database for Mascot searching was Uniprot-Swissprot (Version: May 30th, 2013, 540,261 sequences, 191,876,607 residues). Taxonomy was *mammalia* (540,261 sequences). Digestion enzyme was Trypsin/P, and a maximum of one missed cleavage was allowed. Precursor ion error was 20 parts per million (ppm). Fragment ion error was 0.5 Da. Instrument type was ESI-TRAP. For peptide scoring, the significance threshold was 0.01. For the differential alkylation method, variable modifications were carbamidomethyl and N-ethylmaleimide on cysteine and oxidation on methionine. For the dimedone experiment, variable modifications were dimedone and carbamidomethyl on cysteine and oxidation on methionine.

Analysis of Q-TOF data was performed using MaxQuant 1.5.2.8 (248). The data were searched against a database comprised of the protein sequences from human using the following parameters: peptide mass accuracy 20 ppm for the first search and 10 ppm for the second search; double SILAC as quantitation method. All other parameters were used as preset: trypsin enzyme specificity, variable modifications: biotin-maleimide, N-ethylmaleimide and carbamidomethyl on cysteine, oxidation on methionine. Only peptides and proteins with 99% confidence limit (1% false discovery rate) were considered as accurately identified. Data are available at ProteomeXchange Consortium (217) via the PRIDE partner repository with dataset identifier PXD003354, PXD003363, and PXD003365.

The proteins that underwent sulfenic acid modifications after 6-hour treatment of platelet releasate or $H_2O_2$ were submitted to Ingenuity Pathway Analysis (IPA, Ingenuity® Systems; http://www.ingenuity.com). To reveal which pathways are significantly represented by the quantified proteins, pathway analysis was performed using KEGG (Kyoto Encyclopedia of Genes and Genomes) database available at: http://www.genome.jp/kegg/pathway.html.

### 3.2.8 Primary monocyte isolation and integrin $\beta_2$ activity

Peripheral Blood Mononuclear Cells (PBMC) were separated from whole blood using Ficoll-Paque (GE Healthcare, Canada) according to the manufacturer's protocol. Primary monocytes were isolated from PBMC utilizing the Human Monocyte Enrichment Kit without CD16 depletion (StemCell, Canada) based on the manufacturer's instructions. After isolation, human primary monocytes were treated with RPMI media (control), 100 μM $H_2O_2$ or thrombin- or LPA induced platelet releasate for six hours. Treated monocytes were then washed twice with cold PBS, incubated with 2% BSA in PBS for one hour, followed by fluorophore-conjugated antibodies for CD14, CD16 and LFA-1 or Mac-1 for 30 minutes at 37°C, and stained with propidium iodide (PI) for two minutes prior to subjecting them to flow cytometry analysis on an LSR II Flow Cytometer System (BD Biosciences). Primary monocytes treated with 1 μM $MnCl_2$ for 30 minutes were used as positive control for integrin $\beta_2$ activation. Primary monocytes were first gated based on size and granularity, then on cell viability using PI staining and finally according to CD14 and CD16 channels. LFA-1 or Mac-1 was quantified using the mean fluorescent intensity (MFI) and normalized to the control as fold change.

For NOX inhibitor experiments, the primary monocytes ($CD14^+/CD16^+$) were treated with 10 μM DPI, or 1 μM, 3 μM, or 10 μM ML171 for one hour to block NOX; DMSO was used as control. After incubation, the cells were washed with PBS to remove inhibitors or DMSO and then treated with 100 μM $H_2O_2$ or thrombin- or LPA induced platelet releasate for six hours. Finally, the intracellular ROS level, and the activation levels of LFA-1 and Mac-1 were measured by FACS as described above.

In the P-Selectin (CD62P) binding inhibition experiment, thrombin- or LPA induced platelet releasate was pre-incubated with 1 μg/mL anti-CD62P blocking antibody for 30 minutes. After that, human primary monocytes were treated with the antibody-treated platelet releasate for six hours and non-treated platelet releasate as control. Intracellular level of ROS, the activation levels of LFA-1 and Mac-1 were assessed by flow cytometry.

## 3.3 Results and discussion

### 3.3.1 Validation of arsenite selective reduction using a protein model

The very first step towards quantifying sulfenic acid modifications on proteins is to confirm the selective reducing ability of arsenite. Aldolase contains eight free cysteines without disulfide formation in its native state, which makes it a suitable model to study oxidative modifications on cysteine residues. Besides sulfenic acid, the principle product between $H_2O_2$ and cysteine residues (244), this reaction can also lead to other reversible modifications such as disulfide bonds, but also irreversible modifications such as sulfinic acid and sulfonic acid. To verify the formation of sulfenic acid on aldolase upon treatment with $H_2O_2$, the treated aldolase was incubated with dimedone, which is a reagent specific for sulfenic acid (185). The results obtained

after LC-MS/MS analysis are shown in Appendix B.1 and Table 3-1. Of the four cysteine residues that were identified, Cys 178 and Cys 339 were modified by dimedone, which indicated the initial formation of sulfenic acid on these two cysteines.

**Table 3-1**. **Summary of sulfenic acid identifications in aldolase under treatments of different concentrations of $H_2O_2$.** Four cysteine residuces initially carrying sulfenic acid modification sites were identified by mass spectrometry in aldolase, using two different approaches: the direct approach used dimedone reaction with sulfenic acid (dimedone), the indirect approach used arsenite reduction of modified cystienes after free thiols had been blocked, and iodoacetamide labeling of the newly generated thiols (IAA).

| | **Control** | **10 μM $H_2O_2$** | **20 μM $H_2O_2$** |
|---|---|---|---|
| Cys178 | IAA | IAA+dimedone | IAA |
| Cys202 | IAA | IAA | IAA |
| Cys240 | IAA | IAA | IAA |
| Cys339 | IAA | IAA+dimedone | IAA+dimedone |

To assess the reduction of the newly formed sulfenic acids on aldolase by arsenite, a differential alkylation strategy was adapted as outlined in Figure 3-1. The original free cysteines were reacted with NEM, and the sulfenic acid modifications were converted to free thiols by arsenite and subsequently labeled with IAA. From the extracted ion chromatograms of the Cys-containing peptides (Appendix B.2, B.8), the peak areas of each NEM- and IAA-labeled peptide were calculated. The percentages of IAA-modification, a readout of the initial sulfenic acid modification, for the corresponding cysteines are shown in Figure 3-2. Five Cys-containing peptides were observed at all $H_2O_2$ concentrations, which together covered four cysteine

residues: Cys178, Cys202, Cys240, and Cys339. The extent of IAA-modification on Cys240 increased from ~50% at 10 mM $H_2O_2$ to ~70% at 20 mM $H_2O_2$, and on Cys339 from ~90% to nearly 100%. Cys202 was modified to 40% at both $H_2O_2$ concentrations. On Cys178, the extent of modification increased to over 90% at 10 mM $H_2O_2$, but decreased to around 70% at 20 mM $H_2O_2$. This implied the formation of other oxidative modifications, *e.g.* disulfide, that are not amenable to arsenite reduction. The accessibility of cysteines in aldolase does not seem to be a concern, as Cys135, Cys150, Cys178, and Cys202 are buried while Cys73, Cys240, Cys290, and Cys339 are exposed on the periphery of the protein in the native state (249). The lack of coverage for Cys73, Cys135, Cys150, and Cys290 is likely due to the formation of higher oxidation modifications that cannot be reduced by arsenite. Moreover, unlike dimedone, the differential alkylation method identified two more reactive sites and is adaptable to an affinity enrichment method such as the modified biotin switch assay we had published previously (245). Even though the development of dimedone-based chemical probes enables its application in the affinity enrichment method (184), the concern of the cross reactions between dimedone and aldehydes or amines under basic or organic solvent conditions still remains (250).

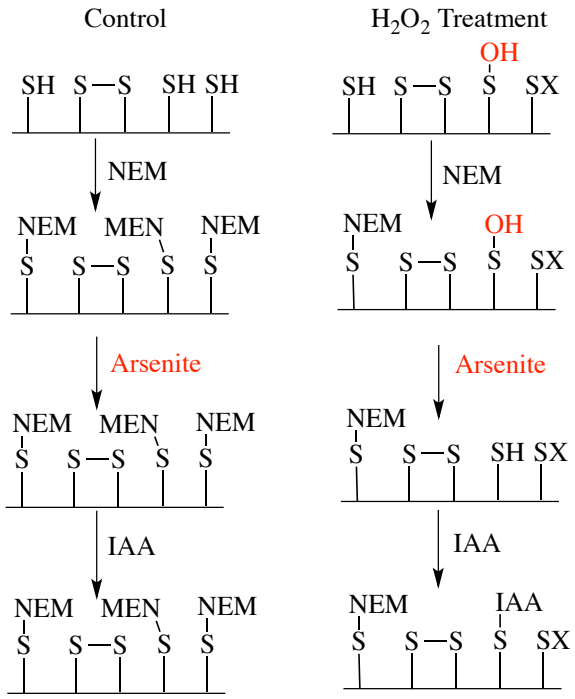


**Figure 3-1. Overview of the differential alkylation strategy for the detection of sulfenic acid modifications in model proteins.** Sulfenic acid modifications (-SOH) are generated by treatments with $H_2O_2$. Remaining free thiols (-SH) are blocked with N-ethylmaleimide (NEM), and sulfenic acid modifications are reduced with arsenite. The newly released free thiols are then labeled with iodoacetamide (IAA). Alternative oxidation states are abbreviated as -SX: cysteine oxidation other than sulfenic acid; -S-S-: disulfide.

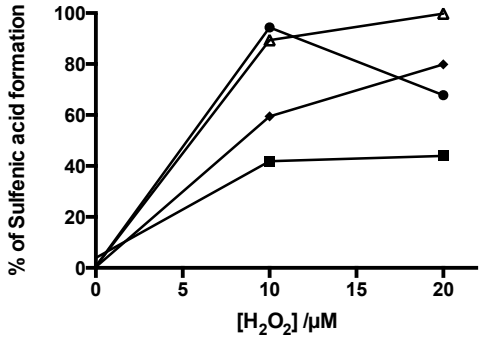


**Figure 3-2**. **The extent of sulfenic acid modification in aldolase in response to different doses of $H_2O_2$.** For each cysteine residue, Cys178 (•), Cys202 (▪), Cys240 (◆), and Cys339 (Δ), for which IAA-modification were detectable by mass spectrometry, the IAA-modification percentage was determined as follows: peak area of IAA-

modification of a specific cysteine divided by the sum of IAA- and NEM-modifications on this cysteine and plotted against the corresponding $H_2O_2$ doses.

To further investigate the formation of other reversible cysteine oxidations such as disulfide on aldolase, arsenite was replaced by DTT in the differential alkylation method to reduce all reversible cysteine oxidations (Appendix B.3). Eleven cysteine-containing peptides were identified at different concentrations of $H_2O_2$, which together covered six cysteine residues: Cys73, Cys178, Cys202, Cys240, Cys290, and Cys339 (Appendix B.4, B.9). Among them, Cys73 and Cys290 are newly covered cysteine residues in comparison with the quantification of the sulfenic acid in aldolase. This evidently supported the hypothesis that $H_2O_2$ reversibly oxidized these two cysteines into oxidation states that could not be reduced by arsenite and so resulted in their absence in the previous experiment. For Cys178, Cys202, Cys240, and Cys290, the percentages of IAA-modification were also higher when reducing all reversible oxidation modifications (Appendix B.5).

To further validate the selectivity of the reducing ability of arsenite on sulfenic acid but not other oxidative modifications especially disulfide, lysozyme was employed in the differential alkylation method. Lysozyme has 8 cysteine residues that all already form disulfide bonds, therefore it was not treated with $H_2O_2$ to avoid further oxidation. Lysozyme reduced by arsenite was compared with lysozyme reduced by DTT, and non-reduced lysozyme was used as control in the differential alkylation method (Appendix B.6, B.10). Cys94, Cys98, and Cys112 were quantified only in the DTT-reducing sample, indicating the inability of arsenite to break disulfide bonds. In contrast, Cys24, Cys82, Cys48, and Cys133 were quantified in all three samples. This

suggests the original existence of the reduced forms in lysozyme, as no significant increases of the percentages of IAA modifications on these four cysteine residues were observed in arsenite-reducing samples in comparison with non-reduced samples. This data suggested that no further reduction of disulfide bonds happened during the treatment with arsenite. Conversely, the percentages of IAA modifications on these four cysteine residues drastically increased in DTT-reducing samples (Appendix B.7).

### 3.3.2 Optimization of the modified biotin switch assay for sulfenic acid quantification

In a previous study, we had modified the biotin switch assay by using TCEP to reduce all reversible cysteine oxidation modifications and introducing SILAC for quantification (245). In order to extend the application of the modified biotin switch assay to selectively quantify sulfenic acid, we needed to incorporate arsenite into this assay and transfer the reaction from model proteins to a more complex system such as whole cell lysate. To determine the optimal concentrations and reaction times of arsenite, a pyridine-2-thione assay was performed using THP-1 cell lysate treated with $H_2O_2$. Different concentrations of arsenite were applied to THP-1 cell lysate to selectively reduce sulfenic acid. The reduced sulfenic acid was then reacted with biotin-HPDP to give rise to pyridine-2 thione. The dose- and time-dependent yields of these reactions are shown in Figure 3-3. The increase of the concentration of arsenite from 20 μM to 100 μM led to an increase of the production of pyridine-2-thione, while a further increase from 100 μM to 200 μM did not dramatically increase the production of pyridine-2-thione. For each different concentration of arsenite, the production of pyridine-2 thione rose quickly within one hour. The reactions reached a maximum around one and half to two hours and remained stable

afterwards. Thus, two-hour incubation with 200 μM arsenite guaranteed the complete reduction of sulfenic acid and was chosen for the modified biotin switch assay.

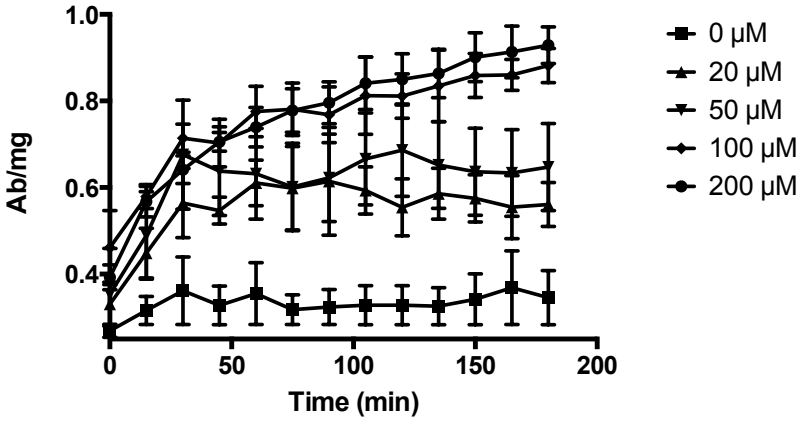


**Figure 3-3**. **Time course of the labeling of free thiols in THP-1 cell lysate with biotin-HPDP.** THP-1 cell lysates were incubated with different concentrations of arsenite, and the resulting free thiols were labeled with biotin-HPDP for different periods of time. The concentration of the reaction product, pyridine-2-thione, was monitored by measuring the absorption at 343 nm.

To quantify sulfenic acid in THP-1 cell lysate, we wanted to combine the SILAC labeling with the modified biotin switch assay as we had done before (245). We therefore examined whether the modified biotin switch assay would affect the quantification results. The heavy SILAC cells were incubated with 100 μM $H_2O_2$ for six hours, while the light SILAC cells were incubated with media as control. The two SILAC cell populations were mixed at a 1:1 ratio, and the lysate was subjected to the modified biotin switch assay (Figure 3-4). The non-enriched THP-1 cell lysate was subjected to SDS PAGE separation and in gel digestion with trypsin, and the resulting peptides analyzed by LC-MS/MS. For the modified biotin switch assay, free thiols were first blocked with NEM, and sulfenic acids then selectively reduced by arsenite, labeled with biotin-

maleimide and enriched with NeutrAvidin. The enriched peptides were then released, separated on SDS PAGE, and analyzed by LC-MS/MS. We plotted the frequency distribution of the logarithm of the heavy / light (H/L) ratios of all proteins quantified in the non-enriched and enriched samples using Gaussian distribution regression (Figure 3-5). Similar means of the H/L ratios for the non-enriched (0.9085) and the enriched (1.0150) sample were observed, indicating that the modified biotin switch assay has no effect on the distribution of H/L ratio.

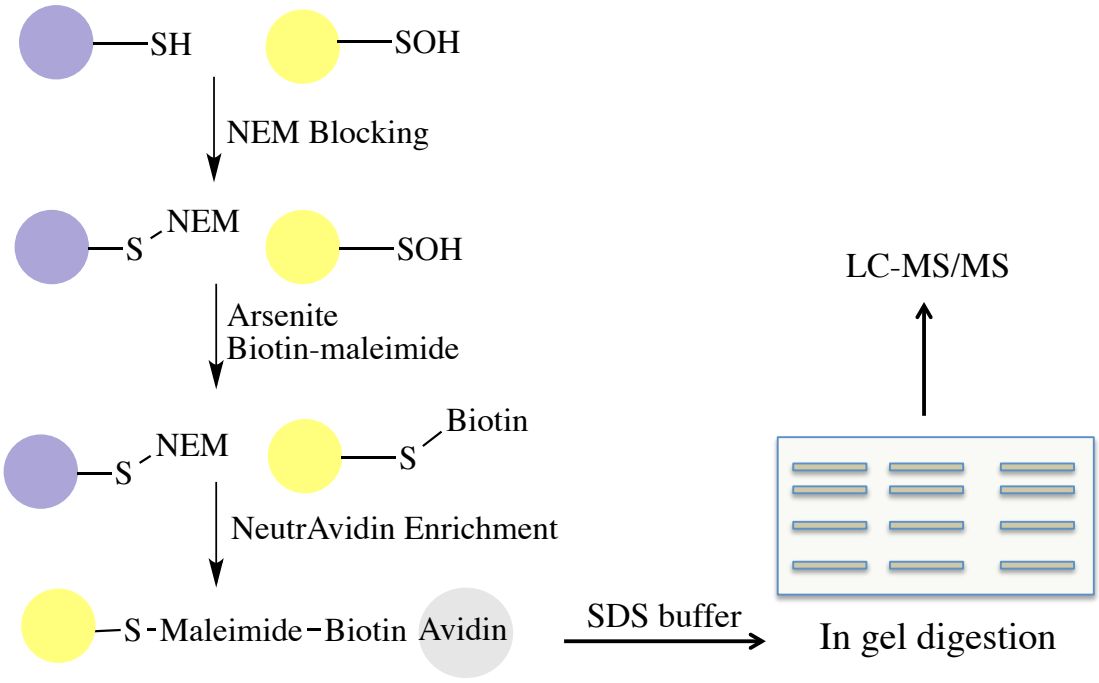


**Figure 3-4. Overview of the workflow in the modified biotin switch assay for protein sulfenic acid quantification.** Any protein may contain cysteines in the free thiol (-SH) or sulfenic acid modification (-SOH) form. Free thiols are first blocked with N-ethylmaleimide (NEM), and sulfenic acid modifications are then selectively reversed by arsenite to generate free thiols, which are then reacted with biotin-maleimide. Proteins enriched by NeutrAvidin are eluted, separated by gel electrophoresis, and subjected to mass spectrometric analysis.

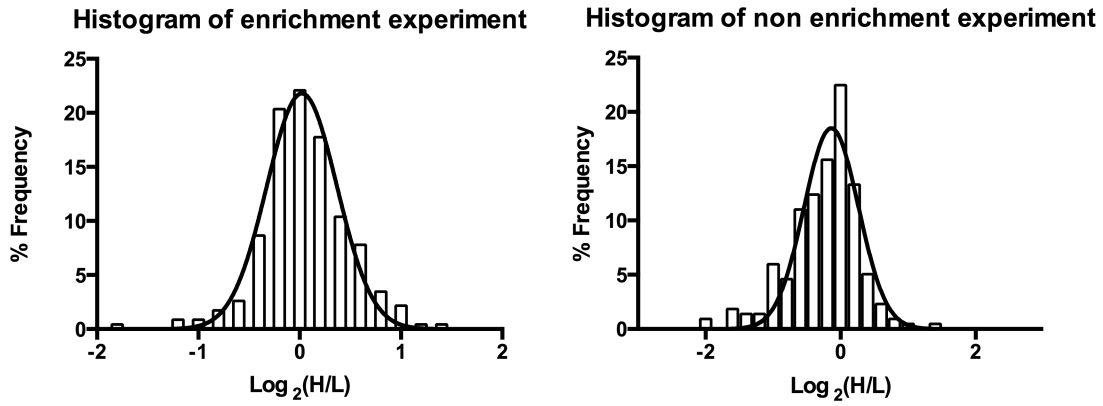


**Figure 3-5**. **The protein H/L ratio with and without the modified biotin switch assay.** Heavy SILAC-labeled THP-1 cells were treated with 100 μM $H_2O_2$ for six hours, and then combined with an equal amount of untreated light SILAC-labeled THP-1 cells. Samples were then subjected to the biotin switch assay, or left as is, followed by separation and mass spectrometric analysis. The frequency distribution of the corresponding protein H/L ratio and regression by Gaussian distribution in the mixed cell lysate was calculated for samples that (A) were subjected to the modified biotin switch assay or (B) was analyzed without enrichment.

### 3.3.3 Application of the biotin switch assay to an atherosclerotic model

In our previous study, we had established a model system in which monocytes were exposed to platelet releasate, and had observed that this elevated intracellular ROS level in monocytes. This had led us to explore redox signaling in this model by studying the total reversible cysteine oxidation proteome (245). In an attempt to improve our understanding of the redox regulation, we decided to study sulfenic acid modification in the same model. For this, heavy SILAC-labeled THP-1 cells were treated with LPA- or thrombin-induced platelet releasate (LPA-PR / Thr-PR) for six hours, and then combined with an equal amount of untreated light SILAC-labeled THP-1 cells. Treatment with 100 μM $H_2O_2$ was used as positive control. The mixed cell lysates were subjected to the modified biotin switch assay, and the enriched proteins were in-gel

digested and analyzed by LC-MS/MS. For each type of treatment, three biological replicates with different batches of THP-1 cells and platelet releasate from different donors were obtained (Table 3-2). By using stringent cutoff criteria, including a minimum of two peptides matched to each protein, an average of 4,156 peptides per repeat were identified corresponding to 1,161 proteins. Of all quantified peptides, an average of 481 peptides contained cysteines, which suggested ~10% enrichment efficiency, and an average of 211 Cys-containing peptides were quantified that had carried sulfenic acid modifications.

**Table 3-2. Enrichment efficiency of the modified biotin switch assay.** Heavy SILAC-labeled THP-1 cells were first treated with with A) 100 μM $H_2O_2$; B) LPA-PR; C) Thr-PR treatment for six hours, and then mixed 1:1 with untreated light SILAC-labeled THP-1 cells. After enrichment, protein separation, in-gel digestion, and mass spectrometric analysis of three replicates for each treatment condition, the corresponding numbers of proteins, peptides, Cys-containing peptides, and sulfenic acid modifications (Cys-SOH) were extracted from MaxQuant result files.

A)

| Replicate | Total number of proteins | Total number of peptides | Number of Cys-containing peptides | Number of Cys-SOH |
|---|---|---|---|---|
| 1 | 1205 | 5191 | 666 | 350 |
| 2 | 1061 | 3783 | 440 | 240 |
| 3 | 1378 | 5705 | 722 | 322 |

B)

| Replicate | Total number of proteins | Total number of peptides | Number of cys-containing peptides | Number of Cys-SOH |
|---|---|---|---|---|
| 1 | 1236 | 4670 | 516 | 210 |
| 2 | 1387 | 4761 | 520 | 217 |
| 3 | 1396 | 4916 | 588 | 250 |

C)

| Replicate | Total number of proteins | Total number of peptides | Number of cys-containing peptides | Number of Cys-SOH |
|---|---|---|---|---|
| 1 | 825 | 2449 | 265 | 109 |
| 2 | 836 | 2537 | 251 | 90 |
| 3 | 1127 | 3393 | 367 | 118 |

The apparent low enrichment efficiency was not unexpected. First, the high reactivity that a sulfenic acid group retains as an intermediate, together with its low abundance reduce the likelihood of arsenite being able to reduce it and biotin-maleimide to trap it. Moreover, only 1.42% of the amino acids in a protein mixture are cysteine residues, even though almost 95% of human proteins contain cysteine residues (251). As the modified biotin switch assay enriches sulfenic acid modifications on the protein level, it contains mostly non-Cys-containing peptides after protein digestion, resulting in a low enrichment efficiency for Cys-containing peptides. However, a key advantage of the protein level enrichment and the presence of non-Cys-containing peptides is the improved identification of proteins during database searching. Indeed, we were able to quantify a higher number of modified proteins than in our previous study utilizing peptide-level enrichment (245). In addition, being able to further separate the protein mixture into five fractions by gel electrophoresis prior to mass spectrometry analysis also helped expand the coverage of proteins/peptides in this study.

For each treatment, only Cys-containing peptides quantified in all three biological replicates were considered to be confirmed sulfenic acid sites. A total of 113, 118 and 40 such peptides

were quantified for $H_2O_2$, LPA-PR and Thr-PR treatments, respectively. Further comparison showed that 17 sulfenic acid modification sites were shared among $H_2O_2$, LPA-PR and Thr-PR treatments as listed in Table 3-3. The number of sulfenic acid modification sites quantified in the current study is comparable with other established methods that utilize dimedone-based direct sulfenic acid labeling probe (252, 253). In addition to identifying these sites, however, we also report the average H/L ratios of each sulfenic acid modification site in three replicates as listed in supplemental tables (Appendix B.11, B.12, B.13), which can be converted to the percentage of sulfenic acid modification by applying the equation: % of sulfenic acid = (H/L)/[1+(H/L)].

**Table 3-3. List of sulfenic acid modification sites of proteins in THP-1 cells that were quantified across all three conditions.** Proteins quantified across all conditions ($H_2O_2$, LPA-PR and Thr-PR treatment) were extracted from the corresponding result files, and listed with their Swiss-Prot identification, their name, the peptide sequence carrying the initial sulfenic acid modification site, and the heavy/light (H/L) ratio obtained using three replicates each.

| Protein ID | Protein name | Sequence | H/L±SD | | |
|---|---|---|---|---|---|
| | | | $H_2O_2$ | LPA-PR | Thr-PR |
| CAP1_HUMAN | Adenylyl cyclase-associated protein 1 | KTDGCHAYLSKNSLDCEIVSAKSSEMNVLIP | 0.95±0.07 | 1.08±0.17 | 0.83±0.14 |
| CAP1_HUMAN | Adenylyl cyclase-associated protein | TGLKLERALLVTASQCQQPAENKLSDLLAPI | 0.96±0.02 | 0.96±0.04 | 0.8±0.07 |
| CATA_HUMAN | Catalase | HRHRLGPNYLHIPVNCPYRARVANYQRDGPM | 0.74±0.03 | 1.09±0.12 | 0.84±0.06 |
| | | SHTFKLVNANGEAVYCKFHYKTDQGIKNLSV | 0.91±0.08 | 1.34±0.31 | 2.25±1.15 |
| CH60_HUMAN | 60 kDa heat shock protein, mitochondrial | ATRAAVEEGIVLGGGCALLRCIPALDSLTPA | 1.26±0.28 | 0.99±0.07 | 0.87±0.09 |
| ENOA_HUMAN | Alpha-enolase | LKVNQIGSVTESLQACKLAQANGWGVMVSHR | 1.1±0.04 | 0.68±0.06 | 1.01±0.19 |

| Protein ID | Protein name | Sequence | H/L±SD | | |
|---|---|---|---|---|---|
| | | | $H_2O_2$ | LPA-PR | Thr-PR |
| ITB2_HUMAN | Integrin β2 | GFEGSACQCERTTEGCL NPRRVECSGRGRCR | 1.23±0.07 | 0.79±0.2 | 0.83±0.02 |
| | | CECDTINCERYNGQVCG GPGRGLCFCGKCRC | 1.11±0.13 | 1.22±0.36 | 1.02±0.02 |
| KPYM_HUMAN | Pyruvate kinase | DIDSPPITARNTGIICTIGP ASRSVETLKEM | 1.13±0.17 | 0.71±0.04 | 0.85±0.16 |
| QCR1_HUMAN | Cytochrome b-c1 complex subunit 1, mitochondrial | IDDMMFVLQGQWMRLC TSATESEVARGKNIL | 0.77±0.08 | 1.08±0.09 | 0.82±0.16 |
| RINI_HUMAN | Ribonuclease inhibitor | LLPLLQQCQVVRLDDCG LTEARCKDISSALR | 0.78±0.06 | 1.1±0.1 | 1.03±0.14 |
| | | QISNNRLEDAGVRELCQ GLGQPGSVLRVLWL | 0.93±0.03 | 0.96±0.11 | 0.76±0.15 |
| TPIS_HUMAN | Triosephosphate isomerase | ARQKLDPKIAVAAQNC YKVTNGAFTGEISPG | 1.07±0.06 | 0.97±0.11 | 0.96±0.04 |
| | | QSTRIIYGGSVTGATCKE LASQPDVDGFLVG | 1.03±0.03 | 1.01±0.11 | 0.87±0.14 |
| TXND5_HUMAN | Thioredoxin domain-containing protein 5 | KVYVAKVDCTAHSDVC SAQGVRGYPTLKLFK | 1.16±0.04 | 0.97±0.31 | 1.15±0.14 |
| | | YNSMEDAKVYVAKVDC TAHSDVCSAQGVRGY | 1.16±0.04 | 0.97±0.31 | 1.15±0.14 |
| VASP_HUMAN | Vasodilator-stimulated phosphoprotein | MSETVICSSRATVMLYD DGNKR | 0.88±0.28 | 1.14±0.13 | 1.23±0.08 |

To better understand how monocytes were affected by platelet releasate treatments, we applied Ingenuity Pathway Analysis (IPA) and KEGG pathway analysis to identify enriched biological processes for the proteins that bear sulfenic acid modifications. IPA reported the top five canonical and tox (toxicity assessment of candidate compounds through toxicogenomics approaches) pathways with p-values <0.05 for each term for $H_2O_2$, LPA-PR and Thr-PR treatments, respectively (Figure 3-6). Glycolysis and gluconeogenesis were enriched for all three treatments, as also observed in our previous study (245). The pathways highlighted by toxicity analysis, i.e. mitochondrial dysfunction, oxidative stress and cell death, also revealed the

involvement of sulfenic acid formation in glucose metabolism. In contrast, KEGG pathway analysis calculated a p-value, but also false discovery rate (FDR) and Bonferroni-method adjusted p-value (cutoff criteria of p-value <0.05 per term). Besides glycolysis, KEGG pathway analysis also highlighted leukocyte transendothelial migration, which is of particular interest in atherosclerosis. The proteins identified within this pathway include integrin $\beta_2$, vasodilator-stimulated phosphoprotein, actin, guanine nucleotide-binding protein G(i) subunit $\alpha_2$, vinculin, and α-actinin-1. We selected integrin $\beta_2$ to validate the effect of platelet releasate on its activation.

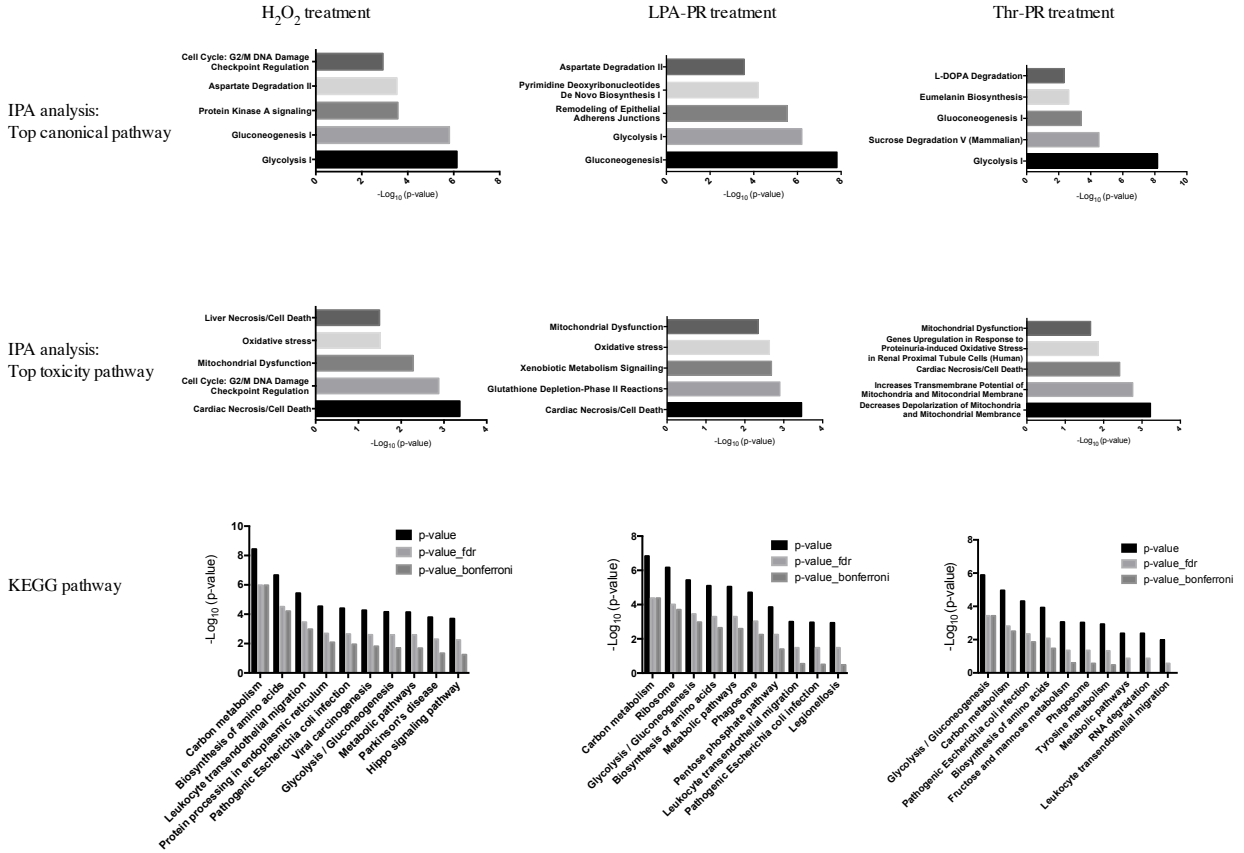


**Figure 3-6**. **Pathway analysis of proteins quantified with sulfenic acid modifications in THP-1 Cells.** The proteins detected with sulfenic acid modifications in THP-1 cells treated with (A) $H_2O_2$, (B) LPA Induced Platelet Releasate (LPA-PR), (C) Thrombin Induced Platelet Releasate (Thr-PR) were subjected to pathway analysis using

Ingenuity Pathway Analysis (top two panels) or KEGG pathway analysis (bottom panel). Shown are the calculated p-value for top canonical pathway and top toxicity pathway using Ingenuity Pathway Analysis, and the three different p-values obtained for KEGG pathway analysis.

### 3.3.4 Flow cytometry validation of integrin $\beta_2$ activated by redox signaling

Integrin $\beta_2$, also designated as CD18, forms complexes with various integrin α subunits and mediates leukocyte adhesion and dynamic cell-surface signaling through interactions with its counter-receptors. The ligation of integrin $\beta_2$ leads to its clustering and transition into a high-affinity state, which then triggers "outside-in" signaling to control acute and chronic inflammatory responses in leukocytes. The integrin $\beta_2$ is also the leading contributor to the recruitment of circulating monocytes from blood vessels into the surrounding tissues during atherosclerosis (254). There are three main forms of integrin $\beta_2$ complexes: LFA-1 (CD11a/CD18, $\alpha_L\beta_2$), Mac-1 (CD11b/CD18, $\alpha_M\beta_2$), and p150/95 (CD11c/18, $\alpha_X\beta_2$). Recent studies *in vitro* and *in vivo* highlighted two subfamilies of the integrin $\beta_2$ complexes, LFA-1 and Mac-1, which have distinct and cooperative roles in monocyte adhesion to, and migration through the endothelium (255, 256). To analyze the effect of platelet releasate or $H_2O_2$ treatments on the activation of monocyte integrin $\beta_2$, we measured the activity level of LFA-1 and Mac-1 on human primary monocytes by FACS. Indeed, LPA-PR, Thr-PR, and $H_2O_2$ all induced a significant 1.5- to 2-fold increase in the activity of LFA-1 and Mac-1 on monocytes compared with untreated monocytes (Figure 3-7 A, Figure 3-8 A). As the positive control, $Mn^{2+}$ strongly induced a 4.5-fold and 3.5-fold increase of LFA-1 and Mac-1 activity, respectively.

In our previous study, we had demonstrated that NADPH oxidase (NOX) was a potent enzyme for ROS production in THP-1 cells as well as primary monocytes during platelet releasate treatments (245). To verify the causality between the activation of NOX and integrin $\beta_2$, two different inhibitors, DPI (an inhibitor of flavoprotein oxireductases) and ML171 (a NOX-specific inhibitor), were applied to monocytes before treatment with platelet releasate or $H_2O_2$. DPI diminished LFA-1 activation to a level even lower than control (Figure 3-7 A), which linked LFA-1 activation to NOX activation. In contrast to LFA-1, DPI pre-treatment did not affect the increase in Mac-1 activity on monocytes induced by platelet releasate (Figure 3-8 A). ML171 is a NOX1-specific inhibitor ($IC_{50}$ of 0.25 μM) that only has marginal activity on other NOX isoforms ($IC_{50}$ > 3 μM in a HEK293-cell-based system) (257). Therefore, three concentrations (1 μM, 3 μM, and 10 μM) of ML171 were used, which all reduced the LFA-1 activation on monocytes induced by platelet releasate or $H_2O_2$ treatment (Figure 3-7 B). Moreover, the lower activity of LFA-1 in monocytes at higher concentrations of ML171 may indicate the inhibition of multiple NOX isoforms. In contrast, ML171 failed to block the activation of Mac-1, and even slightly increased Mac-1 activation at higher doses (Figure 3-8 B).

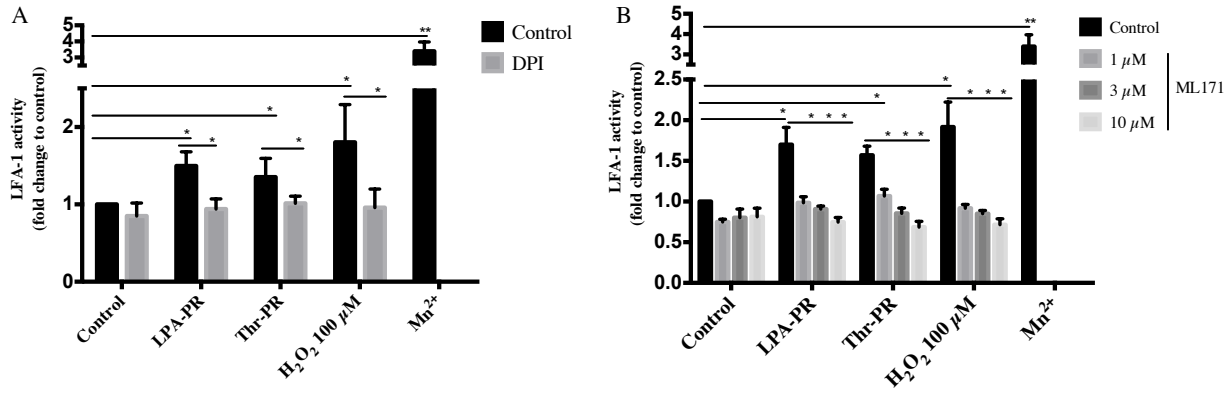


**Figure 3-7**. **Quantification of LFA-1 activation in primary monocytes upon $H_2O_2$ and platelet releasate treatment and DPI and ML171 inhibition of NOX.** Human primary monocytes were first treated with (A) DPI,

(B) different doses of ML171 or DMSO as a control for one hour. After that, monocytes were incubated with $H_2O_2$, different platelet releasate (LPA-PR and Thr-PR) or medium as a negative control for six hours and $Mn^{2+}$ as positive control for 30 minutes. Results are expressed as the mean ± SD; asterisks indicate significance (*, $p < 0.05$, **, $p < 0.01$; two-way ANOVA plus Tukey's post hoc test, $n$=3).

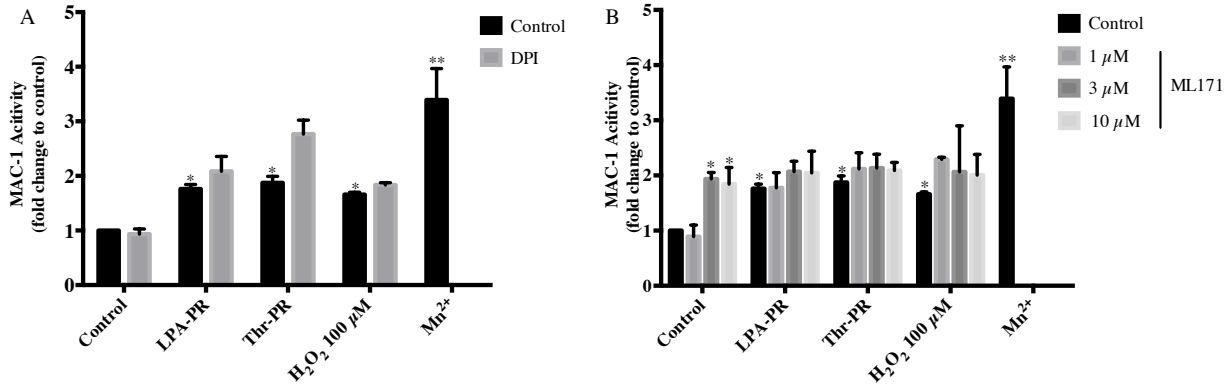


**Figure 3-8**. **Quantification of Mac-1 activation in primary monocytes upon $H_2O_2$ and platelet releasate treatment and DPI and ML171 inhibition of NOX.** Human primary monocytes were first treated with (A) DPI, (B) different doses of ML171 or DMSO as a control for one hour. After that, monocytes were incubated with $H_2O_2$, different platelet releasate (LPA-PR and Thr-PR) or medium as a negative control for six hours and $Mn^{2+}$ as positive control for 30 minutes. Results are expressed as the mean ± SD; asterisks indicate significance (*, $p < 0.05$, **, $p < 0.01$; two-way ANOVA plus Tukey's post hoc test, $n$=3)

Taken together, our results demonstrate the redox regulated LFA-1 and Mac-1 activation on primary monocytes in response to platelet releasate, which confirmed our finding of platelet releasate-induced redox regulation of integrin $\beta_2$ on THP-1 cells. Earlier reports had shown that the addition of exogenously $H_2O_2$ could activate LFA-1 and Mac-1 in neutrophils (258). We now prove that $H_2O_2$ also activates LFA-1 and Mac-1 in human primary monocytes, and platelet releasates show effects similar to $H_2O_2$ in activating LFA-1 and Mac-1. Moreover, our results demonstrate that the activation of LFA-1 is dependent on NOX-derived ROS, but the activation

of Mac-1 is not. Other studies have shown that monocytes interchangeably utilize both LFA-1 (in unstimulated venules) and Mac-1 (in inflammation) for intraluminal crawling (259, 260). Our results also match a previous observation of NOX not being the oxidase involved in the activation of Mac-1 in neutrophils (258).

Finally, we decided to test the effect of a known component of platelet releasates on the activation of integrin $\beta_2$. To this end, we eliminated the P-selectin activity with a blocking antibody, since interactions between P-selectin and PSGL-1 on monocytes trigger the monocyte activation and platelet-monocyte aggregate (PMA) formation (11). The antibody-treated platelet releasates were applied to human primary monocytes for six hours. Depletion of P-selectin did not affect ROS increase in human primary monocytes induced by platelet releasate (Figure 3-9 A). The activation level of LFA-1 on human primary monocytes also significantly increased after six hours incubation with the processed platelet releasates compared to the baseline (Figure 3-9 B). In contrast, depletion of P-selectin in LPA-PR, but not Thr-PR, significantly inhibited the increase Mac-1 activation after six hours platelet releasate treatment (Figure 3-9 C). These results demonstrated that the production of ROS and the activation of LFA-1 did not depend on the P-selectin – PSGL-1 interaction, whereas the activation of Mac-1 did. This corroborates a recent study, which had shown that the induction of pro-inflammatory signaling events in monocytes could be uncoupled from P-selectin signaling through PSGL-1 (238). A previous study in our lab had already identified the platelet releasate-induced up-regulation of very late antigen 5 (VLA-5, or integrin $\alpha_5\beta_1$) on THP-1 cells via a P-selectin-independent mechanism (261). Our findings now add new detail to this novel mechanism, and show that it also involves the production of ROS and the activation of LFA-1.

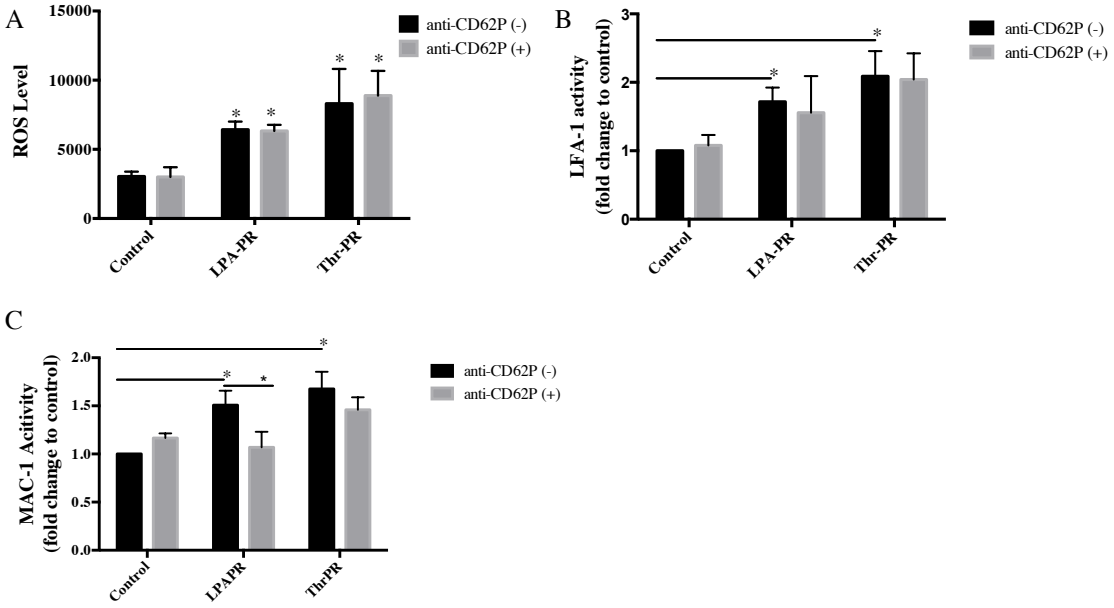


**Figure 3-9**. **Quantification of ROS production and the activation of LFA-1 and Mac-1 in human primary monocytes upon treatment with platelet releasates and P-selectin inhibition.** Platelet releasates were treated with P-selectin blocking antibody for 30 minutes prior to applying them to human primary monocytes for six hours. (A) Intercellular ROS level, the activation level of (B) LFA-1 and (C) Mac-1 were measured. Results are expressed as Mean +/- SD; asterisk indicates significance (*p<0.05, **p<0.01; two-way ANOVA plus Tukey's post hoc test, *n*=3)

Taken together, our novel quantitative proteomics approach enabled us to identify a new aspect of platelet-induced monocyte activation, and revealed a remarkable difference in the regulation of LFA-1 compared to Mac-1 via two separate mechanisms. This highlights the general utility of the approach in profiling sulfenic acid modifications in physiological and pathological conditions associated with oxidative stress.

# Chapter 4: A Novel Inhibitory Mechanism of oxPC Identified on Platelet Activation and its Association with ROS.

## 4.1 Introduction

Atherosclerosis, as well as other pathophysiological states in cardiovascular diseases, is closely associated with platelet hyperactivity (262) and increased prospective risks for arterial thrombosis (263). In high-risk patients, platelet hyperactivity is also highly related to dyslipidemia, the accumulation of oxidized lipids in plasma and vessel walls (264). Dyslipidemia links oxidative stress to the generation of biologically active oxidized phospholipids, which primarily exist in the form of oxidized low-density lipoproteins (oxLDL). Due to the heterogeneous characterization of oxLDL, the mechanisms underlying platelet hyperactivity during dyslipidemia *in vivo* are still largely unclear. Recently, a family of atherogenic oxidized phosphatidylcholines (oxPC) from oxLDL was found to be formed by multiple pathways *in vivo* at sites of intensified oxidative stress (64). These oxPC species are proposed to act through CD36, a scavenger receptor, to alter platelet activity. In human platelets, oxLDL also serve as ligands for CD36 to stimulate tyrosine kinase and protein kinase C (PKC)-dependent activation of NADPH oxidase 2 (NOX2) and the generation of reactive oxygen species (ROS) (47). Superoxide ($O_2^-$) can react rapidly with platelet or endothelium-derived nitric oxide (NO) to form peroxynitrite ($ONOO^-$). It has been suggested that the overwhelming inhibition of the key protective NO-soluble guanylyl cyclase (sGC)-cyclic guanosine monophosphate (cGMP) signaling pathway may result in uncontrolled platelet activity (265). The decreased

bioavailability of NO as a potent inhibitor of platelet activation is of particular importance for atherothrombosis.

ROS acts as intracellular messenger molecule(s) during the interaction of blood platelets with an agonist. The two primary agonists in hemostasis, thrombin and collagen, both lead to the burst of ROS (266, 267), although they act very differently on platelets at the molecular level. Thrombin or thrombin-derived peptide activates NOX to stimulate the production of ROS during platelet activation. The production of intracellular ROS significantly affects the activation of integrin $\alpha_{IIb}\beta_{3,}$ but not the secretion of alpha and dense granules or the shape change of platelets (116). Collagen binding to glycoprotein VI (GPVI) causes the production of ROS, which in return positively regulates the GPVI signaling cascade. ROS oxidizes tyrosine-protein phosphatase non-receptor type 11 (PTPN11) to promote the phosphorylation of spleen tyrosine kinase (Syk), vav guanine nucleotide exchange factor 1 (VAV1), and bruton agammaglobulinemia tyrosine kinase (Btk) in the linker for the activation of T cells (LAT) signaling complex. The LAT signaling complex further enhances the activation of phospholipase Cγ2 (PLCγ2), and elevates the cytosolic calcium level for platelet aggregation and thrombosis formation (114). Moreover, platelet-derived $O_2^-$ is a functionally relevant scavenger of platelet-derived NO to inhibit the anti-aggregatory effects of NO (268). In line with this, inhibitors of integrin $\alpha_{IIb}\beta_3$ enhance platelet NO release while suppressing platelet-derived $O_2^-$ (269). Some observations implicated platelet-derived ROS to have a prominent role in the late phase of platelet aggregation (270, 271). Although crucially involved, the mechanism by which ROS induces and enhances platelet aggregation in the biological context is not yet fully deciphered.

Apart from directly activating platelets, the accumulated evidence *in vitro* and *in vivo* suggests that the platelet-derived ROS increases the adhesion of platelets to vascular endothelium (272). In the meantime, the prothrombotic/proatherosclerotic effects of ROS were observed in the pathophysiology of atherothrombosis *in vivo* (273). However, the relevance of oxLDL to platelet-derived ROS and platelet hyperactivity in atherosclerosis is not yet fully elucidated. The purpose of the current study was to clarify the relationship between ROS and platelet behavior in atherothrombosis compared to that in hemostasis. To be able to apply proteomic tools such as those discussed in the previous chapters on platelets in future studies, we first need to exactly establish that ROS are produced during platelet activation induced by different stimuli occurring in atherothrombosis, hemostasis, and inflammation. Based on the observation that oxPC species are an important component of oxLDL that link ROS to atherothrombosis, we sought to examine the modulation of platelet activity by (ox)PC. By analyzing NOX as the potential ROS source in platelets, we further explored its association with platelet activation.

## 4.2 Materials and methods

### 4.2.1 Antibodies and reagents

Anti-human PAC-1- FITC (clone: PAC-1) was purchased from BD Bioscience and anti-human CD62P-APC (P-selectin) was obtained from BioLegend (CA, USA). Thiobarbituric acid was obtained from TCI (Tokyo, Japan); malondialdehyde derivative tetraethoxypropane from ACROS (NJ, USA); ML171 from Tocris bioscience (ON, Canada); H-Gly-Pro-Arg-Pro-OH (GPRP) from Millipore (ON, Canada); Collagen from Bio/Data Corporation; alkyl-LPA (16:0) from Avanti Polar Lipids (AL, USA); and p91ds-tat and s-gp91ds-tat from AnaSpec (CA, USA). Apyrase, 2', 7'-dichlorodihydrofluorescein diacetate ($H_2$DCFDA), thrombin, adenosine

diphosphate (ADP), dipenyleneiodonium (DPI), 1H- (1, 2, 4) oxadizaole (4, 3-a) quinoxalin-1-one (ODQ), lipopolysaccharide (LPS) (from Salmonella Minnesota), and all the other chemicals were obtained from Sigma (ON, Canada). 1-palmitoyl-2-arachidonoyl-*sn*-phosphatidylcholine (PAPC) was purchased from Santa Cruz biotechnology (CA, USA); KOdiA-PC, KDdiA-PC, POV-PC, and sulfosuccinimidyl oleate (SSO) were obtained from Cayman (ON, Canada).

### 4.2.2 Human platelet preparation

Ethical approval for platelet isolation from whole blood collected from healthy blood donors was obtained from the Clinical Research Ethics Board at the University of British Columbia (H12-00757) and informed consent was granted by blood donors. After discarding the first 2 mL, blood was drawn into vacutainer blood collection tubes containing acid citrate-dextrose (ACD solution A, BD Biosciences, Canada). Platelet-rich plasma was isolated from whole blood by an initial centrifugation at 150 g at room temperature for 15 minutes. Platelet-rich plasma was then supplied with a half volume of ACD buffer (11.5 mM citrate acid, 88.5 mM trisodium citrate, 111 mM glucose, pH=6) and centrifuged at 720 g at room temperature for 10 minutes to pellet platelets. Subsequently, the platelet pellet was carefully washed twice with CGSA buffer (10 mM tri-sodium citrate, 30 mM glucose, 120 mM sodium chloride and 1 U/mL apyrase, pH=6.5) to remove plasma proteins, and suspended in HEPES buffer (10 mM HEPES, 137 mM NaCl, 2.9 mM KCl, 12mM $NaHCO_3$, pH 7.4). Platelet counts were determined on a hemocytometer and adjusted to physiological concentration (300 x $10^9$/L) using HEPES buffer, and supplemented with $CaCl_2$ to a final concentration of 1.8 mM. Platelets were rested at room temperature for 30 minutes before stimulation.

### 4.2.3 Stimulations of human washed platelets

Washed platelets in HEPES buffer containing 1.8 mM $CaCl_2$ were stimulated with various concentrations of thrombin, collagen, ADP, alkyl-LPA, or LPS (from Salmonella Minnesota) for 10 minutes followed by the measurement of intracellular ROS level, P-selectin surface expression, integrin $\alpha_{IIb}\beta_3$ activation, and thromboxane synthase activity as described below.

To investigate whether PC species are agonists or antagonists in a time-dependent manner, washed platelets in HEPES buffer containing 1.8 mM $CaCl_2$ were incubated with 5 μM KOdiA-PC, KDdiA-PC, PAPC, or POV-PC for 0 or 15 minutes and then activated by various doses of thrombin, collagen, or alkyl-LPA for 10 minutes. For the treatment with inhibitors, washed platelets were treated with either 10 μM ODQ or 100 μM SSO for 15 minutes, followed by incubation with 5 μM KOdiA-PC, KDdiA-PC, PAPC, or POV-PC. The treated platelets were then characterized for aggregation, intracellular cAMP/cGMP level, ROS level, P-selectin surface expression, or integrin $\alpha_{IIb}\beta_3$ activation.

### 4.2.4 Aggregation study

Washed platelets (200 μL) in HEPES buffer containing 1.8 mM $CaCl_2$ were incubated at 37°C for 3 minutes before adding agonists. For multiplexed screens, platelet aggregation was monitored using a SpectraMax Plus384 plate reader (Molecular Devices, Sunnyvale, CA, USA) to measure optical density through the sample at 630 nm. The platelets were agitated for 10 seconds before the first reading, after which point readings were taken at intervals of 20 seconds for 10 minutes.

### 4.2.5 Measurements of ROS production, P-selectin expression, and integrin $\alpha_{IIb}\beta_3$ activation by flow cytometry

For detection of intracellular ROS, washed platelets were preloaded with 2', 7'-dichlorodihydrofluorescein diacetate ($H_2$DCF-DA) for half an hour in the dark. For determination of P-selectin expression and integrin $\alpha_{IIb}\beta_3$ activation, washed platelets were stained with anti-P-selectin-APC antibody (5 μg/mL) and anti-activated integrin $\alpha_{IIb}\beta_3$-FITC antibody (5 μg/mL) for half an hour in the dark. Washed platelets were then activated by different stimuli in the presence of GPRP. Flow cytometry analysis of platelets was performed, without fixation, on an LSR II Flow Cytometer System (BD Biosciences, Missisauga, ON, Canada). $H_2$DCF-DA and FITC conjugated-antibody were excited at 488 nm, and APC conjugated-antibody at 633 nm. The fluorescence emission of $H_2$DCF-DA, FITC conjugated-antibody and APC conjugated-antibody were detected through the 520/20, 530/30, and 660/20 nm filters, respectively. A minimum of $5 \times 10^4$ cells per sample was acquired for each measurement.

### 4.2.6 Thromboxane synthase activity

Thromboxane synthase activity was determined by fluorometric quantification of derivatized malondialdehyde as previously described (274). Briefly, 0.7 mL aliquots of washed platelets in HEPES buffer were incubated with various reagents at 37°C in a thermomixer and stopped by addition of 0.4 mL ice-cold trichloroacetic acid (20% wt/vol). The samples were kept on ice for 10 minutes and then centrifuged for 10 minutes at 14000 g. Equal volumes (0.6 mL) of the derivatization reagent thiobarbituric acid (0.5% wt/vol) and the supernatant were combined and incubated for 30 minutes at 70°C. The mixture was incubated for an additional 30 minutes at

room temperature. Fluorescence was measured on an Agilent Cary Eclipse Fluorescence Spectrophotometer (Agilent, Santa Clara, CA, USA) at an excitation wavelength of 533 nm with a slit width of 2.5 nm and an emission wavelength of 550 nm with a slit width of 10 nm. The standards were prepared from the stable malondialdehyde (MDA) derivative tetraethoxypropane with thiobarbituric acid in the presence of trichloroacetic acid (20% wt/vol).

### 4.2.7 Cyclic AMP and cyclic GMP ELISA assays

Washed platelets were treated with different stimuli and pelleted by centrifugation at 720 g for 10 minutes at 4°C. The platelet pellets were then lysed in 0.1 M HCl at room temperature for 20 minutes and centrifuged at ≥ 600 g to remove cellular debris. The platelet lysates were assayed immediately or stored frozen for later analysis according to the manufacturer's protocol (Enzo Life Sciences, Farmingdale, NY, USA). In the meantime, protein concentrations were determined by the BCA assay (Sigma, Oakville, ON, Canada) to normalize the concentration of cAMP or cGMP as pmol of cAMP/cGMP per milligram of total protein.

### 4.2.8 Statistical analysis

All experiments were performed at least in triplicate, and results are presented as mean ± SD. The data were analyzed using analysis of variance (ANOVA) followed by the Tukey post hoc test or Dunnett's test. Differences were considered statistically significant when a p-value was less than 0.05.

## 4.3 Results

### 4.3.1 The response of platelets to LPA or (ox)PC species

Platelet activation induced by the atherosclerotic stimulus alkyl-LPA is donor-dependent, and was categorized into weak (percentage of PAC-1 activity <5%) and strong (percentage of PAC-1 activity >5%) subgroups based on the activation level of integrin $\alpha_{IIb}\beta_3$ (PAC-1) in our study. ROS production was monitored within both subgroups, but in neither of them it significantly increased (Figure 4-1 A, B). For P-selectin expression, platelets from strong responders showed dramatic elevation of P-selectin expression at concentrations of LPA higher than 20 μM (Figure 4-1 C, D), a trend that was similar for the activation of integrin $\alpha_{IIb}\beta_3$ (Figure 4-1 E, F).

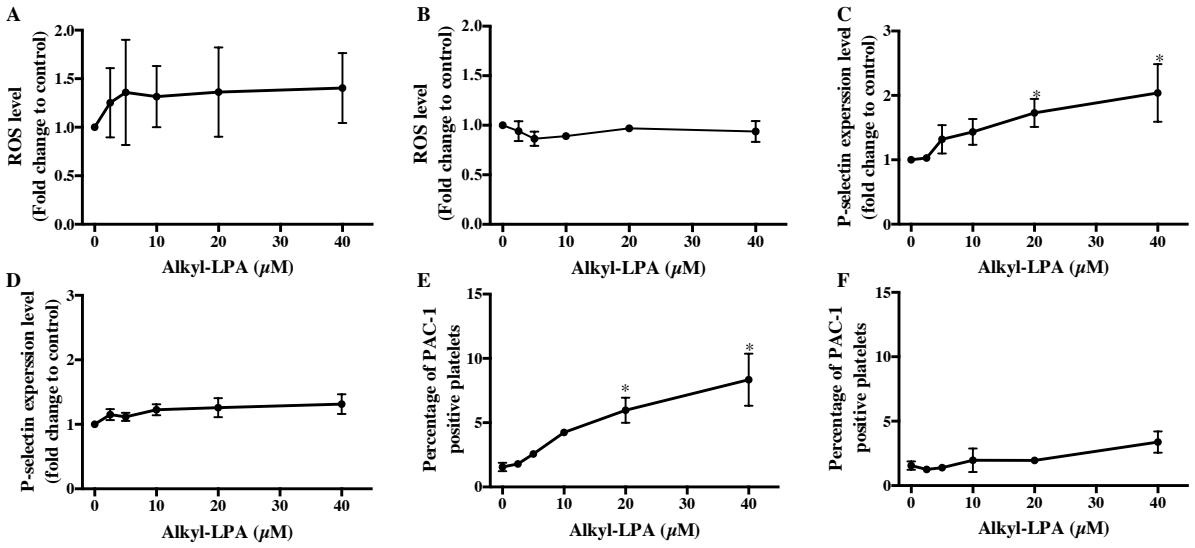


**Figure 4-1. Different concentrations of alkyl-LPA induced the activation of platelets without the production of ROS.** The treated platelets were characterized for intracellular ROS level (A-B), P-selectin expression level (C-D), and integrin $\alpha_{IIb}\beta_3$ (PAC-1) activation level (E-F). Platelets are categorized into strong (percentage of PAC-1 activity >5%) (A, C, E) and weak activation (percentage of PAC-1 activity <5%) (B, D, F) groups based on the activation level of PAC-1. No significantly increase of ROS production was observed within both groups. Results are expressed as mean +/- SD; asterisk indicates significance (*p<0.05, one-way ANOVA plus Dunnett's test, *n*=5)

KOdiA-PC was chosen as the representative of the oxidized 1-palmitoyl-2-arachidonyl-phosphatidylcholine (PAPC) series with PAPC as control, while KDdiA-PC was chosen from the oxidized 1-palmitoyl-2-linoleoyl-phosphatidylcholine (PLPC) series with POV-PC as control (Scheme 4-1). The *sn*-1 position of each of the (ox)PC is bound with palmitic acid, and the *sn*-3 position is bound with a choline group. The *sn*-2 position is linked to different polyunsaturated acyl residues or their oxidized forms (275).

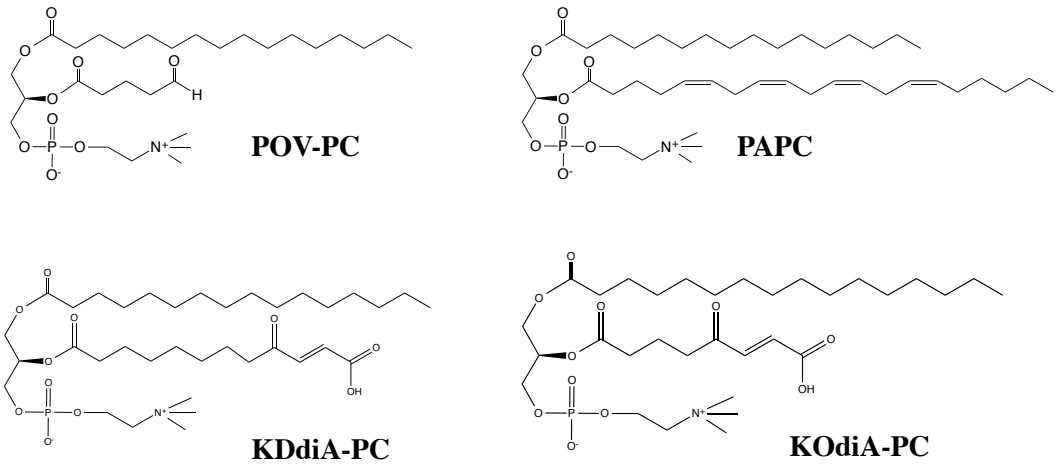


**Scheme 4-1. Chemical structures of different phosphatidylcholine (PC) species and their oxidized derivatives (oxPC).**

Platelets were incubated with 5 μM of each (ox)PC species for 15 minutes, followed by measurements of platelet aggregation, P-selectin expression, integrin $\alpha_{IIb}\beta_3$ activation, and ROS production. However, none of the four species led to significant platelet aggregation (Figure 4-2 A), or platelet activation as measured by P-selectin expression and integrin $\alpha_{IIb}\beta_3$ activation (Figure 4-2 B, C). They also did not elicit ROS production (Figure 4-2 D). In contrast, intracellular cGMP levels in platelets were significantly increased by treatments with the (ox)PC species. KDdiA-PC and POV-PC led to a more than 20-fold increase of cGMP compared with

that in control (Figure 4-2 E). KOdiA-PC and PAPC induced more than 4-fold increase of cGMP level. Intracellular cAMP level was also measured, with a less than two-fold increase upon (ox)PC treatments compared with non-treated platelets being observed (Figure 4-2 F). The extent of change and the absolute concentration of cAMP were lower than those of cGMP in platelets.

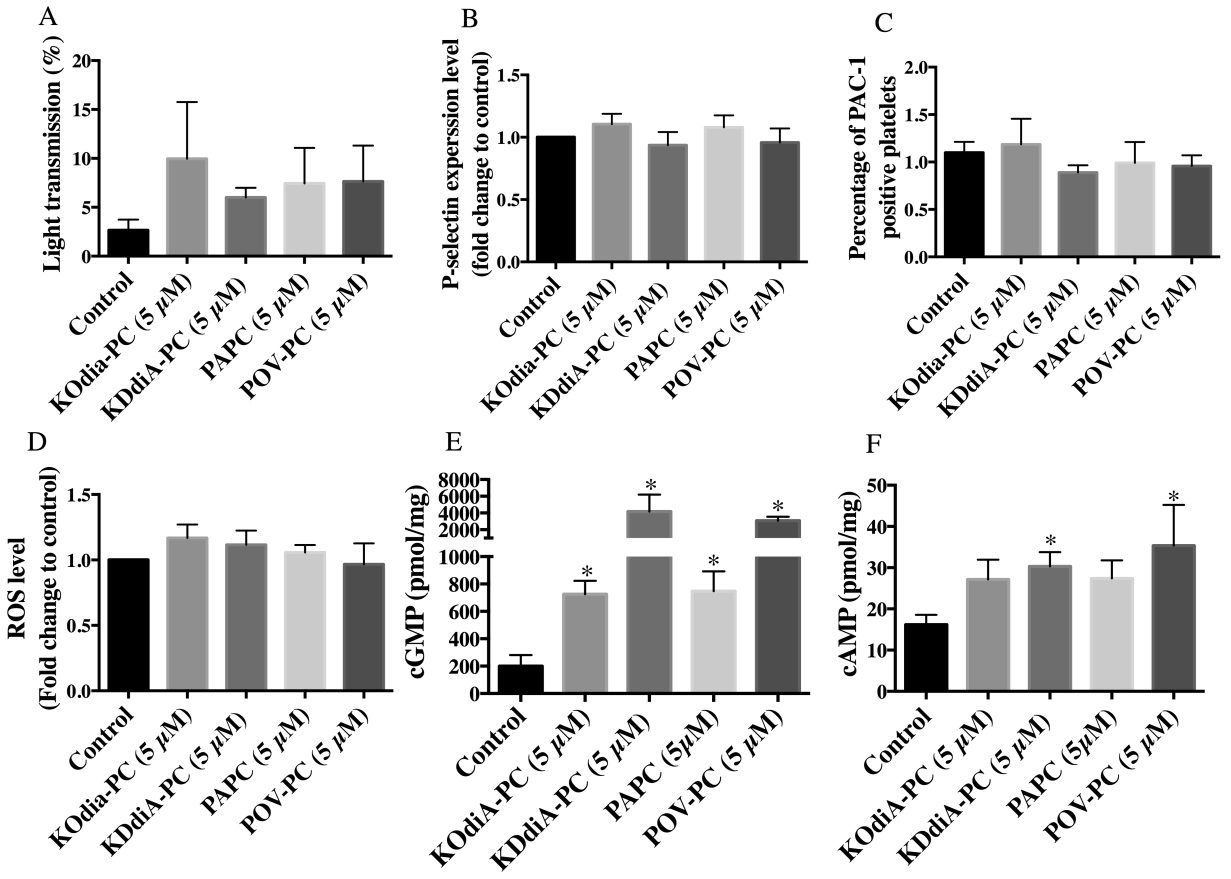


**Figure 4-2. (ox)PC species strongly elevated intracellular cGMP level in human platelets, but not platelet aggregation or activation.** Platelet aggregation (A), P-selectin expression level (B), integrin $\alpha_{IIb}\beta_3$ activation level (C), and ROS production level (D) did not change dramatically after 15 minutes treatment with (ox)PC species. Four (ox)PC species all significantly increased cGMP level (E). KDdiA-PC and POV-PC also increased cAMP level (F). (*$p<0.05$, one-way ANOVA plus Dunnett's test, $n=4$)

### 4.3.2 ROS generation, P-selectin expression, and integrin $\alpha_{IIb}\beta_3$ activation in platelets induced by agonists in hemostasis

To compare the effects of platelet agonists associated with atherosclerotic plaques with those relevant in hemostasis on ROS production and platelet aggregation, platelets were stimulated with thrombin, collagen, or adenosine diphosphate (ADP). The intracellular level of ROS in platelets significantly increased upon stimulation with high doses of thrombin (0.5 U/mL or 1 U/mL) or collagen (0.1 mg/mL or 0.19 mg/mL), but not by low doses of thrombin (0.02 U/mL or 0.2 U/mL) or collagen (0.01 mg/mL) (Figure 4-3 A, B). Unlike thrombin and collagen, ADP did not elicit ROS production at any concentration (Figure 4-3 C). To test platelet activation level, P-selectin expression (Figure 4-3 D-F) and integrin $\alpha_{IIb}\beta_3$ activation (Figure 4-3 G-I) were also monitored with these three agonists. Thrombin at all concentrations significantly induced the surface expression of P-selectin and activated integrin $\alpha_{IIb}\beta_3$ on platelets, as did a high dose (0.1 mg/mL or 0.19 mg/mL) but not a low dose (0.01 mg/mL) of collagen treatment. ADP at different concentrations also led to integrin $\alpha_{IIb}\beta_3$ activation, but had no effect on P-selectin expression. Intracellular cAMP and cGMP levels in platelets were also measured by ELISA, but none of them were significantly changed during platelet activation induced by these three agonists (Figure 4-4)

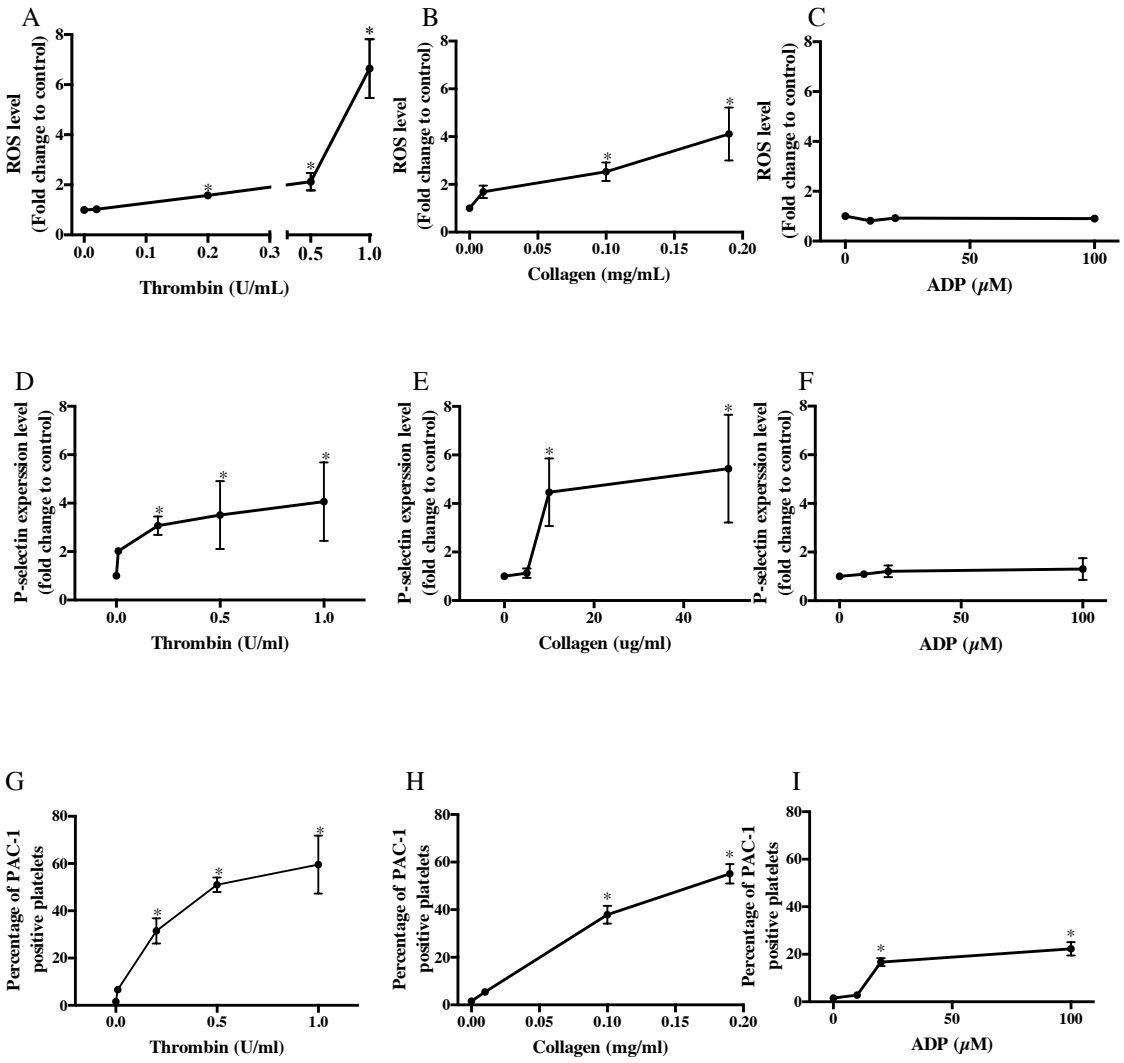


**Figure 4-3. Thrombin and collagen induced ROS production in platelet activation.** Intracellular ROS level increased in a dose-dependent manner in platelets activated by thrombin (A) and collagen (B) but not ADP (C). P-selectin expression and integrin $\alpha_{IIb}\beta_3$ activation also significantly increased in platelets activated by thrombin (D, G) or collagen (E, H). ADP significantly induced integrin $\alpha_{IIb}\beta_3$ activation in platelets. Results are expressed as mean +/- SD; asterisk indicates significance (*$p<0.05$, one-way ANOVA plus Dunnett's test , $n$=5)

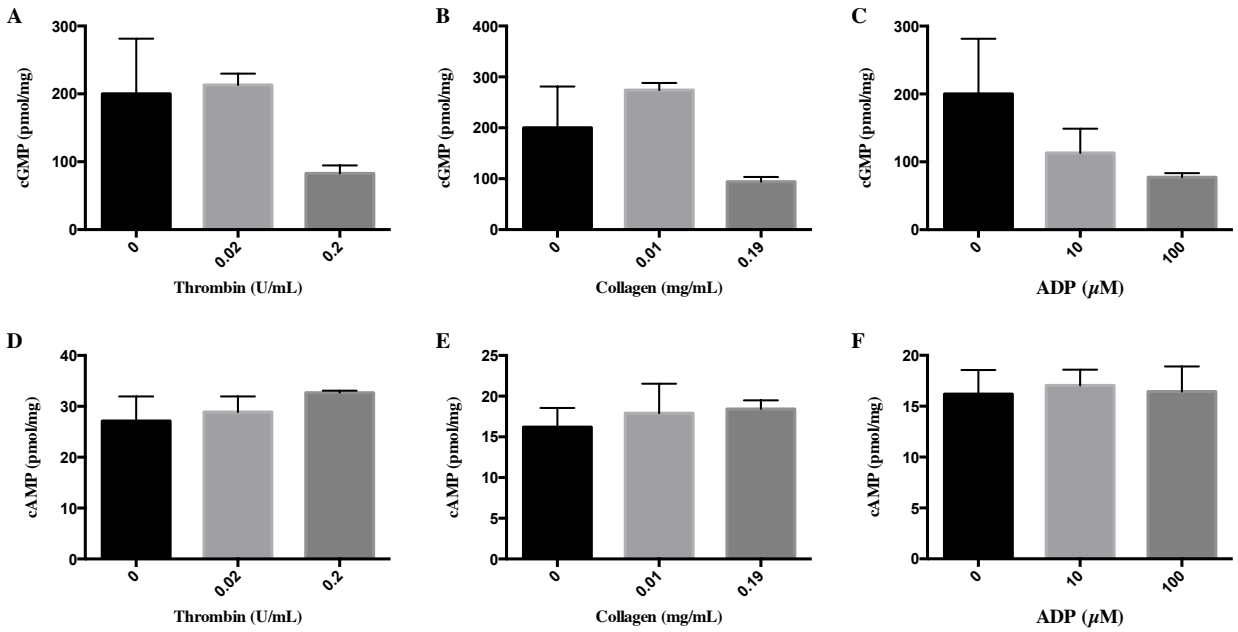


**Figure 4-4. No significant increase of the intracellular level of cGMP and cAMP was observed in platelets upon activation with different stimuli.** Thrombin, collagen, or ADP did not significantly increase or decrease intracellular level of cGMP (A) or cAMP (B) at various concentrations. Results are expressed as mean +/- SD. (one-way ANOVA plus Dunnett's test, *n*=3)

### 4.3.3 Thromboxane synthase activity in platelets stimulated by different agonists

To further compare the role of different agonists in platelet activation, the activity of thromboxane synthase was quantified by the determination of malondialdehyde (MDA) production by means of the thiobarbituric acid (TBA) reaction. In the TBA reactions, MDA reacted with TBA to generate a red, fluorescent 1:2 MDA: TBA adduct at low pH and elevated temperature. Thrombin at concentrations higher than 0.5 U/mL significantly induced the production of MDA, whereas other stimuli like collagen, ADP, or alkyl-LPA did not (Figure 4-5).

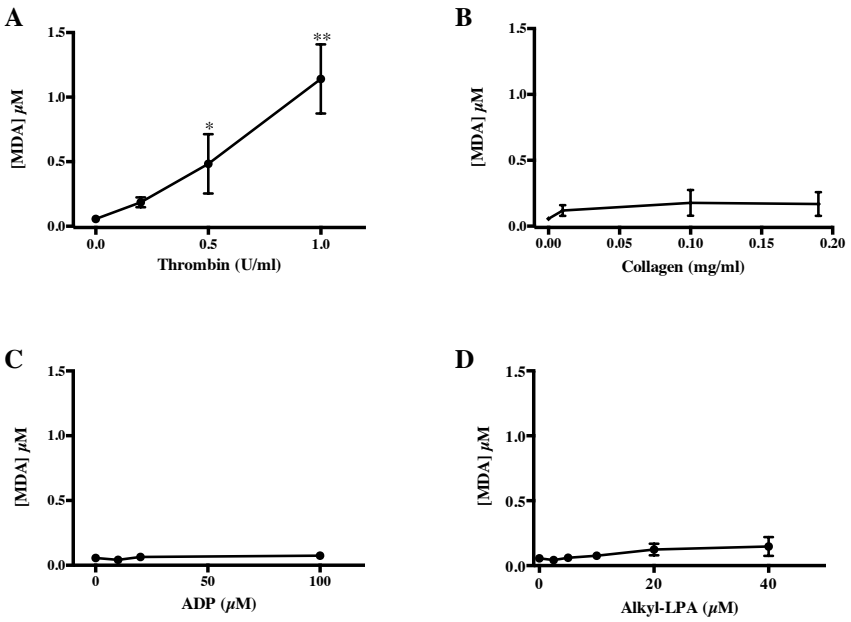


**Figure 4-5. Thrombin significantly induced thromboxane synthase activity in platelets.** Washed platelets were activated by different concentrations of thrombin (A), collagen (B), ADP (C), or alkyl-LPA (D), and the thromboxane synthase activity was measured through the fluorescent determination of MDA production. Results are expressed as Mean +/- SD; asterisk indicates significance (*p<0.05, one-way ANOVA plus Dunnett's test, *n*=3)

### 4.3.4 Platelet NADPH oxidase as the major source of ROS production

We used different NOX inhibitors to investigate the possible NOX isoforms as sources of intracellular ROS production. Thrombin (0.2U/mL) or collagen (0.1mg/mL), which were able to trigger significant ROS production, was employed here. The NOX non-specific inhibitor DPI, as well as the NOX2-specific inhibitor gp91ds-tat, significantly prevented ROS production induced by thrombin or collagen in platelets, while the scrambled peptide S-gp91ds-tat as a control of gp91ds-tat did not have any effect on ROS production (Figure 4-6 A). The NOX-specific inhibitor ML171 exhibited a dose-dependent inhibition effect on ROS production in activated platelets. ML171 at 1 μM specifically inhibited NOX1 over other NOX isoforms (IC50 > 3 μM),

and indeed significantly inhibited ROS production. The inhibition effect of ML171 persisted with increasing concentrations (Figure 4-6 B).

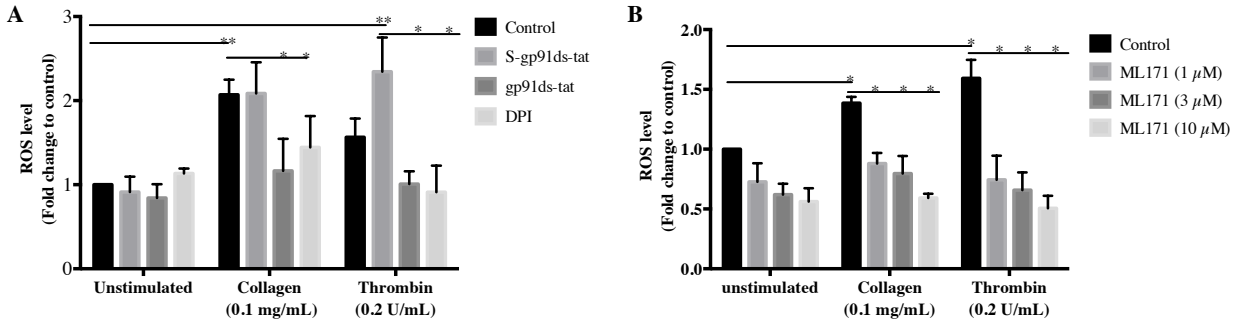


**Figure 4-6. NOX inhibitors prevented thrombin or collagen induced ROS production in platelets.** (A) NOX2 specific inhibitor gp91ds-tat or NOX non-specific inhibitor DPI and (B) different concentrations of NOX1 specific inhibitor ML171 all significantly inhibited ROS production in platelets induced by thrombin or collagen. S-gp91ds-tat, the scrambled peptide of gp91ds-tat, did not interfere ROS production. Results are expressed as mean +/- SD; asterisk indicates significance (*p<0.05, two-way ANOVA plus Tukey's post hoc test, *n*=3)

To further address the role of ROS in regulating platelets, we assessed the effect of NOX inhibitors on P-selectin expression and integrin $\alpha_{IIb}\beta_3$ activation. DPI and gp91ds-tat significantly reduced the increase of P-selectin expression provoked by collagen (0.1 mg/mL) or thrombin (0.2 U/mL), but did not block it completely (Figure 4-7 A). ML171 at all concentrations successfully inhibited the P-selectin expression induced by collagen, whereas only 10 μM ML171 partially reduced P-selectin expression induced by thrombin stimulation (Figure 4-7 B). The effects of different NOX inhibitors on integrin $\alpha_{IIb}\beta_3$ were consistent with those on P-selectin. DPI, gp91ds-tat, or ML171 at 10 μM were able to inhibit the activation of integrin $\alpha_{IIb}\beta_3$ induced by thrombin (0.2 U/mL) or collagen (0.1 mg/mL) (Figure 4-7 C, D). ML171 at low

concentrations, 1 μM or 3 μM, inhibited integrin $\alpha_{IIb}\beta_3$ activation induced by collagen, but not thrombin (Figure 4-7 D).

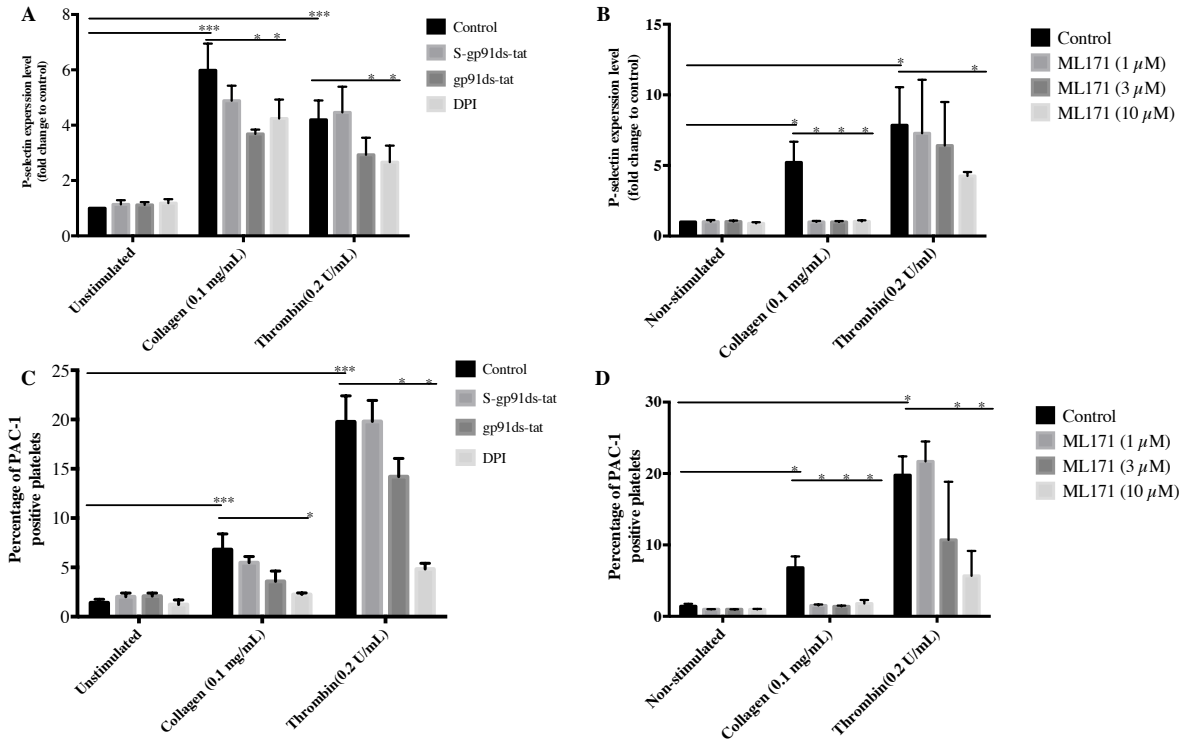


**Figure 4-7. NOX inhibitors partially prevented P-selectin expression and integrin $\alpha_{IIb}\beta_3$ activation induced by thrombin or collagen.** DPI, gp91ds-tat (A), or ML171 (B) significantly inhibited P-selectin expression in platelets induced by thrombin or collagen. Similar results were observed with integrin $\alpha_{IIb}\beta_3$ activation. Results are expressed as Mean +/- SD; asterisk indicates significance (***p<0.001, *p<0.05, two-way ANOVA plus Tukey's post hoc test, *n*=3)

### 4.3.5 ROS production but no activation in human platelets induced by lipopolysaccharide treatment

To assess the effect of stimuli relevant to the inflammation progress on platelet activation, washed platelets were treated with lipopolysaccharide (LPS) (from Salmonella Minnesota) ranging from 1 to 10 μg/mL for 10 minutes, followed by the analysis of ROS production, P-

selectin expression, and integrin $\alpha_{IIb}\beta_3$ activation. LPS at concentrations higher than 5 μg/mL significantly increased ROS levels in platelets (Figure 4-8 A). However, LPS had no effect on P-selectin expression or integrin $\alpha_{IIb}\beta_3$ activation (Figure 4-8 B, C). DPI (non-specific NOX inhibitor) and gp91ds-tat (NOX2-specific inhibitor) significantly inhibited LPS-induced ROS production in platelets, while the scrambled peptide S-gp91ds-tat as the control of gp91ds-tat had no effect on ROS production. ML 171 (NOX1-specific inhibitor) at 10 μM strongly blocked ROS production in platelets stimulated with LPS, but also reduced the ROS level in the non-stimulated platelets (Figure 4-8 D).

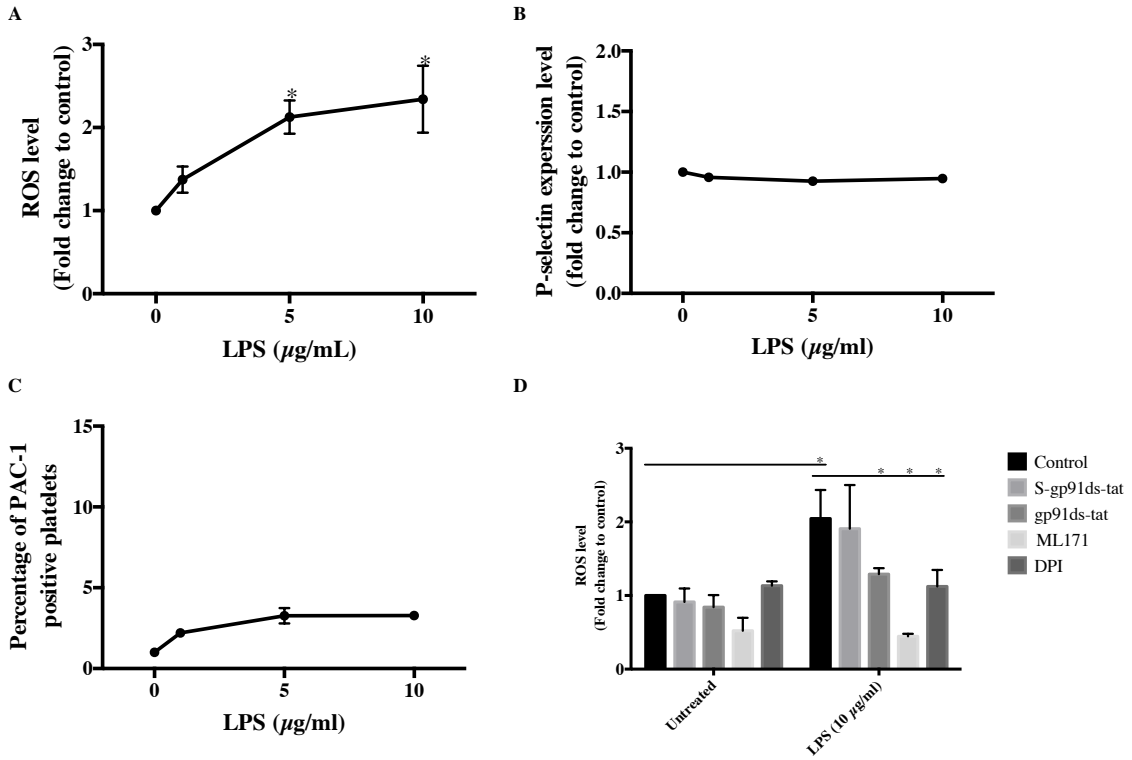


**Figure 4-8. LPS induced NOX-derived ROS production in platelets without induction of platelet activation.** (A) Different concentrations of LPS significantly stimulated the production of ROS in platelets. The P-selectin expression level (B) and integrin $\alpha_{IIb}\beta_3$ activation level (C) did not significantly change in platelets under the treatments of various concentrations of LPS. (D) Different NOX inhibitors (gp91ds-tat, ML171, and DPI)

successfully inhibited ROS production induced by LPS in platelets. The scrambled peptide S-gp91ds-tat as control of gp91ds-tat had no effect on ROS production, while ML171 reduced ROS level in untreated platelets. Results are expressed as Mean +/- SD; asterisk indicates significance. (*$p<0.05$, two-way ANOVA plus Tukey's post hoc test, $n=3$)

### 4.3.6 The inhibition effect of different (ox)PC species on platelet activation

The initial incubation of platelets for 15 minutes with either one of the two oxPC species KOdiA-PC and KDdiA-PC, or their controls PAPC and POV-PC, significantly inhibited platelet aggregation induced by 0.2 U/mL thrombin, 20 μM alkyl-LPA, or collagen at 0.01 or 0.19 mg/mL (Figure 4-9 A). To test the hypothesis that the inhibition effects of (ox)PC species on platelet activity are dependent on the timing of addition, another set of aggregation experiments involving the simultaneous addition of (ox)PC species with different agonists was conducted. Only KOdiA-PC caused a decrease in platelet aggregation induced by 0.2 U/mL thrombin, while other (ox)PC species did not inhibit platelet aggregation initiated by thrombin when added simultaneously. KOdiA-PC and KDdiA-PC showed a statistically significant inhibition of platelet aggregation induced by collagen at 0.01 mg/mL. All four (ox)PC species significantly inhibited platelet aggregation induced by collagen at 0.19 mg/mL or alkyl-LPA at 2.5 or 20 μM (Figure 4-9 B).

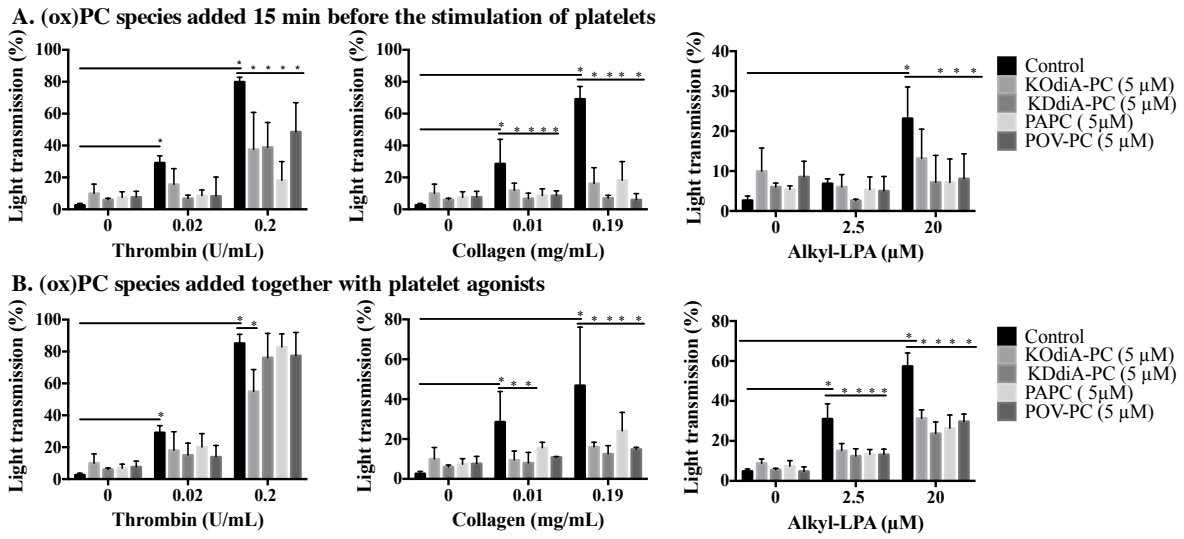


**Figure 4-9. Inhibitory effects of different (ox)PC species in agonist-stimulated platelets were dependent on the timing of addition.** (A) Incubation of platelets with KOdiA-PC, KDdiA-PC, PAPC, and POV-PC for 15 minutes significantly inhibited the activation of platelets induced by thrombin (0.2 U/mL), collagen (0.01 or 0.19 mg/mL), or alkyl-LPA (16:0) (20 μM). (B) The simultaneous addition of (ox)PC species and stimuli to platelets significantly abolished platelet aggregation induced by collagen (0.19 mg/mL) and alkyl-LPA (16:0) (2.5 or 20 μM) . Only KOdiA-PC reduced platelet aggregation induced by thrombin when added at the same time. (Two-way ANOVA with Tukey post hoc test; *$p<0.05$; n= 3 - 5)

In addition to platelet aggregation, P-selectin expression and integrin $\alpha_{IIb}\beta_3$ activation, as well as the production of ROS were also measured in platelets pre-treated with (ox)PC species. Each of the two oxPC species KOdiA-PC and KDdiA-PC, as well as their corresponding controls PAPC and POV-PC, prevented the ROS production induced by thrombin (0.2 U/mL) or collagen (0.2 mg/mL). Alkyl-LPA did not induce ROS production regardless of the presence or absence of (ox)PC (Figure 4-10 A). The increase of the P-selectin expression level in platelets induced by thrombin (0.2 U/mL) or collagen (0.19 mg/mL) was also significantly inhibited by incubation with (ox)PC species for 15 minutes (Figure 4-10 B). Similar results were observed for the

integrin $\alpha_{IIb}\beta_3$ activation level in platelets activated by thrombin (0.2 U/mL) or collagen (0.19 mg/mL) (Figure 4-10 C). Since alkyl-LPA alone did not significantly alter P-selectin expression or integrin $\alpha_{IIb}\beta_3$ activation, no significant changes were observed upon treatments with each of the four (ox)PC species (Figure 4-10 B,C).

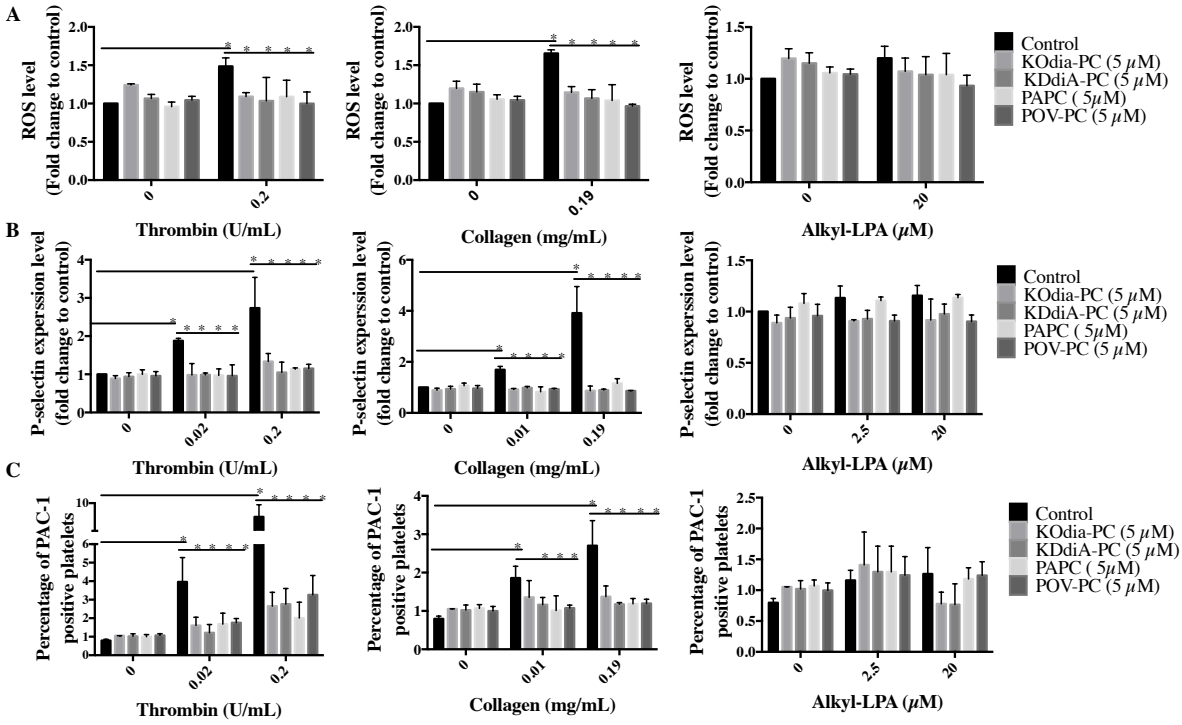


**Figure 4-10. Pre-treatment of human platelets with (ox)PC species prevented the induction of ROS production, P-selectin expression and integrin $\alpha_{IIb}\beta_3$ activation by different stimuli.** Incubation of platelets with KOdiA-PC, KDdiA-PC, PAPC, POV-PC for 15 minutes significantly inhibited ROS production (A), P-selectin expression (B) and integrin $\alpha_{IIb}\beta_3$ activation (C) induced by thrombin, collagen. Alkyl-LPA (16:0) had no significant effect on ROS production (A), P-selectin expression (B) and integrin $\alpha_{IIb}\beta_3$ activation (C), therefore the additions of the four (ox)PC species had no reduction effect. (Two-way ANOVA with Tukey post hoc test; *$p<0.05$; n= 3 - 5)

To examine if cAMP or cGMP are linked to the anti-aggregatory effect of (ox)PC species, intracellular cAMP and cGMP levels were determined by ELISA. Incubation of platelets with

each of the (ox)PC species for 15 minutes followed by stimulation with different agonists led to significant increase of the intracellular cGMP level. The pre-treatment of platelets with KDdiA-PC or POV-PC resulted in roughly 10-fold increase of intracellular cGMP in platelets activated by thrombin (0.02 or 0.2 U/mL), collagen (0.01, or 0.19 mg/mL), or alkyl-LPA (2.5 or 20 μM), and a 20-fold increase of the cGMP level in non-activated platelets. The pre-treatment of platelets with KOdiA-PC or PAPC led to two-fold increase in platelets activated by thrombin, collagen, or alkyl-LPA, and four-fold increase of the cGMP in non-activated platelets (Figure 4-11 A). In contrast, when (ox)PC species and 0.2 U/mL thrombin were added at the same time, they failed to elevate the intracellular cGMP level in platelets. However, the concurrent addition of KDdiA-PC or POV-PC still caused a significant 10-fold increase of cGMP in platelets activated by 0.02 U/mL thrombin, collagen or alkyl-LPA. KOdiA-PC or PAPC also retained their ability to elicit a two-fold increase of intracellular cGMP production in platelets stimulated by 0.02 U/mL thrombin, 0.01 mg/mL collagen or 2.5 μM alkyl-LPA (Figure 4-11 B).

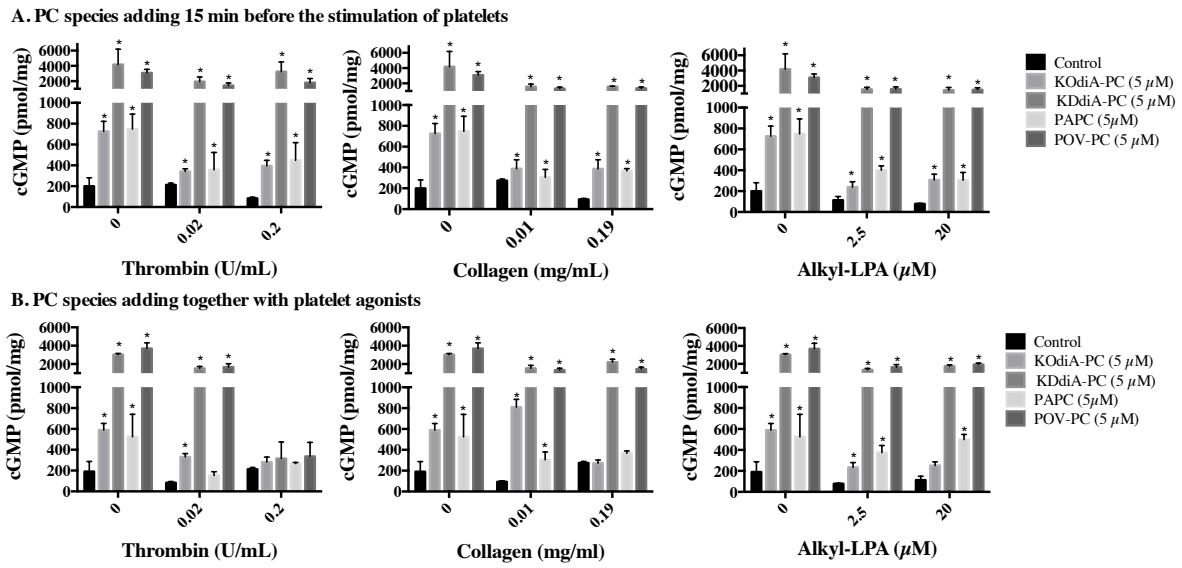


**Figure 4-11. Pre-treatment of human platelets with (ox)PC species suppressed the activation of platelets by different agonists via elevated cGMP level.** (A) Incubation of platelet with KDdiA-PC or POV-PC for 15 minutes

significantly induced 10-fold increase of intracellular cGMP level in platelets in the presence of thrombin, collagen, or alkyl-LPA (16:0), and KOdiA-PC or PAPC only led to a 2-fold increase of cGMP level. (B) Four (ox)PC species significantly increased cGMP level in the presence of 0.02 U/mL thrombin, collagen or alkyl-LPA (16:0), but not for 0.2 U/mL thrombin when added at the same time. (*p<0.05, two-way ANOVA with Tukey post hoc test, n= 3 - 5)

Conversely, the intracellular level of cAMP did not increase as strongly as the intracellular level of cGMP. The 15-minute pre-treatment with KOdiA-PC, KDdiA-PC, PAPC, or POV-PC induced a significant two-fold increase of cAMP in platelets activated by thrombin (0.02 or 0.2 U/mL), collagen (0.19 mg/mL), or non-stimulated control (Figure 4-12 A). In contrast, when each of the four (ox)PC species was added at the same time as thrombin, collagen, or alkyl-LPA (20 μM), they were no longer able to induce significant increase of the intracellular cAMP level (Figure 4-12 B).

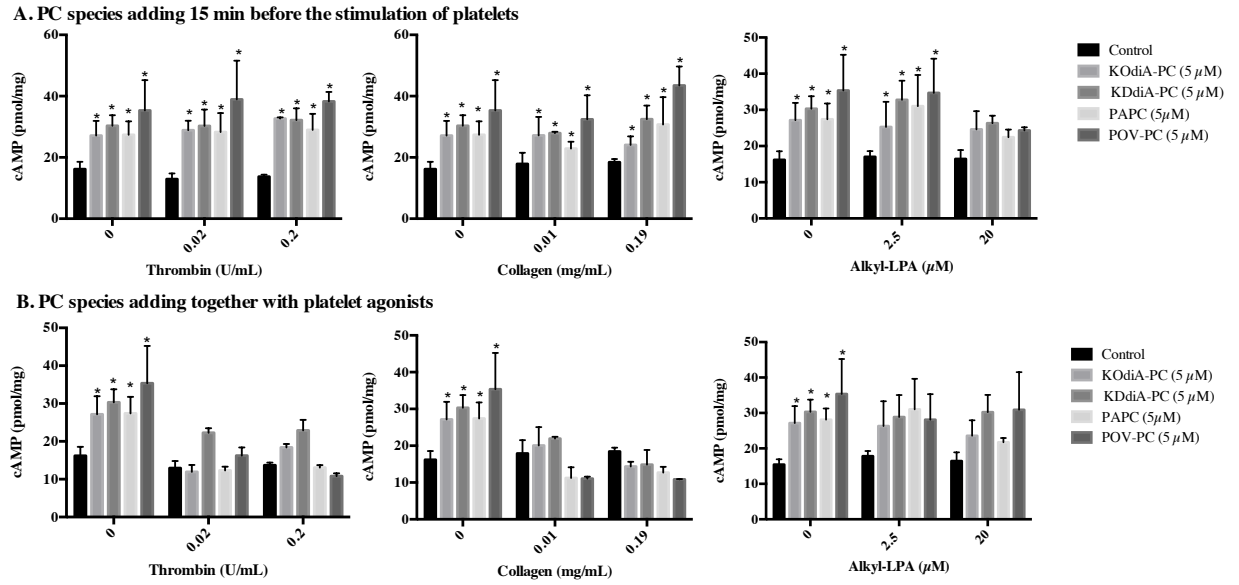


**Figure 4-12. (ox)PC species significantly elevated the intracellular cAMP level in platelets. (A)** Incubation of platelets with four oxPC species for 15 minutes caused a significant 2-fold increase of cAMP level in platelets

activated by thrombin, collagen, or alkyl-LPA. (B) The simultaneous addition of the four (ox)PC species with thrombin, collagen, or alkyl-LPA (16:0) into platelets did not significantly induce intracellular cAMP level. (*p<0.05, two-way ANOVA with Tukey post hoc test, n= 3 - 5)

To further test our hypothesis that (ox)PC species inhibit platelet reactivity via the sGC-cGMP pathway, the sGC inhibitor ODQ was applied to platelets prior to incubation with any one of the (ox)PC species for 15 minutes. ODQ significantly restored the previously observed platelet aggregation in response to thrombin (0.2 U/mL) or collagen (0.19 mg/mL) despite the presence of KOdiA-PC, KDdiA-PC, PAPC, or POV-PC (Figure 4-13). The effect of ODQ on platelet activity induced by alkyl-LPA was not significant, because alkyl-LPA itself did not induce any significant platelet aggregation.

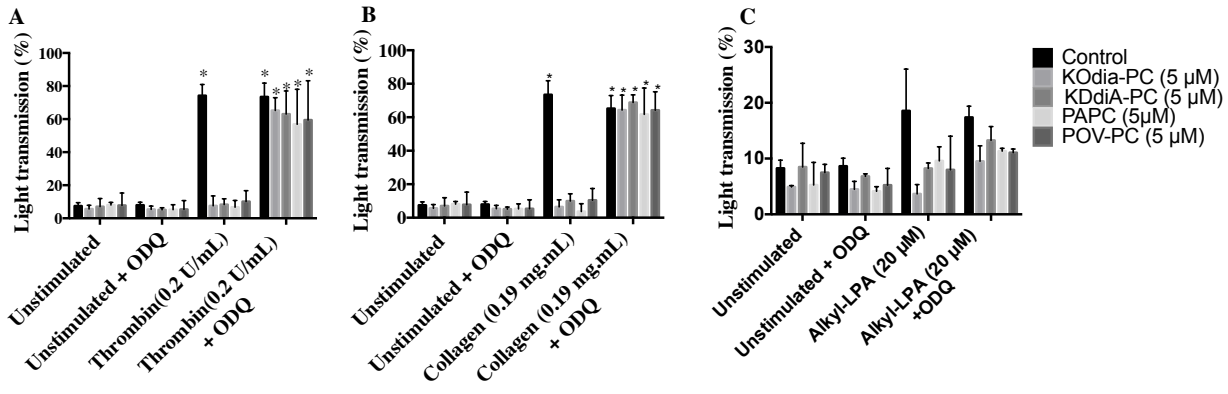


**Figure 4-13. The sGC inhibitor ODQ prevented the inhibition effect of platelet aggregation induced by (ox)PC species.** Incubation of platelets with 10 μM ODQ for 15 minutes significantly prevented the inhibition effect of (ox)PC species on platelet activation induced by thrombin (A) or collagen (B), but not alkyl-LPA (C). (*p<0.05, two-way ANOVA with Tukey post hoc test, n= 3 - 5)

CD36 was suggested to be the primary receptor of oxPC species (65). To determine the involvement of CD36 in the inhibitory effect observed with (ox)PC species, we tested the

inhibitor of scavenger receptor CD36, SSO, on platelets by measuring the integrin $\alpha_{IIb}\beta_3$ activation level. SSO itself prevented platelet activation induced by thrombin (0.2 U/mL), collagen (0.19 mg/mL), or alkyl-LPA (20 μM) (Figure 4-14), as did the addition of SSO and each of the (ox)PC species together.

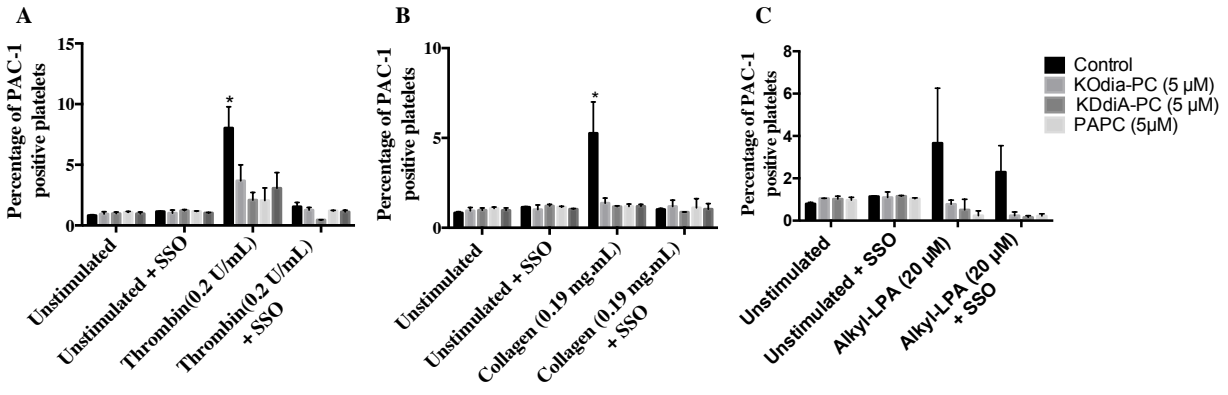


**Figure 4-14. The CD36 inhibitor SSO inhibited platelet activation induced by thrombin, collagen, and alkyl-LPA.** Incubation of platelets with 100 μM SSO for 15 minutes strongly inhibited platelet activation (PAC-1 activation) induced by thrombin, collagen, and alkyl-LPA (16:0). The combination of SSO with (ox)PC significantly blocked PAC-1 activation on platelets induced by thrombin (A), collagen (B), or alkyl-LPA (C). (*$p<0.05$, two-way ANOVA with Tukey post hoc test, n= 3 - 5)

## 4.4 Discussion

In the previous two chapters, we have explored the ROS-induced cysteine oxidation in monocytes using redox proteomic tools. As platelets also contribute to the formation of the atherosclerotic plaque, we need to focus on understanding how platelets are modulated by ROS. In order to apply proteomic tools such as those discussed in the previous chapters on platelets in future studies, we decided to first analyze the interaction between platelets and different stimuli relevant to hemostasis, atherothrombosis, and inflammation The effect of ROS on platelet

activation has been more or less explored in hemostasis (114, 116, 267, 276). Therefore, thrombin, collagen, and ADP as the stimuli relevant to hemostasis were applied as reference for LPA and (ox)PC species, the stimuli derived from atherosclerosis, to study redox regulation in platelets. Using several assays for *in vitro* platelet activation, our results, consistent with previous observations (114, 116), confirmed that primary strong agonists, including thrombin and collagen, were able to generate NOX-derived ROS during platelet activation. The present study also markedly extended the analysis of this phenomenon by resolving the dose-dependent ROS production profiles in platelets, with no significant ROS production at the low dose of thrombin or collagen. This implicated a tight regulated link between ROS production and the extent of platelet activation.

However, the production of ROS is not always associated with platelet activation. ADP as a critical secondary agonist and LPA as a plaque-derived platelet stimulus did not induce ROS production in platelet activation. KOdiA-PC, a representative of oxPC series, had already been shown to stimulated NOX2-derived ROS production to facilitate platelet activation and thrombus formation (47). In contrast, our studies showed that KOdiA-PC and other (ox)PC species we utilized suppressed the production of ROS, and did not induce platelet activation. To further extend our understanding of redox regulation in platelet activity, the pro-inflammatory stimulus lipopolysaccharide (LPS) was also tested. We utilized LPS from Salmonella Minnesota, a rough-form LPS, because rough-form LPS is primarily used in cellular activation studies *in vitro* (277). We found that LPS from Salmonella Minnesota did not trigger the platelet activation cascade, but still induced the NOX-derived ROS production. Future studies to clarify whether LPS-derived ROS sensitize platelets to other stimuli would be worthwhile. Taken together, these

findings indicate that ROS may serve as indispensable signaling molecules only for specific platelet activation pathways.

Platelet hyperactivity in the context of dyslipidemia has been reported to proceed through the action of oxLDL (65, 278). Oxidized PC species are an important component of the atherosclerotic plaque as well as oxLDL. It has been reported that oxPC species increased in the plasma of humans with low high-density lipoprotein (HDL), and enhanced platelet activity (65). Strikingly, those two oxPC species as well as the two control species we utilized did not activate platelets, but acted as inhibitors of platelet activation induced by other stimuli. From this observation, we proceeded to explore the underlying mechanism and demonstrated that an increase in the intracellular cGMP level played a causal role in the inhibition effect of (ox)PC species on platelet activation. The NO-sGC-cGMP signaling pathway is an important inhibitory pathway to keep platelets deactivated. Rescue of (ox)PC-induced inhibitory effect by an sGC inhibitor was observed in platelets, which confirmed the cGMP pathway as the major inhibitory mechanism initiated by (ox)PC species. Furthermore, oxPCs are a component of oxLDL, for which both activating and inhibitory potential have also been reported (45). These results supported the inhibition effects of (ox)PC species on platelet activation. Taken together, our studies suggest that oxPC species profoundly affect GC-cGMP signaling in platelets and inhibit platelet activation (Figure 4-15). However, our observations are different from the literature in regard to the platelet response to oxPC species. Therefore, the exact mechanism of the efforts of oxLDL and oxPC on platelet activity still requires more systematical experiment analysis.

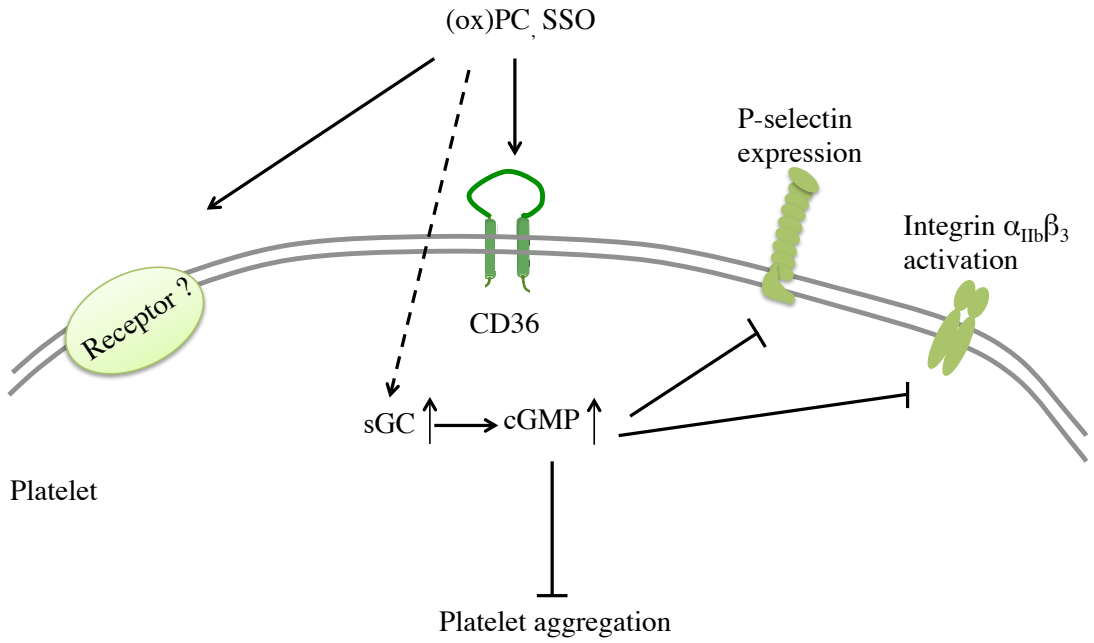


**Figure 4-15. The inhibition effect of (ox)PC species on platelets is mediated by the NO-sGC-cGMP level.** (ox)PC species elicit the intracellular cGMP level in platelets to inhibit platelet activation and ROS production. This inhibitory effect may be regulated by CD36 ligation. NO, nitric oxide; sGC, soluble guanynyl cyclase; cGMP, cyclic guanosine monophosphate; ROS, reactive oxygen species.

The *sn*-1 position of (ox)PC is usually bound with a saturated fatty acid, and the *sn*-2 position is linked to a polyunsaturated fatty acid, which is highly oxidizable. It has been suggested that the biological activities of (ox)PC species may depend on the recognition of the chemical structure of the long-chain fatty acid by specific receptors like CD36 (275). However, the four (ox)PC species we utilized with fatty acids of various structures did not show any significant difference in inhibiting platelet activation. This indicates that the (ox)PC species may be able to induce cellular responses regardless of the structure, or even the position of the fatty acid. In addition, the scavenger receptor CD36 contains a binding pocket for long-chain fatty acid (279). The inhibitor of CD36, SSO, was observed to reduce platelet activity in our studies. On the basis of

its structure, SSO may mimic the fatty acid on the *sn*-2 position but not exclusive of the *sn*-1 position of (ox)PC species. These observations suggest that the inhibition of platelet activation by SSO and (ox)PC species may be mediated by CD36 ligation. In order to unravel the interaction of platelet with (ox)PC through CD36, more research is still needed to understand the precise CD36 signalling pathways in platelets.

ROS reacts rapidly with nitric oxide (NO) to produce peroxynitrite, which depletes the NO level in blood vessels. NO is known to be an important regulator of vascular tone that deactivates platelets through the sGC-cGMP pathway. Low doses of NO-related drugs i.e. aspirin have been very efficacious as an anti-platelet agent in the treatment of thrombotic disorders (280). Moreover, another major therapeutic strategy that has emerged from studying the role of NO as a regulator of platelet activity is phosphodiesterase (PDE) inhibitors. PDEs catalyze the hydrolysis of cAMP and cGMP to regulate their intracellular concentration. PDE3 inhibitors, e.g. milrinone and cilostazol, have been approved by FDA to treat patients with heart failure (281). PDE5 has a relatively high expression in the vascular system, and its inhibitors such as sildenafil, tadalafil, and vardenafil are approved for the treatment of cardiovascular disorders (282). However, all these intervention strategies are associated with increased bleeding risk, because their targets are shared by atherothrombotic and hemostatic pathways. In contrast, manipulation of ROS level to maintain the NO level could be an alternative way to control platelet activation and prevent atherothrombosis.

Numerous studies have now pinpointed platelet-derived ROS as a secondary messenger that drives multiple aspects of platelet function in response to a variety of mediators. Thus the roles

of platelets for atherogenic, inflammatory, and angiogenic processes are all likely to be influenced by platelet-derived ROS. However, the specific significance of different ROS species and ROS-producing enzymatic systems remains to be gradually defined in platelets. As the primary factor that correlates ROS with atherosclerosis, oxLDL influences platelet reactivity through a variety of mechanisms in both prothrombotic and antithrombotic ways. Many questions remain outstanding about the role of oxLDL, in particular different oxPC species, with respect to platelet activity. Therefore, the application of proteomic techniques such phosphoproteomics, glycoproteomics, and redox proteomics will be critical to investigate ROS-induced platelet activation and oxLDL-mediated platelet signaling.

# Chapter 5: Conclusion and Future Direction

Platelet activation and their interaction with monocytes are critical steps in the initiation and progression of atherosclerosis. The comprehensive analysis of the redox proteome in platelets and monocytes is essential for gaining a complete understanding of redox modulations in atherosclerosis. This is the motivation behind the development of versatile proteomic tools in this thesis that can be used to study the platelet-monocyte interaction and platelet activation in the context of atherosclerosis.

The biotin switch assay was originally designed approximately 15 years ago for the investigation of *S*-nitrosylation, the reaction product between nitric oxide (NO) and cysteine residues in proteins (182). After that, mass spectrometric analysis continued to focus on *S*-nitrosylation because of the importance of this modification for signal transduction. In recent years, other oxidative cysteine modifications have also been recognized as prevalent but relatively underexplored regulators of cellular signaling cascades. Studies of those modifications represent the major focus of this thesis, along with development of a tool to characterize such reversible cysteine oxidations. On the basis of results obtained in Chapter 2 and Chapter 3, the modified biotin switch assay coupled with SILAC has proven to be a useful tool for mapping oxidatively modified peptides/proteins from cells under changing conditions, and for isolating modified proteins for subsequent quantification. However, the biotin switch assay has some limitations as it is biased towards the identification of abundant proteins. It has, therefore, been suggested that the quantification of each individual modification should be validated by alternative approaches in order to confirm its physiological relevance (283). Despite these drawbacks, the modified

biotin switch assay developed in this thesis significantly improved previous existing biotin switch assays through incorporation of quantification methods and the use of selective reducing reagents.

To extend our knowledge of redox modulation that occurs in platelet-monocyte interaction, a model system was established using THP-1 cells (a cell line model of monocytes) upon treatment with platelet releasate, and analyzed by the modified biotin switch assay. The analysis of total reversible cysteine oxidation in this model quantified more than one hundred proteins that are relevant to fundamental biological processes, including glycolysis and redox regulation. To gain a better understanding of the redox regulation of monocytes in atherosclerosis, we also assessed the sulfenic acid modification in the same model. This analysis was expected to cover fewer proteins than the study of reversible cysteine oxidation, because sulfenic acid modification is only a small subset of total reversible cysteine oxidation. However, through the use of a high performance mass spectrometer, the investigation of the sulfenic acid modification quantified more than one hundred proteins. Moreover, some of those proteins identified with sulfenic acid modification were involved in the disease-relevant, previously missed biological process of monocyte transendothelial migration, which included integrin $\beta_2$. Thus, the analysis of sulfenic acid modification is more likely to reflect redox regulation relevant to disease than the corresponding total analysis. Future studies of other individual reversible cysteine modifications would be worthwhile.

Most of the enzymes in glycolysis that were quantified with reversible cysteine oxidation were also identified with sulfenic acid modification, such as GAPDH, α-enolase (ENOA), aldolase

(ALDOA), triphosphate isomerase (TPIS), and malate dehydrogenase (MDHM). The consistent quantification of key enzymes in glycolysis may be due to the following reasons. First, because of their short lifetime, ROS species tend to react with targets at the sites where they generated, instead of traveling across subcellular compartments. Glycolysis, i.e. the respiration chain, is an important source of ROS in cellular systems. Therefore, ROS species encounter glycolytic enzymes as soon as they are generated. Second, several enzymes in glycolysis such as GAPDH and TPIS contain reactive cysteine residues that are part of their catalytic site or modulate their function (284). Those cysteine residues are prone to become targets of ROS species (241). In addition, interference with glycolysis initiates the pentose phosphate pathway to produce NADPH to deactivate ROS species (242). Moreover, dysfunctional glycolysis is also associated with the pro-inflammatory state in monocytes (285). The repeated identification of this pathway in our studies as well as literature evidence indicates a profound effect of the platelet releasate on the energy metabolism in monocytes through redox regulation.

In contrast to enzymes in glycolysis, several ribosomal proteins that had been quantified when targeting reversible cysteine oxidations were not quantified as containing sulfenic acid modifications. The ribosome is a molecular machine that is responsible for protein synthesis in cells, and the global inhibition of protein synthesis is a common response to stress conditions. Oxidation of ribosomal proteins may cause errors in the proteins that are produced, and increase the toxicity of the oxidative stress (286). The oxidation of ribosomal proteins is relevant to the general redox state of a cell and reflected in the analysis of total reversible cysteine oxidation. On the other hand, sulfenic acid modification as a reactive intermediate is more likely to be involved in signal transduction. The two studies may therefore emphasize different aspects of the

system, and, consequently, have overlapping but distinct protein profiles.

The novel biological process of interest in the study of sulfenic acid modification is monocyte transendothelial migration, which includes integrin $\beta_2$. LFA-1 ($\alpha_L\beta_2$) and Mac-1 ($\alpha_M\beta_2$), two complexes of integrin $\beta_2$, serve as bridges between activated monocytes and the endothelium (287). The precise mechanism(s) by which integrin $\beta_2$ complexes are activated in monocytes in response to activated platelets are not fully understood, but are believed to involve redox modulation of cysteine residues (258). Integrins are a family of proteins rich in cysteine residues, and cysteine oxidation has been reported to affect the conformation and activation of integrin complexes, including integrin $\beta_2$ (288, 289). On the basis of our proteomic study, we discovered several sulfenic acid modification sites in integrin $\beta_2$. Although the direct functional relevance of those modifications was unclear, flow cytometry experiments clearly showed the activation of LFA-1 but not Mac-1 in monocytes mediated by NOX-derived ROS. In addition, it has been suggested that activated platelets bind to monocytes mainly through P-selectin-PSGL-1 interactions (193), and upregulate the expression and functionality of integrin $\beta_1$ and $\beta_2$ in monocytes (17). We also observed P-selectin-PSGL-1 dependent activation of Mac-1 on monocytes. However, the P-selectin-PSGL-1 interaction was not associated with ROS production, or LFA-1 activation on monocytes in our model. The next step is to determine the effect of sulfenic acid modification on the function of integrin $\beta_2$. This can benefit from the improvement in the quantification of sulfenic acid modification through applying dimedone-based biotin-labeling reagents. Since most sulfenic acid modifications are unstable and lost easily, dimedone-based labeling reagents would preserve them, and have great potential to improve the enrichment accuracy and efficiency (185). Among the dimedone-based sulfenic acid

probes, DAz-1 and DAz-2 have the great advantage of being cell permeable which enables detection of sulfenic acid modifications in living cells (252).

We have contributed to the ever-growing body of knowledge related to mechanisms of platelet-monocyte interaction. As illustrated in Figure 5-1, platelet releasate is sufficient to induce a pro-inflammatory state in monocytes through NOX activation, ROS production, and integrin $\beta_2$ activation. The next step could be the application of current proteomic tools to samples from patients with atherosclerosis to validate the targets quantified in this thesis, e.g. integrin $\beta_2$. Moreover, the quantitative redox proteomic tools we developed enable the monitoring of multiplexed conditions of a biological system associated with atherosclerosis in drug development.

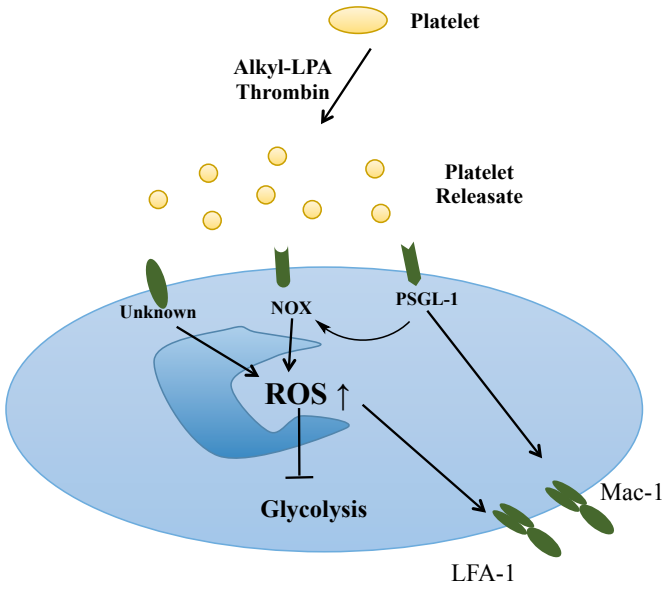


**Figure 5-1. Platelet releasate induces monocyte activation via redox regulation.** Platelets become activated in response to thrombin or alkyl-LPA, and release their content. The platelet releasate then induces ROS production in monocytes through the activation of NOX and other enzymes. The increased intracellular level of ROS leads to the inhibition of glycolysis, and the activation of integrin $\beta_2$ complexes by reversible oxidative modifications of cysteine

residues. ROS, reactive oxygen species; NOX, NADPH oxidase; LFA-1, integrin $\alpha_L\beta_2$; Mac-1, integrin $\alpha_M\beta_2$; PSGL-1, P-selectin glycoprotein ligand-1.

To further extend our understanding of redox regulation in atherosclerosis through proteomics, another reversible cysteine modification that should be considered is *S*-glutathionylation, a mixed disulfide bond formed between cysteine residues and glutathione (GSH). GSH is a potent antioxidant in cells, and more than 90% of the total GSH amount remains in the reduced form in healthy cells. *S*-glutathionylation is regarded as a cellular response to stress, and often found to be increased in diseases (290). Even though protein *S*-glutathionylation has been reported in the THP-1 human monocytic cell line, primary human monocytes (291), and human monocyte-derived macrophages (292), most of these studies have only quantified *S*-glutathionylation at the global level. In contrast, very few *S*-glutathionylated proteins have been validated as redox signaling proteins in monocytes or macrophages (293, 294). A modified biotin switch assay to quantify *S*-glutathionylation through high-throughput proteomic method has already been developed. It uses glutaredoxin (Grx) to enzymatically reduce *S*-glutathionylated proteins, and then enrich the newly reduced proteins/peptides via biotin-avidin (295). In addition, a resin-assisted enrichment has also been developed to directly capture cysteine-containing peptides, and adapted with Grx reduction to offer a more efficient way to analyze *S*-glutathionylation (296).

A remarkable observation arising from the studies was that platelet releasate induced by thrombin or alkyl-LPA did not show any significant difference in triggering ROS production and cysteine oxidation in monocytes. Previous studies in our lab had implemented quantitative proteomics studies to compare proteins released by platelets activated by different agonists.

Those results showed that indeed there was a characteristic proteome profile with each of the agonists, mostly due to difference in the relative abundance of individual components (297). This suggests that various platelet-activating stimuli in atherosclerosis have distinct signaling pathways in platelets. In Chapter 4, we therefore also focused on redox regulation of platelet activation. As observed in monocytes, the measurement of ROS production is the most direct way to monitor redox regulation. Thus, we started with the analysis of ROS production in platelets activation. The two main platelet agonists associated with hemostasis, thrombin and collagen, as well as the infection-specific agonist lipopolysaccharide (LPS), were able to promote ROS production mainly via the activation of NOX, which in turn affected the activation of integrin $\alpha_{IIb}\beta_3$ and P-selectin expression. However, no ROS production was observed in platelets activated by the secondary agonist ADP, or the plaque-derived agonist alkyl-LPA. This suggests that an agonist-dependent variation in the activation of NOX and the resulting ROS production exists in platelets. The cause of this variation is still unclear and whether it occurs *in vivo* still needs to be investigated.

As products of the oxidation of LDL, LPA and (ox)PC species share structural similarity. PCs are first oxidized on their sn-2 position to produce oxPCs. PC and oxPC species then enzymatically convert into lysoPC by PAF acetyl hydrolase (Lp-PLA2) (298), before the removal of the choline group from lysoPC by autotaxin finally generates acyl-LPA (299). Different forms of LPA have been established as platelet agonists. The oxPC species are now also emerging as important regulators of platelet activity, and the platelet activation induced by oxPC species has recently been reported (65). In spite of these findings, the precise role of oxPC in activation/de-activation of platelets has yet to be fully elucidated. In our study, several (ox)PC

species were found to inhibit platelet activation through elevating the intracellular cGMP level. Our observations are different from the literature in regard to the platelet response to oxPC species, which require more systematical analysis.

The agonist-dependent ROS production and the effects of (ox)PC species on platelets indicate active redox regulation in platelets. Proteomics analysis provides one tool to evaluate changes in redox state associated with phenotype changes. A deep exploration of the difference in platelet behavior in hemostasis and atherothrombosis can be achieved through the application of such redox proteomic tools we have developed. Although platelets cannot be metabolically labeled, redox proteomics coupled with chemical labeling approaches, e.g. ICAT, iTRAQ, or iodoTMT, could be applied to systematically quantify redox signaling events. To further extend our understanding of the role platelet plays in atherosclerosis, it would be necessary to apply the redox proteomic assay as well as the functional assays we utilized in chapter 4 to study platelets from patients. A comparison of platelets from patients with platelets from healthy donors would allow us to better understand platelet behavior in atherosclerosis, and develop novel intervention strategies. Given the fact that increased platelet activity is observed in patients with myocardial infarction (300) and stroke (301), modifications in the platelet preparation may also be needed. Platelets are activated during the washing steps of our current platelet preparation protocol, which may lead to false positive results. An alternative way to prepare platelets is gel filtration of platelet-rich plasma, which effectively separates platelets from blood cells and plasma proteins with less activation (302).

Given the involvement of ROS in various aspects of atherosclerosis, antioxidant therapy was considered as one of the most promising strategies to prevent the development of a plaque.

However, the results of large scale clinical trials and randomized controlled trials were mainly disappointing (303, 304). Although antioxidant supplements fail to prevent cardiovascular diseases in clinical trials, the NOX-dependent ROS still remains a compelling target for the prevention and treatment of vascular disease. GKT137831 (http://www.genkyotex.com) as a specific inhibitor for NOX1 and NOX4 has been approved for phase II clinical trials in patients with diabetic nephropathy (305). Our studies have identified NOX as the primary source of ROS in monocytes in contact with platelet releasate, and during platelet activation. However, we are still not able to distinguish which NOX isoforms in monocytes and platelets are responsible for the development of atherosclerosis. Given that NOX has emerged as the most promising therapeutic target for diseases associated with oxidative stress, more studies are therefore required for a complete validation of the role of individual NOX isoforms using inhibitors with improved efficacy and specificity.

It is by now well accepted that chronic and acute events in atherosclerosis, including platelet-monocyte interaction and platelet activation, are associated with redox signaling through reversible cysteine modification. However, the exact mechanism of reversible cysteine modification and its impact on protein function is largely unknown. The development of redox proteomic approaches addresses this need by providing a useful tool that provides direct insight into the redox regulation of proteins in biological processes. Moreover, modulations of redox regulation open up new avenues for design of therapeutic strategies for atherosclerosis. With the capability for multiplexed monitoring of conditions simultaneously, quantitative redox proteomics has guiding potential in discovery and validation of new therapeutic targets.

## Bibliography


1. Global Status Report on noncommunicable disease 2014. World Health Organization. 2014.
2. Epstin FH. Atherosclerosis-an inflammatory disease. the new england journal of medicine. 1999;340:115-26.
3. Davì G, Patrono C. Platelet Activation and Atherothrombosis. New Engl J Med. 2007;357(24):2482-94.
4. Napoli C, D'Armiento FP, Mancini FP, Postiglione A, Witztum JL, Palumbo G, et al. Fatty streak formation occurs in human fetal aortas and is greatly enhanced by maternal hypercholesterolemia. Intimal accumulation of low density lipoprotein and its oxidation precede monocyte recruitment into early atherosclerotic lesions. J Clin Invest. 1997;100(11):2680-90.
5. Sandoo A, van Zanten JJCSV, Metsios GS, Carroll D, Kitas GD.
6. Hadi HAR, Carr CS, Al Suwaidi J.
7. Zibara K, Chignier E, Covacho C, Poston R, Canard G, Hardy P, et al. Modulation of expression of endothelial intercellular adhesion molecule-1, platelet-endothelial cell adhesion molecule-1, and vascular cell adhesion molecule-1 in aortic arch lesions of apolipoprotein E-deficient compared with wild-type mice. Arterioscler Thromb Vasc Biol. 2000;20(10):2288-96.
8. Hidalgo A, Peired AJ, Wild MK, Vestweber D, Frenette PS. Complete identification of E-selectin ligands on neutrophils reveals distinct functions of PSGL-1, ESL-1, and CD44. Immunity. 2007;26(4):477-89.
9. Louis SF, Zahradka P.
10. Cai J, Hatsukami TS, Ferguson MS, Kerwin WS, Saam T, Chu B, et al. In Vivo Quantitative Measurement of Intact Fibrous Cap and Lipid-Rich Necrotic Core Size in Atherosclerotic Carotid Plaque: Comparison of High-Resolution, Contrast-Enhanced Magnetic Resonance Imaging and Histology. Circulation. 2005;112(22):3437-44.
11. Furman MI, Barnard MR, Krueger LA, Fox ML, Shilale EA, Lessard DM, et al. Circulating monocyte-platelet aggregates are an early marker of acute myocardial infarction. J Am Coll Cardiol. 2001;38(4):1002-6.
12. McCabe DJ, Harrison P, Mackie IJ, Sidhu PS, Purdy G, Lawrie AS, et al. Platelet degranulation and monocyte-platelet complex formation are increased in the acute and convalescent phases after ischaemic stroke or transient ischaemic attack. Br J Haematol. 2004;125(6):777-87.
13. Furman MI, Benoit SE, Barnard MR, Valeri CR, Borbone ML, Becker RC, et al. Increased platelet reactivity and circulating monocyte-platelet aggregates in patients with stable coronary artery disease. J Am Coll Cardiol. 1998;31(2):352-8.
14. Ahn KC, Jun AJ, Pawar P, Jadhav S, Napier S, McCarty OJ, et al. Preferential binding of platelets to monocytes over neutrophils under flow. Biochem Biophys Res Commun. 2005;329(1):345-55.
15. Wang HB, Wang JT, Zhang L, Geng ZH, Xu WL, Xu T, et al. P-selectin primes leukocyte integrin activation during inflammation. Nat Immunol. 2007;8(8):882-92.

16. Gawaz M, Neumann FJ, Dickfeld T, Koch W, Laugwitz KL, Adelsberger H, et al. Activated platelets induce monocyte chemotactic protein-1 secretion and surface expression of intercellular adhesion molecule-1 on endothelial cells. Circulation. 1998;98(12):1164-71.
17. da Costa Martins PA, van Gils JM, Mol A, Hordijk PL, Zwaginga JJ. Platelet binding to monocytes increases the adhesive properties of monocytes by up-regulating the expression and functionality of beta1 and beta2 integrins. J Leukoc Biol. 2006;79(3):499-507.
18. Berger G, Hartwell DW, Wagner DD. P-Selectin and platelet clearance. Blood. 1998;92(11):4446-52.
19. Huo Y, Schober A, Forlow SB, Smith DF, Hyman MC, Jung S, et al. Circulating activated platelets exacerbate atherosclerosis in mice deficient in apolipoprotein E. Nat Med. 2003;9(1):61-7.
20. Crow AR, Lazarus AH. Role of Fcgamma receptors in the pathogenesis and treatment of idiopathic thrombocytopenic purpura. Journal of pediatric hematology/oncology. 2003;25 Suppl 1:S14-8.
21. Blair P, Flaumenhaft R. Platelet α–granules: Basic biology and clinical correlates. Blood reviews. 2009;23(4):177-89.
22. Meyers KM, Holmsen H, Seachord CL. Comparative study of platelet dense granule constituents. American Journal of Physiology - Regulatory, Integrative and Comparative Physiology. 1982;243(3):R454-R61.
23. Ciferri S, Emiliani C, Guglielmini G, Orlacchio A, Nenci GG, Gresele P. Platelets release their lysosomal content in vivo in humans upon activation. Thromb Haemost. 2000;83(1):157-64.
24. Ruggeri ZM. Von Willebrand factor, platelets and endothelial cell interactions. Journal of thrombosis and haemostasis : JTH. 2003;1(7):1335-42.
25. Nieswandt B, Watson SP. Platelet-collagen interaction: is GPVI the central receptor? Blood. 2003;102(2):449-61.
26. Davie EW, Ratnoff OD. WATERFALL SEQUENCE FOR INTRINSIC BLOOD CLOTTING. Science. 1964;145(3638):1310-2.
27. O'Toole TE, Mandelman D, Forsyth J, Shattil SJ, Plow EF, Ginsberg MH. Modulation of the affinity of integrin alpha IIb beta 3 (GPIIb-IIIa) by the cytoplasmic domain of alpha IIb. Science. 1991;254(5033):845-7.
28. Coughlin SR. Thrombin signalling and protease-activated receptors. Nature. 2000;407(6801):258-64.
29. Vu TK, Hung DT, Wheaton VI, Coughlin SR. Molecular cloning of a functional thrombin receptor reveals a novel proteolytic mechanism of receptor activation. Cell. 1991;64(6):1057-68.
30. Furman MI, Liu L, Benoit SE, Becker RC, Barnard MR, Michelson AD. The cleaved peptide of the thrombin receptor is a strong platelet agonist. Proceedings of the National Academy of Sciences of the United States of America. 1998;95(6):3082-7.
31. Klages B, Brandt U, Simon MI, Schultz G, Offermanns S. Activation of G12/G13 results in shape change and Rho/Rho-kinase-mediated myosin light chain phosphorylation in mouse platelets. J Cell Biol. 1999;144(4):745-54.
32. Offermanns S, Toombs CF, Hu YH, Simon MI. Defective platelet activation in G alpha(q)-deficient mice. Nature. 1997;389(6647):183-6.

33. Barr AJ, Brass LF, Manning DR. Reconstitution of receptors and GTP-binding regulatory proteins (G proteins) in Sf9 cells. A direct evaluation of selectivity in receptor.G protein coupling. J Biol Chem. 1997;272(4):2223-9.
34. Santoro SA, Zutter MM. The alpha 2 beta 1 integrin: a collagen receptor on platelets and other cells. Thromb Haemost. 1995;74(3):813-21.
35. Kehrel B, Wierwille S, Clemetson KJ, Anders O, Steiner M, Knight CG, et al. Glycoprotein VI is a major collagen receptor for platelet activation: it recognizes the platelet-activating quaternary structure of collagen, whereas CD36, glycoprotein IIb/IIIa, and von Willebrand factor do not. Blood. 1998;91(2):491-9.
36. Nieswandt B, Watson SP. Platelet-collagen interaction: is GPVI the central receptor? Blood. 2003;102(2):449.
37. Moroi M, Jung SM. Platelet glycoprotein VI: its structure and function. Thromb Res. 2004;114(4):221-33.
38. Kauskot A, Hoylaerts MF. Platelet receptors. Handb Exp Pharmacol. 2012(210):23-57.
39. Murugappa S, Kunapuli SP. The role of ADP receptors in platelet function. Frontiers in bioscience : a journal and virtual library. 2006;11:1977-86.
40. Trumel C, Payrastre B, Plantavid M, Hechler B, Viala C, Presek P, et al. A key role of adenosine diphosphate in the irreversible platelet aggregation induced by the PAR1-activating peptide through the late activation of phosphoinositide 3-kinase. Blood. 1999;94(12):4156-65.
41. Hechler B, Cattaneo M, Gachet C. The P2 receptors in platelet function. Seminars in thrombosis and hemostasis. 2005;31(2):150-61.
42. Kunapuli SP, Ding Z, Dorsam RT, Kim S, Murugappan S, Quinton TM. ADP receptors--targets for developing antithrombotic agents. Curr Pharm Des. 2003;9(28):2303-16.
43. Wijeyeratne YD, Heptinstall S. Anti-platelet therapy: ADP receptor antagonists. Br J Clin Pharmacol. 2011;72(4):647-57.
44. Hackeng CM, Relou IA, Pladet MW, Gorter G, van Rijn HJ, Akkerman JW. Early platelet activation by low density lipoprotein via p38MAP kinase. Thromb Haemost. 1999;82(6):1749-56.
45. Korporaal SJA, Gorter G, van Rijn HJM, Akkerman J-WN. Effect of Oxidation on the Platelet-Activating Properties of Low-Density Lipoprotein. Arterioscler Thromb Vasc Biol. 2005;25(4):867-72.
46. Chen K, Febbraio M, Li W, Silverstein RL. A specific CD36-dependent signaling pathway is required for platelet activation by oxidized low-density lipoprotein. Circ Res. 2008;102(12):1512-9.
47. Magwenzi S, Woodward C, Wraith KS, Aburima A, Raslan Z, Jones H, et al. Oxidized LDL activates blood platelets through CD36/NOX2-mediated inhibition of the cGMP/protein kinase G signaling cascade. Blood. 2015;125(17):2693-703.
48. Haseruck N, Erl W, Pandey D, Tigyi G, Ohlmann P, Ravanat C, et al. The plaque lipid lysophosphatidic acid stimulates platelet activation and platelet-monocyte aggregate formation in whole blood: involvement of P2Y1 and P2Y12 receptors. Blood. 2004;103(7):2585-92.
49. Aoki J. Mechanisms of lysophosphatidic acid production. Semin Cell Dev Biol. 2004;15(5):477-89.
50. Eichholtz T, Jalink K, Fahrenfort I, Moolenaar WH. The bioactive phospholipid lysophosphatidic acid is released from activated platelets. Biochem J. 1993;291(Pt 3):677-80.

51. Tokumura A, Sinomiya J, Kishimoto S, Tanaka T, Kogure K, Sugiura T, et al. Human platelets respond differentially to lysophosphatidic acids having a highly unsaturated fatty acyl group and alkyl ether-linked lysophosphatidic acids. Biochem J. 2002;365(Pt 3):617-28.
52. Choi JW, Herr DR, Noguchi K, Yung YC, Lee CW, Mutoh T, et al. LPA receptors: subtypes and biological actions. Annu Rev Pharmacol Toxicol. 2010;50:157-86.
53. Kihara Y, Maceyka M, Spiegel S, Chun J. Lysophospholipid receptor nomenclature review: IUPHAR Review 8. Br J Pharmacol. 2014;171(15):3575-94.
54. Ishii S, Noguchi K, Yanagida K. Non-Edg family lysophosphatidic acid (LPA) receptors. Prostaglandins & other lipid mediators. 2009;89(3-4):57-65.
55. Tabata K, Baba K, Shiraishi A, Ito M, Fujita N. The orphan GPCR GPR87 was deorphanized and shown to be a lysophosphatidic acid receptor. Biochem Biophys Res Commun. 2007;363(3):861-6.
56. Murakami M, Shiraishi A, Tabata K, Fujita N. Identification of the orphan GPCR, P2Y(10) receptor as the sphingosine-1-phosphate and lysophosphatidic acid receptor. Biochem Biophys Res Commun. 2008;371(4):707-12.
57. Oka S, Ota R, Shima M, Yamashita A, Sugiura T. GPR35 is a novel lysophosphatidic acid receptor. Biochem Biophys Res Commun. 2010;395(2):232-7.
58. McIntyre TM, Pontsler AV, Silva AR, St Hilaire A, Xu Y, Hinshaw JC, et al. Identification of an intracellular receptor for lysophosphatidic acid (LPA): LPA is a transcellular PPARgamma agonist. Proc Natl Acad Sci U S A. 2003;100(1):131-6.
59. Khandoga AL, Fujiwara Y, Goyal P, Pandey D, Tsukahara R, Bolen A, et al. Lysophosphatidic acid-induced platelet shape change revealed through LPA(1-5) receptor-selective probes and albumin. Platelets. 2008;19(6):415-27.
60. Retzer M, Essler M. Lysophosphatidic acid-induced platelet shape change proceeds via Rho/Rho kinase-mediated myosin light-chain and moesin phosphorylation. Cell Signal. 2000;12(9-10):645-8.
61. Pamuklar Z, Lee JS, Cheng HY, Panchatcharam M, Steinhubl S, Morris AJ, et al. Individual heterogeneity in platelet response to lysophosphatidic acid: evidence for a novel inhibitory pathway. Arterioscler Thromb Vasc Biol. 2008;28(3):555-61.
62. Berliner JA, Leitinger N, Tsimikas S. The role of oxidized phospholipids in atherosclerosis. J Lipid Res. 2009;50 Suppl:S207-12.
63. Watson AD, Leitinger N, Navab M, Faull KF, Horkko S, Witztum JL, et al. Structural identification by mass spectrometry of oxidized phospholipids in minimally oxidized low density lipoprotein that induce monocyte/endothelial interactions and evidence for their presence in vivo. J Biol Chem. 1997;272(21):13597-607.
64. Podrez EA, Poliakov E, Shen Z, Zhang R, Deng Y, Sun M, et al. Identification of a novel family of oxidized phospholipids that serve as ligands for the macrophage scavenger receptor CD36. J Biol Chem. 2002;277(41):38503-16.
65. Podrez EA, Byzova TV, Febbraio M, Salomon RG, Ma Y, Valiyaveettil M, et al. Platelet CD36 links hyperlipidemia, oxidant stress and a prothrombotic phenotype. Nat Med. 2007;13(9):1086-95.
66. Wong KL, Yeap WH, Tai JJ, Ong SM, Dang TM, Wong SC. The three human monocyte subsets: implications for health and disease. Immunol Res. 2012;53(1-3):41-57.
67. Passlick B, Flieger D, Ziegler-Heitbrock HW. Identification and characterization of a novel monocyte subpopulation in human peripheral blood. Blood. 1989;74(7):2527-34.

68. Geissmann F, Jung S, Littman DR. Blood monocytes consist of two principal subsets with distinct migratory properties. Immunity. 2003;19(1):71-82.
69. Serbina NV, Jia T, Hohl TM, Pamer EG. Monocyte-mediated defense against microbial pathogens. Annu Rev Immunol. 2008;26:421-52.
70. Woollard KJ, Geissmann F. Monocytes in atherosclerosis: subsets and functions. Nature reviews Cardiology. 2010;7(2):77-86.
71. Geissmann F, Auffray C, Palframan R, Wirrig C, Ciocca A, Campisi L, et al. Blood monocytes: distinct subsets, how they relate to dendritic cells, and their possible roles in the regulation of T-cell responses. Immunol Cell Biol. 2008;86(5):398-408.
72. Tacke F, Randolph GJ. Migratory fate and differentiation of blood monocyte subsets. Immunobiology. 2006;211(6-8):609-18.
73. Varol C, Yona S, Jung S. Origins and tissue-context-dependent fates of blood monocytes. Immunol Cell Biol. 2009;87(1):30-8.
74. Shi C, Pamer EG. Monocyte recruitment during infection and inflammation. Nat Rev Immunol. 2011;11(11):762-74.
75. Imhof BA, Aurrand-Lions M. Adhesion mechanisms regulating the migration of monocytes. Nat Rev Immunol. 2004;4(6):432-44.
76. Greaves DR, Gordon S. The macrophage scavenger receptor at 30 years of age: current knowledge and future challenges. J Lipid Res. 2009;50 Suppl:S282-6.
77. Hahn C, Schwartz MA. Mechanotransduction in vascular physiology and atherogenesis. Nat Rev Mol Cell Biol. 2009;10(1):53-62.
78. Smith JB, Willis AL. Aspirin selectively inhibits prostaglandin production in human platelets. Nature: New biology. 1971;231(25):235-7.
79. Clappers N, Brouwer MA, Verheugt FWA. Antiplatelet treatment for coronary heart disease. Heart. 2007;93(2):258-65.
80. Executive Summary of The Third Report of The National Cholesterol Education Program (NCEP) Expert Panel on Detection, Evaluation, And Treatment of High Blood Cholesterol In Adults (Adult Treatment Panel III). Jama. 2001;285(19):2486-97.
81. Hippisley-Cox J, Coupland C. Unintended effects of statins in men and women in England and Wales: population based cohort study using the QResearch database. BMJ (Clinical research ed). 2010;340:c2197.
82. Preiss D, Seshasai SR, Welsh P, Murphy SA, Ho JE, Waters DD, et al. Risk of incident diabetes with intensive-dose compared with moderate-dose statin therapy: a meta-analysis. Jama. 2011;305(24):2556-64.
83. Desai DA, Zakaria S, Ouyang P. Initiation of statin therapy: are there age limits? Current atherosclerosis reports. 2012;14(1):17-25.
84. Alfadda AA, Sallam RM. Reactive oxygen species in health and disease. J Biomed Biotechnol. 2012;2012:936486.
85. Stadtman ER, Levine RL. Protein Oxidation. Ann N Y Acad Sci. 2000;899(1):191-208.
86. Droge W. Free radicals in the physiological control of cell function. Physiol Rev. 2002;82(1):47-95.
87. Liu Y, Zhao H, Li H, Kalyanaraman B, Nicolosi AC, Gutterman DD. Mitochondrial sources of H2O2 generation play a key role in flow-mediated dilation in human coronary resistance arteries. Circ Res. 2003;93(6):573-80.

88. Forman HJ, Torres M, Fukuto J. Redox signaling. Mol Cell Biochem. 2002;234-235(1-2):49-62.
89. Bubici C, Papa S, Dean K, Franzoso G. Mutual cross-talk between reactive oxygen species and nuclear factor-kappa B: molecular basis and biological significance. Oncogene. 2006;25(51):6731-48.
90. Wu HM, Chi KH, Lin WW. Proteasome inhibitors stimulate activator protein-1 pathway via reactive oxygen species production. FEBS Lett. 2002;526(1-3):101-5.
91. Ma Q. Role of nrf2 in oxidative stress and toxicity. Annu Rev Pharmacol Toxicol. 2013;53:401-26.
92. Trachootham D, Lu W, Ogasawara MA, Valle NR-D, Huang P. Redox Regulation of Cell Survival. Antioxidants & Redox Signaling. 2008;10(8):1343-74.
93. Gryglewski RJ, Palmer RMJ, Moncada S. Superoxide anion is involved in the breakdown of endothelium-derived vascular relaxing factor. Nature. 1986;320(6061):454-6.
94. Griendling KK, FitzGerald GA. Oxidative Stress and Cardiovascular Injury: Part I: Basic Mechanisms and In Vivo Monitoring of ROS. Circulation. 2003;108(16):1912-6.
95. Siti HN, Kamisah Y, Kamsiah J. The role of oxidative stress, antioxidants and vascular inflammation in cardiovascular disease (a review). Vascular Pharmacology. 2015;71:40-56.
96. Sun M, Finnemann SC, Febbraio M, Shan L, Annangudi SP, Podrez EA, et al. Light-induced oxidation of photoreceptor outer segment phospholipids generates ligands for CD36-mediated phagocytosis by retinal pigment epithelium: a potential mechanism for modulating outer segment phagocytosis under oxidant stress conditions. J Biol Chem. 2006;281(7):4222-30.
97. O'Brien KD, McDonald TO, Chait A, Allen MD, Alpers CE. Neovascular Expression of E-Selectin, Intercellular Adhesion Molecule-1, and Vascular Cell Adhesion Molecule-1 in Human Atherosclerosis and Their Relation to Intimal Leukocyte Content. Circulation. 1996;93(4):672-82.
98. Lambeth JD, Cheng G, Arnold RS, Edens WA. Novel homologs of gp91phox. Trends Biochem Sci. 2000;25(10):459-61.
99. Drummond GR, Selemidis S, Griendling KK, Sobey CG. Combating oxidative stress in vascular disease: NADPH oxidases as therapeutic targets. Nat Rev Drug Discov. 2011;10(6):453-71.
100. Manea S-A, Constantin A, Manda G, Sasson S, Manea A. Regulation of Nox enzymes expression in vascular pathophysiology: Focusing on transcription factors and epigenetic mechanisms. Redox Biology. 2015;5:358-66.
101. Jandeleit-Dahm K, Lassila M, Davis BJ, Candido R, Johnston CI, Allen TJ, et al. Anti-atherosclerotic and renoprotective effects of combined angiotensin-converting enzyme and neutral endopeptidase inhibition in diabetic apolipoprotein E-knockout mice. Journal of hypertension. 2005;23(11):2071-82.
102. Sheehan AL, Carrell S, Johnson B, Stanic B, Banfi B, Miller Jr FJ. Role for Nox1 NADPH oxidase in atherosclerosis. Atherosclerosis. 2011;216(2):321-6.
103. Gray SP, Di Marco E, Okabe J, Szyndralewiez C, Heitz F, Montezano AC, et al. NADPH Oxidase 1 Plays a Key Role in Diabetes Mellitus–Accelerated Atherosclerosis. Circulation. 2013;127(18):1888-902.
104. Vendrov AE, Madamanchi NR, Niu X-L, Molnar KC, Runge M, Szyndralewiez C, et al. NADPH Oxidases Regulate CD44 and Hyaluronic Acid Expression in Thrombin-treated Vascular Smooth Muscle Cells and in Atherosclerosis. J Biol Chem. 2010;285(34):26545-57.

105. Lee MY, Martin AS, Mehta PK, Dikalova AE, Garrido AM, Datla SR, et al. Mechanisms of Vascular Smooth Muscle NADPH oxidase 1 (Nox1) Contribution to Injury-induced Neointimal Formation. Arterioscler Thromb Vasc Biol. 2009;29(4):480-7.
106. Saul S, Gibhardt CS, Schmidt B, Lis A, Pasieka B, Conrad D, et al. A calcium-redox feedback loop controls human monocyte immune responses: The role of ORAI Ca2+ channels. Science Signaling. 2016;9(418):ra26-ra.
107. Chang ZL, Beezhold DH. Protein kinase C activation in human monocytes: regulation of PKC isoforms. Immunology. 1993;80(3):360-6.
108. Carnevale KA, Cathcart MK. Calcium-Independent Phospholipase A2 Is Required for Human Monocyte Chemotaxis to Monocyte Chemoattractant Protein 1. The Journal of Immunology. 2001;167(6):3414-21.
109. Zheng L, Zomerdijk TPL, Van Den Barselaar MT, Geertsma MF, Van Furth R, Nibbering PH. Arachidonic acid, but not its metabolites, is essential for FcγR-stimulated intracellular killing of Staphylococcus aureus by human monocytes. Immunology. 1999;96(1):90-7.
110. Cathcart MK, McNally AK, Morel DW, Chisolm GM. Superoxide anion participation in human monocyte-mediated oxidation of low-density lipoprotein and conversion of low-density lipoprotein to a cytotoxin. J Immunol. 1989;142(6):1963-9.
111. Dusi S, Donini M, Lissandrini D, Mazzi P, Bianca VD, Rossi F. Mechanisms of expression of NADPH oxidase components in human cultured monocytes: role of cytokines and transcriptional regulators involved. Eur J Immunol. 2001;31(3):929-38.
112. Boring L, Gosling J, Cleary M, Charo IF. Decreased lesion formation in CCR2-/- mice reveals a role for chemokines in the initiation of atherosclerosis. Nature. 1998;394(6696):894-7.
113. Barry-Lane PA, Patterson C, van der Merwe M, xE, Hu Z, Holland SM, et al. p47phox is required for atherosclerotic lesion progression in ApoE–/– mice. The Journal of Clinical Investigation. 2001;108(10):1513-22.
114. Jang JY, Min JH, Chae YH, Baek JY, Wang SB, Park SJ, et al. Reactive oxygen species play a critical role in collagen-induced platelet activation via SHP-2 oxidation. Antioxid Redox Signal. 2014;20(16):2528-40.
115. Arthur JF, Qiao J, Shen Y, Davis AK, Dunne E, Berndt MC, et al. ITAM receptor-mediated generation of reactive oxygen species in human platelets occurs via Syk-dependent and Syk-independent pathways. Journal of thrombosis and haemostasis : JTH. 2012;10(6):1133-41.
116. Begonja AJ, Gambaryan S, Geiger J, Aktas B, Pozgajova M, Nieswandt B, et al. Platelet NAD(P)H-oxidase-generated ROS production regulates alphaIIbbeta3-integrin activation independent of the NO/cGMP pathway. Blood. 2005;106(8):2757-60.
117. Krötz F, Sohn HY, Gloe T, Zahler S, Riexinger T, Schiele TM, et al. NAD(P)H oxidase–dependent platelet superoxide anion release increases platelet recruitment. Blood. 2002;100(3):917-24.
118. Plumb RD, El-Sherbeeny NA, Dixon LJ, Hughes SMT, Devine AB, Leahey WJ, et al. NAD(P)H-dependent superoxide production in platelets: The role of angiotensin II and protein kinase C. Clin Biochem. 2005;38(7):607-13.
119. Seno T, Inoue N, Gao D, Okuda M, Sumi Y, Matsui K, et al. Involvement of NADH/NADPH Oxidase in Human Platelet ROS Production. Thrombosis Research. 2001;103(5):399-409.

120. Dayal S, Wilson KM, Motto DG, Miller FJ, Chauhan AK, Lentz SR. Hydrogen Peroxide Promotes Aging-Related Platelet Hyperactivation and Thrombosis. Circulation. 2013;127(12):1308-16.
121. Pignatelli P, Carnevale R, Di Santo S, Bartimoccia S, Sanguigni V, Lenti L, et al. Inherited Human gp91phox Deficiency Is Associated With Impaired Isoprostane Formation and Platelet Dysfunction. Arterioscler Thromb Vasc Biol. 2011;31(2):423-34.
122. Leo R, Pratico` D, Iuliano L, Pulcinelli FM, Ghiselli A, Pignatelli P, et al. Platelet Activation by Superoxide Anion and Hydroxyl Radicals Intrinsically Generated by Platelets That Had Undergone Anoxia and Then Reoxygenated. Circulation. 1997;95(4):885-91.
123. Morrow JD. Quantification of Isoprostanes as Indices of Oxidant Stress and the Risk of Atherosclerosis in Humans. Arterioscler Thromb Vasc Biol. 2005;25(2):279-86.
124. Morrow JD, Hill KE, Burk RF, Nammour TM, Badr KF, Roberts LJ. A series of prostaglandin F2-like compounds are produced in vivo in humans by a non-cyclooxygenase, free radical-catalyzed mechanism. Proceedings of the National Academy of Sciences of the United States of America. 1990;87(23):9383-7.
125. Pignatelli P, Pulcinelli FM, Lenti L, Paolo Gazzaniga P, Violi F. Hydrogen Peroxide Is Involved in Collagen-Induced Platelet Activation. Blood. 1998;91(2):484-90.
126. Jin RC, Mahoney CE, Anderson L, Ottaviano F, Croce K, Leopold JA, et al. Glutathione Peroxidase-3 Deficiency Promotes Platelet-Dependent Thrombosis In Vivo. Circulation. 2011;123(18):1963-73.
127. Bokoch GM, Prossnitz V. Isoprenoid metabolism is required for stimulation of the respiratory burst oxidase of HL-60 cells. J Clin Invest. 1992;89(2):402-8.
128. Venter JC, Adams MD, Myers EW, Li PW, Mural RJ, Sutton GG, et al. The sequence of the human genome. Science. 2001;291(5507):1304-51.
129. Lander ES, Linton LM, Birren B, Nusbaum C, Zody MC, Baldwin J, et al. Initial sequencing and analysis of the human genome. Nature. 2001;409(6822):860-921.
130. Jewett MC, Noireaux V. Synthetic biology: Tailor-made genetic codes. Nat Chem. 2016;8(4):291-2.
131. Horgan RP, Kenny LC. 'Omic' technologies: genomics, transcriptomics, proteomics and metabolomics. The Obstetrician & Gynaecologist. 2011;13(3):189-95.
132. Saeys Y, Inza I, Larrañaga P. A review of feature selection techniques in bioinformatics. Bioinformatics. 2007;23(19):2507-17.
133. Walsh GM, Rogalski JC, Klockenbusch C, Kast J. Mass spectrometry-based proteomics in biomedical research: emerging technologies and future strategies. Expert reviews in molecular medicine. 2010;12:e30.
134. Tyers M, Mann M. From genomics to proteomics. Nature. 2003;422(6928):193-7.
135. Fenn JB, Mann M, Meng CK, Wong SF, Whitehouse CM. Electrospray ionization for mass spectrometry of large biomolecules. Science. 1989;246(4926):64-71.
136. Tang K, Fu D, Kötter S, Cotter RJ, Cantor CR, Köster H. Matrix-assisted laser desorption/ionization mass spectrometry of immobilized duplex DNA probes. Nucleic Acids Res. 1995;23(16):3126-31.
137. Tanaka K, Waki H, Ido Y, Akita S, Yoshida Y, Yoshida T, et al. Protein and polymer analyses up to m/z 100 000 by laser ionization time-of-flight mass spectrometry. Rapid Communications in Mass Spectrometry. 1988;2(8):151-3.

138. Wolters DA, Washburn MP, Yates JR. An Automated Multidimensional Protein Identification Technology for Shotgun Proteomics. Analytical Chemistry. 2001;73(23):5683-90.
139. Vorm O, Roepstorff P, Mann M. Improved Resolution and Very High Sensitivity in MALDI TOF of Matrix Surfaces Made by Fast Evaporation. Analytical Chemistry. 1994;66(19):3281-7.
140. Aebersold R, Mann M. Mass spectrometry-based proteomics. Nature. 2003;422(6928):198-207.
141. Hager JW. A new linear ion trap mass spectrometer. Rapid Communications in Mass Spectrometry. 2002;16(6):512-26.
142. Marshall AG, Hendrickson CL, Jackson GS. Fourier transform ion cyclotron resonance mass spectrometry: a primer. Mass spectrometry reviews. 1998;17(1):1-35.
143. Peterman SM, Dufresne CP, Horning S. The Use of a Hybrid Linear Trap/FT-ICR Mass Spectrometer for On-Line High Resolution/High Mass Accuracy Bottom-Up Sequencing. Journal of Biomolecular Techniques : JBT. 2005;16(2):112-24.
144. Hu Q, Noll RJ, Li H, Makarov A, Hardman M, Graham Cooks R. The Orbitrap: a new mass spectrometer. J Mass Spectrom. 2005;40(4):430-43.
145. Domon B, Aebersold R. Mass Spectrometry and Protein Analysis. Science. 2006;312(5771):212-7.
146. Chernushevich IV, Loboda AV, Thomson BA. An introduction to quadrupole-time-of-flight mass spectrometry. J Mass Spectrom. 2001;36(8):849-65.
147. Sze SK, Ge Y, Oh H, McLafferty FW. Top-down mass spectrometry of a 29-kDa protein for characterization of any posttranslational modification to within one residue. Proc Natl Acad Sci U S A. 2002;99(4):1774-9.
148. Han X, Jin M, Breuker K, McLafferty FW. Extending top-down mass spectrometry to proteins with masses greater than 200 kilodaltons. Science. 2006;314(5796):109-12.
149. Han X, Aslanian A, Yates JR, 3rd. Mass spectrometry for proteomics. Curr Opin Chem Biol. 2008;12(5):483-90.
150. Steen H, Mann M. The abc's (and xyz's) of peptide sequencing. Nat Rev Mol Cell Biol. 2004;5(9):699-711.
151. Mitchell Wells J, McLuckey SA. Collision‐Induced Dissociation (CID) of Peptides and Proteins. Methods Enzymol. Volume 402: Academic Press; 2005. p. 148-85.
152. Mikesh LM, Ueberheide B, Chi A, Coon JJ, Syka JE, Shabanowitz J, et al. The utility of ETD mass spectrometry in proteomic analysis. Biochimica et biophysica acta. 2006;1764(12):1811-22.
153. McLafferty FW, Horn DM, Breuker K, Ge Y, Lewis MA, Cerda B, et al. Electron capture dissociation of gaseous multiply charged ions by Fourier-transform ion cyclotron resonance. J Am Soc Mass Spectrom. 2001;12(3):245-9.
154. Elviri L. ETD and ECD mass spectrometry fragmentation for the characterization of protein post translational modifications: INTECH Open Access Publisher; 2012.
155. Eng JK, McCormack AL, Yates JR. An approach to correlate tandem mass spectral data of peptides with amino acid sequences in a protein database. J Am Soc Mass Spectrom. 1994;5(11):976-89.
156. Perkins DN, Pappin DJ, Creasy DM, Cottrell JS. Probability-based protein identification by searching sequence databases using mass spectrometry data. Electrophoresis. 1999;20(18):3551-67.

157. Clauser KR, Baker P, Burlingame AL. Role of accurate mass measurement (+/- 10 ppm) in protein identification strategies employing MS or MS/MS and database searching. Anal Chem. 1999;71(14):2871-82.
158. Craig R, Beavis RC. TANDEM: matching proteins with tandem mass spectra. Bioinformatics. 2004;20(9):1466-7.
159. Geer LY, Markey SP, Kowalak JA, Wagner L, Xu M, Maynard DM, et al. Open mass spectrometry search algorithm. J Proteome Res. 2004;3(5):958-64.
160. Bantscheff M, Schirle M, Sweetman G, Rick J, Kuster B. Quantitative mass spectrometry in proteomics: a critical review. Anal Bioanal Chem. 2007;389(4):1017-31.
161. Elliott MH, Smith DS, Parker CE, Borchers C. Current trends in quantitative proteomics. J Mass Spectrom. 2009;44(12):1637-60.
162. Ong SE, Blagoev B, Kratchmarova I, Kristensen DB, Steen H, Pandey A, et al. Stable isotope labeling by amino acids in cell culture, SILAC, as a simple and accurate approach to expression proteomics. Mol Cell Proteomics. 2002;1(5):376-86.
163. Zhu H, Pan S, Gu S, Bradbury EM, Chen X. Amino acid residue specific stable isotope labeling for quantitative proteomics. Rapid communications in mass spectrometry : RCM. 2002;16(22):2115-23.
164. Ong S-E, Kratchmarova I, Mann M. Properties of 13C-Substituted Arginine in Stable Isotope Labeling by Amino Acids in Cell Culture (SILAC). Journal of Proteome Research. 2003;2(2):173-81.
165. Harsha HC, Molina H, Pandey A. Quantitative proteomics using stable isotope labeling with amino acids in cell culture. Nat Protoc. 2008;3(3):505-16.
166. Kruger M, Moser M, Ussar S, Thievessen I, Luber CA, Forner F, et al. SILAC mouse for quantitative proteomics uncovers kindlin-3 as an essential factor for red blood cell function. Cell. 2008;134(2):353-64.
167. Geiger T, Cox J, Ostasiewicz P, Wisniewski JR, Mann M. Super-SILAC mix for quantitative proteomics of human tumor tissue. Nat Meth. 2010;7(5):383-5.
168. Gygi SP, Rist B, Gerber SA, Turecek F, Gelb MH, Aebersold R. Quantitative analysis of complex protein mixtures using isotope-coded affinity tags. Nat Biotechnol. 1999;17(10):994-9.
169. Gevaert K, Impens F, Ghesquiere B, Van Damme P, Lambrechts A, Vandekerckhove J. Stable isotopic labeling in proteomics. Proteomics. 2008;8(23-24):4873-85.
170. Ross PL, Huang YN, Marchese JN, Williamson B, Parker K, Hattan S, et al. Multiplexed protein quantitation in Saccharomyces cerevisiae using amine-reactive isobaric tagging reagents. Mol Cell Proteomics. 2004;3(12):1154-69.
171. Wiese S, Reidegeld KA, Meyer HE, Warscheid B. Protein labeling by iTRAQ: a new tool for quantitative mass spectrometry in proteome research. Proteomics. 2007;7(3):340-50.
172. Thompson A, Schäfer J, Kuhn K, Kienle S, Schwarz J, Schmidt G, et al. Tandem Mass Tags: A Novel Quantification Strategy for Comparative Analysis of Complex Protein Mixtures by MS/MS. Analytical Chemistry. 2003;75(8):1895-904.
173. Qu Z, Meng F, Bomgarden RD, Viner RI, Li J, Rogers JC, et al. Proteomic quantification and site-mapping of S-nitrosylated proteins using isobaric iodoTMT reagents. J Proteome Res. 2014;13(7):3200-11.
174. Marino SM, Gladyshev VN. Analysis and Functional Prediction of Reactive Cysteine Residues. J Biol Chem. 2012;287(7):4419-25.

175. Phalen TJ, Weirather K, Deming PB, Anathy V, Howe AK, van der Vliet A, et al. Oxidation state governs structural transitions in peroxiredoxin II that correlate with cell cycle arrest and recovery. The Journal of Cell Biology. 2006;175(5):779-89.
176. Tonks NK. Protein tyrosine phosphatases: from genes, to function, to disease. Nat Rev Mol Cell Biol. 2006;7(11):833-46.
177. Murphy E, Kohr M, Sun J, Nguyen T, Steenbergen C. S-Nitrosylation: A Radical Way to Protect the Heart. J Mol Cell Cardiol. 2012;52(3):568-77.
178. Martínez-Ruiz A, Cadenas S, Lamas S. Nitric oxide signaling: Classical, less classical, and nonclassical mechanisms. Free Radical Biol Med. 2011;51(1):17-29.
179. Nadtochiy SM, Burwell LS, Brookes PS. Cardioprotection and mitochondrial S-nitrosation: effects of S-nitroso-2-mercaptopropionyl glycine (SNO-MPG) in cardiac ischemia-reperfusion injury. J Mol Cell Cardiol. 2007;42(4):812-25.
180. Lindahl M, Mata-Cabana A, Kieselbach T. The Disulfide Proteome and Other Reactive Cysteine Proteomes: Analysis and Functional Significance. Antioxidants & Redox Signaling. 2011;14(12):2581-642.
181. Hill BG, Bhatnagar A. Protein S-glutathiolation: Redox-sensitive regulation of protein function. J Mol Cell Cardiol. 2012;52(3):559-67.
182. Jaffrey SR, Snyder SH. The biotin switch method for the detection of S-nitrosylated proteins. Science's STKE : signal transduction knowledge environment. 2001;2001(86):pl1.
183. Saurin AT, Neubert H, Brennan JP, Eaton P. Widespread sulfenic acid formation in tissues in response to hydrogen peroxide. Proc Natl Acad Sci U S A. 2004;101(52):17982-7.
184. Nelson KJ, Klomsiri C, Codreanu SG, Soito L, Liebler DC, Rogers LC, et al. Use of Dimedone-Based Chemical Probes for Sulfenic Acid Detection. Methods Enzymol. 2010;473:95-115.
185. Furdui CM, Poole LB. Chemical approaches to detect and analyze protein sulfenic acids. Mass spectrometry reviews. 2014;33(2):126-46.
186. Reynaert NL, Ckless K, Guala AS, Wouters EFM, van der Vliet A, Janssen-Heininger YMW. In situ detection of S-glutathionylated proteins following glutaredoxin-1 catalyzed cysteine derivatization. Biochimica et Biophysica Acta (BBA) - General Subjects. 2006;1760(3):380-7.
187. Brennan JP, Miller JIA, Fuller W, Wait R, Begum S, Dunn MJ, et al. The Utility of N,N-Biotinyl Glutathione Disulfide in the Study of Protein S-Glutathiolation. Molecular & Cellular Proteomics. 2006;5(2):215-25.
188. Clavreul N, Bachschmid MM, Hou X, Shi C, Idrizovic A, Ido Y, et al. S-Glutathiolation of p21ras by Peroxynitrite Mediates Endothelial Insulin Resistance Caused by Oxidized Low-Density Lipoprotein. Arterioscler Thromb Vasc Biol. 2006;26(11):2454-61.
189. Wang S-B, Foster DB, Rucker J, O'Rourke B, Kass DA, Van Eyk JE. Redox Regulation of Mitochondrial ATP synthase: Implications for Cardiac Resynchronization Therapy. Circ Res. 2011;109(7):750-7.
190. Hu W, Tedesco S, McDonagh B, Bárcena JA, Keane C, Sheehan D. Selection of thiol- and disulfide-containing proteins of Escherichia coli on activated thiol-Sepharose. Anal Biochem. 2010;398(2):245-53.
191. Leichert LI, Gehrke F, Gudiseva HV, Blackwell T, Ilbert M, Walker AK, et al. Quantifying changes in the thiol redox proteome upon oxidative stress in vivo. Proceedings of the National Academy of Sciences of the United States of America. 2008;105(24):8197-202.

192. Totani L, Evangelista V. Platelet-leukocyte interactions in cardiovascular disease and beyond. Arterioscler Thromb Vasc Biol. 2010;30(12):2357-61.
193. van Gils JM, Zwaginga JJ, Hordijk PL. Molecular and functional interactions among monocytes, platelets, and endothelial cells and their relevance for cardiovascular diseases. J Leukoc Biol. 2009;85(2):195-204.
194. Rendu F, Brohard-Bohn B. The platelet release reaction: granules' constituents, secretion and functions. Platelets. 2001;12(5):261-73.
195. Scheuerer B, Ernst M, Durrbaum-Landmann I, Fleischer J, Grage-Griebenow E, Brandt E, et al. The CXC-chemokine platelet factor 4 promotes monocyte survival and induces monocyte differentation into macrophages. Blood. 2001;95:1156-66.
196. Nassar T, Sachais BS, Akkawi S, Kowalska MA, Bdeir K, Leitersdorf E, et al. Platelet factor 4 enhances the binding of oxidized low-density lipoprotein to vascular wall cells. J Biol Chem. 2003;278(8):6187-93.
197. Victor M. Victor, Milagros Rocha, Eva Sola, Celia Banuls, Katherine Garcia-Malpartida, Hernandez-Mijares A. Oxidative stress, endothelial dysfunction and atherosclerosis. Curr Pharm Des. 2009(19):2988-3002.
198. Georgia Vogiatzi, Dimitris Tousoulis, Stefanadis C. the role of oxidative stress in atheroslcerosis. Hellenic J Cardiol. 2009(50):402-9.
199. Roger T. Dean, Shanlin Fu, Roland Stocker, Davies MJ. biochemistry and pathology of radical-mediated protein oxidation. Biochem J 1997(324):1-18.
200. Cui MZ. Lysophosphatidic acid effects on atherosclerosis and thrombosis. Clinical lipidology. 2011;6(4):413-26.
201. Alberto Bindoli JMF, Henry Jay Forman. thiol chemistry in peroxidase catalysis and redox signaling. Antioxid Redox Signal. 2008;10:1549-64.
202. Giorgio; M, Trinei; M, Migliaccio; E, Pelicci PG. hydorgen peroxide- a metabolic by-product or a common mediator of aging signals. Nat Rev Mol Cell Biol. 2007;8:722-8.
203. Lui JKC, Lipscombe R, Arthur PG. detecting changes in the thiol redox state of proteins following a decrease in oxygen concentration using a dual labeling technique. Journal of proteome research. 2010;9:383-92.
204. Murray CI, Van Eyk JE. Chasing cysteine oxidative modifications: proteomic tools for characterizing cysteine redox status. Circulation Cardiovascular genetics. 2012;5(5):591.
205. Heinecke JW. mass spectrometric quantification of amino acid oxidation products in proteins-insights into pathways that promote LDL oxidation in the human artery wall. FASEB 1999;13:1113-20.
206. Stocker R, Keaney JF. Role of oxidative modification in atherosclerosis. Physiol Rev. 2003;84:1381-478.
207. Guo J, Gaffrey MJ, Su D, Liu T, Camp DG, 2nd, Smith RD, et al. Resin-assisted enrichment of thiols as a general strategy for proteomic profiling of cysteine-based reversible modifications. Nat Proct. 2014;9(1):64-75.
208. Han P, Chen C. Detergent-free biotin switch combined with liquid chromatography/tandem mass spectrometry in the analysis of S-nitrosylated proteins. Rapid communications in mass spectrometry : RCM. 2008;22(8):1137-45.
209. Ong SE, Mann M. A practical recipe for stable isotope labeling by amino acids in cell culture (SILAC). Nat Protoc. 2006;1(6):2650-60.

210. Qin Z. The use of THP-1 cells as a model for mimicking the function and regulation of monocytes and macrophages in the vasculature. Atherosclerosis. 2012;221(1):2-11.
211. Hoffman MD, Walsh GM, Rogalski JC, Kast J. Identification of nitroxyl-induced modifications in human platelet proteins using a novel mass spectrometric detection method. Mol Cell Proteomics. 2009;8(5):887-903.
212. Cossarizza A, Ferraresi R, Troiano L, Roat E, Gibellini L, Bertoncelli L, et al. Simultaneous analysis of reactive oxygen species and reduced glutathione content in living cells by polychromatic flow cytometry. Nat Protoc. 2009;4(12):1790-7.
213. Jacek R. Wisniewski, Alexandre Zougman, Mann M. Combination of FASP and StageTip-Based Fractionation Allows in-Depth Analysis of the Hippocampal Membrane Proteome. J Proteome Res. 2009;8:5674-8.
214. Rappsilber J, Mann M, Ishihama Y. Protocol for micro-purification, enrichment, pre-fractionation and storage of peptides for proteomics using StageTips. Nat Protoc. 2007;2(8):1896-906.
215. Huang da W, Sherman BT, Lempicki RA. Systematic and integrative analysis of large gene lists using DAVID bioinformatics resources. Nat Protoc. 2009;4(1):44-57.
216. Huang da W, Sherman BT, Lempicki RA. Bioinformatics enrichment tools: paths toward the comprehensive functional analysis of large gene lists. Nucleic acids research. 2009;37(1):1-13.
217. Vizcaíno JA, Côté RG, Csordas A, Dianes JA, Fabregat A, Foster JM, et al. The PRoteomics IDEntifications (PRIDE) database and associated tools: status in 2013. Nucleic Acids Res. 2013;41(Database issue):D1063-9.
218. Shao W, Yeretssian G, Doiron K, Hussain SN, Saleh M. The caspase-1 digestome identifies the glycolysis pathway as a target during infection and septic shock. J Biol Chem. 2007;282(50):36321-9.
219. Benitez-Cardoza CG, Rojo-Domingues A, Hernandze-Arana A. temperature-induced denaturation and renaturation of triosephosphate isomerase for saccharomyces cerevisiae: evidence of dimerization coupled to refolding of the thermaly unfolded protein. Biochemistry 2001(40):9049-58.
220. Muller F, Aquilanti E, DePinho R. In vitro enzymatic activity assay for ENOLASE in mammalian cells in culture. 2012.
221. Agnes M. Gardner, Feng-hao Xu, Catherine Fady, Fred J. Jacoby, Dianne C. Duffey, Yiping Tu, et al. apoptotic vs. nonapoptotic cytotoxicity induced by hydrogen peroxide. Free Radic Biol Med. 1997;22:73-83.
222. Gao C, Guo H, Wei J, Mi Z, Wai PY, Kuo PC. Identification of S-nitrosylated proteins in endotoxin-stimulated RAW264.7 murine macrophages. Nitric oxide : biology and chemistry / official journal of the Nitric Oxide Society. 2005;12(2):121-6.
223. Hao G, Derakhshan B, Shi L, Campagne F, Gross SS. SNOSID, a proteomic method for identification of cysteine S-nitrosylation sites in complex protein mixtures. Proc Natl Acad Sci U S A. 2006;103(4):1012-7.
224. Lopez-Sanchez LM, Corrales FJ, Gonzalez R, Ferrin G, Munoz-Castaneda JR, Ranchal I, et al. Alteration of S-nitrosothiol homeostasis and targets for protein S-nitrosation in human hepatocytes. Proteomics. 2008;8(22):4709-20.
225. Wu C, LIu T, Chen W, Oka S-i, Fu C, Jain MR, et al. redox regulatory mechanism of transnitrosylation by Thioredoxin. Mol Cell Proteomics. 2010:2262-75.

226. Farah ME, Sirotkin V, Haarer B, Kakhniashvili D, Amberg DC. Diverse protective roles of the actin cytoskeleton during oxidative stress. Cytoskeleton. 2011;68(6):340-54.
227. Terman JR, Kashina A. Post-translational modification and regulation of actin. Curr Opin Cell Biol. 2013;25(1):30-8.
228. Klamt F, Zdanov S, Levine RL, Pariser A, Zhang Y, Zhang B, et al. Oxidant-induced apoptosis is mediated by oxidation of the actin-regulatory protein cofilin. Nat Cell Biol. 2009;11(10):1241-6.
229. Kil IS, Shin SW, Park JW. S-glutathionylation regulates GTP-binding of Rac2. Biochem Biophys Res Commun. 2012;425(4):892-6.
230. Lefievre L, Chen Y, Conner SJ, Scott JL, Publicover SJ, Ford WC, et al. Human spermatozoa contain multiple targets for protein S-nitrosylation: an alternative mechanism of the modulation of sperm function by nitric oxide? Proteomics. 2007;7(17):3066-84.
231. Zhou; X, Han; P, Li; J, Zhang; X, Huang; B, Ruan; H-Q, et al. ESNOQ, proteomic quantification of endogenous s-nitrosation. Plos One. 2010;5(4):1-7.
232. Victor Adler ZY, Serge Y. Fuchs, Miriam Benezra, Lilliam Rosario, Kenneth D. Tew, Matthew R. Pincus, MOhinder Sardana, Colin J. Henderson, C. Roland Wolf, Roger J. Davis, Ze'ev Ronai. regulation of JNK signaling by GSTp. The EMBO Journal. 1999;18(5):1321-34.
233. Hegazy UM, Tars K, Hellman U, Mannervik B. Modulating catalytic activity by unnatural amino acid residues in a GSH-binding loop of GST P1-1. J Mol Biol. 2008;376(3):811-26.
234. Chen JW, C.F. D, Feinstein SI, Jain MK, Fisher AB. 1-Cys peroxiredoxin, a bifunctional enzyme with glutathione peroxidase and phospholipase A2 activities. J Biol Chem. 2000(0021-9258 (Print)).
235. Greco TM, Hodara R, Parastatidis I, Heijnen HF, Dennehy MK, Liebler DC, et al. Identification of S-nitrosylation motifs by site-specific mapping of the S-nitrosocysteine proteome in human vascular smooth muscle cells. Proc Natl Acad Sci U S A. 2006;103(19):7420-5.
236. Kim HS, Ullevig SL, Zamora D, Lee CF, Asmis R. Redox regulation of MAPK phosphatase 1 controls monocyte migration and macrophage recruiment. Proc Natl Acad Sci USA. 2012;109(41):2803-12.
237. Bayat H, Schroder K, Pimentel DR, Brandes RP, Verbeuren TJ, Cohen RA, et al. Activation of thromboxane receptor modulates interleukin-1beta-induced monocyte adhesion--a novel role of Nox1. Free Radic Biol Med. 2012;52(9):1760-6.
238. Stephen J, Emerson B, Fox KA, Dransfield I. The uncoupling of monocyte-platelet interactions from the induction of proinflammatory signaling in monocytes. J Immunol. 2013;191(11):5677-83.
239. Bomgarde RD, Viner RI, Kuhn K, Pike I, Rogers JC. Iodoacetyl Tandem Mass Tags for Cysteine Peptide Modification, Enrichment and Quantitation. analysis. 2012;1(2):3.
240. Steven P.Gygi, Beate Rist, Scott A. Gerber, Frantisek Turecek, Michae H. Gelb, Aebersold R. Quantitative analysis of complex protein mixtures using isotope-coded affinity tags. Nat Biotechnol. 1999;17:994-9.
241. Nakajima H, Amano W, Fujita A, Fukuhara A, Azuma Y-T, Hata F, et al. The Active Site Cysteine of the Proapoptotic Protein Glyceraldehyde-3-phosphate Dehydrogenase Is Essential in Oxidative Stress-induced Aggregation and Cell Death. J Biol Chem. 2007;282(36):26562-74.

242. Ralser M, Wamelink MM, Kowald A, Gerisch B, Heeren G, Struys EA, et al. Dynamic rerouting of the carbohydrate flux is key to counteracting oxidative stress. J Biol. 2007;6(4):10.
243. Poole LB, Karplus PA, Claiborne A. Protein sulfenic acids in redox signaling. Annu Rev Pharmacol Toxicol. 2004;44:325-47.
244. Billiet L, Geerlings P, Messens J, Roos G. The thermodynamics of thiol sulfenylation. Free Radic Biol Med. 2012;52(8):1473-85.
245. Li R, Huang J, Kast J. Identification of Total Reversible Cysteine Oxidation in an Atherosclerosis Model Using a Modified Biotin Switch Assay. J Proteome Res. 2015;14(5):2026-35.
246. Meisel SR, Shapiro H, Radnay J, Neuman Y, Khaskia A-R, Gruener N, et al. Increased Expression of Neutrophil and Monocyte Adhesion Molecules LFA-1 and Mac-1 and Their Ligand ICAM-1 and VLA-4 Throughout the Acute Phase of Myocardial InfarctionPossible Implications for Leukocyte Aggregation and Microvascular Plugging. J Am Coll Cardiol. 1998;31(1):120-5.
247. Shevchenko A, Tomas H, Havlis J, Olsen JV, Mann M. In-gel digestion for mass spectrometric characterization of proteins and proteomes. Nat Protoc. 2006;1(6):2856-60.
248. Beck S, Michalski A, Raether O, Lubeck M, Kaspar S, Goedecke N, et al. The Impact II, a Very High-Resolution Quadrupole Time-of-Flight Instrument (QTOF) for Deep Shotgun Proteomics. Mol Cell Proteomics. 2015;14(7):2014-29.
249. Heyduk T, Moniewska A, Kochman M. The reactivity and function of cysteine residues in rabbit liver aldolase B. Biochimica et biophysica acta. 1986;874(3):337-46.
250. Benitez LV, Allison WS. The Inactivation of the Acyl Phosphatase Activity Catalyzed by the Sulfenic Acid Form of Glyceraldehyde 3-Phosphate Dehydrogenase by Dimedone and Olefins. J Biol Chem. 1974;249(19):6234-43.
251. Attila Miseta PC. relationship between occurence of cysteine in proteins and the complexity of organisms. Cysteine and Phylogenesis. 2000;17(8):1232-9.
252. Leonard SE, Reddie KG, Carroll KS. Mining the Thiol Proteome for Sulfenic Acid Modifications Reveals New Targets for Oxidation in Cells. ACS Chem Biol. 2009;4(9):783-99.
253. Charles RL, Schröder E, May G, Free P, Gaffney PRJ, Wait R, et al. Protein Sulfenation as a Redox Sensor: Proteomics Studies Using a Novel Biotinylated Dimedone Analogue. Mol Cell Proteomics. 2007;6(9):1473-84.
254. Gahmberg CG. Leukocyte adhesion: CD11/CD18 integrins and intercellular adhesion molecules. Curr Opin Cell Biol. 1997;9(5):643-50.
255. Auffray C, Fogg D, Garfa M, Elain G, Join-Lambert O, Kayal S, et al. Monitoring of blood vessels and tissues by a population of monocytes with patrolling behavior. Science. 2007;317(5838):666-70.
256. Issekutz AC, Issekutz TB. The contribution of LFA-1 (CD11a/CD18) and MAC-1 (CD11b/CD18) to the in vivo migration of polymorphonuclear leucocytes to inflammatory reactions in the rat. Immunology. 1992;76(4):655-61.
257. Gianni D, Taulet N, Zhang H, DerMardirossian C, Kister J, Martinez L, et al. A Novel and Specific NADPH Oxidase-1 (Nox1) Small-Molecule Inhibitor Blocks the Formation of Functional Invadopodia in Human Colon Cancer Cells. ACS Chem Biol. 2010;5(10):981-93.
258. Blouin E, Halbwache-Mecarelli L, Rieu P. redox regulation of beta-2 integrin CD11b:CD18 activation. Eur J Immunol. 1999;29:3419-31.

259. Sumagin R, Prizant H, Lomakina E, Waugh RE, Sarelius IH. LFA-1 and Mac-1 Define Characteristically Different Intralumenal Crawling and Emigration Patterns for Monocytes and Neutrophils In Situ. J Immunol. 2010;185(11):7057-66.
260. Yakubenko VP, Bhattacharjee A, Pluskota E, Cathcart MK. αMβ2 Integrin Activation Prevents Alternative Activation of Human and Murine Macrophages and Impedes Foam Cell Formation. Circ Res. 2011;108(5):544-54.
261. Huang J, Kast J. Quantitative Glycoproteomic Analysis Identifies Platelet-Induced Increase of Monocyte Adhesion via the Up-Regulation of Very Late Antigen 5. J Proteome Res. 2015;14(8):3015-26.
262. Vericel E, Januel C, Carreras M, Moulin P, Lagarde M. Diabetic patients without vascular complications display enhanced basal platelet activation and decreased antioxidant status. Diabetes. 2004;53(4):1046-51.
263. Lacoste L, Lam JY, Hung J, Letchacovski G, Solymoss CB, Waters D. Hyperlipidemia and coronary disease. Correction of the increased thrombogenic potential with cholesterol reduction. Circulation. 1995;92(11):3172-7.
264. Davi G, Romano M, Mezzetti A, Procopio A, Iacobelli S, Antidormi T, et al. Increased levels of soluble P-selectin in hypercholesterolemic patients. Circulation. 1998;97(10):953-7.
265. Willoughby SR, Stewart S, Holmes AS, Chirkov YY, Horowitz JD. Platelet nitric oxide responsiveness: a novel prognostic marker in acute coronary syndromes. Arterioscler Thromb Vasc Biol. 2005;25(12):2661-6.
266. Caccese D, Pratico D, Ghiselli A, Natoli S, Pignatelli P, Sanguigni V, et al. Superoxide anion and hydroxyl radical release by collagen-induced platelet aggregation--role of arachidonic acid metabolism. Thromb Haemost. 2000;83(3):485-90.
267. Wachowicz B, Olas B, Zbikowska HM, Buczynski A. Generation of reactive oxygen species in blood platelets. Platelets. 2002;13(3):175-82.
268. Tajima M, Sakagami H. Tetrahydrobiopterin impairs the action of endothelial nitric oxide via superoxide derived from platelets. Br J Pharmacol. 2000;131(5):958-64.
269. Chakrabarti S, Clutton P, Varghese S, Cox D, Mascelli MA, Freedman JE. Glycoprotein IIb/IIIa inhibition enhances platelet nitric oxide release. Thromb Res. 2004;113(3-4):225-33.
270. Saeed SA, Connor JD, Imran, Quadri J, Tasneem S, Ahmed S, et al. Inhibitors of phosphatidylinositide 3-kinase: effects on reactive oxygen species and platelet aggregation. Pharmacological reports : PR. 2007;59(2):238-43.
271. Iuliano L, Colavita AR, Leo R, Pratico D, Violi F. Oxygen free radicals and platelet activation. Free Radic Biol Med. 1997;22(6):999-1006.
272. Cerwinka WH, Cooper D, Krieglstein CF, Ross CR, McCord JM, Granger DN. Superoxide mediates endotoxin-induced platelet-endothelial cell adhesion in intestinal venules. American Journal of Physiology - Heart and Circulatory Physiology. 2003;284(2):H535-H41.
273. Funk SD, Jr AY, Orr AW. Hyperglycemia and Endothelial Dysfunction in Atherosclerosis: Lessons from Type 1 Diabetes. International Journal of Vascular Medicine. 2012;2012.
274. Aktas B, Utz A, Hoenig-Liedl P, Walter U, Geiger J. Dipyridamole enhances NO/cGMP-mediated vasodilator-stimulated phosphoprotein phosphorylation and signaling in human platelets: in vitro and in vivo/ex vivo studies. Stroke. 2003;34(3):764-9.
275. Fruhwirth GO, Loidl A, Hermetter A. Oxidized phospholipids: from molecular properties to disease. Biochimica et biophysica acta. 2007;1772(7):718-36.

276. Krotz F, Sohn HY, Pohl U. Reactive oxygen species: players in the platelet game. Arterioscler Thromb Vasc Biol. 2004;24(11):1988-96.
277. Nijland R, Hofland T, van Strijp JAG. Recognition of LPS by TLR4: Potential for Anti-Inflammatory Therapies. Mar Drugs. 2014;12(7):4260-73.
278. Chen K, Li W, Major J, Rahaman SO, Febbraio M, Silverstein RL. Vav guanine nucleotide exchange factors link hyperlipidemia and a prothrombotic state. Blood. 2011;117(21):5744-50.
279. Kuda O, Pietka TA, Demianova Z, Kudova E, Cvacka J, Kopecky J, et al. Sulfo-N-succinimidyl oleate (SSO) inhibits fatty acid uptake and signaling for intracellular calcium via binding CD36 lysine 164: SSO also inhibits oxidized low density lipoprotein uptake by macrophages. J Biol Chem. 2013;288(22):15547-55.
280. Cena C, Lolli ML, Lazzarato L, Guaita E, Morini G, Coruzzi G, et al. Antiinflammatory, gastrosparing, and antiplatelet properties of new NO-donor esters of aspirin. J Med Chem. 2003;46(5):747-54.
281. Maurice DH, Ke H, Ahmad F, Wang Y, Chung J, Manganiello VC. Advances in targeting cyclic nucleotide phosphodiesterases. Nat Rev Drug Discov. 2014;13(4):290-314.
282. Aversa A. Systemic and metabolic effects of PDE5-inhibitor drugs. World Journal of Diabetes. 2010;1(1):3-7.
283. Martinez-Ruiz A, Lamas S. Nitrosylation of thiols in vascular homeostasis and disease. Current atherosclerosis reports. 2005;7(3):213-8.
284. Hara MR, Agrawal N, Kim SF, Cascio MB, Fujimuro M, Ozeki Y, et al. S-nitrosylated GAPDH initiates apoptotic cell death by nuclear translocation following Siah1 binding. Nat Cell Biol. 2005;7(7):665-74.
285. Palmer CS, Cherry CL, Sada-Ovalle I, Singh A, Crowe SM. Glucose Metabolism in T Cells and Monocytes: New Perspectives in HIV Pathogenesis. EBioMedicine.
286. Katz A, Orell O. Protein Synthesis and the Stress Response. 2012.
287. Diamond MS, Staunton DE, de Fougerolles AR, Stacker SA, Garcia-Aguilar J, Hibbs ML, et al. ICAM-1 (CD54): a counter-receptor for Mac-1 (CD11b/CD18). The Journal of Cell Biology. 1990;111(6):3129-39.
288. Kamata T, Ambo H, Puzon-McLaughlin W, Tieu KK, Handa M, Ikeda Y, et al. Critical cysteine residues for regulation of integrin alphaIIbbeta3 are clustered in the epidermal growth factor domains of the beta3 subunit. Biochem J. 2004;378(Pt 3):1079-82.
289. Beglova N, Blacklow SC, Takagi J, Springer TA. Cysteine-rich module structure reveals a fulcrum for integrin rearrangement upon activation. Nat Struct Biol. 2002;9(4):282-7.
290. Ullevig S, Kim HS, Asmis R. S-glutathionylation in monocyte and macrophage (dys)function. Int J Mol Sci. 2013;14(8):15212-32.
291. Ullevig S, Zhao Q, Lee CF, Seok Kim H, Zamora D, Asmis R. NADPH oxidase 4 mediates monocyte priming and accelerated chemotaxis induced by metabolic stress. Arterioscler Thromb Vasc Biol. 2012;32(2):415-26.
292. Lee CF, Ullevig S, Kim HS, Asmis R. Regulation of Monocyte Adhesion and Migration by Nox4. PLoS ONE. 2013;8(6):e66964.
293. Gallogly MM, Mieyal JJ. Mechanisms of reversible protein glutathionylation in redox signaling and oxidative stress. Curr Opin Pharmacol. 2007;7(4):381-91.

294. Butturini E, Carcereri de Prati A, Chiavegato G, Rigo A, Cavalieri E, Darra E, et al. Mild oxidative stress induces S-glutathionylation of STAT3 and enhances chemosensitivity of tumoural cells to chemotherapeutic drugs. Free Radical Biol Med. 2013;65:1322-30.
295. Xie Y, Kole S, Precht P, Pazin MJ, Bernier M. S-Glutathionylation Impairs Signal Transducer and Activator of Transcription 3 Activation and Signaling. Endocrinology. 2009;150(3):1122-31.
296. Su D, Gaffrey MJ, Guo J, Hatchell KE, Chu RK, Clauss TRW, et al. Proteomic identification and quantification of S-glutathionylation in mouse macrophages using resin-assisted enrichment and isobaric labeling. Free Radical Biol Med. 2014;67:460-70.
297. Khosrovi-Eghbal A. Exploring the interaction environment of blood cells : proteomic analysis of platelet releasate and platelet-monocyte interaction [Text]2012.
298. Carlquist JF, Muhlestein JB, Anderson JL. Lipoprotein-associated phospholipase A2: a new biomarker for cardiovascular risk assessment and potential therapeutic target. Expert review of molecular diagnostics. 2007;7(5):511-7.
299. van Meeteren LA, Moolenaar WH. Regulation and biological activities of the autotaxin–LPA axis. Progress in Lipid Research. 2007;46(2):145-60.
300. Trip MD, Cats VM, van Capelle FJ, Vreeken J. Platelet hyperreactivity and prognosis in survivors of myocardial infarction. N Engl J Med. 1990;322(22):1549-54.
301. Vanschoonbeek K, Feijge MA, Keuren JF, Coenraad Hemker H, Lodder JJ, Hamulyak K, et al. Thrombin-induced hyperactivity of platelets of young stroke patients: involvement of thrombin receptors in the subject-dependent variability in Ca2+ signal generation. Thromb Haemost. 2002;88(6):931-7.
302. Fine KM, Ashbrook PC, Brigden LP, Maldonado JE, Didishelm P. Gel-filtered human platelets. Ultrastructure, function, and role of proteins in inhibition of aggregation by aspirin. The American journal of pathology. 1976;84(1):11-24.
303. Sedeek M, Hebert RL, Kennedy CR, Burns KD, Touyz RM. Molecular mechanisms of hypertension: role of Nox family NADPH oxidases. Current opinion in nephrology and hypertension. 2009;18(2):122-7.
304. Munzel T, Gori T, Bruno RM, Taddei S. Is oxidative stress a therapeutic target in cardiovascular disease? Eur Heart J. 2010;31(22):2741-8.
305. Deliyanti D, Wilkinson-Berka JL. Inhibition of NOX1/4 with GKT137831: a potential novel treatment to attenuate neuroglial cell inflammation in the retina. Journal of Neuroinflammation. 2015;12(1):1-13.

# Appendices

## Appendix A

**A.1 Increased ROS production in THP-1 cells upon $H_2O_2$ treatment for one hour and six hours.**

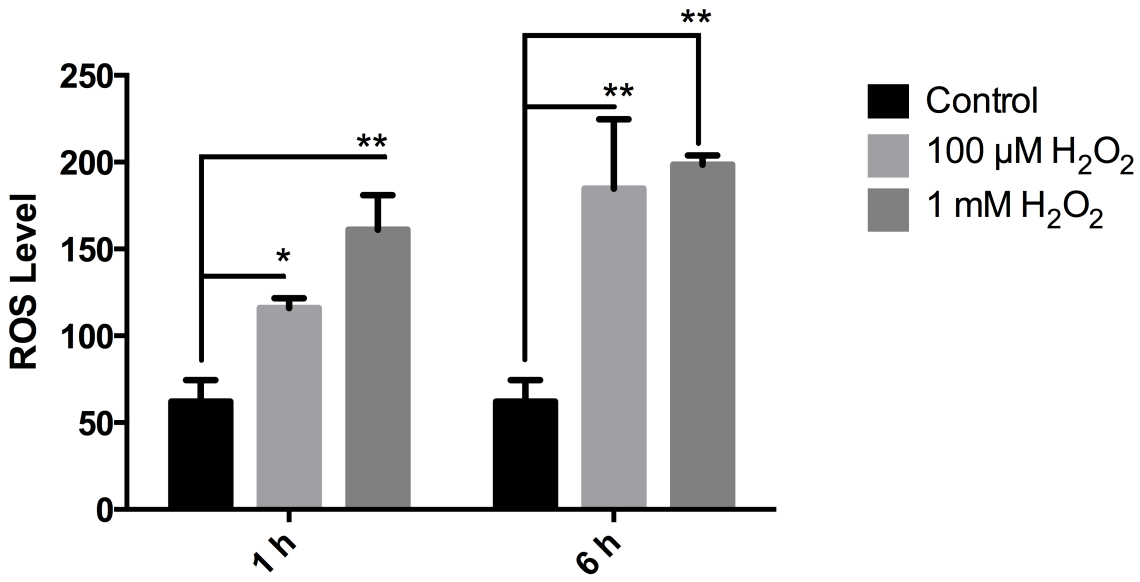


**A.2 The overlap of A. total peptides; B. Cys-containing peptides among three replicates in THP-1 cells with LPA-PR treatment for six hours.**

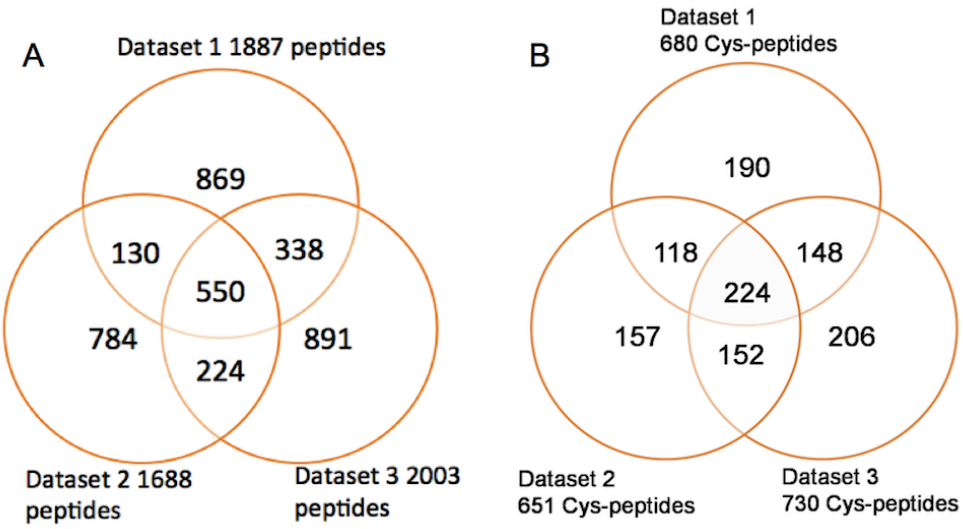

**A.3 The overlap of A. total peptides; B. Cys-containing peptides among three replicates in THP-1 cells with Thr-PR treatment for six hours.**

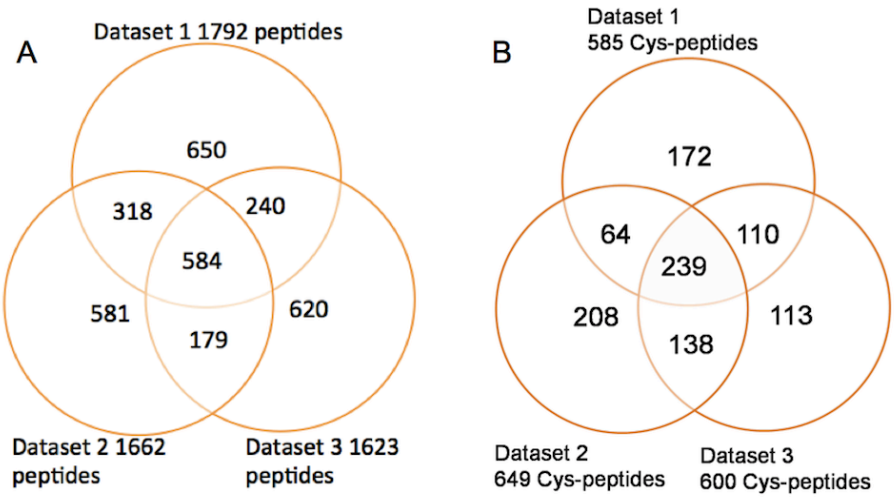


**A.4 The overlap of A. total peptides; B. Cys-containing peptides among three replicates in THP-1 cells with DPI 1h pretreatment following by LPA-PR six hours treatment.**

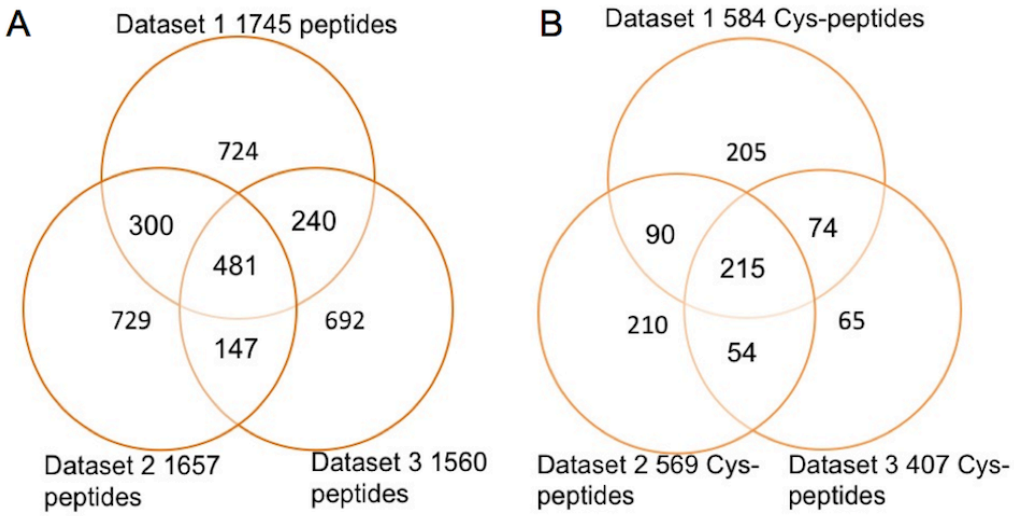

## A.5 Enrichment Efficiency of the Modified Biotin switch assay on THP-1 cells with LPA-PR treatment for six hours.

| # of replicates | Total # of peptides | # of Cys-containing peptides |
|---|---|---|
| 1 | 1887 | 680 |
| 2 | 1688 | 651 |
| 3 | 2003 | 730 |

## A.6 The 120 $Cys_{OX}$ containing peptides in six hours LPA-PR treatment with their H/L ratio.

| UniProt ID | Sequence | H/L | SD |
|---|---|---|---|
| 1433Z_HUMAN | YDDMAACMK | 2.62 | 1.51 |
| | DICNDVLSLLEK | 1.44 | 0.00 |
| ACTB_HUMAN | LCYVALDFEQEMATAASSSSLEK | 2.02 | 0.47 |
| | CDVDIR | 2.67 | 1.10 |
| ALDOA_HUMAN | ALANSLACQGK | 1.39 | 0.17 |
| ANXA6_HUMAN | CLIEILASR | 1.53 | 0.27 |
| ARP2_HUMAN | LCYVGYNIEQEQK | 2.79 | 0.64 |
| ARP3_HUMAN | LPACVVDCGTGYTK | 4.05 | 2.97 |
| | YSYVCPDLVK | 2.44 | 1.05 |
| | LGYAGNTEPQFIIPSCIAIK | 1.61 | 0.23 |
| CALR_HUMAN | HEQNIDCGGGYVK | 1.57 | 0.23 |
| CAP1_HUMAN | ALLVTASQCQQPAENK | 2.36 | 1.06 |
| | CVNTTLQIK | 2.46 | 0.97 |
| | NSLDCEIVSAK | 1.69 | 0.42 |
| | INSITVDNCK | 1.57 | 0.19 |
| | TDGCHAYLSK | 1.53 | 0.16 |
| CAPZB_HUMAN | DYLLCDYNR | 1.69 | 0.83 |
| | NLSDLIDLVPSLCEDLLSSVDQPLK | 2.11 | 0.17 |
| CDC42_HUMAN | YVECSALTQK | 2.54 | 0.69 |
| CH60_HUMAN | AAVEEGIVLGGGCALLR | 3.00 | 0.13 |
| CLCB_HUMAN | VAQLCDFNPK | 1.83 | 0.17 |
| CLIC1_HUMAN | FLDGNELTLADCNLLPK | 2.50 | 1.23 |
| | LHIVQVVCK | 3.07 | 0.66 |
| | IGNCPFSQR | 2.72 | 0.60 |
| COF1_HUMAN | AVLFCLSEDK | 6.60 | 1.06 |
| | HELQANCYEEVK | 3.25 | 0.63 |
| DDX17_HUMAN | STCIYGGAPK | 2.19 | 0.28 |
| DX39B_HUMAN | HFILDECDK | 1.95 | 0.47 |

| UniProt ID | Sequence | H/L | SD |
|---|---|---|---|
| EF2_HUMAN | STLTDSLVCK | 4.15 | 2.17 |
| | TFCQLILDPIFK | 2.31 | 0.97 |
| ENOA_HUMAN | SCNCLLLK | 9.03 | 2.97 |
| | VNQIGSVTESLQACK | 4.18 | 2.25 |
| ETFA_HUMAN | TIYAGNALCTVK | 5.39 | 2.91 |
| | LGGEVSCLVAGTK | 12.91 | 1.18 |
| G3P_HUMAN | IISNASCTTNCLAPLAK | 1.41 | 0.03 |
| GBB1_HUMAN | LFVSGACDASAK | 2.45 | 0.50 |
| GNAI2_HUMAN | IIHEDGYSEEECR | 1.39 | 0.09 |
| GNAI3_HUMAN | IIHEDGYSEDECK | 1.36 | 0.05 |
| GSTP1_HUMAN | ASCLYGQLPK | 2.44 | 0.72 |
| HNRPD_HUMAN | FGEVVDCTLK | 3.35 | 1.67 |
| | GFCFITFK | 2.39 | 0.40 |
| HNRPQ_HUMAN | GFCFLEYEDHK | 1.44 | 0.09 |
| HS105_HUMAN | GCALQCAILSPAFK | 2.93 | 1.33 |
| HSP7C_HUMAN | CNEIINWLDK | 2.47 | 0.65 |
| | VCNPIITK | 2.25 | 0.26 |
| LDHA_HUMAN | VIGSGCNLDSAR | 2.54 | 1.17 |
| LEG1_HUMAN | IKCVAFD | 3.49 | 1.61 |
| | FNAHGDANTIVCNSK | 1.43 | 0.12 |
| MDHM_HUMAN | TIIPLISQCTPK | 1.70 | 0.62 |
| MIF_HUMAN | LLCGLLAER | 1.48 | 0.15 |
| NDK8_HUMAN | GDFCIQVGR | 5.21 | 0.72 |
| NH2L1_HUMAN | PVIACSVTIK | 2.17 | 0.88 |
| PCBP1_HUMAN | LVVPATQCGSLIGK | 2.21 | 1.03 |
| PCBP2_HUMAN | LVVPASQCGSLIGK | 1.54 | 0.53 |
| | AITIAGIPQSIIECVK | 1.51 | 0.04 |
| PGK1_HUMAN | DCVGPEVEK | 1.64 | 0.35 |
| | GCITIIGGGDTATCCAK | 1.71 | 0.13 |
| PLSL_HUMAN | EGICAIGGTSEQSSVGTQHSYSEEE | 1.57 | 0.04 |
| PP1G_HUMAN | IYGFYDECK | 2.05 | 1.06 |
| PPIA_HUMAN | KITIADCGQLE | 1.93 | 0.70 |
| | IIPGFMCQGGDFTR | 1.97 | 0.59 |
| PRDX6_HUMAN | DINAYNCEEPTEK | 1.41 | 0.06 |
| RAC2_HUMAN | AVLCPQPTR | 2.18 | 1.00 |
| | YLECSALTQR | 3.27 | 0.82 |
| RAN_HUMAN | VCENIPIVLCGNK | 2.06 | 0.49 |
| RINI_HUMAN | LDDCGLTEAR | 2.98 | 0.62 |
| RL12_HUMAN | EILGTAQSVGCNVDGR | 2.14 | 0.82 |
| RL14_HUMAN | ALVDGPCTQVR | 1.48 | 0.26 |
| | CMQLTDFILK | 1.44 | 0.05 |
| RL18_HUMAN | GCGTVLLSGPR | 2.29 | 0.70 |
| RL18A_HUMAN | DLTTAGAVTQCYR | 1.45 | 0.15 |
| RL23_HUMAN | ISLGLPVGAVINCADNTGAK | 1.96 | 0.68 |

| UniProt ID | Sequence | H/L | SD |
|---|---|---|---|
| RL24_HUMAN | VELCSFSGYK | 2.32 | 0.80 |
| RL28_HUMAN | NCSSFLIK | 2.22 | 0.42 |
| RL30_HUMAN | VCTLAIIDPGDSDIIR | 1.62 | 0.60 |
| RL32_HUMAN | SYCAEIAHNVSSK | 2.94 | 0.97 |
| RL34_HUMAN | SACGVCPGR | 1.84 | 0.11 |
| RL36L_HUMAN | LECVEPNCR | 1.74 | 0.24 |
| RL4_HUMAN | SGQGAFGNMCR | 1.62 | 0.43 |
| | FCIWTESAFR | 1.49 | 0.04 |
| RL5_HUMAN | DIICQIAYAR | 1.70 | 0.28 |
| RLF_HUMAN | SSEDEEMKASVCK | 15.65 | 4.41 |
| RS11_HUMAN | CPFTGNVSIR | 1.51 | 0.12 |
| RS12_HUMAN | KVVGCSCVVVK | 2.25 | 0.95 |
| | LGEWVGLCK | 2.31 | 0.82 |
| | VVGCSCVVVK | 2.93 | 0.75 |
| | LVEALCAEHQINLIK | 1.69 | 0.20 |
| RS15A_HUMAN | CGVISPR | 1.70 | 0.57 |
| RS17L_HUMAN | VCEEIAIIPSK | 4.98 | 0.09 |
| RS2_HUMAN | GCTATLGNFAK | 2.43 | 0.67 |
| RS21_HUMAN | TYAICGAIR | 3.76 | 1.68 |
| RS27L_HUMAN | LTEGCSFR | 2.70 | 1.17 |
| RS28_HUMAN | TGSQGQCTQVR | 4.25 | 2.10 |
| RS3_HUMAN | GCEVVVSGK | 12.41 | 1.59 |
| | RACYGVLR | 1.37 | 0.19 |
| RS3A_HUMAN | ACQSIYPLHDVFVR | 2.15 | 0.08 |
| RS5_HUMAN | TIAECLADELINAAK | 1.90 | 0.36 |
| | VNQAIWLLCTGAR | 1.98 | 0.32 |
| | AQCPIVER | 1.78 | 0.29 |
| RS6_HUMAN | LNISFPATGCQK | 2.50 | 1.20 |
| RS8_HUMAN | LLACIASR | 1.52 | 0.06 |
| SERA_HUMAN | VLISDSLDPCCRK | 2.82 | 0.42 |
| | NAGNCLSPAVIVGLLK | 1.56 | 0.13 |
| SMD2_HUMAN | HCNMVLENVK | 1.72 | 0.49 |
| TBA1B_HUMAN | SIQFVDWCPTGFK | 1.63 | 0.30 |
| | AVCMLSNTTAIAEAWAR | 1.63 | 0.11 |
| TBA1C_HUMAN | TIQFVDWCPTGFK | 1.91 | 0.72 |
| TBB3_HUMAN | NMMAACDPR | 6.82 | 4.48 |
| | EIVHIQAGQCGNQIGAK | 1.91 | 0.82 |
| TBB5_HUMAN | TAVCDIPPR | 2.68 | 0.52 |
| TCPA_HUMAN | VLCELADLQDK | 1.57 | 0.59 |
| TCPB_HUMAN | SLHDALCVLAQTVK | 1.80 | 0.30 |
| TCPG_HUMAN | TLIQNCGASTIR | 2.73 | 0.23 |
| TEBP_HUMAN | LTFSCLGGSDNFK | 1.73 | 0.31 |
| THIO_HUMAN | CMPTFQFFK | 2.62 | 0.94 |
| TPIS_HUMAN | IAVAAQNCYK | 2.00 | 0.82 |

| UniProt ID | Sequence | H/L | SD |
|---|---|---|---|
| UB2L3_HUMAN | GQVCLPVISAENWKPATK | 1.54 | 0.07 |
| UBA1_HUMAN | YFLVGAGAIGCELLK | 1.46 | 0.29 |
| UBC12_HUMAN | LVICPDEGFYK | 4.34 | 0.66 |
| UBE2N_HUMAN | ICLDILK | 1.60 | 0.17 |

## A.7 Enrichment Efficiency of the Modified Biotin switch assay on THP-1 cells with Thr-PR treatment for six hours.

| # of replicates | Total # of peptides | # of Cys-containing peptides |
|---|---|---|
| 1 | 1792 | 585 |
| 2 | 1662 | 649 |
| 3 | 1623 | 600 |

## A.8 The 105 $Cys_{OX}$ containing peptides in six-hour Thr-PR treatment with their H/L ratio

| UniProt ID | Sequence | H/L | SD |
|---|---|---|---|
| 1433Z_HUMAN | YDDMAACMK | 2.54 | 0.81 |
| | DICNDVLSLLEK | 1.70 | 0.40 |
| ACTB_HUMAN | LCYVALDFEQEMATAASSSSLEK | 2.00 | 0.31 |
| | CDVDIR | 2.70 | 0.82 |
| ALDOA_HUMAN | ALANSLACQGK | 1.41 | 0.06 |
| ARP2_HUMAN | LCYVGYNIEQEQK | 1.53 | 0.07 |
| ARP3_HUMAN | KDYEEIGPSICR | 2.43 | 1.56 |
| | YSYVCPDLVK | 1.67 | 0.11 |
| | LPACVVDCGTGYTK | 1.38 | 0.07 |
| CALR_HUMAN | HEQNIDCGGGYVK | 2.18 | 0.86 |
| CAP1_HUMAN | ALLVTASQCQQPAENK | 2.79 | 1.30 |
| | NSLDCEIVSAK | 1.65 | 0.28 |
| | CVNTTLQIK | 1.69 | 0.49 |
| | INSITVDNCK | 1.79 | 0.29 |
| | TDGCHAYLSK | 1.64 | 0.30 |
| CAPZB_HUMAN | NLSDLIDLVPSLCEDLLSSVDQPLK | 1.74 | 0.04 |
| | DYLLCDYNR | 1.58 | 0.00 |
| CATA_HUMAN | LCENIAGHLK | 3.35 | 2.05 |
| CDC42_HUMAN | YVECSALTQK | 4.30 | 2.31 |
| CH60_HUMAN | AAVEEGIVLGGGCALLR | 1.36 | 0.03 |
| CLCB_HUMAN | VAQLCDFNPK | 1.56 | 0.22 |
| CLIC1_HUMAN | LHIVQVVCK | 6.86 | 3.45 |
| | LHIVQVVCKK | 9.87 | 3.04 |
| | FLDGNELTLADCNLLPK | 2.68 | 0.99 |

| UniProt ID | Sequence | H/L | SD |
|---|---|---|---|
| | IGNCPFSQR | 1.54 | 0.03 |
| CNBP_HUMAN | CGETGHVAINCSK | 2.14 | 0.90 |
| COF1_HUMAN | AVLFCLSEDK | 2.77 | 0.88 |
| | AVLFCLSEDKK | 2.85 | 0.93 |
| | HELQANCYEEVK | 1.37 | 0.07 |
| DDX5_HUMAN | LIDFLECGK | 1.69 | 0.07 |
| ECHM_HUMAN | ICPVETLVEEAIQCAEK | 18.14 | 13.90 |
| EF2_HUMAN | TFCQLILDPIFK | 1.64 | 0.48 |
| | STLTDSLVCK | 1.48 | 0.19 |
| ENOA_HUMAN | SCNCLLLK | 1.95 | 0.23 |
| | SGETEDTFIADLVVGLCTGQIK | 2.44 | 0.33 |
| | VNQIGSVTESLQACK | 2.22 | 0.91 |
| ETFA_HUMAN | LGGEVSCLVAGTK | 6.16 | 3.91 |
| | TIYAGNALCTVK | 10.55 | 0.94 |
| GBB1_HUMAN | LFVSGACDASAK | 1.72 | 0.40 |
| GPV_HUMAN | LRGTLLCAVLGLLR | 7.61 | 6.53 |
| GPX1_HUMAN | LITWSPVCR | 1.39 | 0.05 |
| GSTP1_HUMAN | ASCLYGQLPK | 1.78 | 0.13 |
| HNRPD_HUMAN | FGEVVDCTLK | 1.83 | 0.63 |
| | GFCFITFK | 2.25 | 0.88 |
| HNRPK_HUMAN | GSDFDCELR | 1.41 | 0.03 |
| HNRPQ_HUMAN | GFCFLEYEDHK | 1.75 | 0.55 |
| HSP74_HUMAN | GCALQCAILSPAFK | 2.58 | 0.79 |
| HSP7C_HUMAN | VCNPIITK | 1.54 | 0.33 |
| | CNEIINWLDK | 1.39 | 0.09 |
| IDH3A_HUMAN | IEAACFATIK | 4.53 | 0.91 |
| ITB2_HUMAN | YISCAECLK | 1.89 | 0.58 |
| LDHA_HUMAN | VIGSGCNLDSAR | 16.67 | 0.78 |
| LEG1_HUMAN | FNAHGDANTIVCNSK | 1.37 | 0.04 |
| | DSNNLCLHFNPR | 1.49 | 0.00 |
| | IKCVAFD | 1.75 | 0.44 |
| MDHC_HUMAN | VIVVGNPANTNCLTASK | 1.38 | 0.06 |
| MDHM_HUMAN | TIIPLISQCTPK | 1.43 | 0.06 |
| MIF_HUMAN | LLCGLLAER | 1.49 | 0.08 |
| NDKA_HUMAN | GDFCIQVGR | 1.88 | 0.29 |
| NTAL_HUMAN | FSKPPEDDDANSYENVLICK | 4.94 | 0.91 |
| PCBP2_HUMAN | AITIAGIPQSIIECVK | 2.48 | 0.01 |
| PGK1_HUMAN | DVLFLKDCVGPEVEK | 1.74 | 0.13 |
| | GCITIIGGGDTATCCAK | 1.70 | 0.41 |
| PLSL_HUMAN | EGICAIGGTSEQSSVGTQHSYSEEEK | 1.80 | 0.34 |
| PPIA_HUMAN | KITIADCGQLE | 1.89 | 0.95 |
| PRDX6_HUMAN | DINAYNCEEPTEK | 1.33 | 0.13 |
| PTN6_HUMAN | AYGPYSVTNCGEHDTTEYK | 2.20 | 0.65 |
| RAC2_HUMAN | CVVVGDGAVGK | 6.07 | 0.51 |
| | YLECSALTQR | 1.35 | 0.05 |
| RAN_HUMAN | VCENIPIVLCGNK | 1.46 | 0.08 |
| RHOA_HUMAN | IGAFGYMECSAK | 3.29 | 0.37 |
| | LVIVGDGACGK | 2.00 | 0.46 |

| UniProt ID | Sequence | H/L | SD |
|---|---|---|---|
| RINI_HUMAN | LDDCGLTEAR | 1.88 | 0.23 |
| | SNELGDVGVHCVLQGLQTPSCK | 1.81 | 0.32 |
| RL10A_HUMAN | FSVCVLGDQQHCDEAK | 6.79 | 3.42 |
| RL14_HUMAN | CMQLTDFILK | 3.27 | 0.81 |
| RL23_HUMAN | ISLGLPVGAVINCADNTGAK | 1.85 | 0.17 |
| ROA3_HUMAN | WGTLTDCVVMR | 1.86 | 0.11 |
| RS12_HUMAN | KVVGCSCVVVK | 1.43 | 0.08 |
| | LVEALCAEHQINLIK | 1.67 | 0.11 |
| | LGEWVGLCK | 1.33 | 0.18 |
| RS27L_HUMAN | LTEGCSFR | 2.03 | 0.25 |
| RS3A_HUMAN | ACQSIYPLHDVFVR | 3.46 | 0.88 |
| RS5_HUMAN | TIAECLADELINAAK | 1.72 | 0.36 |
| RSSA_HUMAN | YVDIAIPCNNK | 3.50 | 0.25 |
| SERA_HUMAN | NAGNCLSPAVIVGLLK | 1.91 | 0.46 |
| | VLISDSLDPCCRK | 1.84 | 0.18 |
| SMD2_HUMAN | HCNMVLENVK | 1.89 | 0.44 |
| SRSF9_HUMAN | EAGDVCYADVQK | 2.77 | 0.60 |
| SYWC_HUMAN | GIFGFTDSDCIGK | 11.29 | 7.50 |
| TALDO_HUMAN | ALAGCDFLTISPK | 1.80 | 0.07 |
| TBA1B_HUMAN | SIQFVDWCPTGFK | 1.49 | 0.13 |
| | AVCMLSNTTAIAEAWAR | 1.55 | 0.11 |
| TBA1C_HUMAN | TIQFVDWCPTGFK | 1.73 | 0.22 |
| TBB3_HUMAN | EIVHIQAGQCGNQIGAK | 1.45 | 0.09 |
| | NMMAACDPR | 1.49 | 0.14 |
| TBB5_HUMAN | TAVCDIPPR | 2.17 | 0.51 |
| TCPB_HUMAN | SLHDALCVLAQTVK | 1.64 | 0.41 |
| TCPG_HUMAN | TLIQNCGASTIR | 1.31 | 0.07 |
| TEBP_HUMAN | LTFSCLGGSDNFK | 2.54 | 0.31 |
| THIO_HUMAN | CMPTFQFFK | 2.42 | 0.40 |
| TPIS_HUMAN | IAVAAQNCYK | 1.95 | 0.58 |
| UBC12_HUMAN | LVICPDEGFYK | 1.88 | 0.59 |
| VDAC1_HUMAN | YQIDPDACFSAK | 3.27 | 1.58 |

## A.9 $Cys_{OX}$ containing peptides overlap between LPA-PR and Thr-PR with their H/L ratio.

| UniProt ID | Sequence | LPA-PR | Thr-PR |
|---|---|---|---|
| | | H/L±SD | H/L±SD |
| 1433Z_HUMAN | DICNDVLSLLEK | 1.44±0 | 1.7±0.4 |
| | YDDMAACMK | 2.62±1.51 | 2.54±0.81 |
| ACTB_HUMAN | CDVDIR | 2.67±1.1 | 2.7±0.82 |
| | LCYVALDFEQEMATAASSSSLEK | 2.02±0.47 | 2±0.31 |
| ALDOA_HUMAN | ALANSLACQGK | 1.39±0.17 | 1.41±0.06 |
| ARP2_HUMAN | LCYVGYNIEQEQK | 2.79±0.64 | 1.53±0.07 |

| UniProt ID | Sequence | LPA-PR | Thr-PR |
|---|---|---|---|
| | | H/L±SD | H/L±SD |
| ARP3_HUMAN | LPACVVDCGTGYTK | 4.05±2.97 | 1.38±0.07 |
| | YSYVCPDLVK | 2.44±1.05 | 1.67±0.11 |
| CALR_HUMAN | HEQNIDCGGGYVK | 1.57±0.23 | 2.18±0.86 |
| CAP1_HUMAN | ALLVTASQCQQPAENK | 2.36±1.06 | 2.79±1.3 |
| | CVNTTLQIK | 2.46±0.97 | 1.69±0.49 |
| | INSITVDNCK | 1.57±0.19 | 1.79±0.29 |
| | NSLDCEIVSAK | 1.69±0.42 | 1.65±0.28 |
| | TDGCHAYLSK | 1.53±0.16 | 1.64±0.3 |
| CAPZB_HUMAN | DYLLCDYNR | 1.69±0.83 | 1.58±0 |
| | NLSDLIDLVPSLCEDLLSSVDQPL | 2.11±0.17 | 1.74±0.04 |
| CDC42_HUMAN | YVECSALTQK | 2.54±0.69 | 4.3±2.31 |
| CH60_HUMAN | AAVEEGIVLGGGCALLR | 3±0.13 | 1.36±0.03 |
| CLCB_HUMAN | VAQLCDFNPK | 1.83±0.17 | 1.56±0.22 |
| CLIC1_HUMAN | FLDGNELTLADCNLLPK | 2.5±1.23 | 2.68±0.99 |
| | IGNCPFSQR | 2.72±0.6 | 1.54±0.03 |
| | LHIVQVVCK | 3.07±0.66 | 6.86±3.45 |
| COF1_HUMAN | AVLFCLSEDK | 6.6±1.06 | 2.77±0.88 |
| | HELQANCYEEVK | 3.25±0.63 | 1.37±0.07 |
| EF2_HUMAN | STLTDSLVCK | 4.15±2.17 | 1.48±0.19 |
| | TFCQLILDPIFK | 2.31±0.97 | 1.64±0.48 |
| ENOA_HUMAN | SCNCLLLK | 9.03±2.97 | 1.95±0.23 |
| | VNQIGSVTESLQACK | 4.18±2.25 | 2.22±0.91 |
| ETFA_HUMAN | LGGEVSCLVAGTK | 12.91±1.1 | 6.16±3.91 |
| | TIYAGNALCTVK | 5.39±2.91 | 10.55±0.9 |
| GBB1_HUMAN | LFVSGACDASAK | 2.45±0.5 | 1.72±0.4 |
| GSTP1_HUMAN | ASCLYGQLPK | 2.44±0.72 | 1.78±0.13 |
| HNRPD_HUMAN | FGEVVDCTLK | 3.35±1.67 | 1.83±0.63 |
| | GFCFITFK | 2.39±0.4 | 2.25±0.88 |
| HNRPQ_HUMAN | GFCFLEYEDHK | 1.44±0.09 | 1.75±0.55 |
| HSP74_HUMAN | GCALQCAILSPAFK | 2.93±1.33 | 2.58±0.79 |
| HSP7C_HUMAN | CNEIINWLDK | 2.47±0.65 | 1.39±0.09 |
| | VCNPIITK | 2.25±0.26 | 1.54±0.33 |
| LDHA_HUMAN | VIGSGCNLDSAR | 2.54±1.17 | 16.67±0.7 |
| LEG1_HUMAN | FNAHGDANTIVCNSK | 1.43±0.12 | 1.37±0.04 |
| | IKCVAFD | 3.49±1.61 | 1.75±0.44 |
| MDHM_HUMAN | TIIPLISQCTPK | 1.7±0.62 | 1.43±0.06 |
| MIF_HUMAN | LLCGLLAER | 1.48±0.15 | 1.49±0.08 |
| NDKA_HUMAN | GDFCIQVGR | 5.21±0.72 | 1.88±0.29 |
| PCBP2_HUMAN | AITIAGIPQSIIECVK | 1.51±0.04 | 2.48±0.01 |
| PGK1_HUMAN | GCITIIGGGDTATCCAK | 1.71±0.13 | 1.7±0.41 |
| PLSL_HUMAN | EGICAIGGTSEQSSVGTQHSYSEEE | 1.57±0.04 | 1.8±0.34 |
| PPIA_HUMAN | KITIADCGQLE | 1.93±0.7 | 1.89±0.95 |

| UniProt ID | Sequence | LPA-PR | Thr-PR |
|---|---|---|---|
| | | H/L±SD | H/L±SD |
| PRDX6_HUMAN | DINAYNCEEPTEK | 1.41±0.06 | 1.33±0.13 |
| RAC2_HUMAN | YLECSALTQR | 3.27±0.82 | 1.35±0.05 |
| RAN_HUMAN | VCENIPIVLCGNK | 2.06±0.49 | 1.46±0.08 |
| RINI_HUMAN | LDDCGLTEAR | 2.98±0.62 | 1.88±0.23 |
| RL14_HUMAN | CMQLTDFILK | 1.44±0.05 | 3.27±0.81 |
| RL23_HUMAN | ISLGLPVGAVINCADNTGAK | 1.96±0.68 | 1.85±0.17 |
| RS12_HUMAN | KVVGCSCVVVK | 2.25±0.95 | 1.43±0.08 |
| | LGEWVGLCK | 2.31±0.82 | 1.33±0.18 |
| | LVEALCAEHQINLIK | 1.69±0.2 | 1.67±0.11 |
| RS27L_HUMAN | LTEGCSFR | 2.7±1.17 | 2.03±0.25 |
| RS3A_HUMAN | ACQSIYPLHDVFVR | 2.15±0.08 | 3.46±0.88 |
| RS5_HUMAN | TIAECLADELINAAK | 1.9±0.36 | 1.72±0.36 |
| SERA_HUMAN | NAGNCLSPAVIVGLLK | 1.56±0.13 | 1.91±0.46 |
| | VLISDSLDPCCRK | 2.82±0.42 | 1.84±0.18 |
| SMD2_HUMAN | HCNMVLENVK | 1.72±0.49 | 1.89±0.44 |
| TBA1B_HUMAN | AVCMLSNTTAIAEAWAR | 1.63±0.11 | 1.55±0.11 |
| | SIQFVDWCPTGFK | 1.63±0.3 | 1.49±0.13 |
| TBA1C_HUMAN | TIQFVDWCPTGFK | 1.91±0.72 | 1.73±0.22 |
| TBB3_HUMAN | EIVHIQAGQCGNQIGAK | 1.91±0.82 | 1.45±0.09 |
| | NMMAACDPR | 6.82±4.48 | 1.49±0.14 |
| TBB5_HUMAN | TAVCDIPPR | 2.68±0.52 | 2.17±0.51 |
| TCPB_HUMAN | SLHDALCVLAQTVK | 1.8±0.3 | 1.64±0.41 |
| TCPG_HUMAN | TLIQNCGASTIR | 2.73±0.23 | 1.31±0.07 |
| TEBP_HUMAN | LTFSCLGGSDNFK | 1.73±0.31 | 2.54±0.31 |
| THIO_HUMAN | CMPTFQFFK | 2.62±0.94 | 2.42±0.4 |
| TPIS_HUMAN | IAVAAQNCYK | 2±0.82 | 1.95±0.58 |
| UBC12_HUMAN | LVICPDEGFYK | 4.34±0.66 | 1.88±0.59 |

### A.10 Enrichment Efficiency of the Modified Biotin switch assay on THP-1 cells with DPI one-hour pretreatment following by LPA-PR six-hour treatment.

| # of Replicates | Total # of peptide | # of Cys-containing |
|---|---|---|
| 1 | 1745 | 584 |
| 2 | 1657 | 569 |
| 3 | 1560 | 407 |

## A.11 The 43 $Cys_{OX}$ containing peptides in DPI pre-treatment following by six-hour LPA-PR treatment with their H/L ratio.

| UniProt ID | Sequence | H/L | SD |
|---|---|---|---|
| 1433Z_HUMAN | DICNDVLSLLEK | 1.79 | 0.06 |
| 5HT1E_HUMAN | LIRCREHT | 5.25 | 0.45 |
| APT_HUMAN | GFLFGPSLAQELGLGCVLIR | 1.37 | 0.04 |
| C1TC_HUMAN | STTTIGLVQALGAHLYQNVFACVR | 2.17 | 0.84 |
| CAP1_HUMAN | INSITVDNCKK | 28.15 | 15.85 |
| | GKINSITVDNCK | 1.42 | 0.07 |
| CHCH2_HUMAN | LCEGFNEVLK | 1.80 | 0.35 |
| ENOA_HUMAN | FGANAILGVSLAVCK | 2.70 | 0.05 |
| | SGETEDTFIADLVVGLCTGQIK | 2.31 | 0.03 |
| HNRPK_HUMAN | GSDFDCELR | 1.62 | 0.13 |
| LEG1_HUMAN | SFVLNLGKDSNNLCLHFNPR | 1.75 | 0.20 |
| MDHC_HUMAN | VIVVGNPANTNCLTASK | 1.49 | 0.13 |
| MDHM_HUMAN | TIIPLISQCTPK | 2.89 | 0.12 |
| | GCDVVVIPAGVPR | 1.51 | 0.12 |
| ERP44_HUMAN | TPADCPVIAIDSFR | 1.74 | 0.47 |
| ABRAL_HUMAN | CANLFEALVGTLK | 1.80 | 0.39 |
| CL042_HUMAN | MSTVICMKQR | 1.86 | 0.25 |
| COR1A_HUMAN | ADQCYEDVR | 1.42 | 0.03 |
| DOCK2_HUMAN | TTQRNVEVIMCVCAEDGK | 1.55 | 0.02 |
| DX39B_HUMAN | HFILDECDK | 1.54 | 0.09 |
| PRR9_HUMAN | VQEKCSSPGKGK | 1.57 | 0.09 |
| PUR6_HUMAN | ITSCIFQLLQEAGIK | 2.10 | 0.03 |
| RINI_HUMAN | WAELLPLLQQCQVVR | 1.51 | 0.14 |
| RTCA_HUMAN | VSTALSCLLGLPLRVQK | 2.04 | 0.57 |
| SYAC_HUMAN | NVGCLQEALQLATSFAQLR | 2.02 | 0.03 |
| TBA1B_HUMAN | SIQFVDWCPTGFK | 1.46 | 0.13 |
| TOIP1_HUMAN | YCDHENAAFK | 1.43 | 0.23 |
| ZN579_HUMAN | APLPCPTCGR | 2.65 | 0.01 |
| TPIS_HUMAN | IIYGGSVTGATCK | 1.64 | 0.29 |
| | VAHALAEGLGVIACIGEK | 1.93 | 0.13 |
| CUL7_HUMAN | CQQGGIDTRIR | 1.36 | 0.04 |
| FBN2_HUMAN | SFCYRSYNGTTCENELPFNVTK | 1.74 | 0.47 |
| KAD2_HUMAN | NLETPLCK | 1.96 | 0.68 |
| | LVSDEMVVELIEKNLETPLCK | 1.93 | 0.13 |
| LDHA_HUMAN | GLYGIKDDVFLSVPCILGQNGISDLVK | 1.75 | 0.20 |
| NLRC4_HUMAN | LQIKRCAGVAGSLSLVLSTCK | 1.58 | 0.21 |
| PARK7_HUMAN | GLIAAICAGPTALLAHEIGFGSK | 1.46 | 0.13 |
| PROF1_HUMAN | CYEMASHLR | 1.35 | 0.21 |
| RTCA_HUMAN | VSTALSCLLGLPLRVQK | 1.52 | 0.15 |

| UniProt ID | Sequence | H/L | SD |
|---|---|---|---|
| TDRD6_HUMAN | MCSTPGMPAPGASLALR | 1.51 | 0.14 |
| TF3C1_HUMAN | CTMVEAFDR | 2.61 | 3.49 |
| Z804B_HUMAN | YSPQSCLSR | 1.59 | 0.49 |
| ZBT38_HUMAN | CKYPAELDCAVGK | 1.81 | 0.49 |

## Appendix B

### B.1 Extracted ion chromatograms of the sulfenic acid modification-containing peptides in aldolase upon the treatment with $H_2O_2$, identified after labeling with dimedone.

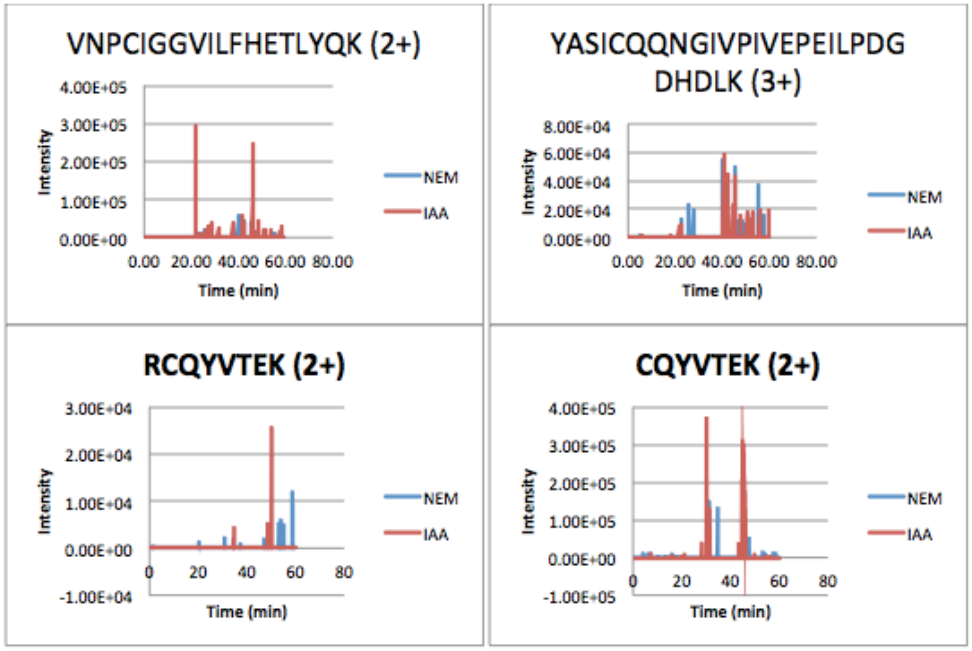


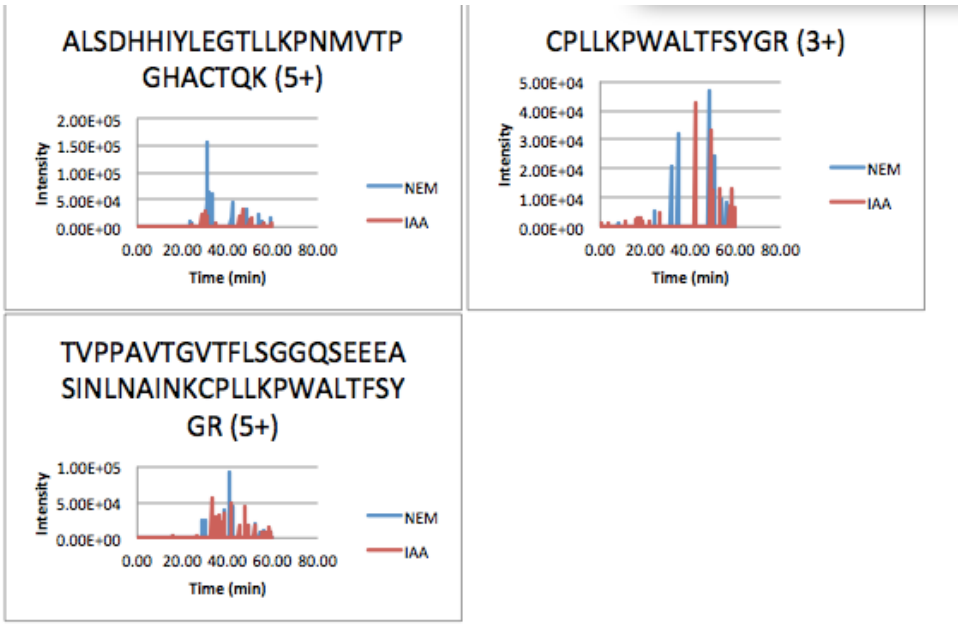

**B.2 Extracted ion chromatograms of the sulfenic acid modification-containing peptides in aldolase upon the treatment with $H_2O_2$, identified after arsenite reduction and iodoacetamide labeling.**

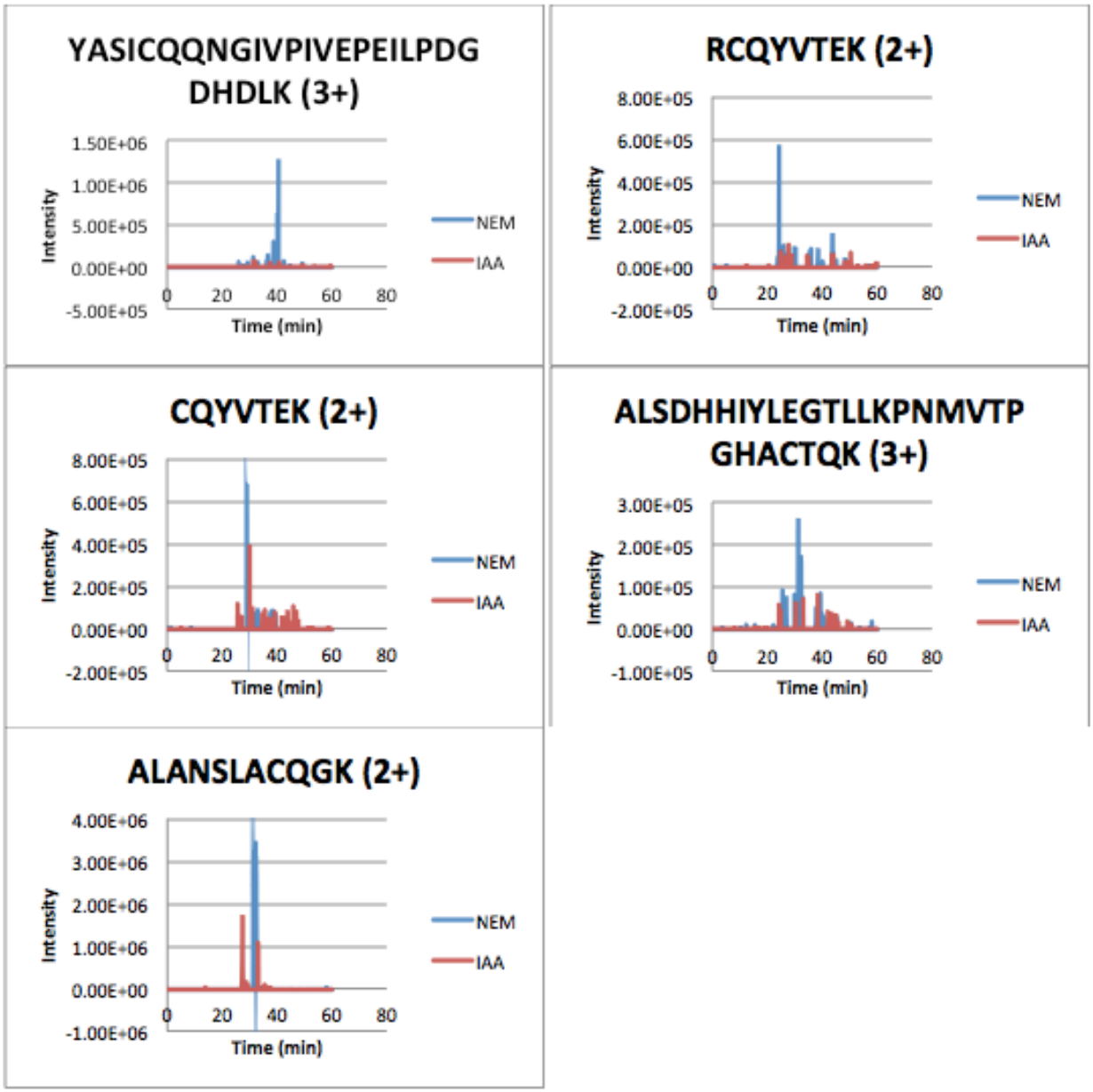

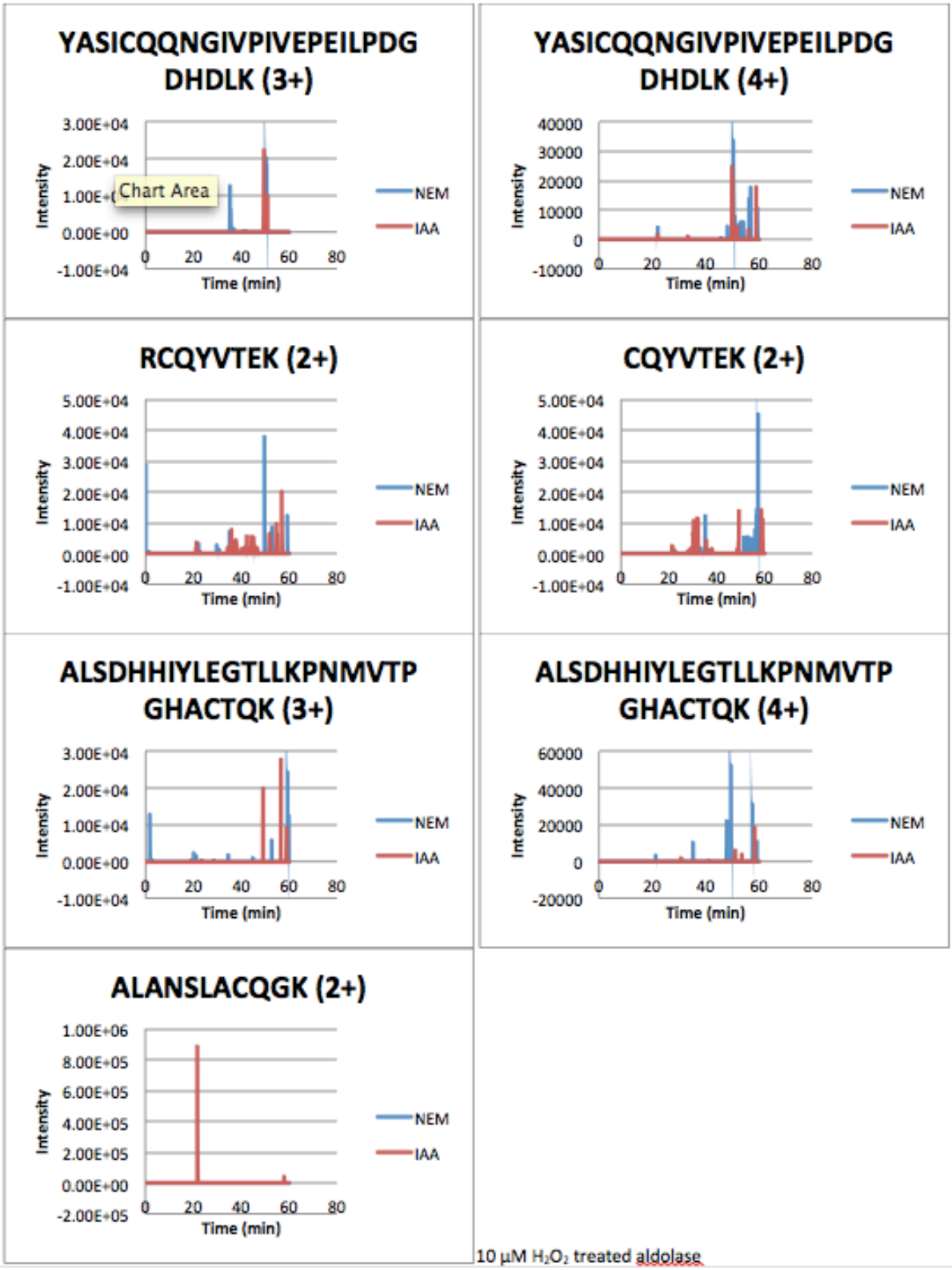


10 µM $H_2O_2$ treated aldolase

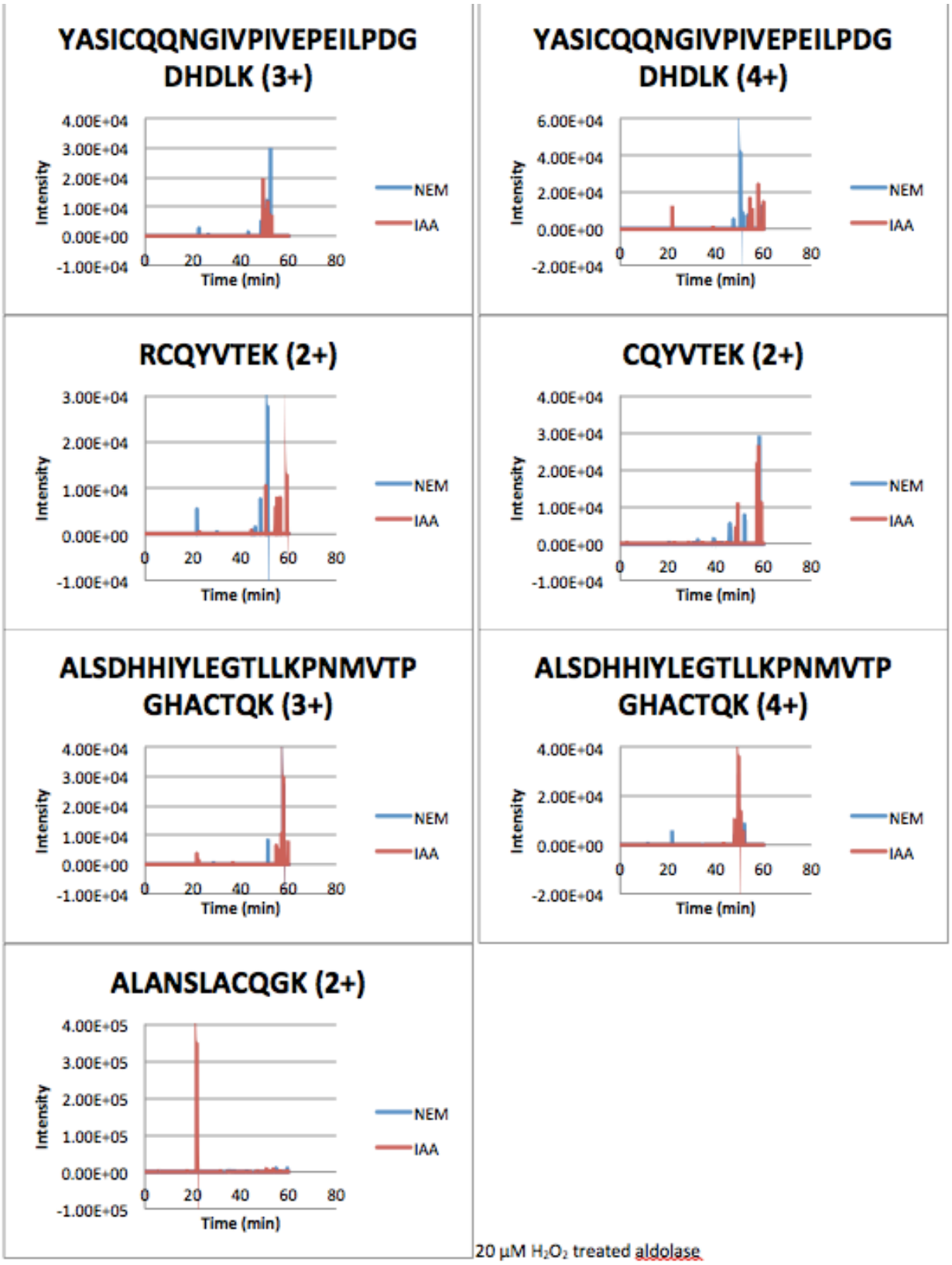


20 µM $H_2O_2$ treated aldolase

B.3 **Overview of differential alkylation strategy for the detection of reversible cysteine oxidation in model protein.** Reversible cysteine oxidations are introduced by treatment with $H_2O_2$. Remaining free thiols (-SH) are blocked with N-ethylmaleimide (NEM), and reversible cysteine oxidations are reduced with dithiothreitol (DTT). The newly released free thiols are then labeled with iodoacetamide (IAA). Alternative oxidation states are abbreviated as -SX: irreversible cysteine oxidation; -S-S-: disulfide.

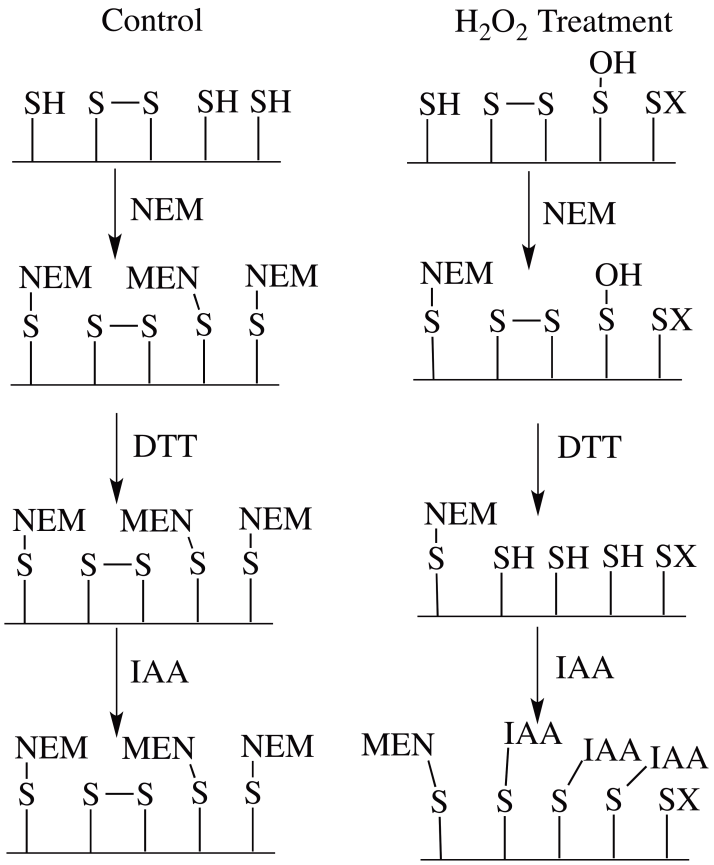

**B.4 Extracted ion chromatograms of the cysteine-containing peptides in aldolase upon the treatment with $H_2O_2$, identified after DTT reduction and iodoacetamide labeling.**

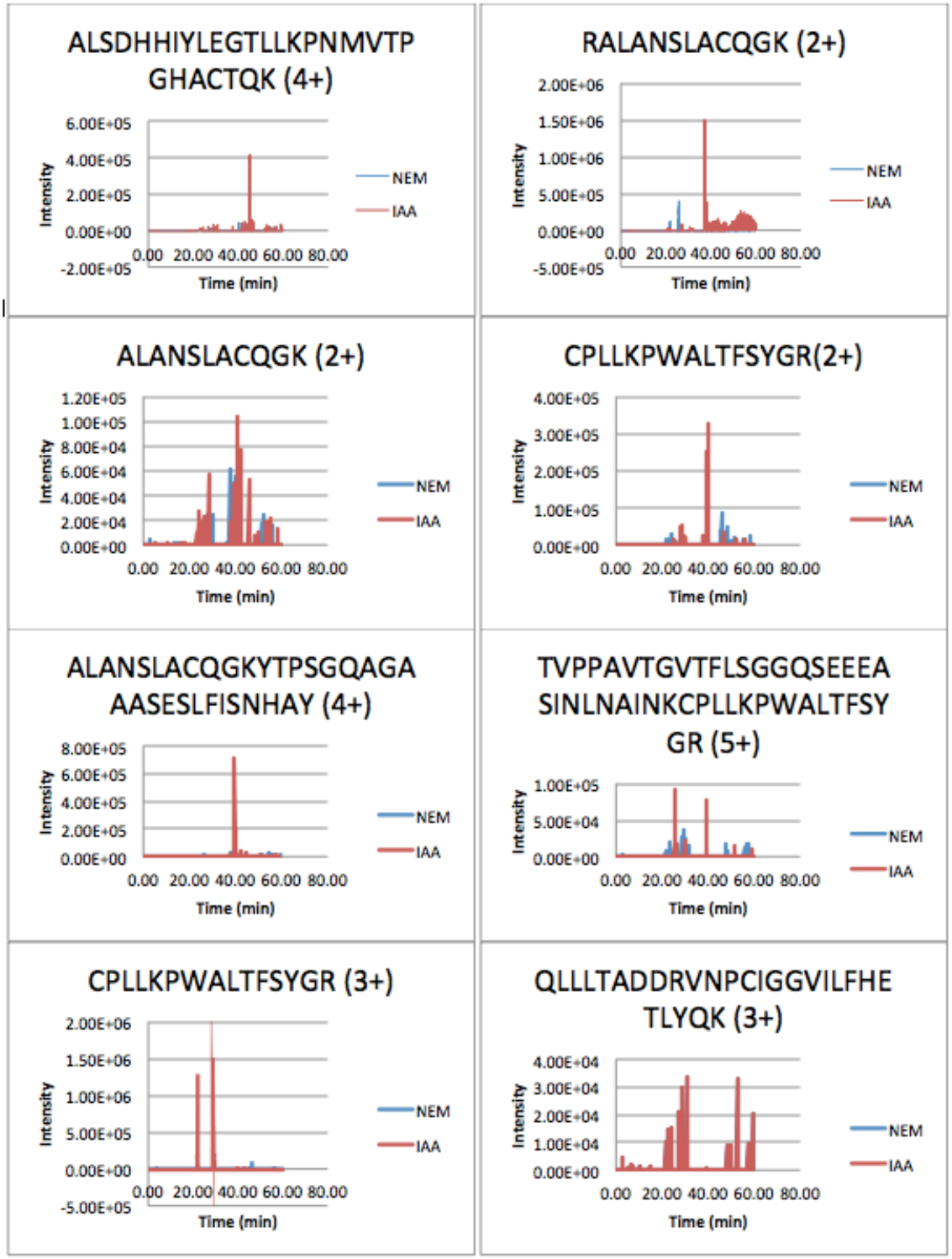

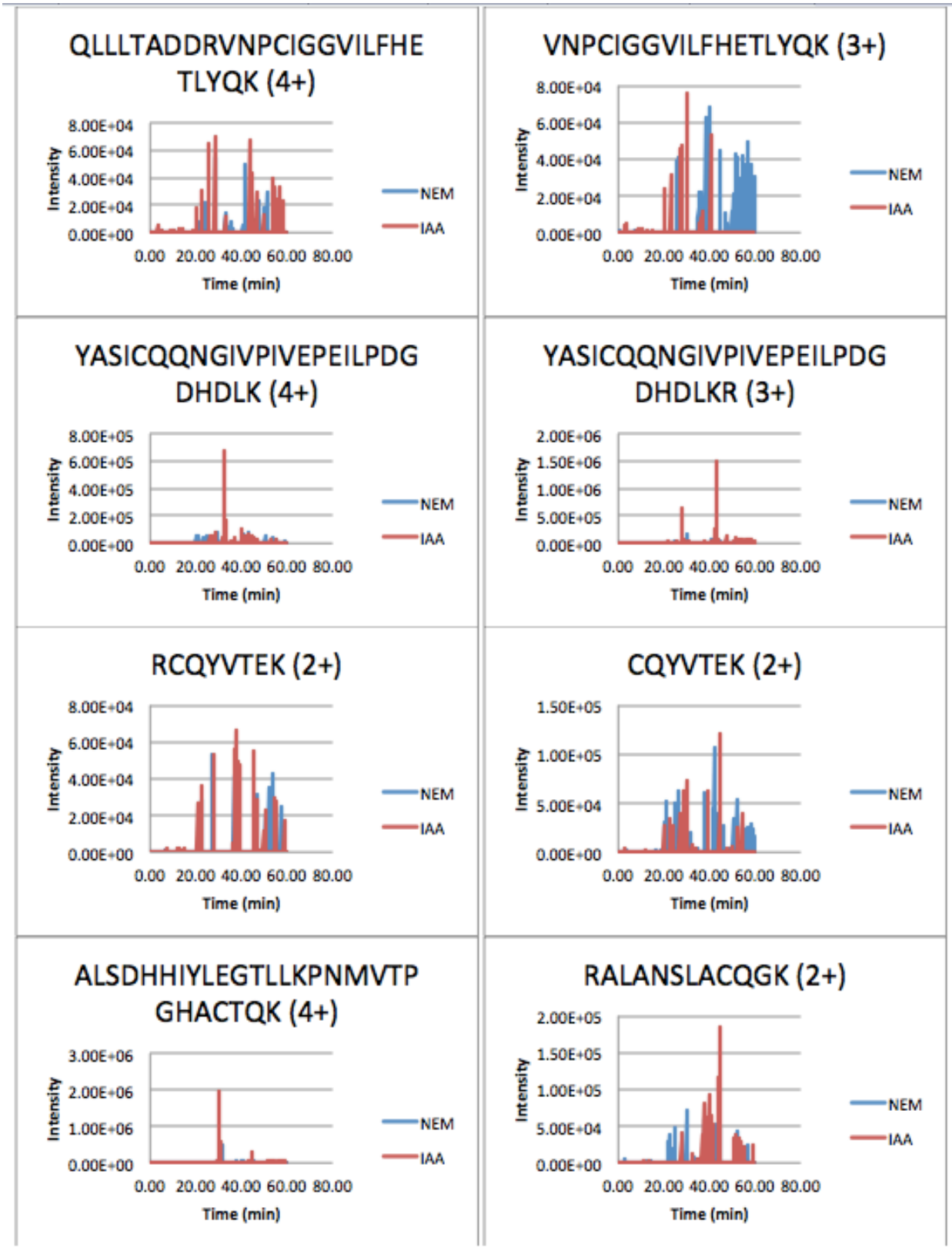
QLLLTADDRVNPCIGGVILFHE TLYQK (4+)
Intensity
8.00E+04
6.00E+04
4.00E+04
2.00E+04
0.00E+00
0.00 20.00 40.00 60.00 80.00
Time (min)
NEM
IAA
VNPCIGGVILFHETLYQK (3+)
Intensity
8.00E+04
6.00E+04
4.00E+04
2.00E+04
0.00E+00
0.00 20.00 40.00 60.00 80.00
Time (min)
NEM
IAA
YASICQQNGIVPIVEPEILPDG DHDLK (4+)
Intensity
8.00E+05
6.00E+05
4.00E+05
2.00E+05
0.00E+00
0.00 20.00 40.00 60.00 80.00
Time (min)
NEM
IAA
YASICQQNGIVPIVEPEILPDG DHDLKR (3+)
Intensity
2.00E+06
1.50E+06
1.00E+06
5.00E+05
0.00E+00
0.00 20.00 40.00 60.00 80.00
Time (min)
NEM
IAA
RCQYVTEK (2+)
Intensity
8.00E+04
6.00E+04
4.00E+04
2.00E+04
0.00E+00
0.00 20.00 40.00 60.00 80.00
Time (min)
NEM
IAA
CQYVTEK (2+)
Intensity
1.50E+05
1.00E+05
5.00E+04
0.00E+00
0.00 20.00 40.00 60.00 80.00
Time (min)
NEM
IAA
ALSDHHIYLEGTLLKPNMVTP GHACTQK (4+)
Intensity
3.00E+06
2.00E+06
1.00E+06
0.00E+00
0.00 20.00 40.00 60.00 80.00
Time (min)
NEM
IAA
RALANSLACQGK (2+)
Intensity
2.00E+05
1.50E+05
1.00E+05
5.00E+04
0.00E+00
0.00 20.00 40.00 60.00 80.00
Time (min)
NEM
IAA

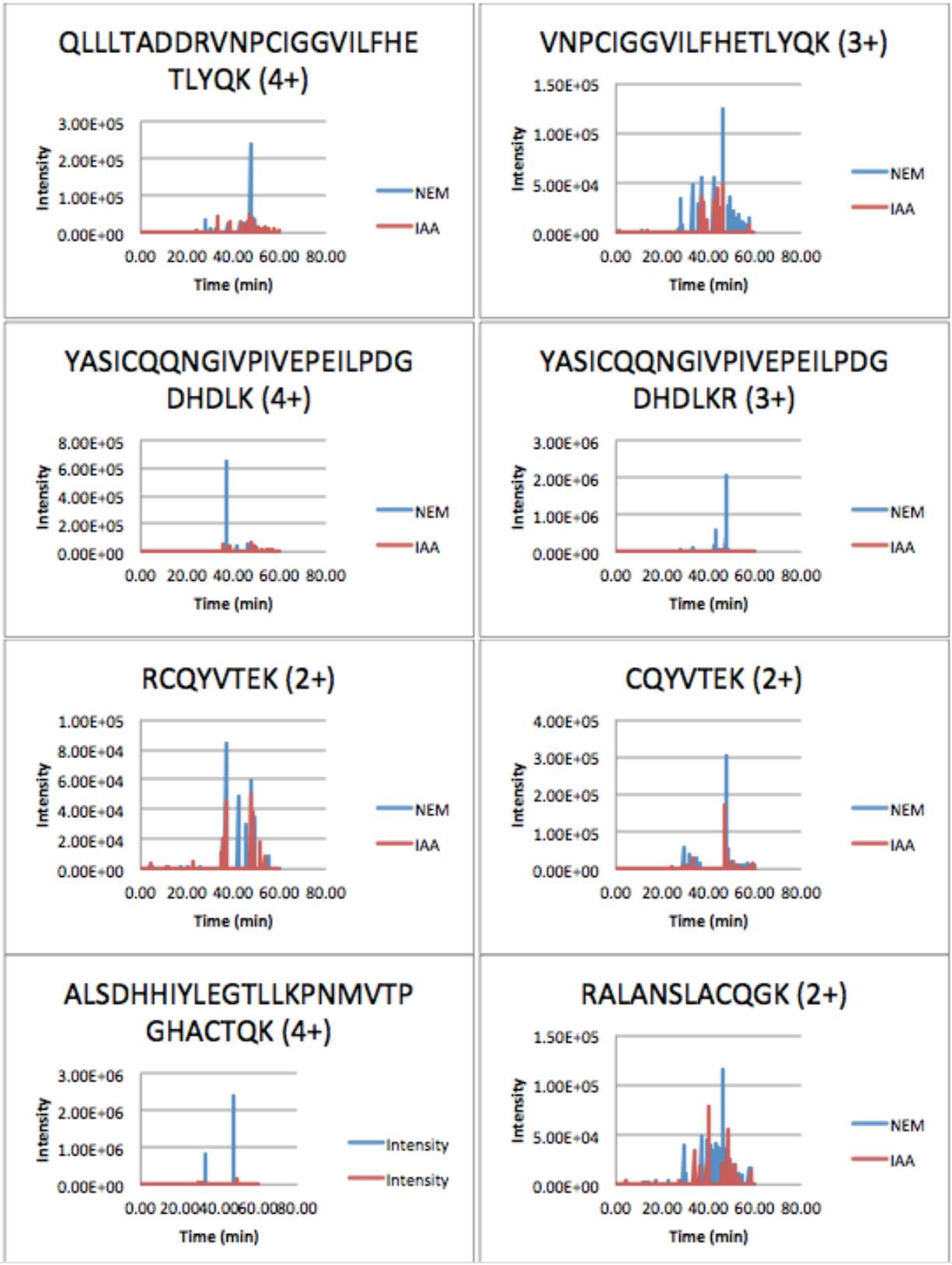
QLLLTADDRVNPCIGGVILFHE TLYQK (4+)
Intensity
3.00E+05
2.00E+05
1.00E+05
0.00E+00
0.00 20.00 40.00 60.00 80.00
Time (min)
NEM
IAA
VNPCIGGVILFHETLYQK (3+)
Intensity
1.50E+05
1.00E+05
5.00E+04
0.00E+00
0.00 20.00 40.00 60.00 80.00
Time (min)
NEM
IAA
YASICQQNGIVPIVEPEILPDG DHDLK (4+)
Intensity
8.00E+05
6.00E+05
4.00E+05
2.00E+05
0.00E+00
0.00 20.00 40.00 60.00 80.00
Time (min)
NEM
IAA
YASICQQNGIVPIVEPEILPDG DHDLKR (3+)
Intensity
3.00E+06
2.00E+06
1.00E+06
0.00E+00
0.00 20.00 40.00 60.00 80.00
Time (min)
NEM
IAA
RCQYVTEK (2+)
Intensity
1.00E+05
8.00E+04
6.00E+04
4.00E+04
2.00E+04
0.00E+00
0.00 20.00 40.00 60.00 80.00
Time (min)
NEM
IAA
CQYVTEK (2+)
Intensity
4.00E+05
3.00E+05
2.00E+05
1.00E+05
0.00E+00
0.00 20.00 40.00 60.00 80.00
Time (min)
NEM
IAA
ALSDHHIYLEGTLLKPNMVTP GHACTQK (4+)
Intensity
3.00E+06
2.00E+06
1.00E+06
0.00E+00
0.00 20.0040.0060.0080.00
Time (min)
Intensity
Intensity
RALANSLACQGK (2+)
Intensity
1.50E+05
1.00E+05
5.00E+04
0.00E+00
0.00 20.00 40.00 60.00 80.00
Time (min)
NEM
IAA

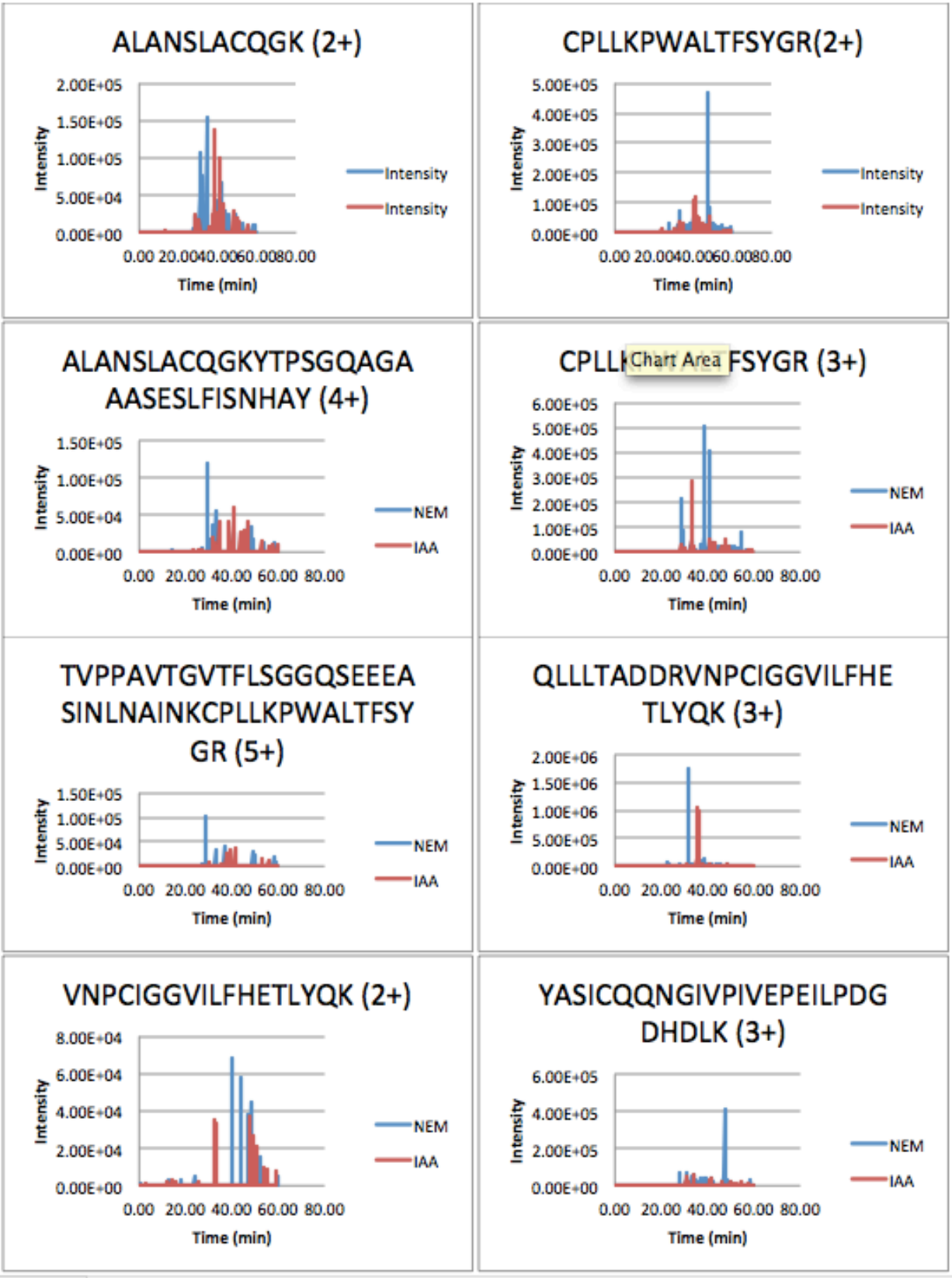
ALANSLACQGK (2+)
2.00E+05
1.50E+05
1.00E+05
5.00E+04
0.00E+00
Intensity
0.00 20.0040.0060.0080.00
Time (min)
Intensity
Intensity
CPLLKPWALTFSYGR(2+)
5.00E+05
4.00E+05
3.00E+05
2.00E+05
1.00E+05
0.00E+00
Intensity
0.00 20.0040.0060.0080.00
Time (min)
Intensity
Intensity
ALANSLACQGKYTPSGQAGA
AASESLFISNHAY (4+)
1.50E+05
1.00E+05
5.00E+04
0.00E+00
Intensity
0.00 20.00 40.00 60.00 80.00
Time (min)
NEM
IAA
CPLL Chart Area FSYGR (3+)
6.00E+05
5.00E+05
4.00E+05
3.00E+05
2.00E+05
1.00E+05
0.00E+00
Intensity
0.00 20.00 40.00 60.00 80.00
Time (min)
NEM
IAA
TVPPAVTGVTFLSGGQSEEEA
SINLNAINKCPLLKPWALTFSY
GR (5+)
1.50E+05
1.00E+05
5.00E+04
0.00E+00
Intensity
0.00 20.00 40.00 60.00 80.00
Time (min)
NEM
IAA
QLLLTADDRVNPCIGGVILFHE
TLYQK (3+)
2.00E+06
1.50E+06
1.00E+06
5.00E+05
0.00E+00
Intensity
0.00 20.00 40.00 60.00 80.00
Time (min)
NEM
IAA
VNPCIGGVILFHETLYQK (2+)
8.00E+04
6.00E+04
4.00E+04
2.00E+04
0.00E+00
Intensity
0.00 20.00 40.00 60.00 80.00
Time (min)
NEM
IAA
YASICQQNGIVPIVEPEILPDG
DHDLK (3+)
6.00E+05
4.00E+05
2.00E+05
0.00E+00
Intensity
0.00 20.00 40.00 60.00 80.00
Time (min)
NEM
IAA

B.5 **The analysis of reversible cysteine oxidation in Aldolase with the treatment with $H_2O_2$.** For each cysteine residue, Cys73 (•), Cys178 (■), Cys202 (◆), Cys240 (△), Cys290 (○), and Cys339 (□), for which IAA-modification were detectable by mass spectrometry, the IAA-modification percentage was determined as follows: peak area of IAA-modification of a specific cysteine divided by the sum of IAA- and NEM-modifications on this cysteine, and plotted against the corresponding $H_2O_2$ dose.

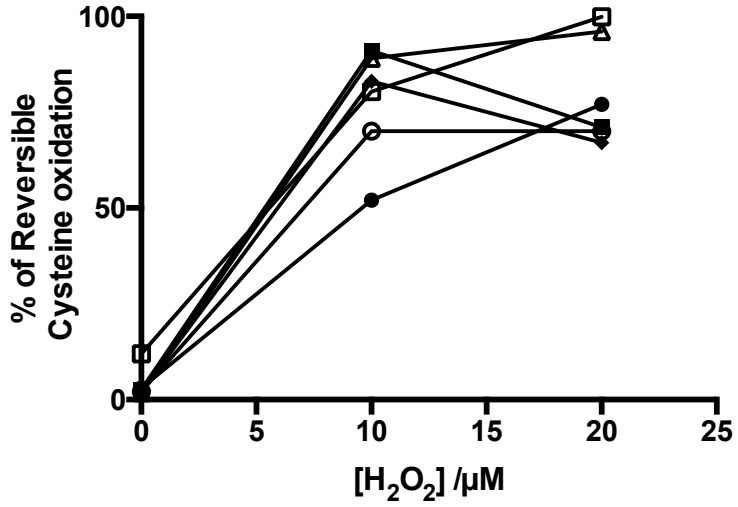

**B.6 Extracted ion chromatograms of the cysteine-containing peptides in lysozyme upon the treatment with $H_2O_2$, identified after DTT reduction and iodoacetamide labeling.**

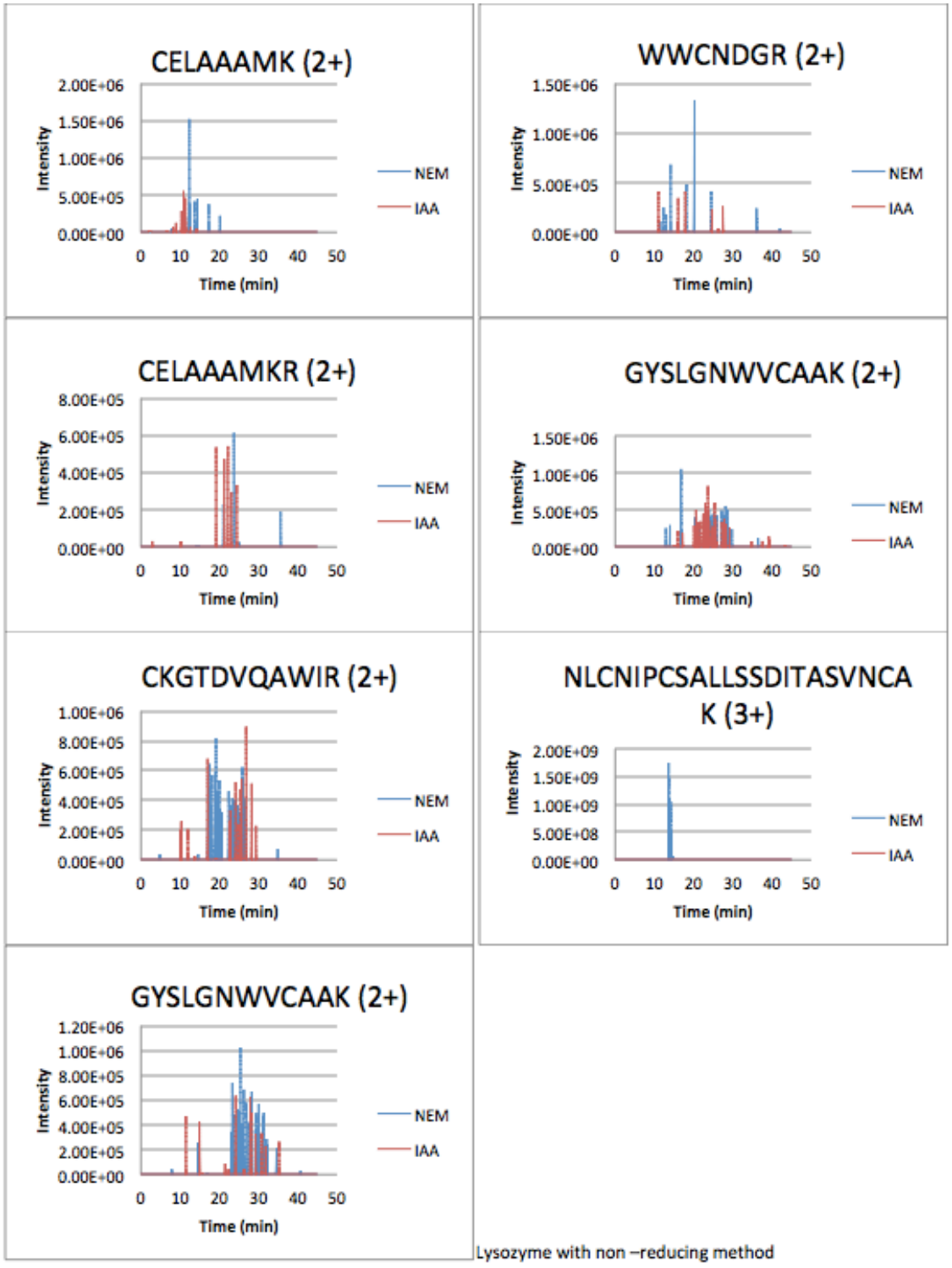


Lysozyme with non –reducing method

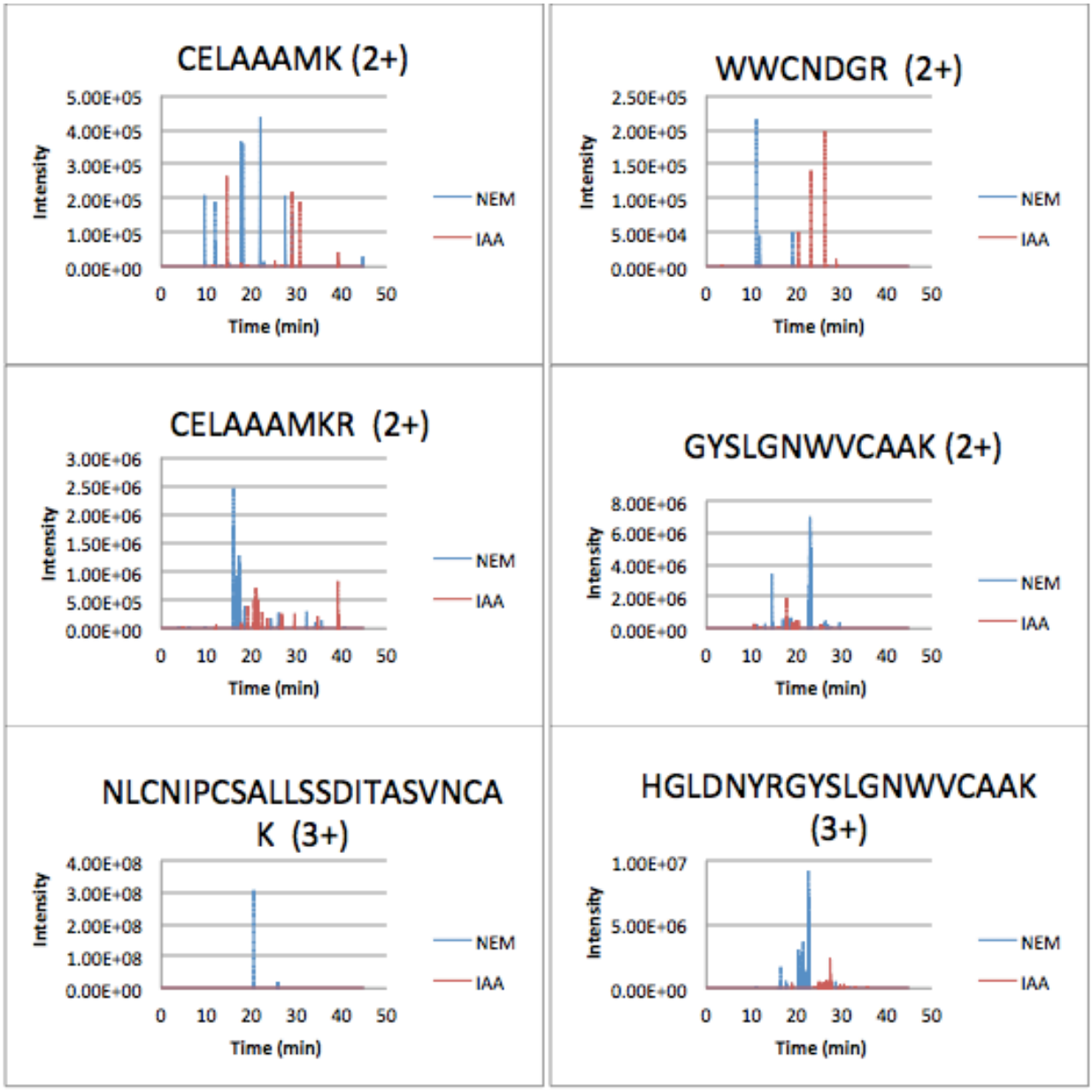


Lysozyme with arsenite as reducing reagent

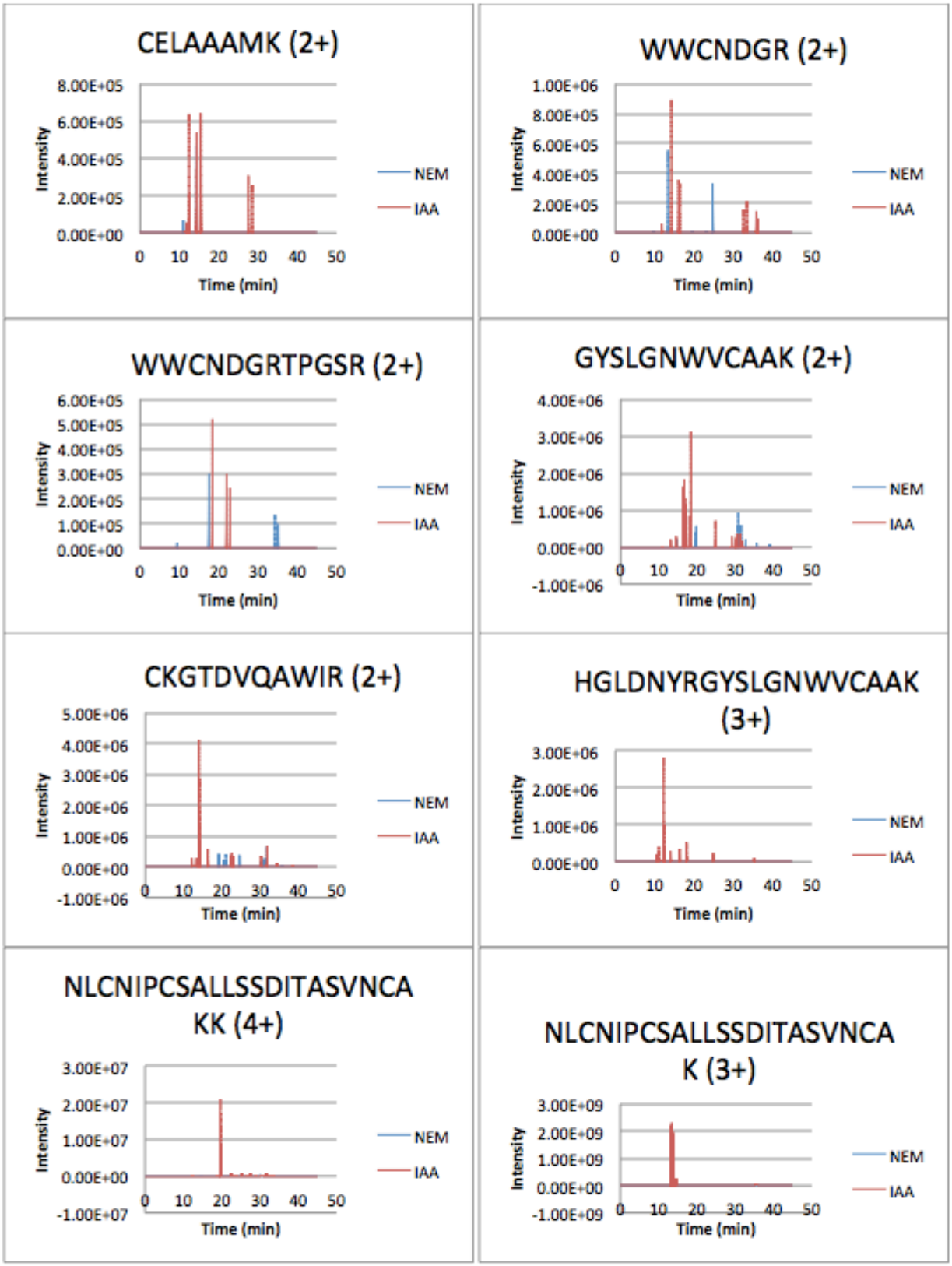
CELAAAMK (2+)
8.00E+05
6.00E+05
4.00E+05
2.00E+05
0.00E+00
Intensity
0 10 20 30 40 50
Time (min)
NEM
IAA
WWCNDGR (2+)
1.00E+06
8.00E+05
6.00E+05
4.00E+05
2.00E+05
0.00E+00
Intensity
0 10 20 30 40 50
Time (min)
NEM
IAA
WWCNDGRTPGSR (2+)
6.00E+05
5.00E+05
4.00E+05
3.00E+05
2.00E+05
1.00E+05
0.00E+00
Intensity
0 10 20 30 40 50
Time (min)
NEM
IAA
GYSLGNWVCAAK (2+)
4.00E+06
3.00E+06
2.00E+06
1.00E+06
0.00E+00
-1.00E+06
Intensity
0 10 20 30 40 50
Time (min)
NEM
IAA
CKGTDVQAWIR (2+)
5.00E+06
4.00E+06
3.00E+06
2.00E+06
1.00E+06
0.00E+00
-1.00E+06
Intensity
0 10 20 30 40 50
Time (min)
NEM
IAA
HGLDNYRGYSLGNWVCAAK (3+)
3.00E+06
2.00E+06
1.00E+06
0.00E+00
Intensity
0 10 20 30 40 50
Time (min)
NEM
IAA
NLCNIPCSALLSSDITASVNCA KK (4+)
3.00E+07
2.00E+07
1.00E+07
0.00E+00
-1.00E+07
Intensity
0 10 20 30 40 50
Time (min)
NEM
IAA
NLCNIPCSALLSSDITASVNCA K (3+)
3.00E+09
2.00E+09
1.00E+09
0.00E+00
-1.00E+09
Intensity
0 10 20 30 40 50
Time (min)
NEM
IAA

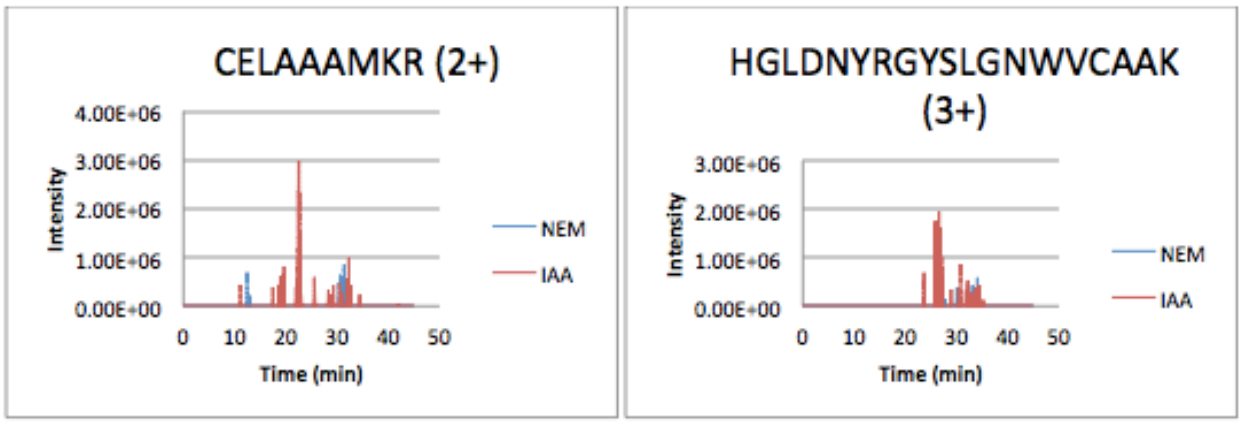


B.7 **The analysis of disulfide bonds in lysozyme by using differential alkylation method.**

For each cysteine residue, Cys24 (•), Cys48 (■), Cys82 (◆), Cys133 (▲), Cys94 (o), Cys98 (□), and Cys122 (△), for which IAA-modification were detectable by mass spectrometry, the IAA-modification percentage was determined as follows: peak area of IAA-modification of a specific cysteine divided by the sum of IAA- and NEM-modifications on this cysteine, and plotted against different reducing agents.

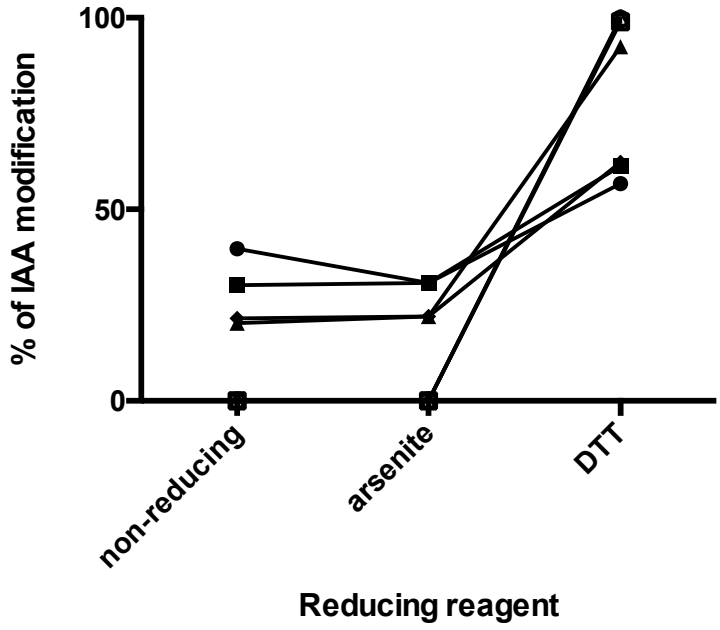

**B.8 The sequences of the five sulfenic acid modification-containing peptides in aldolase upon the treatment with $H_2O_2$, identified after arsenite reduction and iodoacetamide labeling.**

| Protein | Peptide sequence |
|---|---|
| Aldolase_rabbit | YASICQQNGIVPIVEPEILPDGDHDLK(174-200)<br>RCQYVTEK(201-208)<br>CQYVTEK(202-208)<br>ALSDHHIYLEGTLLKPNMVTPGHACTQK(216-243)<br>ALANSLACQGK(332-342) |

**B.9 The sequences of the eleven cysteine-containing peptides in aldolase upon the treatment with $H_2O_2$, identified after DTT reduction and iodo5acetamide labeling.**

| Protein | Peptide sequence |
|---|---|
| Aldolase_rabbit | CQYVTEK(202-208)<br>ALANSLACQGK(332-342)<br>RALANSLACQGK(331-342)<br>CPLLKPWALTFSYGR(290-304)<br>VNPCIGGVILFHETLYQK(70-87)<br>YASICQQNGIVPIVEPEILPDGDHDLK(174-200)<br>QLLLTADDRVNPCIGGVILFHETLYQK(61-87)<br>ALSDHHIYLEGTLLKPNMVTPGHACTQK(216-243)<br>YASICQQNGIVPIVEPEILPDGDHDLKR(174-201)<br>ALANSLACQGKYTPSGQAGAAASESLFISNHAY(332-364)<br>TVPPAVTGVTFLSGGQSEEEASINLNAINKCPLLKPWALTFSYGR(260- |

**B.10 The sequences of the nine cysteine-containing peptides in lysozyme, identified by iodoacetamide labeling.**

| Protein | Peptide sequence |
|---|---|
| Lysozyme_chicken | CELAAAMK(24-31)<br>WWCNDGR(80-86)<br>CELAAAMKR(24-32)<br>GYSLGNWVCAAK(40-51)<br>CKGTDVQAWIR(133-143)<br>WWCNDGRTPGSR(80-91) |

| Protein | Peptide sequence |
|---|---|
| | HGLDNYRGYSLGNWVCAAK(33-51)<br>NLCNIPCSALLSSDITASVNCAK(92-114)<br>NLCNIPCSALLSSDITASVNCAKK(92-115) |

## B.11 The 113 sulfenic acid modification sites identified in THP-1 cells upon six-hour 100 μM $H_2O_2$ treatment with H/L ratio.

| Protein ID | Protein Name | Sequence | H/L | SD |
|---|---|---|---|---|
| 1433G_HUMAN | 14-3-3 protein gamma | CQDVLSLLDNYLIKNCSETQYESKVFYLKMK | 1.00 | 0.11 |
| 1433T_HUMAN | 14-3-3 protein theta | LKMKGDYFRYLAEVACGDDRKQTIDNSQGAY | 1.11 | 0.01 |
| 1433Z_HUMAN | 14-3-3 protein zeta/delta | AKLAEQAERYDDMAACMKSVTEQGAELSNEE | 1.11 | 0.05 |
| 6PGD_HUMAN | 6-phosphogluconate dehydrogenase, decarboxylating | QNLLLDDFFKSAVENCQDSWRRAVSTGVQAG | 1.03 | 0.02 |
| ACTB_HUMAN | Actin, cytoplasmic 1 | DDDIAALVVDNGSGMCKAGFAGDDAPRAVFP | 1.17 | 0.11 |
| ACTN1_HUMAN | Alpha-actinin-1 | DYYDSPSVNARCQKICDQWDNLGALTQKRRE | 1.06 | 0.12 |
| ALDOA_HUMAN | Fructose-bisphosphate aldolase A | AQEEYVKRALANSLACQGKYTPSGQAGAAAS | 1.05 | 0.07 |
| ANXA4_HUMAN | Annexin A4 | EKKWGTDEVKFLTVLCSRNRNHLLHVFDEYK | 0.97 | 0.01 |
| ANXA6_HUMAN | Annexin A6 | SGDKTSLETRFMTILCTRSYPHLRRVFQEFI | 1.32 | 0.11 |
| AP1B1_HUMAN | AP-1 complex subunit beta-1 | KDIPNENEAQFQIRDCPLNAEAASSKLQSSN | 1.02 | 0.15 |
| ARP3_HUMAN | Actin-related protein 3 | SLETAKAVKERYSYVCPDLVKEFNKYDTDGS | 0.87 | 0.07 |
| ARPC2_HUMAN | Actin-related protein 2/3 complex subunit 2 | SKDSIVHQAGMLKRNCFASVFEKYFQFQEEG | 1.09 | 0.01 |
| CALR_HUMAN | Calreticulin | TLVVQFTVKHEQNIDCGGGYVKLFPNSLDQT | 1.17 | 0.05 |
| CAP1_HUMAN | Adenylyl cyclase-associated protein 1 | KTDGCHAYLSKNSLDCEIVSAKSSEMNVLIP | 0.95 | 0.07 |
| CAP1_HUMAN | Adenylyl cyclase-associated protein 1 | TGLKLERALLVTASQCQQPAENKLSDLLAPI | 0.96 | 0.02 |
| CAP1_HUMAN | Adenylyl cyclase-associated protein 1 | TLQIKGKINSITVDNCKKLGLVFDDVVGIVE | 1.05 | 0.13 |
| CATA_HUMAN | Catalase | HRHRLGPNYLHIPVNCPYRARVANYQRDGPM | 0.74 | 0.03 |
| CATA_HUMAN | Catalase | SHTFKLVNANGEAVYCKFHYKTDQGIKNLSV | 0.91 | 0.08 |
| CH60_HUMAN | 60 kDa heat shock protein, mitochondrial | ATRAAVEEGIVLGGGCALLRCIPALDSLTPA | 1.26 | 0.28 |
| CHRD1_HUMAN | Cysteine and histidine-rich domain-containing protein 1 | MALLCYNRGCGQRFDPETNS | 1.34 | 0.28 |
| CLIC1_HUMAN | Chloride intracellular channel protein 1 | ELFVKAGSDGAKIGNCPFSQRLFMVLWLKGV | 0.82 | 0.08 |
| COR1A_HUMAN | Coronin-1A | DTIYSVDWSRDGGLICTSCRDKRVRIIEPRK | 0.97 | 0.02 |
| COR1A_HUMAN | Coronin-1A | YSVDWSRDGGLICTSCRDKRVRIIEPRKGTV | 0.97 | 0.02 |
| COR1A_HUMAN | Coronin-1A | SKFRHVFGQPAKADQCYEDVRVSQTTWDSGF | 1.08 | 0.09 |

| Protein ID | Protein Name | Sequence | H/L | SD |
|---|---|---|---|---|
| COR1A_HUMAN | Coronin-1A | YEDVRVSQTTWDSGFCAVNPKFVALICEASG | 1.11 | 0.04 |
| CYBP_HUMAN | Calcyclin-binding protein | EGSSKKVKTDTVLILCRKKVENTRWDYLTQV | 1.06 | 0.05 |
| ECH1_HUMAN | Delta | KRNAMNKVFWREMVECFNKISRDADCRAVVI | 1.23 | 0.15 |
| EF2_HUMAN | Elongation factor 2 | AIHRGGGQIIPTARRCLYASVLTAQPRLMEP | 0.85 | 0.14 |
| EF2_HUMAN | Elongation factor 2 | VVSYRETVSEESNVLCLSKSPNKHNRLYMKA | 1.02 | 0.07 |
| EF2_HUMAN | Elongation factor 2 | SVVAGFQWATKEGALCEENMRGVRFDVHDVT | 0.99 | 0.01 |
| EF2_HUMAN | Elongation factor 2 | AHVDHGKSTLTDSLVCKAGIIASARAGETRF | 1.18 | 0.04 |
| ELNE_HUMAN | Neutrophil elastase | LNVTVVTSLCRRSNVCTLVRGRQAGVCFGDS | 0.76 | 0.24 |
| ENOA_HUMAN | alpha enolase | LKVNQIGSVTESLQACKLAQANGWGVMVSHR | 1.10 | 0.04 |
| ENOA_HUMAN | alpha enolase | NPKRIAKAVNEKSCNCLLLKVNQIGSVTESL | 1.19 | 0.03 |
| ENOA_HUMAN | alpha enolase | VTNPKRIAKAVNEKSCNCLLLKVNQIGSVTE | 1.19 | 0.03 |
| ENPL_HUMAN | Endoplasmin | KIEKAVVSQRLTESPCALVASQYGWSGNMER | 1.08 | 0.13 |
| ERP44_HUMAN | Endoplasmic reticulum resident protein 44 | EEFPNENQVVFARVDCDQHSDIAQRYRISKY | 0.97 | 0.03 |
| ETFB_HUMAN | Electron transfer flavoprotein subunit beta | KLVKEVIAVSCGPAQCQETIRTALAMGADRG | 0.88 | 0.01 |
| ETFB_HUMAN | Electron transfer flavoprotein subunit beta | RLKEKKLVKEVIAVSCGPAQCQETIRTALAM | 0.88 | 0.01 |
| FAS_HUMAN | Fatty acid synthase | LQELSSKADEASELACPTPKEDGLAQQQTQL | 1.06 | 0.15 |
| FSCN1_HUMAN | Fascin | HLGRYLAADKDGNVTCEREVPGPDCRFLIVA | 1.13 | 0.06 |
| G3P_HUMAN | Glyceraldehyde-3-phosphate dehydrogenase | AFRVPTANVSVVDLTCRLEKPAKYDDIKKVV | 1.00 | 0.05 |
| GBB1_HUMAN | Guanine nucleotide-binding protein G | SLSLAPDTRLFVSGACDASAKLWDVREGMCR | 0.88 | 0.07 |
| GLU2B_HUMAN | Glucosidase 2 subunit beta | DHDKFSAMKYEQGTGCWQGPNRSTTVRLLCG | 0.82 | 0.08 |
| GNAI2_HUMAN | Guanine nucleotide-binding protein G | KQMKIIHEDGYSEEECRQYRAVVYSNTIQSI | 1.01 | 0.03 |
| GSLG1_HUMAN | Golgi apparatus protein 1 | DRHLYFACRDDRERFCENTQAGEGRVYKCLF | 1.07 | 0.02 |
| GSTM3_HUMAN | Glutathione S-transferase Mu 3 | LLEFTDTSYEEKRYTCGEAPDYDRSQWLDVK | 1.07 | 0.03 |
| HNRPD_HUMAN | Heterogeneous nuclear ribonucleoprotein D0 | KDLKDYFSKFGEVVDCTLKLDPITGRSRGFG | 0.95 | 0.04 |
| HNRPQ_HUMAN | Heterogeneous nuclear ribonucleoprotein Q | DPLTGLNRGYAFVTFCTKEAAQEAVKLYNNH | 1.05 | 0.31 |
| HNRPU_HUMAN | Heterogeneous nuclear ribonucleoprotein U | LDQTNVSAAAQRRKMCLFAGFQRKAVVVCPK | 1.05 | 0.13 |
| HSP7C_HUMAN | Heat shock cognate 71 kDa protein | EKEEFEHQQKELEKVCNPIITKLYQSAGGMP | 0.84 | 0.18 |
| HYOU1_HUMAN | Hypoxia up-regulated protein 1 | TTVMLKEKLAELRKLCQGLFFRVEERKKWPE | 1.38 | 0.24 |
| IDHP_HUMAN | Isocitrate dehydrogenase [NADP], mitochondrial | GNQDLIRFAQMLEKVCVETVESGAMTKDLAG | 1.32 | 0.30 |
| ITB2_HUMAN | Integrin beta-2 | PGCPSPCGKYISCAECLKFEKGPFGKNCSAA | 1.30 | 0.48 |
| ITB2_HUMAN | Integrin beta-2 | QECPGCPSPCGKYISCAECLKFEKGPFGKNC | 1.30 | 0.48 |
| ITB2_HUMAN | Integrin beta-2 | HPDKLRNPCPNKEKECQPPFAFRHVLKLTNN | 1.19 | 0.07 |

| Protein ID | Protein Name | Sequence | H/L | SD |
|---|---|---|---|---|
| ITB2_HUMAN | Integrin beta-2 | CECDTINCERYNGQVCGGPGRGLCFCGKCRC | 1.23 | 0.07 |
| ITB2_HUMAN | Integrin beta-2 | GFEGSACQCERTTEGCLNPRRVECSGRGRCR | 1.11 | 0.13 |
| ITB2_HUMAN | Integrin beta-2 | ECQTQGRSSQELEGSCRKDNNSIICSGLGDC | 1.43 | 0.07 |
| KAD2_HUMAN | Adenylate kinase 2, mitochondrial | EMVVELIEKNLETPLCKNGFLLDGFPRTVRQ | 0.88 | 0.09 |
| KPYM_HUMAN | Pyruvate kinase PKM | DIDSPPITARNTGIICTIGPASRSEVELKKG | 0.88 | 0.08 |
| KPYM_HUMAN | Pyruvate kinase PKM | DIDSPPITARNTGIICTIGPASRSVETLKEM | 1.13 | 0.17 |
| LMNA_HUMAN | Prelamin-A/C | SPPTDLVWKAQNTWGCGNSLRTALINSTGEE | 1.24 | 0.32 |
| MCM3_HUMAN | DNA replication licensing factor MCM3 | GDPSVAKSQLLRYVLCTAPRAIPTTGRGSSG | 1.42 | 0.13 |
| MDHC_HUMAN | Malate dehydrogenase, cytoplasmic | TASKSAPSIPKENFSCLTRLDHNRAKAQIAL | 1.15 | 0.07 |
| MDHM_HUMAN | Malate dehydrogenase, mitochondrial | KGYLGPEQLPDCLKGCDVVVIPAGVPRKPGM | 0.85 | 0.04 |
| MDHM_HUMAN | Malate dehydrogenase, mitochondrial | IGGHAGKTIIPLISQCTPKVDFPQDQLTALT | 0.87 | 0.03 |
| MDHM_HUMAN | Malate dehydrogenase, mitochondrial | FSLVDAMNGKEGVVECSFVKSQETECTYFST | 1.30 | 0.17 |
| MPRI_HUMAN | Cation-independent mannose-6-phosphate receptor | QDGCEYVFIWRTVEACPVVRVEGDNCEVKDP | 0.62 | 0.11 |
| P3H1_HUMAN | Prolyl 3-hydroxylase 1 | TELDAKTVTAEVQPQCGRAVGFSSGTENPHG | 0.46 | 0.28 |
| PARK7_HUMAN | Protein deglycase DJ-1 | LAGKDPVQCSRDVVICPDASLEDAKKEGPYD | 0.90 | 0.11 |
| PDC6I_HUMAN | Programmed cell death 6-interacting protein | HEGALETLLRYYDQICSIEPKFPFSENQICL | 1.90 | 0.68 |
| PLOD3_HUMAN | Procollagen-lysine,2-oxoglutarate 5-dioxygenase 3 | GLDYEGGGCRFLRYDCVISSPRKGWALLHPG | 1.22 | 0.09 |
| PLSL_HUMAN | Plastin-2 | GYISFNELNDLFKAACLPLPGYRVREITENL | 0.81 | 0.01 |
| PLSL_HUMAN | Plastin-2 | PPYPKLGGNMKKLENCNYAVELGKNQAKFSL | 0.96 | 0.13 |
| PLSL_HUMAN | Plastin-2 | AFVNWINKALENDPDCRHVIPMNPNTNDLFN | 0.92 | 0.04 |
| PLSL_HUMAN | Plastin-2 | DMSGLREKDDIQRAECMLQQAERLGCRQFVT | 1.04 | 0.10 |
| PNCB_HUMAN | Nicotinate phosphoribosyltransferase | PDTDPAFFEHLRALDCSEVTVRALPEGSLAF | 1.11 | 0.13 |
| PRDX6_HUMAN | Peroxiredoxin-6 | SWGILFSHPRDFTPVCTTELGRAAKLAPEFA | 1.23 | 0.25 |
| PTPRC_HUMAN | Receptor-type tyrosine-protein phosphatase C | QLHDCTQVEKADTTICLKWKNIETFTCDTQN | 1.00 | 0.17 |
| QCR1_HUMAN | Cytochrome b-c1 complex subunit 1, mitochondrial | IDDMMFVLQGQWMRLCTSATESEVARGKNIL | 0.77 | 0.08 |
| RCC2_HUMAN | Protein RCC2 | YRNLGQNLWGPHRYGCLAGVRVRTVVSGSCA | 0.94 | 0.07 |
| RINI_HUMAN | Ribonuclease inhibitor | QISNNRLEDAGVRELCQGLGQPGSVLRVLWL | 0.78 | 0.06 |
| RINI_HUMAN | Ribonuclease inhibitor | LEALKLESCGVTSDNCRDLCGIVASKASLRE | 0.88 | 0.05 |
| RINI_HUMAN | Ribonuclease inhibitor | LKDSPCQLEALKLESCGVTSDNCRDLCGIVA | 0.88 | 0.05 |
| RINI_HUMAN | Ribonuclease inhibitor | LLPLLQQCQVVRLDDCGLTEARCKDISSALR | 0.93 | 0.03 |
| ROA2_HUMAN | Heterogeneous nuclear ribonucleoproteins A2/B1 | ESLRNYYEQWGKLTDCVVMRDPASKRSRGFG | 0.91 | 0.03 |

| Protein ID | Protein Name | Sequence | H/L | SD |
|---|---|---|---|---|
| SERC_HUMAN | Phosphoserine aminotransferase | VVIVRDDLLGFALRECPSVLEYKVQAGNSSL | 0.76 | 0.12 |
| SF01_HUMAN | Splicing factor 1 | PWQSSETRSITNTTVCTKCGGAGHIASDCKF | 0.98 | 0.01 |
| SNAA_HUMAN | Alpha-soluble NSF attachment protein | FFSGLFGGSSKIEEACEIYARAANMFKMAKN | 1.28 | 0.33 |
| CAP1_HUMAN | Adenylyl cyclase-associated protein 1 | VIEDTELKQVAYIYKCVNTTLQIKGKINSIT | 1.02 | 0.08 |
| SRSF1_HUMAN | Serine/arginine-rich splicing factor 1 | SWQDLKDHMREAGDVCYADVYRDGTGVVEF V | 0.98 | 0.05 |
| SYAC_HUMAN | Alanine--tRNA ligase, cytoplasmic | MLFTVDNEAGKITCLCQVPQNAANRGLKASE | 0.61 | 0.18 |
| SYAC_HUMAN | Alanine--tRNA ligase, cytoplasmic | SAMLFTVDNEAGKITCLCQVPQNAANRGLKA | 0.61 | 0.18 |
| SYAC_HUMAN | Alanine--tRNA ligase, cytoplasmic | ANEMIEAAKAVYTQDCPLAAAKAIQGLRAVF | 0.76 | 0.16 |
| SYEP_HUMAN | Bifunctional glutamate/proline--tRNA ligase | MWEEMKKGSQFGQSCCLRAKIDMSSNNGCMR | 0.87 | 0.15 |
| SYEP_HUMAN | Bifunctional glutamate/proline--tRNA ligase | QMWEEMKKGSQFGQSCCLRAKIDMSSNNGCM | 0.87 | 0.15 |
| SYEP_HUMAN | Bifunctional glutamate/proline--tRNA ligase | GVPIRLEVGPRDMKSCQFVAVRRDTGEKLTV | 0.71 | 0.35 |
| SYEP_HUMAN | Bifunctional glutamate/proline--tRNA ligase | WVQSHRDLPIKLNQWCNVVRWEFKHPQPFLR | 2.20 | 1.24 |
| TCEA1_HUMAN | Transcription elongation factor A protein 1 | HQMAKTGGTQTDLFTCGKCKKKNCTYTQVQT | 0.67 | 0.10 |
| TCPG_HUMAN | T-complex protein 1 subunit gamma | VAQALEVIPRTLIQNCGASTIRLLTSLRAKH | 1.94 | 0.15 |
| TPIS_HUMAN | Triosephosphate isomerase | GTLNAAKVPADTEVVCAPPTAYIDFARQKLD | 0.89 | 0.04 |
| TPIS_HUMAN | Triosephosphate isomerase | ARQKLDPKIAVAAQNCYKVTNGAFTGEISPG | 1.07 | 0.06 |
| TPIS_HUMAN | Triosephosphate isomerase | QSTRIIYGGSVTGATCKELASQPDVDGFLVG | 1.03 | 0.03 |
| TXND5_HUMAN | Thioredoxin domain-containing protein 5 | KVYVAKVDCTAHSDVCSAQGVRGYPTLKLFK | 1.16 | 0.04 |
| TXND5_HUMAN | Thioredoxin domain-containing protein 5 | YNSMEDAKVYVAKVDCTAHSDVCSAQGVRGY | 1.16 | 0.04 |
| TXND5_HUMAN | Thioredoxin domain-containing protein 5 | KEFPGLAGVKIAEVDCTAERNICSKYSVRGY | 1.11 | 0.05 |
| UBA1_HUMAN | Ubiquitin-like modifier-activating enzyme 1 | AMVSMVTKDNPGVVTCLDEARHGFESGDFVS | 0.76 | 0.16 |
| VASP_HUMAN | Vasodilator-stimulated phosphoprotein | MSETVICSSRATVMLYDDGNKR | 0.88 | 0.28 |
| VDAC3_HUMAN | Voltage-dependent anion-selective channel protein 3 | DTGKASGNLETKYKVCNYGLTFTQKWNTDNT | 1.29 | 0.19 |
| VINC_HUMAN | Vinculin | KQCTDKRIRTNLLQVCERIPTISTQLKILST | 0.83 | 0.04 |
| VPS35_HUMAN | Vacuolar protein sorting-associated protein 35 | QHPLRGLFLRNYLLQCTRNILPDEGEPTDEE | 1.33 | 0.24 |
| ZYX_HUMAN | Zyxin | DMEHPQRQNVAVNELCGRCHQPLARAQPAVR | 1.11 | 0.05 |

## B.12 The 118 sulfenic acid modification sites identified in THP-1 cells upon six-hour LPA-PR treatment with H/L ratio.

| Protein ID | Protein Name | Sequence | H/L | SD |
|---|---|---|---|---|
| TBA4A_HUMAN | Tubulin alpha-4A chain | TVVPGGDLAKVQRAVCMLSNTTAIAEAWARL | 1.02 | 0.13 |
| TBA8_HUMAN | Tubulin alpha-4A chain;Tubulin alpha-1B chain | IAAIKTKRSIQFVDWCPTGFKVGINYQPPTV | 0.90 | 0.23 |
| LDH6A_HUMAN | L-lactate dehydrogenase | WKISGFPKNRVIGSGCNLDSARFRYLMGERL | 1.29 | 0.58 |
| RAC2_HUMAN | Ras-related C3 botulinum toxin substrate 2 | RGLKTVFDEAIRAVLCPQPTRQQKRACSLL_ | 1.08 | 0.10 |
| P3H1_HUMAN | Prolyl 3-hydroxylase 1 | TELDAKTVTAEVQPQCGRAVGFSSGTENPHG | 0.55 | 0.07 |
| TEBP_HUMAN | Prostaglandin E synthase 3 | DPNDSKHKRTDRSILCCLRKGESGQSWPRLT | 0.90 | 0.09 |
| TCPG_HUMAN | T-complex protein 1 subunit gamma | VAQALEVIPRTLIQNCGASTIRLLTSLRAKH | 0.82 | 0.16 |
| ARP3_HUMAN | Actin-related protein 3 | SLETAKAVKERYSYVCPDLVKEFNKYDTDGS | 0.95 | 0.10 |
| PGK1_HUMAN | Phosphoglycerate kinase 1 | ELKSLLGKDVLFLKDCVGPEVEKACANPAAG | 0.92 | 0.09 |
| PGK1_HUMAN | Phosphoglycerate kinase 1 | VLFLKDCVGPEVEKACANPAAGSVILLENLR | 1.04 | 0.13 |
| PIMT_HUMAN | Protein-L-isoaspartate O-methyltransferase | AKALDVGSGSGILTACFARMVGCTGKVIGID | 0.60 | 0.18 |
| MDHC_HUMAN | Malate dehydrogenase, cytoplasmic | MVIVVGNPANTNCLTASKSAPSIPKENF | 1.12 | 0.16 |
| MDHC_HUMAN | Malate dehydrogenase, cytoplasmic | TASKSAPSIPKENFSCLTRLDHNRAKAQIAL | 1.44 | 0.30 |
| RS27L_HUMAN | 40S ribosomal protein S27 | VLCQPTGGKARLTEGCSFRRKQH | 0.91 | 0.10 |
| RSSA_HUMAN | 40S ribosomal protein SA | PLTEASYVNLPTIALCNTDSPLRYVDIAIPC | 0.46 | 0.24 |
| PPIH_HUMAN | Peptidyl-prolyl cis-trans isomerase | FADVVPKTAENFRQFCTGEFRKDGVPIGYKG | 0.99 | 0.15 |
| RL30_HUMAN | 60S ribosomal protein L30 | NNIELGTACGKYYRVCTLAIIDPGDSDIIRS | 0.58 | 0.12 |
| PTPRC_HUMAN | Receptor-type tyrosine-protein phosphatase C | IKTDFGSPGEPQIIFCRSEAAHQGVITWNPP | 1.03 | 0.26 |
| HNRH1_HUMAN | Heterogeneous nuclear ribonucleoprotein H | GGEGFVVKVRGLPWSCSADEVQRFFSDCKIQ | 0.69 | 0.18 |
| RS3_HUMAN | 40S ribosomal protein S3 | GSVELYAEKVATRGLCAIAQAESLRYKLLGG | 0.67 | 0.10 |
| TALDO_HUMAN | Transaldolase | GASFRNTGEIKALAGCDFLTISPKLLGELLQ | 0.86 | 0.19 |
| STIP1_HUMAN | Stress-induced-phosphoprotein 1 | KAMDVYQKALDLDSSCKEAADGYQRCMMAQY | 0.79 | 0.03 |
| CAP1_HUMAN | Adenylyl cyclase-associated protein 1 | KTDGCHAYLSKNSLDCEIVSAKSSEMNVLIP | 1.08 | 0.17 |
| CAP1_HUMAN | Adenylyl cyclase-associated protein 1 | VIEDTELKQVAYIYKCVNTTLQIKGKINSIT | 1.17 | 0.13 |
| CAP1_HUMAN | Adenylyl cyclase-associated protein 1 | TLQIKGKINSITVDNCKKLGLVFDDVVGIVE | 1.15 | 0.15 |
| CAP1_HUMAN | Adenylyl cyclase-associated protein 1 | TGLKLERALLVTASQCQQPAENKLSDLLAPI | 0.96 | 0.04 |

| Protein ID | Protein Name | Sequence | H/L | SD |
|---|---|---|---|---|
| AP1B1_HUMAN | AP-1 complex subunit beta-1 | KDIPNENEAQFQIRDCPLNAEAASSKLQSSN | 0.83 | 0.13 |
| DUT_HUMAN | Deoxyuridine 5'-triphosphate nucleotidohydrolase, mitochondrial | EKFEVKKGDRIAQLICERIFYPEIEEVQALD | 0.27 | 0.06 |
| GSLG1_HUMAN | Golgi apparatus protein 1 | DRHLYFACRDDRERFCENTQAGEGRVYKCLF | 0.84 | 0.05 |
| QCR2_HUMAN | Cytochrome b-c1 complex subunit 2, mitochondrial | LHAAAYRNALANPLYCPDYRIGKVTSEE | 0.80 | 0.02 |
| PCBP2_HUMAN | Poly(rC)-binding protein 2 | IREESGARINISEGNCPERIITLTGPTNAIF | 0.70 | 0.14 |
| CLIC1_HUMAN | Chloride intracellular channel protein 1 | ELFVKAGSDGAKIGNCPFSQRLFMVLWLKGV | 1.10 | 0.15 |
| PLOD3_HUMAN | Procollagen-lysine,2-oxoglutarate 5-dioxygenase 3 | GLDYEGGGCRFLRYDCVISSPRKGWALLHPG | 1.13 | 0.07 |
| 6PGL_HUMAN | 6-phosphogluconolactonase | ELGAALAQLVAQRAACCLAGARARFALGLSG | 1.41 | 0.15 |
| LMNA_HUMAN | Prelamin-A/C | SPPTDLVWKAQNTWGCGNSLRTALINSTGEE | 1.42 | 0.36 |
| CATA_HUMAN | Catalase | HRHRLGPNYLHIPVNCPYRARVANYQRDGPM | 1.09 | 0.12 |
| CATA_HUMAN | Catalase | SHTFKLVNANGEAVYCKFHYKTDQGIKNLSV | 1.34 | 0.31 |
| ALDOA_HUMAN | Fructose-bisphosphate aldolase A | QSEEEASINLNAINKCPLLKPWALTFSYGRA | 1.01 | 0.16 |
| ALDOA_HUMAN | Fructose-bisphosphate aldolase A | AQEEYVKRALANSLACQGKYTPSGQAGAAAS | 1.30 | 0.65 |
| G3P_HUMAN | Glyceraldehyde-3-phosphate dehydrogenase | AFRVPTANVSVVDLTCRLEKPAKYDDIKKVV | 0.99 | 0.05 |
| G3P_HUMAN | Glyceraldehyde-3-phosphate dehydrogenase | DNSLKIISNASCTTNCLAPLAKVIHDNFGIV | 0.87 | 0.06 |
| G3P_HUMAN | Glyceraldehyde-3-phosphate dehydrogenase | HEKYDNSLKIISNASCTTNCLAPLAKVIHDN | 1.00 | 0.10 |
| ITB2_HUMAN | Integrin beta-2 | GFEGSACQCERTTEGCLNPRRVECSGRGRCR | 0.79 | 0.20 |
| ITB2_HUMAN | Integrin beta-2 | CECDTINCERYNGQVCGGPGRGLCFCGKCRC | 1.22 | 0.36 |
| ITB2_HUMAN | Integrin beta-2 | FCSNGVTHRNQPRGDCDGVQINVPITFQVKV | 0.85 | 0.22 |
| ITB2_HUMAN | Integrin beta-2 | HNALPDTLKVTYDSFCSNGVTHRNQPRGDCD | 0.79 | 0.21 |
| ENOA_HUMAN | Alpha-enolase | LKVNQIGSVTESLQACKLAQANGWGVMVSHR | 0.68 | 0.06 |
| ENOA_HUMAN | Alpha-enolase | NPKRIAKAVNEKSCNCLLLKVNQIGSVTESL | 1.10 | 0.19 |
| ENOA_HUMAN | Alpha-enolase | VTNPKRIAKAVNEKSCNCLLLKVNQIGSVTE | 1.04 | 0.09 |
| CATG_HUMAN | Cathepsin G | VALPRAQEGLRPGTLCTVAGWGRVSMRRGTD | 0.33 | 0.22 |
| GSTP1_HUMAN | Glutathione S-transferase P | VVTVETWQEGSLKASCLYGQLPKFQDGDLTL | 0.89 | 0.01 |
| LEG1_HUMAN | Galectin-1 | AKSFVLNLGKDSNNLCLHFNPRFNAHGDANT | 0.77 | 0.09 |
| LEG1_HUMAN | Galectin-1 | FNPRFNAHGDANTIVCNSKDGGAWGTEQREA | 0.85 | 0.12 |
| LEG1_HUMAN | Galectin-1 | ACGLVASNLNLKPGECLRVRGEVAPDAKSFV | 0.87 | 0.01 |
| LEG1_HUMAN | Galectin-1 | MACGLVASNLNLKPGECL | 0.58 | 0.31 |
| CH60_HUMAN | 60 kDa heat shock protein, mitochondrial | ATRAAVEEGIVLGGGCALLRCIPALDSLTPA | 0.99 | 0.07 |
| HSP7C_HUMAN | Heat shock cognate 71 kDa protein | EKEEFEHQQKELEKVCNPIITKLYQSAGGMP | 0.61 | 0.09 |
| ACTN1_HUMAN | Alpha-actinin-1 | DYYDSPSVNARCQKICDQWDNLGALTQKRRE | 1.47 | 0.08 |
| RINI_HUMAN | Ribonuclease inhibitor | LLPLLQQCQVVRLDDCGLTEARCKDISSALR | 1.10 | 0.10 |

| Protein ID | Protein Name | Sequence | H/L | SD |
|---|---|---|---|---|
| RINI_HUMAN | Ribonuclease inhibitor | QISNNRLEDAGVRELCQGLGQPGSVLRVLWL | 0.96 | 0.11 |
| RINI_HUMAN | Ribonuclease inhibitor | LRTLWIWECGITAKGCGDLCRVLRAKESLKE | 1.12 | 0.15 |
| EF2_HUMAN | Elongation factor 2 | AIHRGGGQIIPTARRCLYASVLTAQPRLMEP | 0.59 | 0.16 |
| EF2_HUMAN | Elongation factor 2 | SVVAGFQWATKEGALCEENMRGVRFDVHDVT | 0.87 | 0.11 |
| PLSL_HUMAN | Plastin-2 | DMSGLREKDDIQRAECMLQQAERLGCRQFVT | 1.08 | 0.10 |
| PLSL_HUMAN | Plastin-2 | PPYPKLGGNMKKLENCNYAVELGKNQAKFSL | 1.01 | 0.15 |
| PLST_HUMAN | Plastin-2 | AFVNWINKALENDPDCRHVIPMNPNTNDLFN | 1.01 | 0.23 |
| PLST_HUMAN | Plastin-2 | GYISFNELNDLFKAACLPLPGYRVREITENL | 1.08 | 0.13 |
| KPYM_HUMAN | Pyruvate kinase | DIDSPPITARNTGIICTIGPASRSVETLKEM | 0.71 | 0.04 |
| ENPL_HUMAN | Endoplasmin | KIEKAVVSQRLTESPCALVASQYGWSGNMER | 0.74 | 0.07 |
| NDKA_HUMAN | Nucleoside diphosphate kinase A | TNPADSKPGTIRGDFCIQVGRNIIHGSDSVE | 1.16 | 0.18 |
| NDKB_HUMAN | Phosphoglycerate mutase 1 | KDRRYADLTEDQLPSCESLKDTIARALPFWN | 0.86 | 0.17 |
| GSTM3_HUMAN | Glutathione S-transferase Mu 3 | LLEFTDTSYEEKRYTCGEAPDYDRSQWLDVK | 1.18 | 0.22 |
| UBA1_HUMAN | Ubiquitin-like modifier-activating enzyme 1 | AMVSMVTKDNPGVVTCLDEARHGFESGDFVS | 1.00 | 0.04 |
| TCEA1_HUMAN | Transcription elongation factor A protein 1 | TQTDLFTCGKCKKKNCTYTQVQTRSADEPMT | 0.80 | 0.29 |
| TCEA2_HUMAN | Elongation factor 1-gamma | SFRQAFPNTNRWFLTCINQPQFRAVLGEVKL | 0.88 | 0.17 |
| CALR_HUMAN | Calreticulin | TLVVQFTVKHEQNIDCGGGYVKLFPNSLDQT | 1.03 | 0.13 |
| PRDX6_HUMAN | Peroxiredoxin-6 | SWGILFSHPRDFTPVCTTELGRAAKLAPEFA | 0.89 | 0.22 |
| RL12_HUMAN | 60S ribosomal protein L12 | PPKFDPNEIKVVYLRCTGGEVGATSALAPKI | 0.74 | 0.08 |
| COR1A_HUMAN | Coronin-1A | YSVDWSRDGGLICTSCRDKRVRIIEPRKGTV | 1.19 | 0.20 |
| COR1A_HUMAN | Coronin-1A | DTIYSVDWSRDGGLICTSCRDKRVRIIEPRK | 1.14 | 0.18 |
| COR1A_HUMAN | Coronin-1A | YEDVRVSQTTWDSGFCAVNPKFVALICEASG | 1.14 | 0.05 |
| COR1A_HUMAN | Coronin-1A | SKFRHVFGQPAKADQCYEDVRVSQTTWDSGF | 1.03 | 0.15 |
| QCR1_HUMAN | Cytochrome b-c1 complex subunit 1, mitochondrial | IDDMMFVLQGQWMRLCTSATESEVARGKNIL | 1.08 | 0.09 |
| MDHM_HUMAN | Malate dehydrogenase, mitochondrial | KAAVKGYLGPEQLPDCLKGCDVVVIPAGVPR | 0.63 | 0.02 |
| MDHM_HUMAN | Malate dehydrogenase, mitochondrial | KGYLGPEQLPDCLKGCDVVVIPAGVPRKPGM | 1.03 | 0.18 |
| MDHM_HUMAN | Malate dehydrogenase, mitochondrial; | EGVVECSFVKSQETECTYFSTPLLLGKKGIE | 1.04 | 0.16 |
| RS5_HUMAN | 40S ribosomal protein S5 | DVSPLRRVNQAIWLLCTGAREAAFRNIKTIA | 0.59 | 0.12 |
| HCFC1_HUMAN | Host cell factor 1 | QPGTAYKFRVAGINACGRGPFSEISAFKTCL | 0.88 | 0.14 |
| TPIS_HUMAN | Triosephosphate isomerase | GTLNAAKVPADTEVVCAPPTAYIDFARQKLD | 0.84 | 0.13 |
| TPIS_HUMAN | Triosephosphate isomerase | ARQKLDPKIAVAAQNCYKVTNGAFTGEISPG | 0.97 | 0.11 |
| TPIS_HUMAN | Triosephosphate isomerase | QSTRIIYGGSVTGATCKELASQPDVDGFLVG | 1.01 | 0.11 |
| TPIS_HUMAN | Triosephosphate isomerase | QKVAHALAEGLGVIACIGEKLDEREAGITEK | 1.14 | 0.05 |
| ACTB_HUMAN | Actin, cytoplasmic 1 | DDDIAALVVDNGSGMCKAGFAGDDAPRAVFP | 0.83 | 0.13 |
| RS20_HUMAN | 40S ribosomal protein S20 | RITLTSRNVKSLEKVCADLIRGAKEKNLKVK | 0.91 | 0.07 |

| Protein ID | Protein Name | Sequence | H/L | SD |
|---|---|---|---|---|
| CNBP_HUMAN | Cellular nucleic acid-binding protein | TGHVAINCSKTSEVNCYRCGESGHLARECTI | 0.65 | 0.09 |
| GBB1_HUMAN | Guanine nucleotide-binding protein G(I)/G(S)/G(T) subunit beta-1 | SLSLAPDTRLFVSGACDASAKLWDVREGMCR | 1.25 | 0.07 |
| PPIA_HUMAN | Peptidyl-prolyl cis-trans isomerase A | GYKGSCFHRIIPGFMCQGGDFTRHNGTGGKS | 0.79 | 0.19 |
| PPIA_HUMAN | Peptidyl-prolyl cis-trans isomerase A | GSRNGKTSKKITIADCGQLE | 0.67 | 0.19 |
| AIMP1_HUMAN | Aminoacyl tRNA synthase complex-interacting multifunctional protein 1 | DSKPIDVSRLDLRIGCIITARKHPDADSLYV | 0.96 | 0.03 |
| PRDX4_HUMAN | Peroxiredoxin-4 | QGWETEERPRTREEECHFYAGGQVYPGEASR | 0.36 | 0.04 |
| SF01_HUMAN | Splicing factor 1 | PWQSSETRSITNTTVCTKCGGAGHIASDCKF | 0.58 | 0.10 |
| ZYX_HUMAN | Zyxin | DMEHPQRQNVAVNELCGRCHQPLARAQPAVR | 0.70 | 0.16 |
| FSCN1_HUMAN | Fascin | HLGRYLAADKDGNVTCEREVPGPDCRFLIVA | 0.82 | 0.14 |
| TBB5_HUMAN | Tubulin beta chain | SYFVEWIPNNVKTAVCDIPPRGLKMAVTFIG | 1.14 | 0.17 |
| HNRPK_HUMAN | Heterogeneous nuclear ribonucleoprotein K | PTLEEYQHYKGSDFDCELRLLIHQSLAGGII | 0.78 | 0.06 |
| PNCB_HUMAN | Nicotinate phosphoribosyltransferase | PDTDPAFFEHLRALDCSEVTVRALPEGSLAF | 1.01 | 0.03 |
| TXND5_HUMAN | Thioredoxin domain-containing protein 5 | KVYVAKVDCTAHSDVCSAQGVRGYPTLKLFK | 0.97 | 0.31 |
| TXND5_HUMAN | Thioredoxin domain-containing protein 5 | YNSMEDAKVYVAKVDCTAHSDVCSAQGVRGY | 0.97 | 0.31 |
| TXND5_HUMAN | Thioredoxin domain-containing protein 5 | KEFPGLAGVKIAEVDCTAERNICSKYSVRGY | 1.05 | 0.10 |
| PARK7_HUMAN | Protein DJ-1 | IKVTVAGLAGKDPVQCSRDVVICPDASLEDA | 0.65 | 0.14 |
| PARK7_HUMAN | Protein DJ-1 | LAGKDPVQCSRDVVICPDASLEDAKKEGPYD | 0.71 | 0.12 |
| ESYT1_HUMAN | Extended synaptotagmin-1 | KSDPYALVRLGTQTFCSRVIDEELNPQWGET | 1.08 | 0.09 |
| ZN576_HUMAN | Zinc finger protein 576 | FVAQKLQGVLFICFTCARSFPSSKALITHQR | 5.25 | 1.13 |
| ZN576_HUMAN | Zinc finger protein 576 | PADFVAQKLQGVLFICFTCARSFPSSKALIT | 5.25 | 1.13 |
| DPP2_HUMAN | Dipeptidyl peptidase 2 | SGSEHCYDIYRLYHSCADPTGCGTGPDARAW | 1.41 | 0.20 |
| DPP2_HUMAN | Dipeptidyl peptidase 2 | YDIYRLYHSCADPTGCGTGPDARAWDYQACT | 1.41 | 0.20 |
| RL36_HUMAN | 60S ribosomal protein L36 | LTKHTKFVRDMIREVCGFAPYERRAMELLKV | 0.75 | 0.14 |
| VASP_HUMAN | Vasodilator-stimulated phosphoprotein | MSETVICSSRATVMLYDDGNKR | 1.14 | 0.13 |

### B.13 The 40 sulfenic acid modification sites identified in THP-1 cells upon six-hour Thr-PR treatment with H/L ratio.

| Protein ID | Protein name | Sequence | H/L | SD |
|---|---|---|---|---|
| ACTB_HUMAN | Actin, cytoplasmic 1 | TTAEREIVRDIKEKLCYVALDFEQEMATAAS | 1.07 | 0.11 |

| Protein ID | Protein name | Sequence | H/L | SD |
|---|---|---|---|---|
| ADPGK_HUMAN | ADP-dependent glucokinase | LAAVAAGARVAGTQACATETIDTSRVSLRAP | 0.95 | 0.15 |
| ALDOC_HUMAN | Fructose-bisphosphate aldolase C | AILENANVLARYASICQQNGIVPIVEPEILP | 0.60 | 0.02 |
| CAP1_HUMAN | Adenylyl cyclase-associated protein 1 | VMGKVPTISINKTDGCHAYLSKNSLDCEIVS | 0.76 | 0.08 |
| CAP1_HUMAN | Adenylyl cyclase-associated protein 1 | KTDGCHAYLSKNSLDCEIVSAKSSEMNVLIP | 0.83 | 0.14 |
| CAP1_HUMAN | Adenylyl cyclase-associated protein 1 | TGLKLERALLVTASQCQQPAENKLSDLLAPI | 0.80 | 0.07 |
| CATA_HUMAN | Catalase | HRHRLGPNYLHIPVNCPYRARVANYQRDGPM | 0.84 | 0.06 |
| CATA_HUMAN | Catalase | SHTFKLVNANGEAVYCKFHYKTDQGIKNLSV | 2.25 | 1.15 |
| CATG_HUMAN | Cathepsin G | VALPRAQEGLRPGTLCTVAGWGRVSMRRGTD | 0.50 | 0.09 |
| CH60_HUMAN | 60 kDa heat shock protein, mitochondrial | ATRAAVEEGIVLGGGCALLRCIPALDSLTPA | 0.87 | 0.09 |
| COMT_HUMAN | Catechol O-methyltransferase | LSPGARLITIEINPDCAAITQRMVDFAGVKD | 1.01 | 0.05 |
| DEST_HUMAN | Destrin | MASGVQVADEVCRIFYDMKVRKCSTPE | 0.86 | 0.02 |
| DPP2_HUMAN | Dipeptidyl peptidase 2 | SGSEHCYDIYRLYHSCADPTGCGTGPDARAW | 0.76 | 0.06 |
| DPP2_HUMAN | Dipeptidyl peptidase 2 | YDIYRLYHSCADPTGCGTGPDARAWDYQACT | 0.76 | 0.06 |
| EF2_HUMAN | Elongation factor 2 | KSATSPEGKKLPRTFCQLILDPIFKVFDAIM | 0.82 | 0.01 |
| ENOA_HUMAN | Alpha-enolase | LKVNQIGSVTESLQACKLAQANGWGVMVSHR | 1.01 | 0.19 |
| ITB2_HUMAN | Integrin beta-2 | GFEGSACQCERTTEGCLNPRRVECSGRGRCR | 0.83 | 0.02 |
| ITB2_HUMAN | Integrin beta-2 | CECDTINCERYNGQVCGGPGRGLCFCGKCRC | 1.02 | 0.02 |
| KPYM_HUMAN | Pyruvate kinase | DIDSPPITARNTGIICTIGPASRSVETLKEM | 0.85 | 0.16 |
| KPYM_HUMAN | Pyruvate kinase | PTEATAVGAVEASFKCCSGAIIVLTKSGRSA | 0.95 | 0.08 |
| KPYM_HUMAN | Pyruvate kinase | TEATAVGAVEASFKCCSGAIIVLTKSGRSAH | 0.95 | 0.08 |
| LDHA_HUMAN | L-lactate dehydrogenase A chain | WKISGFPKNRVIGSGCNLDSARFRYLMGERL | 1.36 | 0.14 |
| LEG1_HUMAN | Galectin-1 | FNPRFNAHGDANTIVCNSKDGGAWGTEQREA | 0.96 | 0.18 |
| LEG1_HUMAN | Galectin-1 | AKSFVLNLGKDSNNLCLHFNPRFNAHGDANT | 1.27 | 0.15 |
| LEG1_HUMAN | Galectin-1 | MACGLVASNLNLKPGECL | 0.60 | 0.17 |
| LEG1_HUMAN | Galectin-1 | ACGLVASNLNLKPGECLRVRGEVAPDAKSFV | 0.60 | 0.17 |
| LSM7_HUMAN | U6 snRNA-associated Sm-like protein LSm7 | QYKLTEDTRQLGLVVCRGTSVVLICPQDGME | 1.70 | 0.56 |
| MIF_HUMAN | Macrophage migration inhibitory factor | GKIGGAQNRSYSKLLCGLLAERLRISPDRVY | 0.88 | 0.17 |
| PAL4A_HUMAN | Peptidyl-prolyl cis-trans isomerase | GSRNGKTSKKITIADCGQLE | 0.89 | 0.27 |
| PCBP2_HUMAN | Poly(rC)-binding protein 2 | IREESGARINISEGNCPERIITLTGPTNAIF | 0.97 | 0.10 |
| PPIA_HUMAN | Peptidyl-prolyl cis-trans isomerase | GYKGSCFHRIIPGFMCQGGDFTRHNGTGGKS | 0.94 | 0.20 |
| QCR1_HUMAN | Cytochrome b-c1 complex subunit 1, mitochondrial | IDDMMFVLQGQWMRLCTSATESEVARGKNIL | 0.82 | 0.16 |
| RINI_HUMAN | Ribonuclease inhibitor | LLPLLQQCQVVRLDDCGLTEARCKDISSALR | 1.03 | 0.14 |
| RINI_HUMAN | Ribonuclease inhibitor | QISNNRLEDAGVRELCQGLGQPGSVLRVLWL | 0.76 | 0.15 |

| Protein ID | Protein name | Sequence | H/L | SD |
|---|---|---|---|---|
| RL30_HUMAN | 60S ribosomal protein L30 | NNIELGTACGKYYRVCTLAIIDPGDSDIIRS | 0.83 | 0.16 |
| TBA1B_HUMAN | Tubulin alpha-4A chain | TVVPGGDLAKVQRAVCMLSNTTAIAEAWARL | 0.97 | 0.03 |
| TBA4A_HUMAN | Tubulin alpha-4A chain | IAAIKTKRSIQFVDWCPTGFKVGINYQPPTV | 0.93 | 0.00 |
| TPIS_HUMAN | Triosephosphate isomerase | ARQKLDPKIAVAAQNCYKVTNGAFTGEISPG | 0.96 | 0.04 |
| TPIS_HUMAN | Triosephosphate isomerase | QSTRIIYGGSVTGATCKELASQPDVDGFLVG | 0.87 | 0.14 |
| TXND5_HUMAN | Thioredoxin domain-containing protein 5 | KVYVAKVDCTAHSDVCSAQGVRGYPTLKLFK | 1.15 | 0.14 |
| TXND5_HUMAN | Thioredoxin domain-containing protein 5 | YNSMEDAKVYVAKVDCTAHSDVCSAQGVRGY | 1.15 | 0.14 |
| VASP_HUMAN | Vasodilator-stimulated phosphoprotein | MSETVICSSRATVMLYDDGNKR | 1.23 | 0.08 |

**Appendix C : Publication list**

Li, R., Huang, J., Kast, J. I**dentification of Total Reversible Cysteine Oxidation in an Atherosclerosis Model Using a Modified Biotin Switch Assay**. J. Proteome Res., 2015, 14 (5), 2026–2035.

Zhang, C.-C., Li, R., Jiang, H., Lin, S., Rogalski, JC., Liu K., Kast J. **Development and Application of a Quantitative Multiplexed Small GTPase Activity Assay Using Targeted Proteomics.** J. Proteome Res., 2015, 14(2), 967-976.

Li, R., Klockenbusch, C., Lin, L., Lin, S., Kast, J. Quantitative Protein Sulfenic Acid Analysis Identifies Platelet Releasate-induced Activation of Integrin $\beta_2$ on Monocytes via NADPH Oxidase. (Submitted)